

University of Silesia in Katowice

Faculty of Natural Sciences

Institute of Earth Sciences

MSc Anna Gumsley

**Variscan to Early Alpine magmatic and  
metamorphic evolution of the Strandja Zone  
(SE Bulgaria/NW Turkey)**

PhD Dissertation

Supervisor: dr hab. Krzysztof Szopa, Prof. UŚ

Sosnowiec, 2023



*'It is amazing what the chronicles are silent about  
and we will remember.'*

I want to thank you very much for all help and support which I got.

Without people who believed in me, I will not be here.

I want to thank all of you who are here and  
those who are already gone.

The research was conducted thanks to a Preludium Grant awarded by Anna Gumsley from the National Science Centre (NCN) in Poland (grant agreement no. UMO-2018/29/N/ST10/00368).



**A. Articles included in the PhD dissertation of Anna Gumsley (maiden name: Anna Sałacińska) entitled: '*Variscan to Early Alpine magmatic and metamorphic evolution of the Strandja Zone (SE Bulgaria/NW Turkey)*'.**

1. **Sałacińska, A.**, Gerdjikov, I., Gumsley, A., Szopa, K., Chew, D., Gawęda, A., Kocjan, I. (2021). Two stages of Late Carboniferous to Triassic magmatism in the Strandja Zone of Bulgaria and Turkey. *Geological Magazine*, 158: 2151–2164. <https://doi.org/10.1017/S0016756821000650>

*List of Ministry of Science and Higher Education: 100 points, IF 2.66*

2. **Sałacińska, A.**, Gerdjikov, I., Kounov, A., Chew, D., Szopa, K., Gumsley, A., Kocjan, I., Marciniak-Maliszewska, B., Drakou, F. (2022). Variscan magmatic evolution of the Strandja Zone (Southeast Bulgaria and Northwest Turkey) and its relationship to other North Gondwanan margin terranes. *Gondwana Research*, 109: 253–273. <https://doi.org/10.1016/j.gr.2022.04.013>

*List of Ministry of Science and Higher Education: 200 points, IF 6.15*

3. **Gumsley, A.**, Szopa, K., Chew, D., Gerdjikov, I., Jokubauskas, P., Marciniak-Maliszewska, B., Drakou, F. (2023). An Early Cretaceous thermal event in the Sakar Unit (Strandja Zone, SE Bulgaria/NW Turkey) revealed based on U-Pb rutile geochronology. *Lithos* 448-449, 1-17. <https://doi.org/10.1016/j.lithos.2023.107186>

*List of Ministry of Science and Higher Education: 140 points, IF 4.02*

**B. Other publications of PhD student:**

1. Gumsley, A., de Kock, M., Ernst, R., **Gumsley, A.**, Hanson, R., Kamo, S., Knoper, M., Lewandowski, M., Luks, B., Mamuse, A., Söderlund, U., (2023). The Mutare-Fingeren Dyke Swarm: the enigma of the Kalahari Craton's exit from supercontinent Rodinia. *Journal of the Geological Society Special Publication*, 537. <https://doi.org/10.1144/SP537-2022-206>

*List of Ministry of Science and Higher Education: 140 points, IF 2.64*

2. Gumsley, A., Stamsnijder, J., Larsson, E., Söderlund, U., Naeraa, T., de Kock, M., **Sałacińska, A.**, Gawęda, A., Humbert, F., Ernst, R., (2020) Neoarchean large igneous provinces on the Kaapvaal Craton in southern Africa re-define the formation of the Ventersdorp Supergroup and its temporal equivalents. *Geological Society of America Bulletin*, 177, 31-49. <https://doi.org/10.1130/B35237.1>

*List of Ministry of Science and Higher Education: 140 points, IF 5.41*

3. Szopa, K., **Sałacińska, A.**, Gumsley, A.P., Chew, D., Petrov, P., Gawęda, A., Zagórska, A., Deput, E., Gospodinov, N., Banasik, K., (2020). Two-Stage Late

Jurassic to Early Cretaceous Hydrothermal Activity in the Sakar Unit of Southeastern Bulgaria. *Minerals*, 10: 266. <https://doi.org/10.3390/min10030266>

*List of Ministry of Science and Higher Education: 100 points, IF 2.66*

4. Dunkley, D.J., Kusiak, M.K., Wilde, S., Whitehouse, M., **Śałacińska, A.**, Kielman, R., Konečný, P., (2020). Two Neoarchean tectonothermal events on the western edge of the North Atlantic Craton, as revealed by SIMS dating of the Saglek Block, Nain Province, Labrador. *Journal of the Geological Society Special Publication*. 177:31-49. <https://doi.org/10.1144/jgs2018-153>

*List of Ministry of Science and Higher Education: 140 points, IF 2.64*

5. **Śałacińska, A.**, Kusiak, M.A., Whitehouse, M.J., Dunkley, D.J., Wilde, S.A., Kielman, R., Król, P., (2019) Gneiss-forming events in the Saglek Block, Labrador; a reappraisal of the Uivak gneiss, *International Journal of Earth Sciences*. *International Journal of Earth Sciences*, 108:753–778. [doi.org/10.1007/s00531-019-01677-y](https://doi.org/10.1007/s00531-019-01677-y)

*List of Ministry of Science and Higher Education: 100 points, IF 2.52*

6. **Śałacińska, A.**, Kusiak, M.A., Whitehouse, M.J., Dunkley, D.J., Wilde, S.A., Kielman, R. (2018) Complexity of the early Archean Uivak Gneiss: insights from Tigigakyuk Inlet, Saglek Block, Labrador, Canada and possible correlations with south West Greenland. *Precambrian Research* 315:103-119 <https://doi.org/10.1016/j.precamres.2018.07.011>

*List of Ministry of Science and Higher Education: 200 points, IF 4.26*

7. Kusiak, M.A., Dunkley, D.J., Whitehouse, M.J., Wilde, S.A., **Śałacińska, A.**, Konečný, P., Szopa, K., Gawęda, A., Chew, D. (2018) Peak to post-peak thermal history of the Saglek Block of Labrador: a multiphase and multi-instrumental approach to geochronology. *Chemical Geology*. <https://doi.org/10.1016/j.chemgeo.2017.10.033>

*List of Ministry of Science and Higher Education: 140 points, IF 4.68*

## Table of contents

Summary of PhD Dissertation in Polish.....	9
Summary of PhD Dissertation in English.....	11
1. Introduction.....	13
2. Aim of the PhD Dissertation.....	16
3. Study area.....	16
4. Methodology.....	19
5. Summary of the articles included in the PhD Dissertation.....	21
5.1. Two stages of Late Carboniferous to Triassic magmatism in the Strandja Zone of Bulgaria and Turkey.....	21
5.2. Variscan magmatic evolution of the Strandja Zone (Southeast Bulgaria and Northwest Turkey) and its relationship to other North Gondwanan margin terranes.....	24
5.3. An Early Cretaceous thermal event in the Sakar Unit (Strandja Zone, SE Bulgaria/NW Turkey) revealed based on U-Pb rutile geochronology and Zr-in-rutile thermometry.....	27
6. Conclusions.....	30
7. Literature.....	33
8. Contribution statement of the co-authors.....	39





## Summary of PhD Dissertation in Polish

Strefa Strandży to pasmo górskie rozciągające się z północnego-zachodu do południowego-wschodu na granicy bułgarsko-tureckiej. Strefa ta składa się z jednostek autochtonicznych i allochtonicznych, starszych niż późna kreda. Obszar ten jest jednym z najmniej rozpoznanych w rejonie Morza Czarnego i jest różnie klasyfikowany. Część badaczy zalicza go do Bałkanidów, a inni do Pontydów. Choć we wszystkich sąsiednich jednostkach geologicznych zachowały się pozostałości waryscyjskich masywów, ich ewolucja została w wielu miejscach zatarta przez młodsze wydarzenia tektoniczne lub pokryta skałami osadowymi.

Strefy Strandży w okresie od późnej jury do wczesnej kredy została objęta oddziaływaniem metamorfizmu *sensu stricto* i deformacji, zwanych w lokalnej literaturze metamorfizmem wczesnoalpejskim, który znacząco zatarał ślady jej paleozoicznej i wczesno mezozoicznej ewolucji. Na podstawie różnego stopnia metamorfizmu i deformacji wczesnoalpejskiej, wyróżniono trzy jednostki strefy Strandży na terytorium Bułgarii: Strandja, Sakar i Veleka. Jednostki Strandża i Sakar wykazują wiele podobieństw. Obie składają się ze skał (starsze niż późno karbońskie) podłoża, w które intrudowały granitoidy od późnego karbonu do triasu. Skały podłoża i granitoidy jednostki Sakar są pokryte przez permsko-triasowe skały meta-osadowe, które zostały zmetamorfizowane w warunkach facji amfibolitowej podczas metamorfizmu wczesnoalpejskiego. Natomiast równowiekowe skały osadowe w jednostce Strandży zostały zmetamorfizowane w niższym stopniu.

Pozycja paleogeograficzna Strefy Strandży w paleozoiku i mezozoiku budzi wiele kontrowersji. Wcześniejsze badania sugerowały, że Strefa Strandży tworzyła łuk magmowy 1) od późnego dewonu do wczesnego karbonu razem z Bałkanami, Sredną Górą, Sakaryą i Kaukazem; 2) lub od późnego karbonu do triasu wraz z Rodopami i Serbsko-Macedońskim Kompleksem Metamorficznym, związany z subdukcją Oceanu Paleo-Tetydy. Pierwszy model został podważony przez występowanie waryscyjskiej strefy ścinania między słabo- i silnie- zmetamorfizowanymi skałami podłoża kolejno w strefach Bałkanów i Srednej Góry. Natomiast drugi model został zakwestionowany w tej rozprawie doktorskiej.

Niniejsza praca koncentruje się na Jednostce Sakar (Strefa Strandży), zdominowanej przez późno karbońskie do triasowych granitoidów budujących Batolit Sakar, Blok Magmaowy Harmanli oraz południowe plutony Izvorovo, Levka i Ustrem.

W rozprawie przedstawiono nowe dane z datowania U-Pb cyrkonu, tytanitu i rutylu w połączeniu z badaniami geochemicznymi, petrograficznymi i terenowymi. Najważniejszymi wynikami badań są: **1)** określenie po raz pierwszy wieków krystalizacji plutonów Izvorovo (ok. 251-256 mln lat) i Levka (ok. 306 mln lat); **2)** korekta wieku Batolitu Sakar (ok. 319 mln lat); **3)** wskazanie dowodów na wpływ metamorfizmu deformacji waryscyjskich w jednostce Sakar (> ok. 319 mln lat) oraz **4)** wykazanie obecności dwóch etapów metamorfizmu i deformacji wczesnoalpejskiej i jej korelacja z fazą regionalną w późnej jurze (ok. 154 mln lat temu) i lokalną aktywnością hydrotermalną we wczesnej kredzie (ok. 125-116 mln lat temu) związaną z albityzacją. Oba te etapy osiągnęły podobne temperatury (~530-620°C).

Badania wykazały również, że późno karbońsko-triasowy magmatyzm w Strefie Strandży reprezentuje dwie grupy granitoidów. Starsza grupa, późno karbońska, jest interpretowana jako post-kolizyjna, podobnie do równowiekowego magmatyzmu w strefach Srednej Góry i Sakaryi. Natomiast młodsza grupa (permsko-triasowa), powstała prawdopodobnie w warunkach związanych z ryftami lub subdukcją.

Podobieństwa skał podłoża i granitoidów stref Strandży i Sredna Gora wskazały, że dzielą one wspólną ewolucję paleozoiczną. Obie te strefy, wraz z Serbsko-Macedońskim Kompleksem Metamorficznym i Strefą Sakarya, prawdopodobnie były częścią metamorficznego jądra orogenu waryscyjskiego. Następnie strefa Strandży w późnej jurze do wczesnej kredy została dotknięta metamorfizmem i deformacją. W tym samym czasie metamorfizm w Rodopach osiągnął (ultra-) wysoki stopień. Chociaż wydarzenia te są równowiekowe, różnice w warunkach metamorficznych nie pozwalają na bezpośrednie korelowanie mezozoicznej ewolucji tych dwóch stref.

Rozprawa doktorska przedstawia również wyzwania w interpretacji danych geochemicznych i geochronologicznych, takie jak: **1)** problem z rozróżnieniem środowisk tektonicznych w których formowały się granitoidy na podstawie wyłącznie danych geochemicznych. Ten problem podparty jest dowodami z charakterystyki populacji cyrkonu i temperatur generacji magmy; **2)** problem z interpretacją danych z datowania U-Pb cyrkonu rozłożonych wzdłuż konkordii, dla którego proponowane rozwiązanie zakłada częściową utratę ołowiu w wyniku zdarzenia metamorficznego; **3)** interpretacja wysoko radiogenicznego pierwotnego składu izotopów ołowiu w rutylu, przedstawiona na podstawie przesłanek izotopowych i teksturalnych na to, że tytanit magmowy był prekursorem rutylu.

## Summary of PhD Dissertation in English

The Strandja Zone is an NW-SE-trending mountain belt consisting of pre-Late Cretaceous autochthonous and allochthonous units located on the Bulgarian-Turkey border. This zone is one of the least studied areas in the Black Sea region, variously assigned as part of the Balkanides or Pontides. All neighbouring units contain remnants of the Variscan basement massifs; however, the Variscan evolution was in many places obliterated by younger tectonic events or covered by sedimentary rocks.

In the Strandja Zone, the Paleozoic and Early Mesozoic geological evolution is obscured by Late Jurassic to Early Cretaceous metamorphism and deformation called in local literature the 'Early Alpine' event. The heterogeneity of this event was a key feature in distinguishing three units of the Strandja Zone in Bulgarian territory: the Strandja, Sakar and Veleka units. The Sakar and Strandja units display many similarities. Both units contain Gondwana-derived pre-Late Carboniferous high-grade country rocks intruding by Late Carboniferous to Triassic granitoids. In the Sakar Unit, the country rocks and granitoids are covered by Permian-Triassic metasedimentary rocks metamorphosed at amphibolite-facies conditions during Early Alpine metamorphism. In contrast, only low-grade metamorphism affected the coeval sedimentary succession in the Strandja Unit.

The paleogeographic position of the Strandja Zone during the Paleozoic and Mesozoic is a topic of debate. Previous studies proposed that the Strandja Zone formed a magmatic arc 1) either from Late Devonian to Early Carboniferous together with Balkan, Sredna Gora, Sakarya and Caucasus; 2) or from Late Carboniferous to Triassic together with Rhodope Zone and Serbo-Macedonian Metamorphic Complex as the westernmost extension of the Euroasian active continental margin related to the subduction of the Paleo-Tethys Ocean. The first model was questioned by the occurrence of the Variscan shear zone between low- and high-grade metamorphic country rocks of Balkan and Sredna Gora zones, respectively, whereas the second model was challenged in this study.

This study focuses on the Sakar Unit of the Strandja Zone, dominated by Late Carboniferous to Triassic granitoids of the Sakar Batholith in the central part, the Harmanli Block Magmatic Complex in the south-western part, and the southern plutons of Izvorovo, Levka and Ustrem, previously grouped as the Lesovo Complex.

The dissertation presents new U-Pb zircon, titanite and rutile dating coupled with geochemical, petrographic and field studies. It provided 1) the first crystallization ages of the Izvorovo (ca. 251-256 Ma) and Levka (ca. 306 Ma) plutons; 2) a better constraint on the emplacement age of the Sakar Batholith (ca. 319 Ma); 3) evidence of Variscan metamorphism and deformation in the Sakar Unit (>ca. 319 Ma); 4) evidence of two stages of Early Alpine metamorphism and deformation with a Late Jurassic (ca. 154 Ma) regional phase and Early Cretaceous (ca. 125-116 Ma) localized hydrothermal activity associated with albitization, which both reached similar temperatures (~530-620°C).

The study also revealed that Late Carboniferous to Triassic magmatism in the Strandja Zone represents two groups of granitoids formed in the Late Carboniferous and Permian-Triassic. The older group is interpreted to be related to a post-collisional setting, similar to coeval magmatism in the Sredna Gora and Sakarya zones, whereas the younger group was formed probably in rift- or subduction-related settings.

The similarities of the Gondwana-derived country rocks affected by Variscan metamorphism and deformation and intruded by Late Carboniferous granitoids in the Strandja and Sredna Gora zones led to the conclusion that they share a common Paleozoic evolution. Both these zones, probably together with Serbo-Macedonian Metamorphic Complex and Sakarya Zone, were a part of the metamorphic core of the Variscan Orogen. Subsequently, the Strandja Zone was affected by Late Jurassic to Early Cretaceous metamorphism and deformation contemporarily with (ultra-) high-grade metamorphism and deformation in the Rhodope Zone. Although the events are coeval, the differences in metamorphic conditions do not allow direct connections between the Strandja and Rhodope zones in the Mesozoic.

The thesis also presents challenges in interpreting the geochemical and geochronological data, such as 1) the problem with discrimination of tectonic settings for granitoids based only on geochemical data, which is presented together with the support of zircon population characteristics and magma generation temperatures; 2) the problem with the interpretation of U-Pb geochronological zircon data spread along the Concordia, for which the proposed solution assumes partial lead loss due to a metamorphic event; 3) interpretation of highly-radiogenic initial lead composition in rutile, presented with isotopic and textural evidence of igneous titanite being a precursor.

## 1. Introduction

The final collision between Gondwana (and Gondwana-derived terranes) and Laurussia in the Late Carboniferous was the critical assembly event of the last known supercontinent, Pangea. This collision led to the formation of the Acadian-Variscan-Alleghanian Orogen exposed the West African Craton margin in Morocco and Algeria, in Western and Central Europe, and the Appalachian Mountains in northeastern North America (e.g., McCann 2008; Michard et al. 2010; Stephan et al. 2019; Franke et al. 2020). The remnants of the Variscan basement massifs, overprinted by younger tectonic events or covered by sedimentary rocks, are also known from other locations from Europe in the Alps, the Hellenides, the Carpatho-Balkanides, portions of the Pontides, and the Caucasus (Sengör et al. 1988; Haydoutov 1989; Stampfli 2000; Himmerkus et al. 2007; Gawęda and Golonka 2011; Mayringer et al. 2011; von Raumer 2013; Zulauf et al. 2014; Antić et al. 2016; Okay and Topuz, 2017; Spahić and Gaudenyu, 2018; Franke et al. 2020).

The focus of this dissertation, the Strandja Zone, is one of the least studied areas in southeastern Europe, variously assigned as either part of neighbouring Balkanides (Sredna Gora and Rhodope zones) or Pontides (Istanbul and Sakarya zones; Figure 1; e.g., Chatalov 1990; Okay et al. 2001; Sunal et al. 2006; Ustaömer et al. 2012; Aysal et al. 2018). The paleogeographic position of the Strandja Zone during the Paleozoic and Mesozoic is also unclear. Okay and Topuz (2017) were the first to note that all neighbouring units of the Balkan, Sredna Gora, Strandja and Sakarya zones (Figure 1a) consist of predominantly Gondwana-derived Late Neoproterozoic to Early Paleozoic sedimentary and igneous rocks affected by Early Carboniferous metamorphism and intruded by Late Carboniferous to Permian granitoids. These authors proposed that these zones, together with the Caucasus, formed a continental magmatic arc during the Late Devonian, which collided with Laurussia at the Early/Late Carboniferous boundary. However, a common magmatic arc for these regions is questioned by the occurrence of a Variscan shear zone between the low- and high-grade metamorphic country rocks of the Balkan and Sredna Gora zones, respectively (e.g., Haydoutov 1989; Carrigan et al. 2005; Gerdjikov et al. 2007; Balkanska et al. 2021). High-grade metamorphism and deformation of the Sredna Gora Zone took place in the Early Carboniferous (e.g., Carrigan et al. 2006; Žák et al. 2022), and coeval high-grade metamorphism also affected the Sakarya Zone (Okay 1996; Topuz et al.

2004). A Variscan metamorphic event has also been suggested from the eastern part of the Strandja Zone (e.g., Okay et al. 2001; Sunal et al. 2011), but its exact timing and conditions remain an open question.

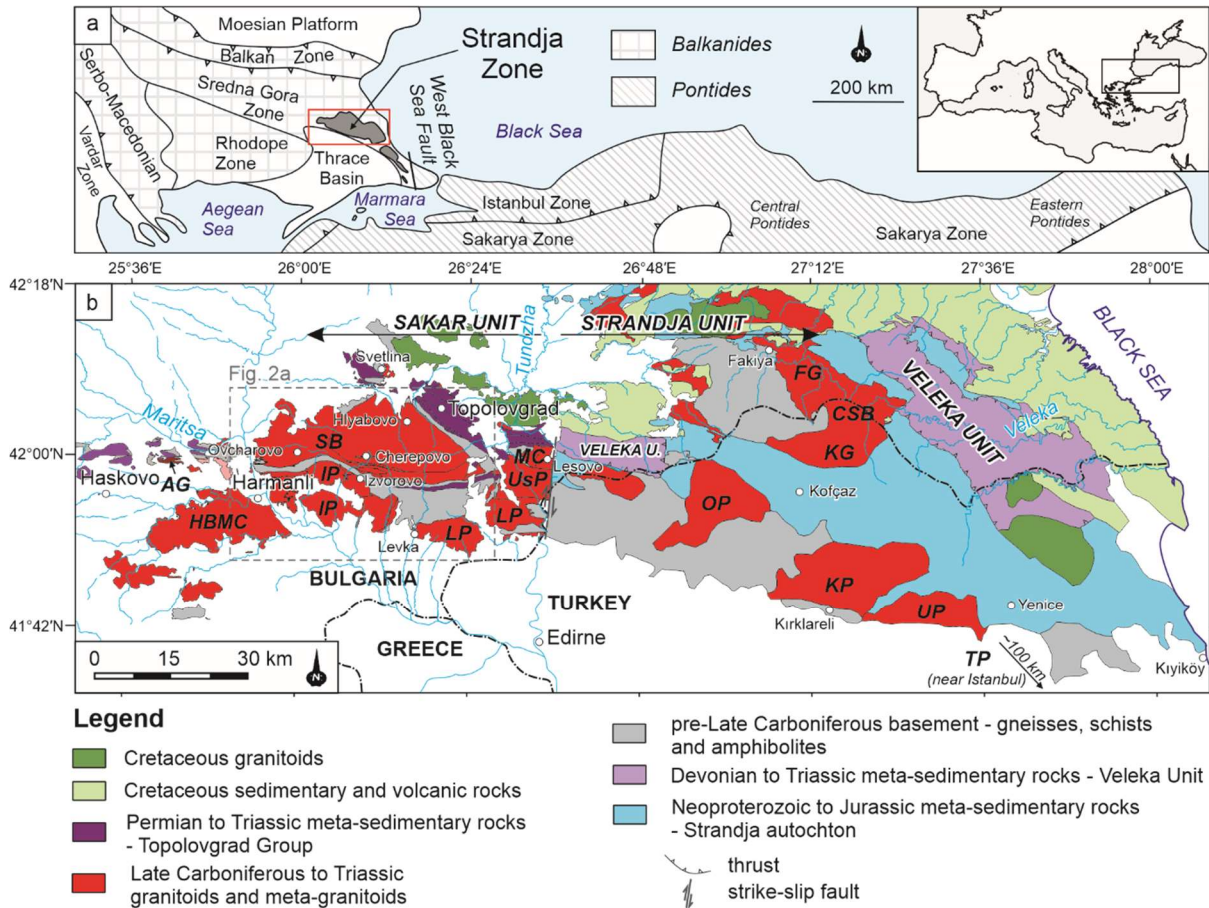


**Figure 1.** (a) Map presenting the Strandja Zone and the surrounding major tectonic units (inset); (b) Geological map of the Strandja Zone with major Late Carboniferous to Triassic plutonic bodies: AG – Aleksandrovo Granite, CSB – Central Strandja Batholith consist of FG – Fakiya granite and KG – Kula granite, HBMC – Harmanli Block Magmatic Complex, IP – Izvorovo Pluton, KP – Kırklareli Pluton, LP – Levka Pluton, MC – Melnitsa Complex, OP – Ömeroba Pluton, SB – Sakar Batholith, UP – Üsküp Pluton, UsP – Ustrem Pluton, TP – Tepecik Pluton (Sałacińska et al. 2022).

Bonev et al. (2019, 2022) also advocate a long-lived magmatic arc consisting of Strandja and Rhodope zones together with the Serbo-Macedonian Complex (Figure 1a), which occurred from the Late Carboniferous to the Triassic, and was associated with the subduction of the Paleo-Tethys Ocean beneath Laurussia. However, the westernmost known subduction-accretionary complex related to the Paleo-Tethys Ocean occurred in the Pontides (Karakaya complex, Sakarya Zone; e.g., Okay and Göncüoğlu 2004), and a similar complex has not been documented in the Strandja

Zone and other neighbouring units (Okay and Topuz 2017). The magmatic arc is suggested based on geochemical signatures of voluminous Late-Carboniferous to Triassic granitoids of the Strandja Zone reported by various authors (e.g., Georgiev et al. 2012; Machev et al. 2015; Peytcheva et al. 2016; Natal'in et al. 2016; Aysal et al. 2018; Pristavova et al. 2019; Bonev et al. 2019, 2022; Akgündüz et al. 2021). Some authors suggested that Late-Carboniferous to Early Permian granitoids of the Strandja Zone can be late- or post-collisional (e.g., Okay et al. 2001; Kamenov et al. 2010; Peytcheva et al. 2016).

Extensive Late Carboniferous to Triassic magmatism is also known from neighbouring areas, such as the Sredna Gora and Balkan zones of the Balkanides (e.g., Kamenov 2002; Malinov et al. 2004; Peytcheva et al. 2006, 2018; Carrigan et al. 2005; Nedialkov et al. 2007; Antonov et al. 2010; Dyulgerov et al. 2018; Georgiev et al. 2020; Balkanska et al. 2021) and often is interpreted as post-tectonic and related to the last stages of the Variscan orogeny (e.g. Haydoutov and Yanev 1997; Carrigan et al. 2005; Balkanska et al. 2021). In the Sakarya Zone of Pontides, the Early Carboniferous granitoids and associated extrusive rocks predominate Late Carboniferous to Early Permian intrusions and are interpreted as syn- and post-tectonic, respectively (Topuz et al. 2010; Ustaömer et al. 2012, 2013; Karslı et al. 2016; Dokuz et al. 2017; Şengün and Korlay 2017; Okay and Topuz 2017; Şengün et al. 2020).

In contrast to the Sredna Gora and Balkan zones, the Strandja Zone was affected by a Late Jurassic to Early Cretaceous upper greenschist- to amphibolite-facies metamorphism. This metamorphism is known in the local literature as the Early Alpine or Cimmerian event (Şengör et al. 1984; Ivanov et al. 2001; Gerdjikov 2005; Cattò et al. 2018; Szopa et al. 2020; Bonev et al. 2020) and is interpreted as either a single event (Sunal et al. 2011; Bonev et al. 2020) or two discrete thermal events (Szopa et al. 2020) from which one is probably related to local albitization of the northwestern part of the Strandja Zone (e.g., Pristavova et al. 2019; Szopa et al. 2020). A coeval metamorphic event is well documented in the Rhodope Zone (Figure 1a), where it reached (ultra-) high-grade metamorphic conditions (e.g., Burg 2012; Gautier et al. 2017) and both the Strandja and Rhodope zones are considered to have a common evolution at this time (e.g., Bonev et al. 2020).

## **2. Aim of the PhD Dissertation**

This PhD dissertation aims to unravel the Late Paleozoic and Mesozoic magmatic and metamorphic evolution of the Strandja Zone (SE Bulgaria/NW Turkey). The voluminous Late Carboniferous to Triassic granitoids of the Sakar Unit (western part of the Strandja Zone; Figure 1b) were selected to be a major subject of the study, which allows to answer the research problems presented in the introduction. The fundamental questions concern Late Carboniferous to Triassic magmatism: 1) are there any differences between granitoids of various ages; 2) were they formed in the same tectonic setting; 3) is there any evidence apart from geochemical signature for prolonged magmatic arc magmatism or were the granitoids formed in more than one magmatic episode? These granitoids were variously deformed and metamorphosed during Late Jurassic to Early Cretaceous. The research was also conducted to test if there are any unaffected granitoids and where they occur. The least deformed and metamorphosed portions of the Late Carboniferous plutons containing country rock xenoliths were used to answer the question about the possible influence of pre-Late Carboniferous high-grade metamorphism in the Strandja Zone. The albitized granitoids and associated rocks of the northwestern Sakar Unit were selected to estimate the timing and conditions of the albitization and its connections with Late Jurassic to Early Cretaceous metamorphism. These complex studies of Late Carboniferous to Triassic granitoids were also conducted to better correlate the Sakar and Strandja units of the Strandja Zone (Figure 1b), as well as the Strandja Zone and surrounding regions (Figure 1a) during Paleozoic and Mesozoic, which helps with understanding the evolution of the southeastern part of Europe.

## **3. Study area**

The Strandja (or Strandzha, Sakar-Strandja, Sakar-Strandzha) Zone, also called Strandja (or Strandzha, Istranca) Massif (e.g., Boyadijev and Lilov 1972; Okay et al. 2001; Gerdjikov 2005; Bedi et al. 2013; Natal'in et al. 2016; Bonev et al. 2019), is a northwest-southeast-trending mountain belt located in southeastern Bulgaria and northwestern Turkey (Figure 1). To the north, the Strandja Zone is covered by volcano-sedimentary rocks of the Sredna Gora Zone, related to the Late Cretaceous Apuseni-Banat-Timok-Sredna Gora magmatic arc (e.g., Chatalov 1990; Gallhofer et al. 2015). In the west, the relationship between Strandja and Rhodope zones is poorly



understood because most of their contact is covered by sedimentary rocks. To the south, the Strandja Zone is covered by Cenozoic sedimentary rocks of the Thrace Basin. The West Black Sea fault separates the Strandja and Istanbul zones (Figure 1a).

The Strandja Zone comprises pre-Late Cretaceous autochthonous and allochthonous units (e.g., Boyadijev and Lilov 1972; Okay et al. 2001; Bedi et al. 2013; Natal'in et al. 2016; Ivanov 2017; Aysal et al. 2018) affected in various degrees by upper greenschist- to amphibolite-facies Late Jurassic to Early Cretaceous metamorphism and deformation (e.g., Ivanov et al. 2001; Okay et al. 2001; Gerdjikov 2005; Natal'in et al. 2016; Aysal et al. 2018; Cattò et al. 2018; Vladinova et al. 2019; Szopa et al. 2020; Bonev et al. 2020, 2022). Additionally, at least parts of the units were also affected by Variscan high-grade metamorphism (e.g., Okay et al. 2001). There is no unified division of units of the Strandja Zone because of the lack of comprehensive, joint research in both Bulgaria and Turkey. Three units are distinguished in the Bulgarian part of the Strandja Zone: Sakar, Strandja and Veleka (Figure 1b; Chatalov 1990; Gerdjikov 2005). Both Sakar and Strandja units consist of pre-Late Carboniferous high-grade country rocks of para- and orthogneisses, garnet two-mica schists, amphibolites, meta-gabbros and migmatites (Şahin et al. 2014; Natal'in et al. 2016). The protoliths of the country rocks include Neoproterozoic-Cambrian and Ordovician felsic magmatic rocks (Şahin et al. 2014; Natal'in et al. 2016; Bonev et al. 2019) and sedimentary rocks with a Cambrian maximum depositional age (Vladinova et al. 2018; Vladinova and Georgieva 2020). They are considered as a part of the terrane(s) formed along the northern margin of Gondwana (e.g., Stampfli 2000; Okay and Topuz 2017). The country rocks were intruded by Late Carboniferous to Triassic intermediate to felsic magmatic rocks, which form significant parts of the Strandja Zone (Figure 1b; e.g., Okay et al. 2001; Natal'in et al. 2016; Bonev et al. 2019, 2022). One main distinction between the Sakar and Strandja units is the metamorphic grade affecting the Permian to Triassic meta-sedimentary rock cover, with the Topolovgrad Group in the Sakar Unit (Figure 1b) being metamorphosed to amphibolite facies with lower-grade coeval rocks in the Strandja Unit (Chatalov 1990).

The Sakar Unit in Bulgaria is the study area of the three publications included in the dissertation (Figure 2). The predominant component of the Sakar Unit are Late Carboniferous to Triassic intermediate to felsic magmatic rocks, which intruded the

high-grade metamorphic country rocks and both, together with their metasedimentary cover of Topolovgrad Group, were variously affected by Late Jurassic to Early Cretaceous metamorphism and deformation (e.g., Kamenov et al. 2010; Bonev et al. 2019, 2022). The largest coherent magmatic body of the Sakar Unit is the Late Carboniferous to Early Permian Sakar Batholith (ca. 305-295 Ma; Kamenov et al. 2010; Peytcheva et al. 2016; Bonev et al. 2019; Pristavova et al. 2019), which is separated from the southern plutons by a belt of country rocks (Figure 2). The southern plutons are deformed and metamorphosed and have been a subject of debate as initially they were grouped as the Lesovo Magmatic Complex (Boyanov et al. 1965; Kozhoukharova and Kozhoukharov 1973) from which Chatalov (1992) distinguished the Late Paleozoic volcanic-plutonic Melnitsa Complex (dated at ca. 300-297 Ma by Bonev et al. 2019), and Ivanov et al. (2001) separated the Ustrem, Levka and Izvorovo plutons within the complex (Figure 2). The contact between the Ustrem and Levka plutons does not crop out (Figure 2); therefore, it is uncertain whether it represents one single or two separate magmatic body/ies. However, Bonev et al. (2019) used the initial classification, leading them to conclude a Late Carboniferous age of the entire Lesovo Complex based on U-Pb zircon dating of a sample from the Ustrem Pluton (ca. 306 Ma). To the west of the Izvorovo Pluton, the ca. 243-241 Ma Harmanli Block Magmatic Complex occurs (Bonev et al. 2022), but the contact with the Izvorovo Pluton is covered by Cenozoic sedimentary rocks (Figure 2). The lithological similarities of the metamorphosed and deformed granites in these magmatic bodies led Jordanov et al. (2008) to suggest that the Harmanli Block Magmatic Complex and Izvorovo Pluton could be the largest magmatic body in the Sakar Unit.

More information about Late Carboniferous to Triassic intermediate to felsic magmatic rocks, pre-Late Carboniferous and Late Jurassic to Early Cretaceous metamorphism are presented in the publications included in the dissertation: the Izvorovo Pluton (article 1), possible correlation of the Izvorovo Pluton and the Harmanli Block Magmatic Complex (article 2), the Sakar Batholith (article 2 and 3), the Levka Pluton and possible correlation with the Ustrem Pluton (article 2), pre-Late Carboniferous metamorphism (article 2), and finally Late Jurassic to Early Cretaceous metamorphism and albitization (article 3). These three articles also include a detailed comparison of geochemical and geochronological data from the Sakar and Strandja units.

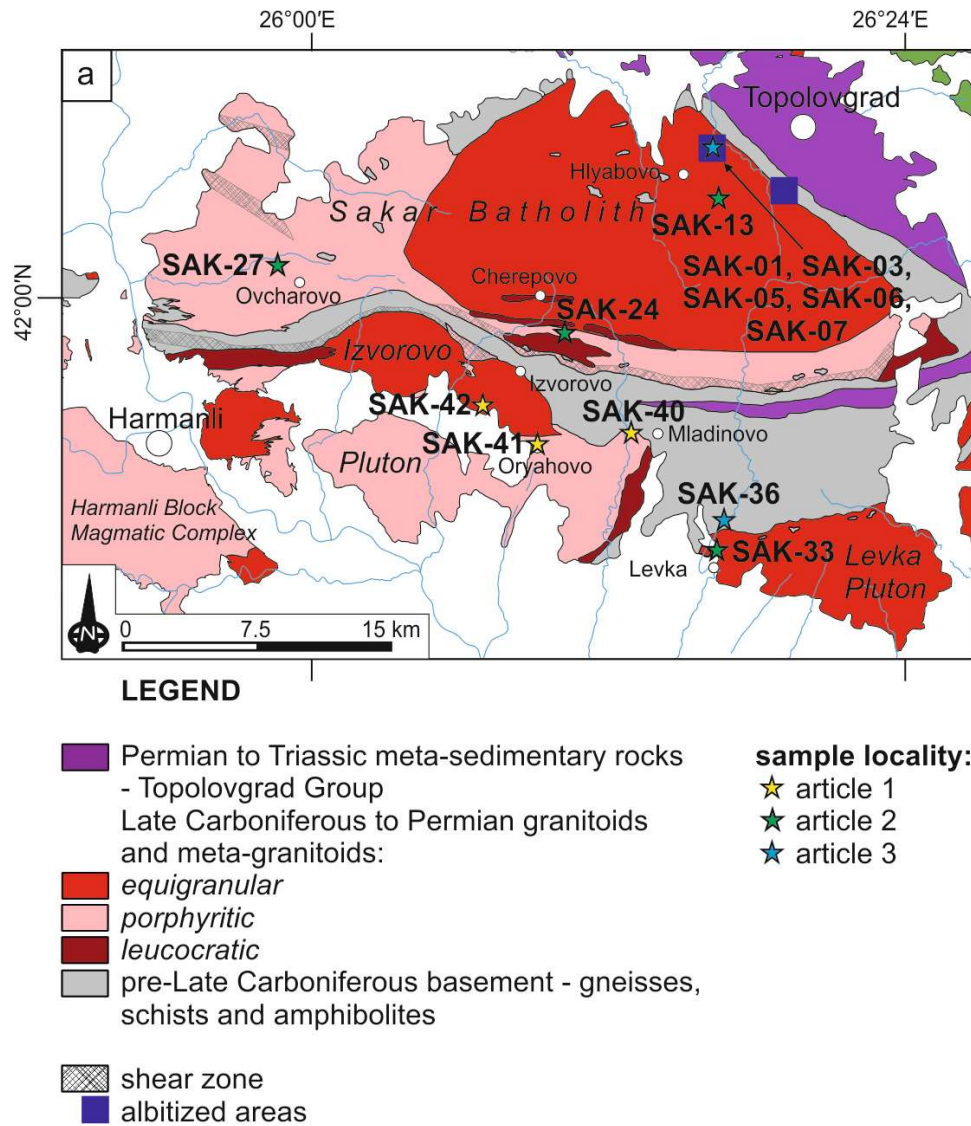


**Figure 2.** Geological map of the Sakar Unit with sample localities marked (modified after Gerdjikov 2005; Sałacińska et al. 2021, 2022; Gumsley et al. 2023).

#### 4. Methodology

In total, seventy-two rock samples from various lithological units were collected during two fieldtrips in the Sakar Unit of the Strandja Zone (southeast Bulgaria). It includes granitoids of the Sakar Batholith, Izvorovo Pluton, Levka Pluton, Harmanli Block Magmatic Complex and their country rocks (i.e., orthogneiss, paragneiss, amphibolite and migmatite; Figure 2). Rock samples for further analysis were selected based on field and petrographic observations. From the collected results, thirteen rock samples of granitoids and metagranitoids and associated rocks were used in the three publications (Table 1; Figure 2). The remaining data obtained during the project are unpublished.

**Table 1.** Location of rock samples selected for the publications (see Figure 1).

Sample	Lithology	Locality	Latitude	Longitude
<b>Article 1 - Two stages of Late Carboniferous to Triassic magmatism in the Strandja Zone of Bulgaria and Turkey</b>				
<b>SAK-40</b>	orthogneiss with feldspar porphyroclasts	Izvorovo Pluton, W Mladinovo	41°56'11.7"N	26°13'05.8"E
<b>SAK-41</b>	augen gneiss	Izvorovo Pluton, Oryahovo	41°55'34.4"N	26°09'35.7"E
<b>SAK-42</b>	metagranite	Izvorovo Pluton, SW Izvorovo	41°56'59.9"N	26°07'13.7"E
<b>Article 2 - Variscan magmatic evolution of the Strandja Zone (Southeast Bulgaria and Northwest Turkey) and its relationship to other North Gondwanan margin terranes.</b>				
<b>SAK-13</b>	porphyritic monzogranite	Sakar Batholith, SE Hlyabovo	42°02'59.0"N	26°16'11.0"E
<b>SAK-24</b>	porphyritic monzogranite	Sakar Batholith, SE Cherepovo	41°59'03.4"N	26°10'16.1"E
<b>SAK-27</b>	porphyritic monzogranite	Sakar Batholith, NW Ovcharovo	42°01'09.1"N	25°59'05.2"E
<b>SAK-33</b>	granodiorite	Levka Pluton, in Levka	41°52'44.9"N	26°16'21.2"E
<b>Article 3 -</b>				
<b>SAK-01</b>	melanocratic metadiorite	NE margin of Sakar Batholith, Kanarata quarry, NE Hlyabovo	42°05'00.0"N	26°16'24.0"E
<b>SAK-03</b>	metadiorite with an amphibolite xenolith (contact zone)			
<b>SAK-05</b>	leucocratic metadiorite			
<b>SAK-06</b>	granodiorite			
<b>SAK-07</b>	amphibolite xenolith			
<b>SAK-36</b>	orthogneiss cut by a quartz vein	country rock, N Levka	41°53'31.3"N	26°17'0.1"E

The research methods are summarised in table 2. For more details, the reader is referred to the methodology sections in the publications.

**Table 2.** Summary of research methods used in the PhD dissertation

Method/Apparatus	Aim/task	Laboratory
crushing, sieving, milling, panning and density separation of heavy minerals, preparation of epoxy mounts	Preparation of rock samples for further analyses	Sample Preparation Laboratory, Institute of Geological Sciences, Polish Academy of Sciences, Kraków, Poland.
Olympus BX-51 optical polarising microscope	Petrographic observation of thin sections, Imaging of accessory minerals in epoxy mounts.	Institute of Earth Sciences, Faculty of Natural Sciences, University of Silesia in Katowice, Poland
ThermoFisher Scientific Phenom XL Scanning Electron Microscope (SEM) with back-scattered electron (BSE) detector coupled to an energy-dispersive spectrometer (EDS)	Petrographic observation of thin section and imaging of accessory minerals in epoxy mount	

FET Phillips 30 SEM Scanning Electron Microscope (SEM) with cathodoluminescence (CL)	Zircon imaging	
Electron Microprobe: 1) Cameca SX100 2) Cameca SXFiveFE	Chemical composition of the rock-forming and accessory minerals	Laboratory of Electron Microscopy, Microanalysis and X-Ray Diffraction, Faculty of Geology, University of Warsaw, Poland
Photon Machines Analyte Excite 193 nm ArF excimer laser-ablation system with a HelEx 2-volume ablation cell, coupled to an Agilent 7900 mass spectrometer	U-Pb zircon, rutile, titanite dating, trace element composition of titanite	Department of Geology, Trinity College Dublin, Ireland
X-ray fluorescence (XRF) spectrometry and inductively coupled plasma-mass spectrometry (ICP-MS)	Whole-rock geochemical analyses (major and trace elements)	Bureau Veritas Analytical Laboratories in Vancouver, Canada

## 5. Summary of the articles included in the PhD Dissertation

### 5.1. Two stages of Late Carboniferous to Triassic magmatism in the Strandja Zone of Bulgaria and Turkey

**Salacińska, A., Gerdjikov, I., Gumsley, A., Szopa, K., Chew, D., Gawęda, A., Kocjan, I. (2021).** *Two stages of Late Carboniferous to Triassic magmatism in the Strandja Zone of Bulgaria and Turkey. Geological Magazine, 158: 2151–2164.*  
<https://doi.org/10.1017/S0016756821000650>

The article presents new insights into Late-Carboniferous to Triassic magmatism of the Strandja Zone and tests the hypothesis of a long-lived magmatic arc, which occurred from the Late Carboniferous to the Triassic, and was associated with subduction of the Paleo-Tethys Ocean beneath Laurussia (Bonev et al. 2019, 2022).

The new data presented in this study include U-Pb zircon ages, coupled with petrography and geochemistry from the Izvorovo Pluton (Sakar Unit, Strandja Zone). The Izvorovo Pluton contains variably metamorphosed and deformed granites that yield crystallization ages of ca. 251-256 Ma. It was the first geochronological and geochemical study of this pluton and showed the genetic relationship between the Izvorovo Pluton and Late Jurassic to Early Cretaceous metamorphism suggested by Ivanov et al. (2001) and Gerdjikov (2005) was incorrect.

Compilation of geochronological data from Late Carboniferous to Triassic granitoids of the Strandja Zone allowed assigning granitoids to two groups of 1) Late Carboniferous and 1) Permian to Triassic magmatism with approximately 20 Myr of quiescence between them (Figura 3). However, geochemical data do not suggest any direct differences between these two groups of granitoids, plotting them within the post-collisional granite (post-COLG) field, which overlaps with the volcanic-arc granite (VAG) field on the Rb vs Y+Nb diagram (Pearce, 1996, after Pearce et al. 1984). However, it led Bonev et al. (2019, 2022) to interpret these two groups as related to a long-lived magmatic arc.

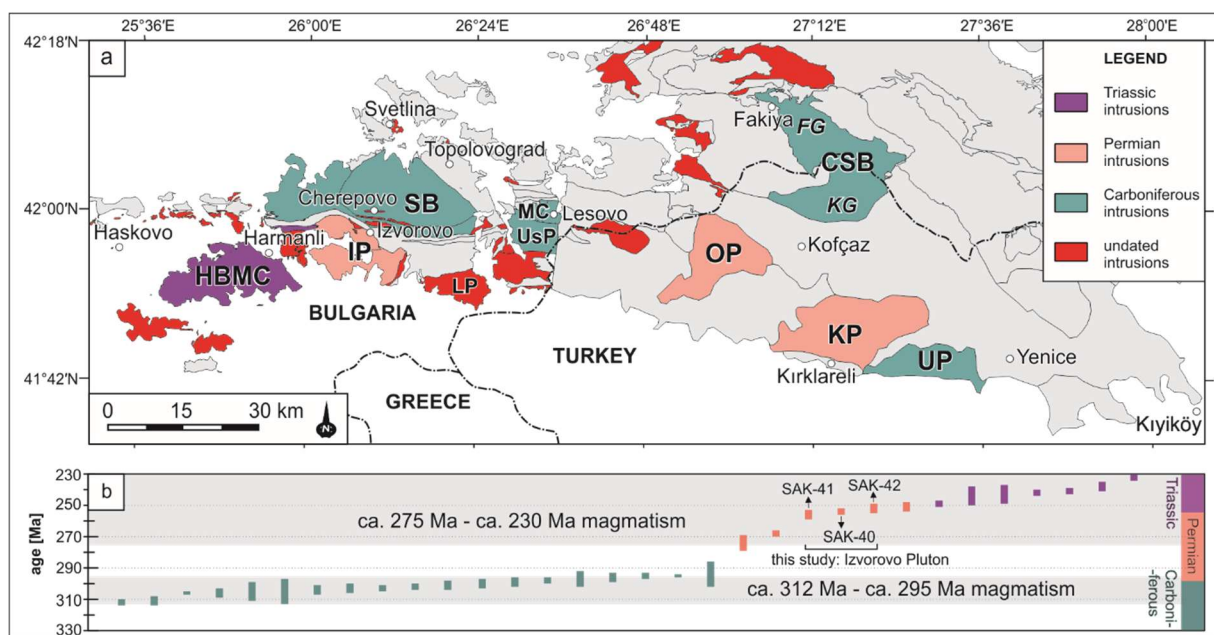


**Figure 3.** Spatial and temporal distribution of the Late Carboniferous to Triassic magmatic rocks in the Strandja Zone: (a) geological map classifying plutonic bodies according to their age of emplacement (HBMC – Harmanli Block Magmatic Complex, IP – Izvorovo Pluton, SB – Sakar Batholith, LP – Levka Pluton, MC – Melnitsa Complex, UsP – Ustrem Pluton, OP – Ömeroba Pluton, KP – Kırklareli Pluton, UP – Üsküp Pluton, CSB – Central Strandja Batholith consist of FG – Fakiya granite and KG – Kula granite); (b) Summary of U-Pb zircon age determinations from all dated plutonic bodies within the Strandja Zone (Sałacińska et al. 2021).

The only noticeable difference between the two groups is the characteristics of the zircon populations with significant amounts of antecrysts and xenocrysts in the Late Carboniferous granitoids (i.e., inheritance-rich) and inheritance-poor populations of Permian to Triassic granitoids. When coupled with the calculation of zircon saturation temperatures ( $T_{Zr}$ ) from bulk-rock compositions (after Watson and Harrison, 1983) it

can estimate temperatures that the magma solidified at. Although the differences between  $T_{Zr}$  are insignificant, with  $<775^{\circ}\text{C}$  for the inheritance-rich Late Carboniferous granitoids and  $\geq 800^{\circ}\text{C}$  for most of the Permian-Triassic inheritance-poor intrusions, the characteristics of the zircon populations implies significant changes in interpretation. According to Miller et al. (2003), inherited zircons in the granitoids indicate that the source was zircon saturated and Zr was present mainly in crystals rather than melt, and  $T_{Zr}$  provides the upper limit on magma temperature. The inheritance-poor zircon populations indicate that the source was undersaturated, and the  $T_{Zr}$  calculated for such granitoids implies a minimum initial magma temperature (Miller et al. 2003). Therefore, 'hotter' Permian to Triassic granitoids with minimum magma temperature of  $\geq 800^{\circ}\text{C}$  are interpreted according to currently accepted modes of felsic magma generation (i.e., dehydration melting in the crust; fractionation of mantle melts, with or without crustal contamination) and without incorporation of inherited components during transport. Late Carboniferous 'colder' granitoids with maximum magma temperatures of  $<775^{\circ}\text{C}$  required a water source to lower the melt temperature. The most visible mechanism for large-scale melting at temperatures  $<800^{\circ}\text{C}$  is infiltration of a water-rich fluid phase (Miller et al. 2003). It implies a possible change in the tectonic setting across the Carboniferous-Permian boundary.

Therefore, it was proposed that Late Carboniferous to Triassic magmatism represents two stages, with older Late Carboniferous granitoids likely correlated with post-collisional magmatism of the Balkanides, similar to the suggestion of Peytcheva et al. (2016). Permian to Triassic granitoids come from either subduction-related magmatism which is consistent with Bonev et al. (2019) or a rift-related setting, similar to the interpretation for the Western Pontides (Okay and Nikishin, 2015). It is also possible that there was a transition from a Permian arc setting to a Middle Permian to Early Triassic back-arc setting, as proposed by Aysal et al. (2018). A rift-related environment may facilitate the high-temperature conditions required for magma generation (Miller et al. 2003) and therefore is more likely.



## 5.2. Variscan magmatic evolution of the Strandja Zone (Southeast Bulgaria and Northwest Turkey) and its relationship to other North Gondwanan margin terranes

**Salacińska, A.,** Gerdjikov, I., Kounov, A., Chew, D., Szopa, K., Gumsley, A., Kocjan, I., Marciniak-Maliszewska, B., Drakou, F. (2022). *Variscan magmatic evolution of the Strandja Zone (Southeast Bulgaria and Northwest Turkey) and its relationship to other North Gondwanan margin terranes. Gondwana Research, 109: 253–273.*  
<https://doi.org/10.1016/j.gr.2022.04.013>

This article focuses on the Variscan magmatic evolution of the Strandja Zone and its similarities to surrounding regions. As presented in the previous article, the Late Carboniferous granitoids from the Strandja Zone are considered to be post-collisional.

The new data presented in this study include U-Pb zircon ages coupled with field, petrographic and geochemical studies of various granitoids from the Sakar Batholith and Levka Pluton. The crystallization age of the ca. 319 Ma Levka Pluton placed this intrusion as the oldest known Late Carboniferous granitoid in the Strandja Zone. The ages obtained from various samples from the Sakar Batholith range between ca. 306-301 Ma and demand a re-evaluation of previously published crystallization ages from this intrusion and other granitoids from the Sakar Unit. Previously published ages of the Sakar Batholith scatter between ca. 305 Ma and ca. 295 Ma, with the oldest age of ca. 305 Ma measured by ID-TIMS (Peytcheva et al. 2016) and younger ca. 298 Ma (Pristavova et al. 2019) and ca. 296-295 (Bonev et al. 2019) ages obtained from LA-ICP-MS. The younger ages of both authors were calculated based on a few of the youngest analyses interpreted as coming from autocrystic zircons, whereas older analyses were excluded from the calculations because they were assumed to represent antecrystic zircons. As interpreted in this study, zircons have thin rims (~5 to ~10 µm in width), and other minerals show recrystallization features. Therefore, Late Jurassic to Early Cretaceous deformation and metamorphism affected the granitoids to various degrees; however, the published literature does not consider this influence. Assuming that Late Jurassic to Early Cretaceous metamorphism caused at least a partial Pb loss in zircons, the effect may not be visible as discordant data (Figure 4). Such spread along the Concordia data is often reported from magmatic rocks which have experienced complex Pb loss during



a subsequent metamorphic event (e.g., Ashwal et al., 1999; Halpin et al., 2007, 2005; Bomparola et al., 2007). Therefore, the interpreted division of data for auto- and antecrysts based only on ages is insufficient; the ‘young age’ represents a minimum crystallization age, and such scatter of ages along Concordia should be presented as an age range when the data do not provide statistically significant results when considering mean squared weighted deviation (MSWD). Assuming such an interpretation, the crystallization age of the Sakar Batholith is closest to ca. 306 Ma in this study, which is within analytical uncertainties of the ca. 305 Ma ID-TIMS zircon age (Peytcheva et al. 2016). Following the above assumptions, the ca. 306 Ma age of the Ustrem Pluton (Bonev et al. 2019) was also recalculated. Taking all 36 concordant data for calculation from the Ustrem rock sample of Bonev et al. (2019), spreading between ca. 327 and ca. 303 Ma, a weighted mean  $^{206}\text{Pb}$ - $^{238}\text{U}$  age of  $315 \pm 2$  Ma (MSWD = 2.3) was obtained, which is within analytical uncertainties of the ca. 319 Ma age of the Levka Pluton from this study. It suggests that probably these two plutons form one continuous magmatic body, as was assumed by Boyanov et al. (1965) and Kozhoukharova and Kozhoukharov (1973).

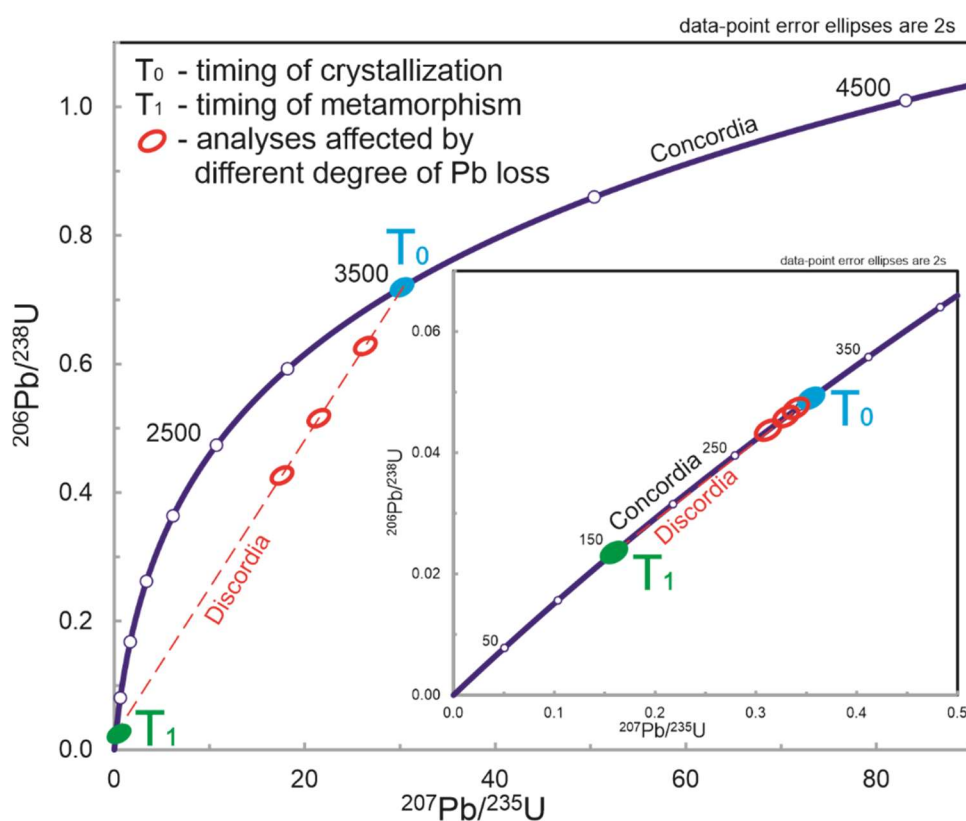


**Figure 4.** ‘Wetherill concordia diagram showing analyses affected by different degrees of Pb loss. In some cases, analyses which are affected by Pb loss can appear to be concordant.

The strongly deformed and metamorphosed xenoliths of the country rocks within almost undeformed parts of the ca. 306 Ma Sakar Batholith are evidence of high-grade Variscan metamorphism and deformation affecting the Sakar Unit (Figure 5). Xenoliths of the country rocks are common within marginal parts of ca. 319 Ma Levka Pluton, which provides an upper age limit for the timing of Variscan metamorphism. Unfortunately, their pre-Late Carboniferous features are often obscured by Late Jurassic to Early Cretaceous deformation and metamorphism.



**Figure 5.** Field photographs of xenoliths from deformed and metamorphosed country rocks in the Sakar Batholith, Kanarata Quarry, north of Hlyabovo (location: 26°16'28,00"E; 42°5'2,00"N; modified after Sałacińska et al. 2022).

The article also presents an extended comparison of Variscan magmatism in the Strandja Zone and surrounding areas. When coupled with evidence of pre-Late Carboniferous high-grade metamorphism in the Strandja Zone, it concluded that the Late Carboniferous to Early Permian magmatic evolution of the Strandja Zone shows a strong resemblance to that of the Sredna Gora Zone (Figure 6). The Strandja and Sredna Gora zones, probably together with the Serbo-Macedonian Metamorphic Complex and Sakarya Zone, were part of the metamorphic core of the Variscan Orogen.

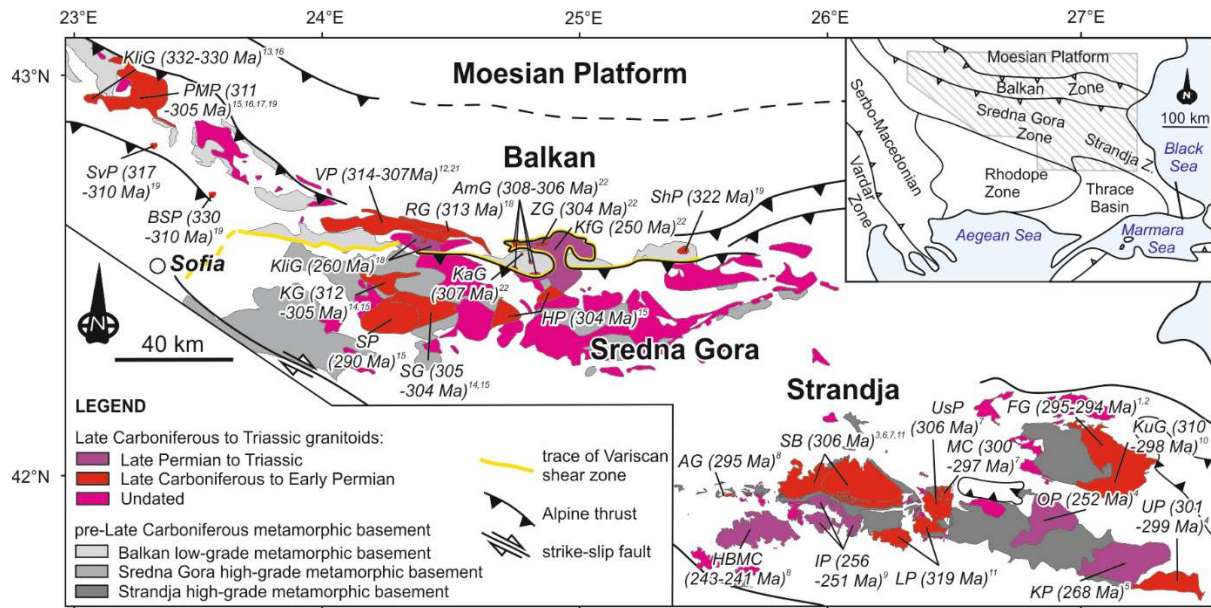


**Figure 6.** Summary geological map of the Late Carboniferous to Triassic granitoids and its basement rocks in the Strandja, Sredna Gora and Balkan zones. The reader is referred to Sałacińska et al. (2022) for abbreviations and references.

### 5.3. An Early Cretaceous thermal event in the Sakar Unit (Strandja Zone, SE Bulgaria/NW Turkey) revealed based on U-Pb rutile geochronology and Zr-in-rutile thermometry

**Gumsley, A., Szopa, K., Chew, D., Gerdjikov, I., Jokubauskas, P., Marciniak-Maliszewska, B., Drakou, F. (2023).** *An Early Cretaceous thermal event in the Sakar Unit (Strandja Zone, SE Bulgaria/NW Turkey) revealed based on U-Pb rutile geochronology.* *Lithos* 448-449, 1-17. <https://doi.org/10.1016/j.lithos.2023.107186>

This article focuses on albitization caused by post-magmatic hydrothermal fluids of external origin affecting the northern part of the Sakar Unit and its connections with Late Jurassic to Early Cretaceous upper greenschist- to amphibolite-facies metamorphism. Contemporaneous metamorphism occurred in the Rhodope Metamorphic Complex, which has led to many authors to correlate both zones (e.g., Bonev et al. 2020).

The new data in the article include U-Pb zircon, titanite and rutile dating, electron microprobe analyses of various minerals, especially rutile, used for Zr-in-rutile thermometry, coupled with field, petrographic and geochemical studies of various rocks affected by albitization. For comparison, country-rock orthogneiss unaffected by

albitization but affected by Late Jurassic to Early Cretaceous metamorphism was also analyzed.

U-Pb zircon and titanite dating were conducted to confirm a Late Carboniferous crystallization age for various granitoids forming the Sakar Batholith. U-Pb rutile dating of albitized metagranitoids yields Early Cretaceous ages (ca. 125-116 Ma; Figure 7a,b), similar to the U-Pb titanite age of ca. 114 Ma from hydrothermal veins from the same locality of the northern part of the Sakar Unit studied by Szopa et al. (2020). U-Pb rutile dating of an orthogneiss (ca. 154 Ma) unaffected by albitization, confirms Late Jurassic amphibolite-facies conditions occurred in the Strandja Zone (e.g., Tzankova and Pristavova 2007; Chavdarova and Machev 2017; Vladinova et al. 2019; Bonev et al. 2020).

Geochemical and petrological studies indicate that albitization was coupled with the removal of quartz and the growth of rutile-rich aggregates replacing titanite (Figure 7c,d), which is supported by isotopic and textural evidence. The  $^{207}\text{Pb}/^{206}\text{Pb}$  initial ratios for rutiles from samples of metadiorites (SAK-01 and SAK-05) are much lower ( $0.126 \pm 0.016$  and  $0.101 \pm 0.013$ , respectively; Figure 7a,b) than the values estimated through the terrestrial Pb-evolution model by Stacey and Kramers (1975). According to this model, ratios should be between 0.844 and 0.843 for an age of ca. 125-116 Ma. This indicates that the local geochemical reservoir in which rutile grew was enriched in radiogenic Pb isotopes, possibly by the breakdown of U-rich minerals (e.g., Romer 2001). As Late Carboniferous titanite from the unalbitized part of granodiorite (SAK-06) from the same quarry is a potential precursor (Figure 7e), the initial lead isotopic composition of the rutile was compared with the mean lead composition of the titanite (a weighted mean  $^{207}\text{Pb}/^{206}\text{Pb}$  ratio of  $0.1057 \pm 0.0066$ ). The similarities in the ratios for titanite and rutile (see also data-point ellipse 'avTtn' Figure 7a) are evidence that the initial lead composition in rutile was inherited from igneous titanite. It suggests that rutile-rich aggregates in albitized metadiorites (samples SAK-01 and SAK-05) are pseudomorphs after the Early Alpine breakdown of Late Carboniferous titanite, which also confirms the textural evidence of similar shape of aggregates to titanite (Figure 7c-e).



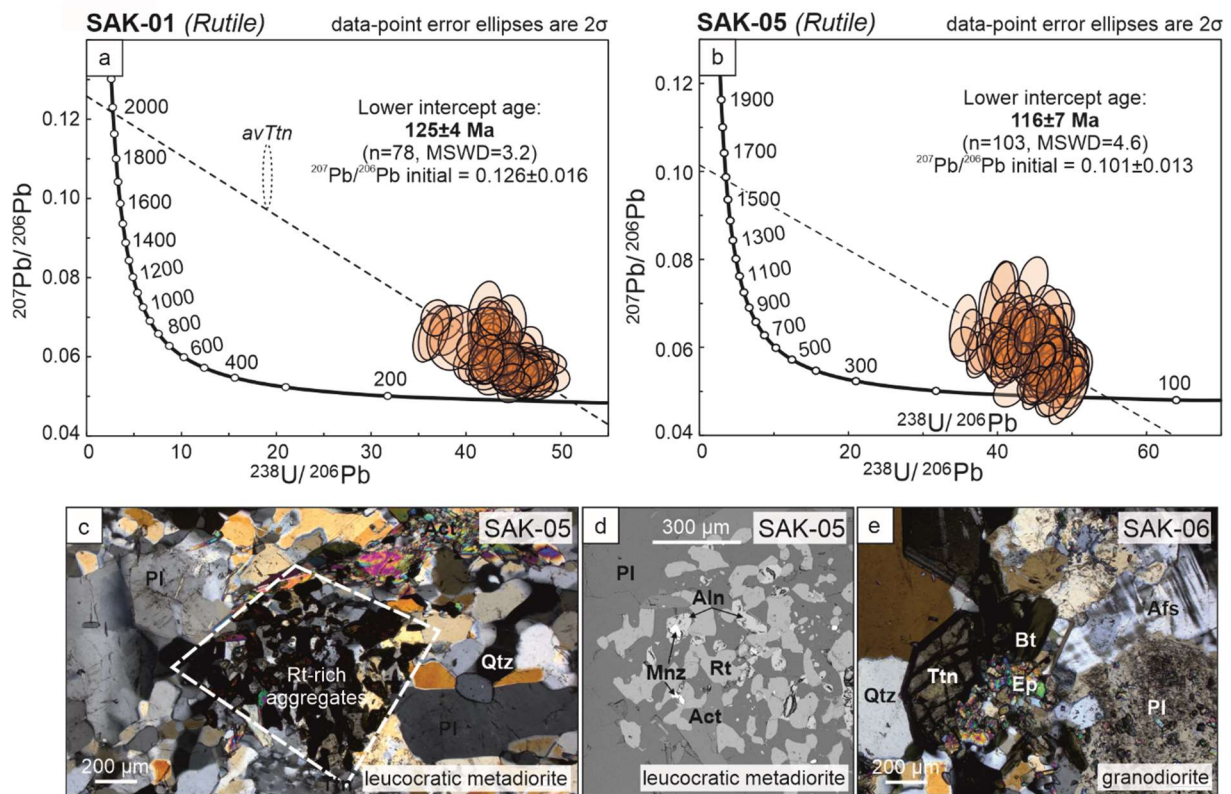


**Figure 7.** LA-ICP-MS rutile U-Th-Pb analyses presented on Tera-Wasserburg Concordia diagrams for samples of metadiorites (a-b); and petrographic images of the rutile-rich aggregates and igneous titanite in rock samples from the Kanarata quarry (north part of the Sakar Batholith) (c-e). Data (a) for melanocratic metadiorite SAK-01; (b) for leucocratic metadiorite SAK-05; the data shown as filled ellipses are used for age calculations. An average titanite data-point ellipse 'AvTtn' was constructed from a weighted mean  $^{207}\text{Pb}/^{206}\text{Pb}$  ratio of  $0.1057 \pm 0.0066$ , coupled with a weighted mean  $^{238}\text{U}/^{206}\text{Pb}$  ratio of  $19.09 \pm 0.38$  of the titanite. (c) Rutile-rich aggregates and primary quartz with undulose extinction (SAK-05); (d) BSE image of rutile, allanite and monazite aggregates (SAK-05); (e) thin section in XPL showing K-feldspar with tartan twinning characteristic of microcline, sericitized plagioclase and euhedral crystals of titanite surrounded by epidote (SAK-06); Abbreviations in the pictures: Act, actinolite; Afs, alkali feldspar; Aln, allanite; Bt, biotite; Ep, epidote; Mnz, monazite; Pl, plagioclase; Rt, rutile; Ttn, titanite; Qz, quartz (modified after Gumsley et al. 2023).

Zr-in-rutile thermometry yields similar crystallization temperatures ( $\sim 530\text{--}620^\circ\text{C}$ ) for the albitized Sakar granitoids and country rock orthogneiss. The results indicate that some parts of the Sakar Unit were affected by two thermal events in the Late Jurassic and Early Cretaceous. However, the younger thermal event did not lead to the formation of a penetrative new fabric.

It is worth noticing that there is no evidence of a high-grade metamorphic event in the Strandja Zone, similar to that documented in the Rhodope Metamorphic

Complex, which reached (ultra-) high-pressure granulite-facies conditions in the Late Jurassic to Early Cretaceous (e.g., Liati, 2005; Bauer et al., 2007; Liati et al., 2016; Moulas et al., 2017). Furthermore, the Rhodope Zone was affected by polycyclic amphibolite-facies Alpine metamorphism in the Late Cretaceous and the Cenozoic (see summary in Burg 2012, Gautier et al., 2017). Therefore, the relationships between Strandja and Rhodope zones during the Mesozoic are still unclear.

## **6. Conclusions**

The articles included in the PhD dissertation present the complex evolution of the Strandja Zone during the Late Paleozoic to Mesozoic. Detailed studies of the Late Carboniferous to Triassic granitoids, including U-Pb zircon dating coupled with the characteristic of zircon populations and magma generation temperatures, allowed for distinguishing two groups of Late Carboniferous and Permian-Triassic granitoids formed in different tectonic settings (article 1). The older group are interpreted as post-collisional granitoids, whereas the younger group was formed in either a subduction-related or a rift-related setting. The study also enhances the knowledge of the local geology, presenting the first U-Pb zircon ages for the ca. 251-256 Ma Izvorovo and ca. 319 Ma Levka plutons and their potential correlation with Harmanli Block Magmatic Complex and Ustrem Pluton, respectively (article 1 and 2). The dissertation provides robust data for the previously proposed division of the Lesovo Complex into separate plutons. The reinterpretation of the previously published results allowed better estimation of the timing of Sakar Batholith emplacement (ca. 306 Ma; article 2).

The field observations along the contact of the Levka Pluton with its country rocks confirm the influence of high-grade Variscan metamorphism and deformation in the Strandja Zone, as well as the upper age limit of this event (>319 Ma) as the Levka Pluton is the oldest Late Carboniferous intrusion so far known in the Strandja Zone (article 2). All above allowed comparison of the Strandja Zone with neighbouring regions, and concludes that the Late Carboniferous to Early Permian magmatic evolution of the Strandja and Sredna Gora zones displays the strongest similarities. When comparing country rocks with Gondwanan affinities affected by Variscan metamorphism and deformation in both these zones, together with Serbo-Macedonian Metamorphic Complex and Sakarya Zone, it can be suggested that all these regions were a part of the metamorphic core of the Variscan Orogen.

The complex study of Early Alpine metamorphism and subsequent albitization revealed two separate events in the Late Jurassic and Early Cretaceous, reaching similar temperatures (~530-620°C). However, the Late Jurassic event was regional, whereas the Early Cretaceous event associated with albitization affected only the northern part of the Sakar Unit (article 3). It shows that both the Strandja and Rhodope zones were affected by coeval metamorphic/hydrothermal events, but their relationship remains unclear.

This PhD dissertation also emphasizes the geochronological and geochemical problems that commonly occur in general geological knowledge. The problem of indications of tectonic setting based on geochemical data of granitoids is presented in article 1. The geochemically invisible differences between Late Carboniferous and Permian-Triassic granitoids of the Strandja Zone are revealed based on the characteristic of zircon populations in granitoids combined with the temperatures of magma generation, which were interpreted according to Miller et al. (2003). Article 2 presents a problem in interpreting geochronological data which spread along Concordia. Potential partial Pb loss due to Late Jurassic to Early Cretaceous metamorphism is indicated to be responsible for such spread (scatter). Therefore, previously published data required a re-evaluation. Article 3 presents a case study where the rutile growth during albitization occurred after the breakdown of igneous titanite, which is supported by isotopic and textural evidence. This study is the first where both the igneous precursor and metamorphic phase are available and allowed testing of the inherited initial lead composition hypothesis presented by Romer (2001).





## 7. Literature

- Akgündüz, S., Aysal, N., Peytcheva, I., Yilmaz, Ş. and Güngör, Y., 2021. Geochronology, geochemistry and tectono-magmatic evolution of the upper Carboniferous–lower Permian Kula pluton in the Istranca (Strandja) Massif, NW Turkey. *Geol. Carpathica* 72(5), 373–394.
- Antić, M., Peytcheva, I., von Quadt, A., Kounov, A., Trivić, B., Serafimovski, T., Tasev, G., Gerdjikov, I. and Wetzel, A., 2016. Pre-Alpine evolution of a segment of the North-Gondwanan margin: Geochronological and geochemical evidence from the central Serbo-Macedonian Massif. *Gondwana Res.* 36, 523–544.
- Antonov, M., Gerdjikov, S., Metodiev, L., Kiselinov, Ch., Sirakov, V. and Valev, V., 2010. Explanatory note to the geological map of the Republic of Bulgaria scale 1:50000: Map sheet K-35-37-B Pirdop, Geocomplex, Sofia.
- Ashwal, L.D., Tucker, R.D. and Zinner, K., 1999. Slow cooling of deep crustal granulites and Pb-loss in zircon. *Geochim. Cosmochim. Acta* 63(18), 2839–2851.
- Aysal, N., Şahin, S.Y., Güngör, Y., Peytcheva, I. and Öngen, S., 2018. Middle Permian–Early Triassic magmatism in the Western Pontides, NW Turkey: geodynamic significance for the evolution of the Paleo-Tethys. *J. Asian Earth Sci.* 164, 83–103.
- Balkanska, E., Gerdjikov, I., Georfiyev, S., Lazarova, A., Dörr, W. and Kounov, A., 2021. Structural and geochronological constraints on the magmatic and tectonic events in the pre-Alpine basement of the central parts of the Balkan fold-thrust belt (Central Stara Planina Mountains, Bulgaria). *Int. J. Earth Sci.* 110, 1181–1211.
- Bauer, C., Rubatto, D., Krenn, K., Proyer, A., Hoinkes, G., 2007. A zircon study from the Rhodope metamorphic complex, N-Greece: Time record of a multistage evolution. *Lithos* 99, 207–228.
- Bedi, Y., Vasilev, E., Dabovski, C., Ergen, A., Okuyucu, C., Dogan, A., Kagan Tekin, U., Ivanova, D., Boncheva, I., Lakova, I., Sachanski, V., Kuscü, I., Tumcay, E., Gülnur Demiray, D., Soycan, H. and Cemal Goncuoglu, M., 2013. New age data from the tectonostratigraphic units of the Istranca “Massif” in NW Turkey: a correlation with SE Bulgaria. *Geol. Carpathica* 64(4), 255–277.
- Bomparola, R.M., Ghezzi, C., Belousova, E., Griffin, W.L., and O'Reilly, S.Y., 2007. Resetting of the U-Pb Zircon System in Cambro-Ordovician Intrusives of the DeepFreeze Range, Northern Victoria Land, Antarctica. *Journal of Petrology* 48(2), 327–364.
- Bonev, N., Spikings, R. and Moritz, R., 2020.  $^{40}\text{Ar}/^{39}\text{Ar}$  age constraints for an early Alpine metamorphism of the Sakar unit, Sakar-Strandzha zone, Bulgaria. *Geol. Mag.* 157(12), 2106–2112.
- Bonev, N., Filipov, P., Raicheva, R. and Moritz, R., 2019. Timing and tectonic significance of Paleozoic magmatism in the Sakar unit of the Sakar-Strandzha Zone, SE Bulgaria. *Int. Geol. Rev.* 61(16), 1957–1979.
- Bonev, N., Filipov, P., Raicheva, R. and Moritz, R., 2022. Evidence of late Palaeozoic and Middle Triassic magmatism in the Sakar-Strandzha Zone, SE Bulgaria: Regional geodynamic implications. *Int. Geol. Rev.* 64(9), 1199–1225.
- Boyadjiev, S. and Lilov, P., 1972. On the K-Ar dating of the South Bulgarian granitoids from Srednogorie and Sakar-Strandja Zones: in *Proceedings of the Geological Institute, ser. Geochemistry, Mineralogy, Petrography* 26(2), 121–220 (in Bulgarian).
- Boyanov, I., Kozhoukharov, D. and Savov, S., 1965. Geological structure of the southern slope of Sakar Mountain between the villages Radovets and Kostur. *Review of the Bulgarian Geological Society* 26(2), 121–134 (in Bulgarian).
- Burg, J-P., 2012. Rhodope: from Mesozoic convergence to Cenozoic extension. *Review of petro-structural data in the geochronological frame. J. Virtual Explor.* 42, 1–44.
- Carrigan, C.W., Mukasa, S.B., Haydoutov, I. and Kolcheva, K., 2005. Age of Variscan magmatism from the Balkan sector of the orogen, central Bulgaria. *Lithos* 82, 125–147.

- Carrigan, C., Mukasa, S., Haydoutov, I. and Kolcheva, K., 2006. Neoproterozoic magmatism and Carboniferous high-grade metamorphism in the Sredna Gora Zone, Bulgaria: An extension of the Gondwana-derived Avalonian-Cadomian belt?. *Precambrian Res.* 147, 404–416.
- Cattò, S., Cavazza, W., Zattin, M. and Okay, A., 2018. No significant Alpine tectonic overprint on the Cimmerian Strandja Massif (SE Bulgaria and NW Turkey). *Int. Geol. Rev.* 60(4), 513–529.
- Chatalov, G.A., 1990. Geology of the Strandja zone in Bulgaria: *Geologica Balcanica*, series operum singulorum 4. Sofia, Publishing house of Bulgarian Academy of Sciences, 263 p. (in Bulgarian).
- Chatalov, A., 1992. Petrological characteristics of the rocks of the Melnitsa orthometamorphic complex, Sakar Mountains. *Review of the Bulgarian Geological Society*, 53, 99–112 (in Bulgarian).
- Chavdarova, S., Machev, P., 2017. Amphibolites from Sakar Mountain – geological position and petrological features. In: *Proceeding of the National Conference with International Participation “GEOSCIENCES 2017” Bulgarian Geological Society* 49–50.
- Dokuz, A., Külekçi, E., Aydınçakır, E., Kandemir, R., Alçiçek, M.C., Pecha, M.E. and Sünnetçi, K., 2017. Cordierite-bearing strongly peraluminous Cebre Rhyolite from the eastern Sakarya Zone, NE Turkey: constraints on the Variscan Orogeny. *Lithos* 278–281, 285–302.
- Dyulgerov, M., Ovtcharova-Schaltegger, M., Ulianov, A., and Schaltegger, U., 2018. Timing of high-K alkaline magmatism in the Balkan segment of southeast European Variscan edifice: ID-TIMS and LA-ICP-MS study. *Int. J. Earth Sci.* 107, 1175–1192.
- Franke, W., Ballèvre, M., Cocks, L.R.M., Torsvik, T.H. and Żelaźniewicz, A., 2020. Variscan Orogeny. *Encyclopedia of Geology (Second Edition)*, 338–349.
- Gallhofer, D., Von Quadt, A., Peytcheva, I., Schmid, S.M. and Heinrich, C.A., 2015. Tectonic, magmatic, and metallogenic evolution of the Late Cretaceous arc in the Carpathian-Balkan orogen. *Tectonics* 34(9), 1813–1836.
- Gautier, P., Bosse, V., Cherneva, Z., Didier, A., Gerdjikov, I., Tiepolo, M., 2017. Polycyclic alpine orogeny in the Rhodope metamorphic complex: The record in migmatites from the Nestos shear zone (N. Greece). *Bulletin de la Societe Geologique de France* 188(6), 1–28.
- Gawęda, A., Golonka, J., 2011. Variscan plate dynamics in the circum-carpathian area. *Geodin. Acta.* 24(3–4), 141–155.
- Georgiev, S., Gerdjikov, I., Peytcheva, I. and Makaveev, P., 2020. Time frame of the Carboniferous tectonic and magmatic activity in the area of Vezhen pluton, Bulgaria. In *Proceedings of the annual geological conference “Geosciences 2020”, Bulgarian Geological Society* 81, 72–74.
- Georgiev, S., Von Quadt, A., Heinrich, C., Peytcheva, I. and Machev, P., 2012. Time evolution of rifted continental arc: integrated ID-TIMS and LA-ICPMS study of magmatic zircons from the Eastern Srednogorie, Bulgaria. *Lithos* 154, 53–67.
- Gerdjikov, I., 2005. Alpine Metamorphism and Granitoid Magmatism in the Strandja Zone: New Data from the Sakar Unit, SE Bulgaria. *Turkish J. Earth Sci.* 14, 167–183.
- Gerdjikov, I., Georgiev, N., Dimov, D. and Lazarova A., 2007. The different faces of supposedly single thrust: a reevaluation of the Vezhen thrust, Central Balkanides. In *Proceedings of the annual geological conference “Geosciences 2007”, Bulgarian Geological Society*, 24–26.
- Gumsley, A., Szopa, K., Chew, D., Gerdjikov, I., Jokubauskas, P., Marciniak-Maliszewska, B., Drakou, F. (2023). An Early Cretaceous thermal event in the Sakar Unit (Strandja Zone, SE Bulgaria/NW Turkey) revealed based on U-Pb rutile geochronology. *Lithos* 448–449, 1–17. <https://doi.org/10.1016/j.lithos.2023.107186>
- Halpin, J.A., Daczko, N.R., Milan, L.A., and Clarke, G.L., 2012. Decoding near-concordant U–Pb zircon ages spanning several hundred million years: recrystallisation, metamictisation or diffusion?. *Contrib. to Mineral. Petrol.* 163, 67–85.
- Halpin, J.A., Gerakiteys, C.L., Clarke, G.L., Belousova, E.A. and Griffin, W.L., 2005. In-situ U–Pb geochronology and Hf isotope analyses of the Rayner Complex, east Antarctica. *Contrib. to Mineral. Petrol.* 148, 689–706.
- Haydoutov, I., 1989. Precambrian ophiolites, Cambrian island arc, and Variscan suture in the South Carpathian-Balkan region. *Geology* 17(10), 905–908.
- Haydoutov, I. and Yanev, S., 1997. The Protomoesian microcontinent of the Balkan Peninsula – a peri-Gondwanaland piece. *Tectonophysics* 272, 303–313.

- Himmerkus, F., Reischmann, T. and Kostopoulos, D., 2009. Triassic rift-related meta-granites in the Internal Hellenides, Greece. *Geol. Mag.* 146(2), 252–265.
- Ivanov, Ž., 2017. *Tectonics of Bulgaria*. Sofia University Press, Sofia, 331 p. (in Bulgarian).
- Ivanov, Z., Gerdjikov, I. and Kounov, A., 2001. New data and considerations about structure and tectonic evolution of Sakar region, SE Bulgaria. *Annuaire de l' University de Sofia, Geology and Geography* 91, 35–80 (in Bulgarian).
- Jordanov, M., Sarov, S., Georgiev, S.T., Marinova, R., Dobrev, G., Grozdev, V., Balkanska, E., Moskovska, L., 2008. Explanatory notes to the Geological Map of the Republic of Bulgaria 1: 50000, sheet K-35-76-B (Harmanly). *Geocomplex*, Sofia, p. 1–60.
- Kamenov, B.K., Vergilov, V., Dabovski, C., Vergilov, I. and Ivchinova, L., 2010. The Sakar batholith – petrology, geochemistry and magmatic evolution. *Bulgarian Academy of Sciences, Geochemistry, Mineralogy and Petrology* 48, 1–37.
- Kamenov, B.K., von Quadt, A. and Peytcheva, I., 2002. New insight into petrology, geochemistry and dating of the Vejen pluton, Bulgaria. *Bulgarian Academy of Sciences, Geochemistry, Mineralogy and Petrology* 39, 3–25.
- Karsli, O., Dokuz, A. and Kandemir, R., 2016. Subduction-related Late Carboniferous to Early Permian Magmatism in the Eastern Pontides, the Camlik and Casurluk plutons: Insights from geochemistry, whole-rock Sr–Nd and in situ zircon Lu–Hf isotopes, and U–Pb geochronology. *Lithos* 266–267, 98–114.
- Kozhoukharov, D. and Kozhoukharova, E., 1973. Stratigraphy and petrology of the Precambrian metamorphic rocks from the Sakar Mountain: *Bulletin of the Geological Institute – Series Geochemistry, Mineralogy and Petrography* 22, 193–210 (in Bulgarian).
- Liati, A., 2005. Identification of repeated Alpine (ultra) high-pressure metamorphic events by U–Pb SHRIMP geochronology and REE geochemistry of zircon: the Rhodope zone of Northern Greece. *Contrib. to Mineral. Petrol.* 150, 608–630.
- Liati, A., Theye, T., Fanning, C.M., Gebauer, D., Rayner, N., 2016. Multiple subduction cycles in the Alpine orogeny, as recorded in single zircon crystals (Rhodope zone, Greece). *Gondwana Res.* 29, 199–207.
- Machev, P.H., Ganev, V. and Klain, L., 2015. New LA-ICP-MS U–Pb zircon dating for Strandja granitoids (SE Bulgaria): evidence for two-stage late Variscan magmatism in the internal Balkanides. *Turkish J. Earth Sci.* 24, 230–48.
- Malinov, O., von Quadt, A., Peytcheva, I., Aladjov, T., Aladjov, A., Naydenova, S. and Djambazov, S., 2004. The Klissura Granite in the Western Balkan – questions and answers from new field and isotopic studies. Annual Scientific Conference “Geology 2004”, 16–17.12.2004, Bulgarian Geological Society, abstract, p. 51–53.
- Mayringer, F., Treloar, P.J., Gerder, A., Finger, F., Shengelia, D., 2011. New age data from the Dzirula massif, Georgia: implications for the evolution of the Caucasian Variscides. *Am. J. Sci.* 311(5), 404–441.
- McCann, T., 2008. *The Geology of Central Europe: Volume 1: Precambrian and Palaeozoic*. *Geol. Soc. Lond.* 748 pages.
- Michard, A., Soulaïmani, A., Hoepffner, C., Ouanaimi, H., Baidder, L., Rjimati, E.C., Saddiqi, O., 2010. The South-Western branch of the Variscan Belt: Evidence from Morocco. *Tectonophysics* 492, 1–24.
- Miller, C.F., McDowell, S.M. and Mapes, R.W., 2003. HOT AND COLD GRANITES? Implications of zircon saturation temperatures and preservation of inheritance. *Geology* 31, 529–532.
- Moulas, E., Schenker, F.L., Burg, J-P., Kostopoulos, D., 2017. Metamorphic conditions and structural evolution of the Kesebir-Kardamos dome: Rhodope metamorphic complex (Greece-Bulgaria). *International Journal of Earth Sciences* 106, 2667–2685.
- Natal'in, B., Sunal, G., Gün, E., Wang, B. and Zhiqing, Y., 2016. Precambrian to Early Cretaceous rocks of the Strandja Massif (northwestern Turkey): evolution of a long lasting magmatic arc. *Can. J. Earth Sci.* 53(11), 1312–1335.

- Nedialkov, R., Platevoet, B., Peytcheva, I., von Quadt, A. and Vangelova, V. 2007. Geochemistry and U-Pb zircon dating of the Mezdrea granitic pluton: Bulgarian Geological Society, National Conference with International Participation "Geosciences 2007", Abstracts, p. 101–102.
- Okay, A.I. and Göncüoğlu, M.C., 2004. Karakaya Complex: a review of data and concepts: Turkish J. Earth Sci. 13, 77–95.
- Okay, A.I. and Nikishin, A.M., 2015. Tectonic evolution of the southern margin of Laurasia in the Black Sea region. *Int. Geol. Rev.* 1051–1076.
- Okay, A., Satur, M., Tüysüz, O., Akyüz, S. and Chen, F., 2001. The tectonics of Strandja Massif: late-Variscan and mid-Mesozoic deformation and metamorphism in the northern Aegean. *Int. J. Earth Sci.* 90, 217–233.
- Okay, A.I., Şengör, A.M.C., Görür, N., 1994. Kinematic history of the opening of the Black Sea and its effects on the surrounding regions. *Geology* 22, 267–270.
- Okay, A. and Topuz, G., 2017. Variscan orogeny in the Black Sea region. *Int. J. Earth Sci.* 106, 569–592.
- Pearce, J. 1996. Sources and settings of granitic rocks. *Episodes* 19(4), 120–125.
- Pearce, J., Harris, N. and Tindle, A.G., 1984. Trace Element Discrimination Diagrams for the Tectonic Interpretation of Granitic Rocks. *J. Petrol.* 25, 956–983.
- Peytcheva, I., Georgiev, S. and Von Quadt, A., 2016. U/Pb ID-TIMS dating of zircons from the Sakar-Strandzha Zone: New data and old questions about the Variscan orogeny in SE Europe. In *Proceedings of Annual Conference of the Bulgaria Geological Society "Geosciences 2016"*: Sofia, Bulgarian Geological Society, 71–72.
- Peytcheva, I., Tacheva, E., von Quadt, A. and Nedialkov, R., 2018. U-Pb zircon and titanite ages and Sr-Nd-Hf isotope constraints on the timing and evolution of the Petrohan-Mezdrea pluton (Western Balkan Mts, Bulgaria). *Geol. Balcanica* 47(2), 25–46.
- Peytcheva, I., von Quadt, A., Malinov, O., Tacheva, E. and Nedialkov, R., 2006. Petrochan and Klissura plutons in Western Balkan: relationships, in situ and single grain U-Pb zircon/monazite dating and isotope tracing. In *Proceedings of the Joint Conference of the Bulgarian Geophysical and Geological Societies "Geosciences 2006"*, abstracts, p. 221–224.
- Pristavova, S., Tzankova, N., Gospodinov, N. and Filipov, P., 2019. Petrological study of metasomatic altered granitoids from Kanarata Deposit, Sakar Mountain, southeastern Bulgaria. *Journal of Mining and Geological Sciences* 62, 53–61.
- Romer, R.L., 2001. Lead incorporation during crystal growth and the misinterpretation of geochronological data from low-<sup>238</sup>U/<sup>204</sup>Pb metamorphic minerals. *Terra Nova* 13(4), 258–263.
- Şahin, S.Y., Aysal, N., Güngör, Y., Peytcheva, I., Neubauer, F., 2014. Geochemistry and U–Pb zircon geochronology of metagranites in Istranca (Strandja) Zone, NW Pontides, Turkey: Implications for the geodynamic evolution of Cadomian orogeny. *Gondwana Res.* 26(2), 755–771.
- Salacińska, A., Gerdjikov, I., Gumsley, A., Szopa, K., Chew, D., Gawęda, A., Kocjan, I., 2021. Two stages of Late Carboniferous to Triassic magmatism in the Strandja Zone of Bulgaria and Turkey. *Geol. Mag.* 158(12), 2151–2164.
- Salacińska, A., Gerdjikov, I., Kounov, A., Chew, D., Szopa, K., Gumsley, A., Kocjan, I., Marciniak-Maliszewska, B., Drakou, F., 2022. Variscan magmatic evolution of the Strandja Zone (Southeast Bulgaria and northwest Turkey) and its relationship to other north Gondwanan margin terranes. *Gondwana Res.* 109, 253–273.
- Sengör, A.M.C., Altiner, D., Cin, A., Ustaömer, T., Hsü, K.J., 1988. Origin and assembly of the Tethyside orogenic collage at the expense of Gondwana Land. *Gondwana and Tethys. Geol. Soc. Spec. Publ.* 37, 119–181.
- Şengör, A. M. C., Yılmaz, Y., and Sungurlu, O., 1984. Tectonics of the Mediterranean Cimmerides: Nature and evolution of the western termination of Paleo-Tethys, in Dixon, J. E., and Robinson, A. H. F., eds., *The geological evolution of the Eastern Mediterranean: Geol. Soc. Spec. Publ.* 17, 77–112.
- Şengün, F. and Koralay, O.E., 2017. Early Variscan magmatism along the southern margin of Laurasia: Geochemical and geochronological evidence from the Biga Peninsula, NW Turkey. *Int. J. Earth Sci.* 106, 811–826.

- Şengün, F., Koralay, O.E. and Kristoffersen, M., 2020. Zircon U-Pb age and Hf isotopic composition of the Carboniferous Gönen granitoid in the western Sakarya Zone of Turkey. *Turkish J. Earth Sci.* 29, 617–628.
- Spahić, D., Gaudenyu, T., 2018. Primordial geodynamics of Southern Carpathian-Balkan basements (Serbo-Macedonian Mass): Avalonian vs. Cadomian arc segments. *Proc. Geol. Assoc.* 130(2), 142–156.
- Stacey, J.S., Kramers, J.D., 1975. Approximation of terrestrial lead isotope evolution by a two-stage model. *Earth Planet. Sci. Lett.* 26(2), 207–221.
- Stampfli, G.M., 2000. Tethyan oceans. In: Bozkurt, E., Winchester, J.A., and Piper, J.D.A., (Eds.), *Tectonics and Magmatism in Turkey and the Surrounding Area: Geol. Soc. Spec. Publ.* 173, 1–23.
- Stephan, T., Kroner, U., Romer, R.L. and Rösel, D., 2019. From a bipartite Gondwanan shelf to an arcuate Variscan belt: The early Paleozoic evolution of northern Peri-Gondwana. *Earth-Sci. Rev.* 192, 491–512.
- Sunal, G., Natal'in, B.A., Satir, M. and Toraman, E., 2006. Paleozoic magmatic events in the Strandja Massif, NW Turkey. *Geodin. Acta* 19(5), 283–300.
- Sunal, G., Satir, M., Natal'in, B.A., Topuz, G. and Vonderschmidt, O., 2011. Metamorphism and diachronous cooling in a contractional orogen: the Strandja Massif, NW Turkey. *Geol. Mag.* 148(4), 580–596.
- Szopa, K., Sałacińska, A., Gumsley, A.P., Chew, D., Petrov, P., Gawęda, A., Zagórska, A., Deput, E., Gospodinov, N. and Banasik, K., 2020. Two-Stage Late Jurassic to Early Cretaceous Hydrothermal Activity in the Sakar Unit of Southeastern Bulgaria. *Minerals* 10, 266.
- Stampfli, G.M., 2000. Tethyan oceans. In *Tectonics and Magmatism in Turkey and the Surrounding Area* (eds. E. Bozkurt, J.A. Winchester & J.D.A. Piper), pp. 1–23. *Geol. Soc. Spec. Publ.* no. 173.
- Topuz, G., Alther, R., Kalt, A., Satir, M., Werner, O. and Schwartz, W.H., 2004. Aluminous granulites from the Pulur Complex, NE Turkey: a case of partial melting, efficient melt extraction and crystallisation. *Lithos* 72, 183–207.
- Topuz, G., Altherr, R., Siebel, W., Schwarz, !.H., Zack, T., Hasözbek, A., Barth, M., Satir, M. and Şen, C., 2010. Carboniferous high-potassium I-type granitoid magmatism in the Eastern Pontides: The Gümüşhane pluton (NE Turkey). *Lithos* 116, 92–110.
- Tzankova, N., Pristavova, S., 2007. Metamorphic evolution of garnet-bearing schists from Sakar mountain southeastern Bulgaria. *Comptes Rendus L'Academie Bulgare des Sciences* 60(3), 271–278.
- Ustaömer, P.A., Ustaömer, T. and Robertson, A.H.F., 2012. Ion Probe U–Pb Dating of the Central Sakarya Basement: a peri-Gondwana Terrane intruded by Late Lower Carboniferous Subduction/Collision-related Granitic Rocks. *Turkish J. Earth Sci.* 21(6), 905–932.
- Ustaömer, T., Robertson A.H.F., Ustaömer, P.A., Gerdes, A. and Peytcheva, I., 2013. Constraints on Variscan and Cimmerian magmatism and metamorphism in the Pontides (Yusufeli–Artvin area), NE Turkey from U–Pb dating and granite geochemistry. *Geol. Soc. Spec. Publ.* 372(1), 49–74.
- Vladinova, T. and Georgieva, M., 2020. New data on the westernmost part of the Sakar unit metamorphic basement, SE Bulgaria, In *Proceedings of National Conference “Geosciences 2020”*: Sofia, Bulgarian Geological Society, 81(3), 105–107.
- Vladinova, T., Georgieva, M., Bosse, V., Cherneva, Z., 2018. U-Pb detrital zircons geochronology from metasedimentary rocks of the Sakar Unit, Sakar-Strandzha zone, SE Bulgaria, In *Proceedings of National Conference “Geosciences 2018”*: Sofia, Bulgarian Geological Society 79(3), 67–68.
- Vladinova, T., Georgieva, M. and Peytcheva, I., 2019. U-Pb geochronology and geochemistry of rutiles from metaconglomerate in the Sakar-Strandzha zone, SE Bulgaria, In *Proceedings of National Conference “Geosciences 2019”*: Sofia, Bulgarian Geological Society, 80(3), 91–93.
- Von Raumer, J.F., 2013. Pre-Mesozoic Alpine basements - their place in the European Paleozoic framework. *GSA Bulletin* 125 (1-2), 89–108.
- Watson, E.B. and Harrison, T.M., 1983. Zircon saturation revisited: Temperature and composition effects in a variety of crustal magma types. *Earth Planet. Sci. Lett.* 64, 295–304.
- Zulauf, G., Dörr, W., Fisher-Spurlock, S.C., Gerder, A., Chatzaras, V., Xypolias, P., 2014. Closure of the Paleotethys in the External Hellenides: constraints from U–Pb ages of magmatic and detrital zircons (Crete). *Gondwana Res.* 28(2), 642–667.

Žák, J., Svojtka, M., Gerdjikov, I., Kounov, A. and Vangelov, D.A., 2022. The Balkan terranes: a missing link between the eastern and western segments of the Avalonian–Cadomian orogenic belt? *Int. Geol. Rev.* 64(17), 2389–2415.

## 8. Contribution statement of the co-authors

### Article 1

**Title:** Two stages of Late Carboniferous to Triassic magmatism in the Strandja Zone of Bulgaria and Turkey

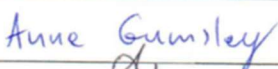


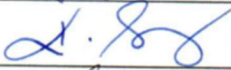
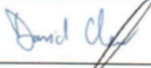


**Journal:** Geological Magazine

**Impact factor:** 2.656

**Publishing date:** 2021

**DOI:** <https://doi.org/10.1017/S0016756821000650>

### Authors:

Name and surname	Contribution [%]	Signature
Anna Sałacińska	70	
Ianko Gerdjikov	5	
Ashley Gumsley	5	
Krzysztof Szopa	5	
David Chew	5	
Aleksandra Gawęda	5	
Izabela Kocjan	5	

## Article 2

**Title:** Variscan magmatic evolution of the Strandja Zone (Southeast Bulgaria and Northwest Turkey) and its relationship to other North Gondwanan margin terranes

**Journal:** Gondwana Research

**Impact factor:** 6.151

**Publishing date:** 2022

**DOI:** <https://doi.org/10.1016/j.j.gr.2022.04.013>

Name and surname	Contribution [%]	Signature
Anna Sałacińska	60	Anna Gumsley
Ianko Gerdjikov	5	I. Gerdjikov
Alexandre Kounov	5	Alexandre Kounov
David Chew	5	David Chew
Krzysztof Szopa	5	K. Szopa
Ashley Gumsley	5	A. Gumsley
Izabela Kocjan	5	Izabela Kocjan
Beata Marciniak-Maliszewska	5	B. Marciniak-Maliszewska
Foteini Drakou	5	F. Drakou



### Article 3

**Title:** An Early Cretaceous thermal event in the Sakar Unit (Strandja Zone, SE Bulgaria/NW Turkey) revealed based on U-Pb rutile geochronology and Zr-in-rutile thermometry

**Journal:** Lithos

**Impact factor:** 4.02

**Publishing date:** 19.04.2023 (available online)

**DOI:** <https://doi.org/10.1016/j.lithos.2023.107186>

Name and surname	Contribution [%]	Signature
Anna Gumsley	60	Anne Gumsley
Krzysztof Szopa	10	K. Szopa
David Chew	10	David Chew
Ianko Gerdjikov	5	I. Gerdjikov
Petras Jokubauskas	5	P. Jokubauskas
Beata Marciniak-Maliszewska	5	B. Marciniak-Maliszewska
Foteini Drakou	5	F. Drakou

## Original Article

**Cite this article:** Sałacińska A, Gerdjikov I, Gumsley A, Szopa K, Chew D, Gawęda A, and Kocjan I (2021) Two stages of Late Carboniferous to Triassic magmatism in the Strandja Zone of Bulgaria and Turkey. *Geological Magazine* **158**: 2151–2164. <https://doi.org/10.1017/S0016756821000650>

Received: 9 February 2021

Revised: 3 June 2021

Accepted: 8 June 2021

First published online: 21 July 2021


**Keywords:**

Strandja Zone; Sakar unit; U–Pb zircon dating; Izvorovo Pluton

**Author for correspondence:**

Anna Sałacińska,  
Email: [anna.salacinska@twarda.pan.pl](mailto:anna.salacinska@twarda.pan.pl)

# Two stages of Late Carboniferous to Triassic magmatism in the Strandja Zone of Bulgaria and Turkey

Anna Sałacińska<sup>1,2</sup> , Ianko Gerdjikov<sup>3</sup>, Ashley Gumsley<sup>1</sup>, Krzysztof Szopa<sup>1</sup>, David Chew<sup>4</sup>, Aleksandra Gawęda<sup>1</sup> and Izabela Kocjan<sup>2</sup>

<sup>1</sup>Institute of Earth Sciences, Faculty of Natural Sciences, University of Silesia in Katowice, Będzińska 60, 41-200 Sosnowiec, Poland; <sup>2</sup>Institute of Geological Sciences, Polish Academy of Sciences, Warsaw, Poland; <sup>3</sup>Faculty of Geology and Geography, Sofia University 'St. Kliment Ohridski', 15 Tzar Osvoboditel Blvd., 1504 Sofia, Bulgaria and <sup>4</sup>Department of Geology, School of Natural Sciences, Trinity College Dublin, Dublin, Ireland

**Abstract**

Although Variscan terranes have been documented from the Balkans to the Caucasus, the southeastern portion of the Variscan Belt is not well understood. The Strandja Zone along the border between Bulgaria and Turkey encompasses one such terrane linking the Balkanides and the Pontides. However, the evolution of this terrane, and the Late Carboniferous to Triassic granitoids within it, is poorly resolved. Here we present laser ablation – inductively coupled plasma – mass spectrometry (LA-ICP-MS) U–Pb zircon ages, coupled with petrography and geochemistry from the Izvorovo Pluton within the Sakar Unit (Strandja Zone). This pluton is composed of variably metamorphosed and deformed granites which yield crystallization ages of c. 251–256 Ma. These ages are older than the previously assumed age of the Izvorovo Pluton based on a postulated genetic relationship between the Izvorovo Pluton and Late Jurassic to Early Cretaceous metamorphism. A better understanding of units across the Strandja Zone can now be achieved, revealing two age groups of plutons within it. An extensive magmatic episode occurred c. 312–295 Ma, and a longer-lived episode between c. 275 and 230 Ma. Intrusions associated with both magmatic events were emplaced into pre-Late Carboniferous basement, and were overprinted by Early Alpine metamorphism and deformation. These two stages of magmatism can likely be attributed to changes in tectonic setting in the Strandja Zone. Such a change in tectonic setting is likely related to the collision between Gondwana-derived terranes and Laurussia, followed by either subduction of the Palaeo-Tethys Ocean beneath Laurussia or rifting in the southern margin of Laurussia, with granitoids forming in different tectonic environments.

**1. Introduction**

The Late Carboniferous to Triassic was marked by the assembly of a significant portion of the European crust, and these tectonic events are critical to our understanding of the amalgamation of Pangaea and its evolution. A key event in the assembly of Pangaea was the collision of Gondwana (and Gondwana-derived terranes) with Laurussia during the Acadian–Variscan–Alleghanian Orogeny in the Late Carboniferous (i.e. McCann, 2008; Stephan *et al.* 2019; Franke *et al.* 2020;). The Variscan Orogen is exposed in Western and Central Europe, but also occurs north of the West African Craton in Morocco and Algeria, and in the Appalachian Mountains in northeastern North America, where it is termed the Alleghanian Orogeny (Michard *et al.* 2010; Stephan *et al.* 2019; Franke *et al.* 2020). To the southeast of the Bohemian Massif in central Europe, the Variscan Belt is either overprinted by younger orogens or covered by sedimentary rocks. However, Variscan basement massifs are known from the Alps, the Carpatho-Balkanides, the Hellenides, parts of the Pontides and further to the east into the Caucasus (Sengör *et al.* 1988; Haydoutov, 1989; Stampfli, 2000; Himmerkus *et al.* 2007; Gawęda & Golonka, 2011; Mayringer *et al.* 2011; von Raumer, 2013; Zulauf *et al.* 2014; Antić *et al.* 2016; Okay & Topuz, 2017; Spahić & Gaudeny, 2018; Franke *et al.* 2020).

The Strandja Zone straddling the border between Bulgaria and Turkey forms the focus of this study. The Strandja Zone occurs between the Carpatho-Balkanides to the north and west and the Pontides to the east, and has been variously assigned to either zone (e.g. Okay *et al.* 2001; Sunal *et al.* 2006; Aysal *et al.* 2018). It contains a series of units related to the Variscan and Alpine orogens, and is key to a better understanding of the Variscan Belt in this sector of Pangaea. The post-Variscan evolution of the Strandja Zone is interpreted by many authors as related to the subduction of the Palaeo-Tethys Ocean beneath the southern margin of Laurussia (e.g. Natal'in *et al.* 2016; Aysal *et al.* 2018; Bonev *et al.* 2019a). The Palaeo-Tethys Ocean remained open to the south of the Variscan Belt until the late Palaeozoic, and then the initiation

© The Author(s), 2021. Published by Cambridge University Press. This is an Open Access article, distributed under the terms of the Creative Commons Attribution licence (<http://creativecommons.org/licenses/by/4.0>), which permits unrestricted re-use, distribution and reproduction, provided the original article is properly cited.

**CAMBRIDGE**  
UNIVERSITY PRESS

of northward subduction led to the final closure of the Palaeo-Tethys Ocean in the Middle Triassic (Sengör, 1979, 1984; Sengör *et al.* 1988; Zulauf *et al.* 2014). Furthermore, this northward subduction likely triggered rifting and the opening of back-arc basins along the Laurussian margin, e.g. the Maliac and Kure basins (e.g. Stampfli, 2000; Stampfli & Kozur, 2006).

The Variscan Belt in Europe is characterized by an abundance of granitoids (e.g. Bonin *et al.* 1998; McCann, 2008). Many of the granitoids in the Variscan Belt of southeastern Europe remain undated and intrude into poorly characterized basement which was also affected by Alpine metamorphic overprinting of variable intensity. In this study, we present the first laser ablation – inductively coupled plasma – mass spectrometry (LA-ICP-MS) U–Pb zircon ages and geochemical results from one of the largest intrusive bodies in the Sakar Unit of the Strandja Zone: the Izvorovo Pluton. The emplacement of this pluton was interpreted by Ivanov *et al.* (2001) and Gerdjikov (2005) as the heat source for Late Jurassic to Early Cretaceous metamorphism in the Sakar Unit of the Strandja Zone. Bonev *et al.* (2019a), however, regarded the pluton as Carboniferous based on ages from the Ustrem Pluton. Therefore, obtaining accurate and precise U–Pb geochronological data for the Izvorovo Pluton is a critical test of this interpretation. The new ages of the Izvorovo Pluton are also coupled with petrographic and geochemical data, and integrated with a compilation of published data from the surrounding plutonic suites of the Strandja Zone. Such a data compilation allows us to demonstrate two major magmatic events in the Late Carboniferous and Permian–Triassic. It also allows for better understanding and correlation of the units within the Strandja Zone and across the region.

## 2. Geological setting

The Strandja (or Strandzha) Zone, also known as the Sakar–Strandja Zone (SSZ; Boyadiev & Lilov 1972; Ivanov, 2017), Strandja (Strandzha) Massif (SM; Okay *et al.* 2001; Natal'in *et al.* 2016 and references therein) or Istranca Massif (Bedi *et al.* 2013), is a NW–SE-trending mountain belt, located in the border area between Bulgaria and Turkey (Fig. 1). To the south, the Strandja Zone is covered by Cenozoic sedimentary rocks of the Thrace Basin. The relationship between the Rhodope Metamorphic Complex to the west and the Strandja Zone is poorly understood, and their contact is mostly covered by Cenozoic sedimentary rocks.

### 2.a. Units

In Bulgaria, the Strandja Zone is defined as a pre-Late Cretaceous orogen, that is covered by sedimentary rocks and intruded by plutons related to the formation of Apuseni–Banat–Timok–Sredna Gora Late Cretaceous magmatic arc (Chatalov, 1990; Gallhofer *et al.* 2015). A key feature of the Strandja Zone is that the main phase of deformation and metamorphism occurred during the Late Jurassic to Early Cretaceous. This event is known as the Early Alpine Orogeny in Bulgarian literature (i.e. Ivanov *et al.* 2001), and the Cimmerian Orogeny in Turkish literature (i.e. Cattò *et al.* 2018). Based on their structural position during the Early Alpine Orogeny, the degree of metamorphism and stratigraphic characteristics, three units have been defined in the Bulgarian part of the Strandja Zone: the Sakar, Strandja and Veleka units (Chatalov, 1990; Gerdjikov, 2005).

The Sakar Unit is exposed within the Sakar Mountains, but also continues westward of the Maritsa River into the Harmanli Block west of Harmanli, as well as the Maritsa region (Fig. 1). The

Strandja Unit is located to the east of the Sakar Unit, within the Strandja Mountains and Derwent Heights along the Bulgarian–Turkish border, and further to the southeast in Turkey towards the vicinity of Istanbul. The Veleka Unit is an allochthon of the Zubernovo Nappe (Chatalov, 1990), that has been emplaced over the less intensely metamorphosed Strandja Unit itself (Gerdjikov, 2005).

### 2.b. Evolution of the units and the granitoids

The Sakar and Strandja units share a similar geological history (e.g. Chatalov, 1990). Late Carboniferous to Triassic granitoids and meta-granitoids in both units were intruded into metamorphic basement, which is composed of gneisses, schists and amphibolites. This pre-Late Carboniferous basement includes Neoproterozoic–Cambrian (Natal'in *et al.* 2016) and Ordovician (Bonev *et al.* 2019a) felsic magmatic rocks, and is considered to represent peri-Gondwanan terrane(s) that formed along the northern Gondwanan margin (e.g. Stampfli, 2000; Okay & Topuz, 2017). Late Carboniferous to Triassic magmatism forms significant parts of the Strandja Zone, with the most important batholiths and plutons shown in Figure 1, along with smaller unnamed intrusions within the basement. One of the largest magmatic bodies in the Sakar Unit is the Late Carboniferous Sakar Batholith (~450 km<sup>2</sup>, Kamenov *et al.* 2010; Peytcheva *et al.* 2016; Bonev *et al.* 2019a; Pristavova *et al.* 2019). Neighbouring intrusions include the Late Carboniferous Ustrem Pluton and Melnitsa Complex (Bonev *et al.* 2019a), and the Izvorovo and Levka plutons which are less extensively studied.

The Izvorovo Pluton was defined as a weakly deformed body of equigranular granites, very similar to the intrusive bodies from the Sakar Pluton (Kouzhokharov & Kouzhokharova, 1973). According to the same authors, these granites, with an assumed Precambrian age, may have been emplaced into the lower part of the metamorphic basement represented by migmatitic paragneisses. Based on detailed field mapping and microfabric data, Ivanov *et al.* (2001) significantly enlarged the areal extent of the Izvorovo Pluton by including strongly foliated K-feldspar porphyritic and equigranular granites, previously regarded as the local country rock. Between 1999 and 2000, the westernmost part of the Sakar Mountains and the Harmanli Block area was mapped at 1:25 000 scale. It was demonstrated by Jordanov *et al.* (2008) that this mapped region is almost entirely composed of metamorphosed and deformed granitoids (orthogneisses) of the Izvorovo Pluton in the Sakar area. Due to the extensive Cenozoic cover, the true extent of the Izvorovo Pluton cannot be easily ascertained, but field mapping indicates that the pluton extends westward toward the area south of Haskovo, thus allowing a crude estimate of the areal extent of the pluton at ~500 km<sup>2</sup>. Based on these field constraints, the Harmanli Block is regarded as the western part of the Izvorovo Pluton.

In the Sakar Unit, the metamorphic basement and the Late Carboniferous to Triassic granitoids and meta-granitoids are overlain by Permian to Triassic meta-sedimentary rock of the Topolovgrad Group (Fig. 1; e.g. Chatalov, 1990). All these units are penetratively deformed and metamorphosed during the Late Jurassic to Early Cretaceous Early Alpine Orogeny (Chatalov, 1988, 1990; Gerdjikov 2005; Bonev *et al.* 2020b; Szopa *et al.* 2020). The highest grades (amphibolite-facies) associated with Early Alpine metamorphism are encountered in the Sakar Mountains (Chatalov, 1990; Tsankova & Pristavova 2007a, b) and in the Harmanli Block (Jordanov *et al.* 2008) of the Sakar Unit. Elsewhere within the Sakar Unit, metamorphism was within the greenschist facies. This spatial distribution of higher peak



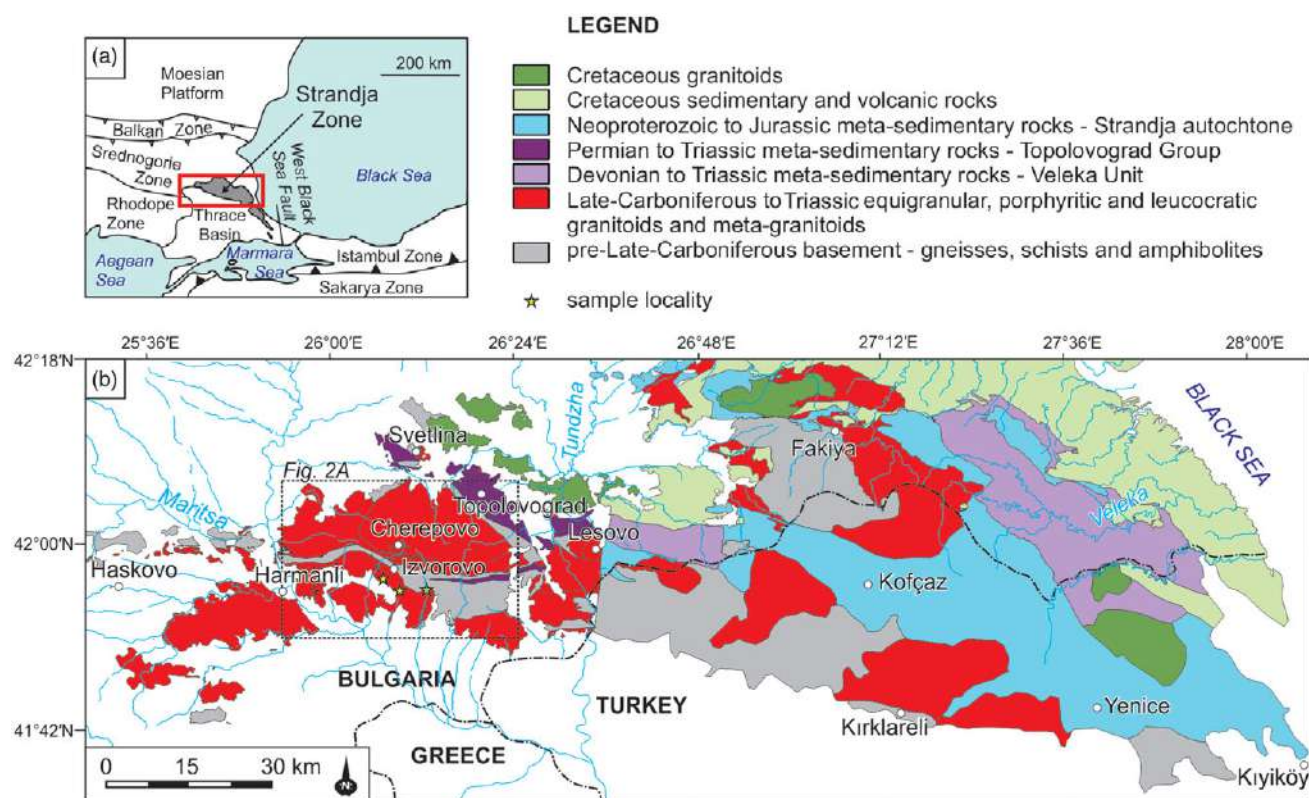


**Fig. 1.** (Colour online) Maps of the Strandja Zone along the Bulgarian–Turkish border: (a) Strandja Zone and surrounding major tectonic units; (b) geological map of the Strandja Zone with the sample localities (modified after Okay *et al.* 2001; Gerdjikov, 2005; Natal'in *et al.* 2016).

metamorphic temperatures compared to the rest of the Sakar Unit of the Strandja Zone led Chatalov (1990) to propose the existence of the so-called Sakar palaeothermal dome. Subsequently, Ivanov *et al.* (2001) and Gerdjikov (2005) argued that these anomalously high temperatures were caused by syn-kinematic Late Jurassic to Early Cretaceous emplacement of large plutonic bodies (i.e. the Sakar, Izvorovo and Varnik plutons). However, new geochronological data have shown that the Sakar Batholith was emplaced in the Late Carboniferous to Early Permian (c. 305 – c. 295 Ma; Peytcheva *et al.* 2016; Bonev *et al.* 2019a; Pristavova *et al.* 2019). Obtaining accurate and precise U–Pb geochronological data for the Izvorovo Pluton is a further test of this hypothesis.

### 3. Sample localities

The region investigated in the Izvorovo Pluton is located to the south of Izvorovo Village. The Izvorovo Pluton is separated from the Sakar Batholith by an east–west-trending belt of basement rocks (Fig. 2a). The Izvorovo Pluton consists of foliated porphyritic and equigranular meta-granites and porphyroclastic gneisses referred to as the Lesovo Orthometamorphic Complex (Kamenov *et al.* 2010) or described as the ‘Sakar-type’ schistose granites of the Izvorovo Dome (Dimitrov 1956, 1959; Boyanov *et al.* 1965; Ivanov *et al.* 2001). The absolute age of the Izvorovo Pluton has not been determined by isotopic dating, and there is also a lack of any other geochemical and mineralogical data from this pluton. A recent study by Bonev *et al.* (2019a) regarded the Izvorovo Pluton as a part of the Carboniferous Lesovo Complex (gneisses and granites), with an age of c. 306 Ma, based on U–Pb zircon dating of meta-quartz–diorite collected from the Ustrem Pluton southeast of Lesovo Village.

In this study, three samples of orthogneiss (SAK-40), augen gneiss (SAK-41) and weakly foliated granite (SAK-42) were collected from the Izvorovo Pluton (Fig. 2). All of these samples represent different types of the Izvorovo meta-granites. The weakly foliated equigranular meta-granite sample SAK-42 is one of the variations of the Izvorovo Pluton, regarded as the ‘Lesovo-type’ pre-metamorphic granite (Kozhoukharov & Kozhoukharova, 1973). The orthogneiss sample SAK-40 and augen gneiss sample SAK-41 are other types of porphyritic meta-granite within the Izvorovo Pluton. However, our field observations showed that significant strain variations occur between the massive, weakly foliated sample SAK-42 and gneiss samples SAK-40 and SAK-41, as the latter are strongly sheared due to their proximity to the country-rock contact.

Sample locations, rock types and mineral assemblages are listed in Table 1. The sample of orthogneiss with feldspar porphyroclasts (SAK-40) was collected from outcrop in a river valley c. 1 km to the west of Mladinovo (Fig. 2a, b). The contact between orthogneiss and deformed amphibolite with leucosome layers (basement rock) is observed in the vicinity of this sample locality (~200 m to the north). The orthogneiss with feldspar porphyroclasts shows a strong resemblance to porphyritic granitoids from the Sakar Batholith, but is more deformed. The augen gneiss sample (SAK-41) was collected from a large outcrop (~3000 m<sup>2</sup>) of pinkish felsic gneisses in the northern part of Oryahovo Village. This rock contains feldspar porphyroclasts up to 3–4 cm in length (Fig. 2a, c). Samples of meta-granite (SAK-42) were collected from an outcrop in close proximity to a dam located c. 2 km to the southwest of Izvorovo itself. This meta-granite is equigranular and coarse-grained (Fig. 2a, d). As the Sakar Mountains study area is covered by steppe, the rock outcrops are usually strongly weathered outside of quarries. However, the freshest rock samples were collected for this study.

**Table 1.** Sample localities and modal mineral assemblages

Sample	Lithology					Locality			Latitude		Longitude	
SAK-40	Orthogneiss with feldspar porphyroclasts					W Mladinovo			41° 56′ 11.7″ N		26° 13′ 05.8″ E	
SAK-41	Augen gneiss					Oryahovo			41° 55′ 34.4″ N		26° 09′ 35.7″ E	
SAK-42	Meta-granite					SW Izvorovo			41° 56′ 59.9″ N		26° 07′ 13.7″ E	
Sample	Mineral assemblage											
	Qz	Pl	Afs	Bt	Ms	Zrn	Ap	Ttn	Mnz	Fe-ox	Mag	Ilm
	...	...	...	..	..	.	.			.	.	
	...	...	...	..	..	.	.	.	.			.
	...	...	...	..	..	.	.		.	.		

Major (…), minor (..) and accessory (.) amounts of minerals. Qz, quartz; Pl, plagioclase; Afs, alkali feldspar; Bt, biotite; Ms, muscovite; Zrn, zircon; Ap, apatite; Ttn, titanite; Mnz, monazite; Fe-ox, Fe-oxides; Mag, magnetite; Ilm, ilmenite.

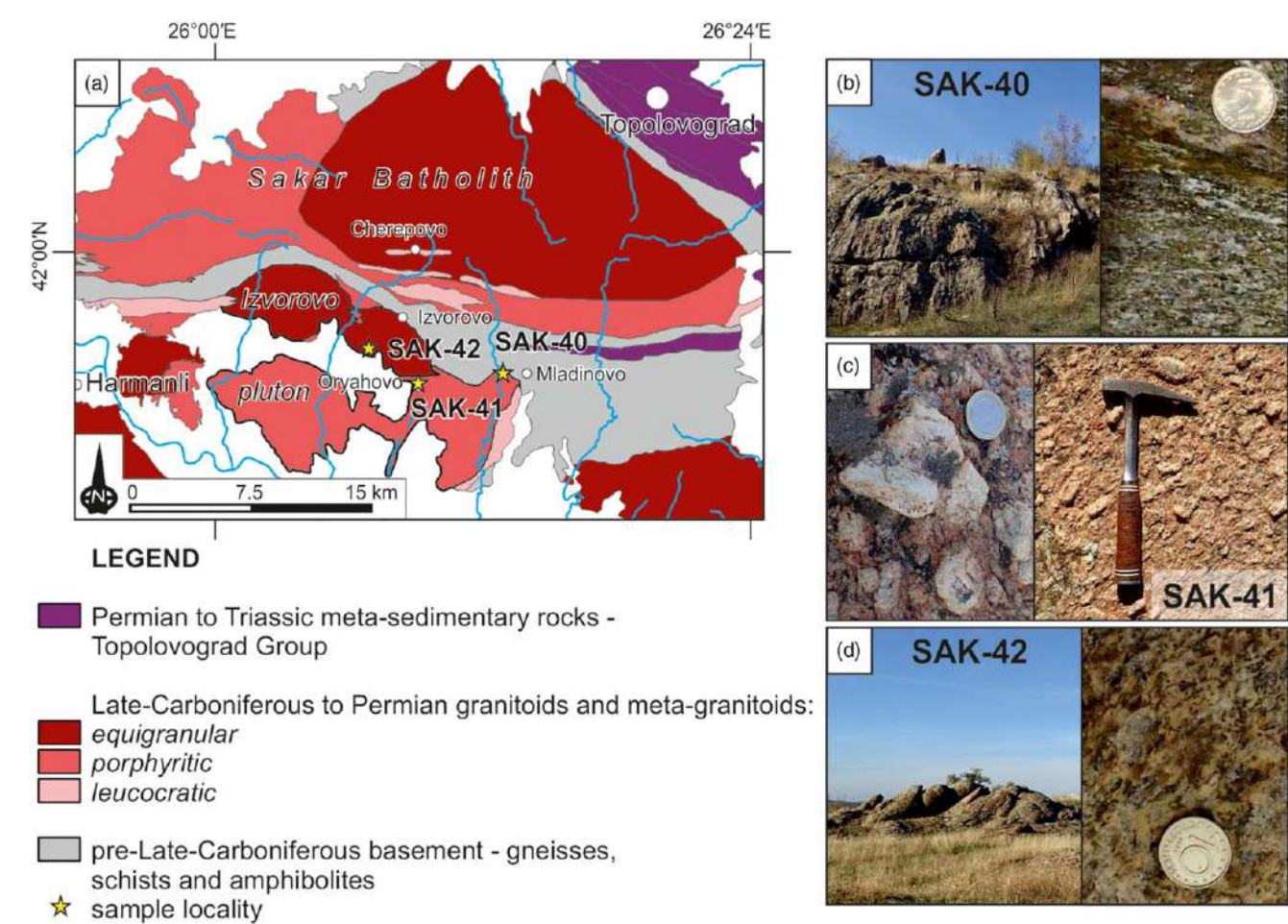


**Fig. 2.** (Colour online) Sample localities in the Izvorovo Pluton: (a) geological map of the Sakar Unit (modified after Okay et al. 2001; Gerdjikov, 2005; Natal'in et al. 2016); (b) strongly deformed orthogneiss with feldspar porphyroblasts (sample SAK-40), from the west of Mladinovo; (c) augen gneiss from which sample SAK-41 was collected from Oryahovo; (d) meta-granite (sample SAK-42) from southwest of Izvorovo.

**4. Analytical procedures**

**4.a. Sample preparation**

Three rock samples (SAK-40, SAK-41, SAK-42) were analysed in this study. Thin-sections were made from each sample and then petrographic observations in transmitted and reflected light were made using an Olympus BX-51 optical polarizing microscope at

the Institute of Earth Sciences, University of Silesia in Katowice, Poland. This was followed by scanning electron microscopy using back-scattered electron (BSE) imagery coupled to an energy-dispersive spectrometry (EDS) using a ThermoFisher Scientific Phenom XL Scanning Electron Microscope (SEM). For whole-rock geochemistry, all weathered material was removed from the samples, and the most homogeneous parts were



selected. The samples were then crushed using a jaw crusher before being pulverized in an agate ball mill to a powder. A representative aliquot was then despatched for analysis of major and trace elements at the Bureau Veritas Analytical Laboratories in Vancouver, Canada, after being coned and quartered. The litho-geochemical package selected included X-ray fluorescence (XRF) spectrometry for major elements and solution ICP-MS for trace elements, including rare earth elements (REE). Loss on ignition (LOI) on each sample was determined to obtain the volatile content. The resultant geochemical data were then plotted using the GeoChemical Data toolkit (GCDkit) of Janoušek *et al.* (2016).

Separation of zircon was undertaken at the Sample Preparation Laboratory, Institute of Geological Sciences, Polish Academy of Sciences, Kraków, Poland. These separations were made using conventional density separation techniques (i.e. crushing, sieving through a 0.315 mm mesh, washing and panning). Using a standard binocular microscope, zircon was then isolated from other accessory heavy minerals and placed into epoxy resin mounts of 25 mm diameter. The mounts were subsequently ground and the zircon grains polished to half thickness to expose their cores. Prior to U–Pb isotopic analyses, all zircon grains were imaged in transmitted and reflected light microscopy using the same Olympus BX-51 microscope, followed by scanning electron microscopy to reveal their internal textures for spot selection. Scanning electron microscopy was also undertaken with a Thermo Fischer Scientific Phenom XL SEM for BSE imagery of the zircon grains. Additionally, the zircon grains in the epoxy mounts were imaged by cathodoluminescence (CL) on a FET Phillips 30 SEM using a 15 kV accelerating voltage and a beam current of 1 nA to highlight the internal structures of the zircon grains. Prior to CL imaging, the epoxy mounts were carbon-coated. All of the respective petrographic imaging was made at the Institute of Earth Sciences, University of Silesia in Katowice. The carbon coating was then removed and the epoxy mounts were cleaned in an ultrasonic bath before U–Th–Pb isotopic measurements were undertaken.

#### 4.b. Sample analysis

Samples SAK-40, SAK-41 and SAK-42 then underwent U–Th–Pb isotopic analyses at the Department of Geology, Trinity College Dublin, Ireland, using a Photon Machines Analyte Excite 193 nm ArF excimer laser-ablation system with a HelEx 2-volume ablation cell, which was coupled to an Agilent 7900 mass spectrometer. The NIST612 standard glass was used to tune the instruments to obtain a Th/U of unity, and produce low oxide production rates (i.e.  $\text{ThO}^+/\text{Th}^+$  typically <0.15 %). A circular laser spot of 24  $\mu\text{m}$  was used, with a repetition rate of 11 Hz. Helium carrier gas was fed into the laser cell at  $\sim 0.4 \text{ L min}^{-1}$ , and was mixed with an aerosol of  $\sim 0.6 \text{ L min}^{-1}$  Ar make-up gas and  $11 \text{ mL min}^{-1}$   $\text{N}_2$ . Eight isotopes ( $^{90}\text{Zr}$ ,  $^{202}\text{Hg}$ ,  $^{204}\text{Pb}$ ,  $^{206}\text{Pb}$ ,  $^{207}\text{Pb}$ ,  $^{208}\text{Pb}$ ,  $^{232}\text{Th}$  and  $^{238}\text{U}$ ) were measured during each analysis. These analyses comprised 27.3 s of ablation (300 shots) and 12 s of washout time. The latter portions of the washout time were used for baseline measurements. The ‘VizualAge’ data reduction scheme (Petrus & Kamber, 2012) in the freeware IOLITE package (Paton *et al.* 2011) was used to undertake data reduction of the raw U–Th–Pb isotopic data. Downhole fractionation corrections to the raw data were then made to account for the long-term drift in isotopic or elemental ratios by normalizing all ratios to those of the U–Th–Pb reference materials. Conventional sample-standard bracketing was then applied. The 91500 zircon ( $^{206}\text{Pb}$ – $^{238}\text{U}$  age of  $1065.4 \pm 0.6 \text{ Ma}$ ;

Wiedenbeck *et al.* 1995, 2004) was used as the primary U–Pb calibration standard. The Plešovice zircon ( $^{206}\text{Pb}$ – $^{238}\text{U}$  age of  $337.13 \pm 0.37 \text{ Ma}$ ; Sláma *et al.* 2008) and WRS 1348 zircon ( $^{206}\text{Pb}$ – $^{238}\text{U}$  age of  $526.26 \pm 0.70$ ; Pointon *et al.* 2012) were used as secondary standards, and yielded respective ages of  $336.9 \pm 2.4 \text{ Ma}$  ( $^{206}\text{Pb}$ – $^{238}\text{U}$  weighted mean age,  $n = 13$ ) and  $526.6 \pm 3.7 \text{ Ma}$  ( $^{206}\text{Pb}$ – $^{238}\text{U}$  weighted mean age,  $n = 17$ ).

Following isotopic analysis, all analysed zircon grains in the epoxy mounts were again imaged by BSE, and subsequently interpreted using the pre-analysis BSE and CL images to verify any inadvertent mixtures of growth zones in the laser ablation sampling and measurements. The final geochronological calculations, Concordia diagrams as well as weighted mean diagrams were made using the Isoplot 3.75 macro for Microsoft Excel (Ludwig, 2012). In Table S1 (in the Supplementary Material available online at <https://doi.org/10.1017/S0016756821000650>), the data are provided at the  $2\sigma$  analytical uncertainty level. Weighted mean calculations and discordia intercept ages are also given at the  $2\sigma$  levels and include decay constant errors. Data with absolute discordance of <5 % ( $^{206}\text{Pb}/^{238}\text{U}$  vs  $^{205}\text{Pb}/^{237}\text{U}$ ) were treated as concordant data.

## 5. Results

### 5.a. Petrographic observations and whole-rock geochemistry

Sample SAK-40 is the most deformed rock investigated in this study. It was sampled from the area located closest to the orthogneiss – country-rock contact, with the country rock composed of amphibolites and biotite paragneisses. Sample SAK-40 represents a foliated porphyroclastic gneiss (Fig. 2b), which contains quartz, plagioclase, K-feldspar and two micas (muscovite and biotite), with accessory magnetite, as well as various Fe-oxides, zircon and fluorapatite (Fig. 3a, b). The gneiss has a well-defined foliation, composed of alternating layers of dark minerals (biotite, magnetite and Fe-oxides) and light minerals, mostly quartz and feldspars (Fig. 3a). The deformed porphyroclasts are composed of K-feldspar, are elongated and irregular in shape and are surrounded by fine-grained recrystallized quartz with an undulose extinction.

Sample SAK-41 (Fig. 2c) is an augen gneiss that contains large porphyroclasts of K-feldspar within a quartz, plagioclase and biotite–muscovite matrix, with accessory fluorapatite, zircon, titanite, monazite and ilmenite (Fig. 3c, d). The K-feldspar has characteristic microcline twinning (Fig. 3d) and is up to 3–4 cm in length. Titanite occurs within nests of co-genetic intergrowths of the two micas (Fig. 3c). The K-feldspar porphyroclasts are interpreted as phenocrysts inherited from the igneous protolith.

Sample SAK-42 is a coarse-grained, equigranular and weakly foliated meta-granite (Fig. 2d), which consists of plagioclase, quartz, K-feldspar, biotite and muscovite with accessory fluorapatite, zircon, monazite and Fe-oxides (Fig. 3e, f). Accessory minerals occur mostly within randomly distributed, irregular patches of two-mica intergrowths, surrounded by feldspars and quartz. This meta-granite is the least deformed rock sample collected in this study.

Whole-rock major- and trace-element compositions for three samples (SAK-40, SAK-41, SAK-42), and a compilation of the published data from other Late Carboniferous to Early Triassic plutons in the Strandja Zone are presented in Table S2 (in the Supplementary Material available online at <https://doi.org/10.1017/S0016756821000650>). The samples from Izvorovo Pluton are silica-rich (70.4–75.4 wt %  $\text{SiO}_2$ ) meta-granitoids and orthogneisses, which plot in the granite field on a  $\text{SiO}_2$  vs  $\text{Na}_2\text{O} + \text{K}_2\text{O}$

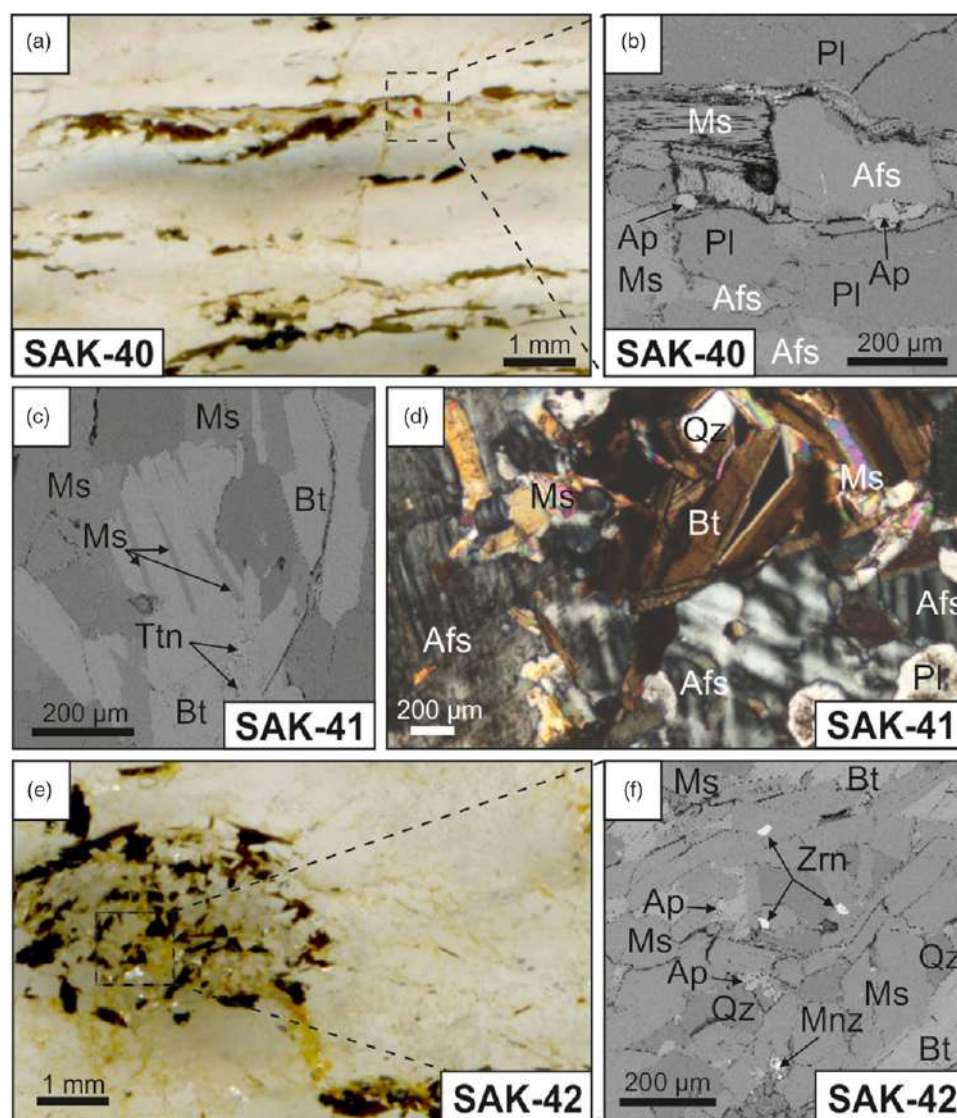


**Fig. 3.** (Colour online) Petrographic images of the gneisses and meta-granite from the Izvorovo Pluton: (a, b) orthogneiss sample SAK-40, (a) thin-section in plane-polarized light (PPL) showing foliation within the orthogneiss, (b) mineral assemblages in the BSE images; (c, d) augen gneiss sample SAK-41, (c) BSE image showing two-mica intergrowths surrounding accessory titanite, (d) thin-section image showing microcline twinning of K-feldspar porphyroclasts (under cross-polarized light); (e, f) meta-granite sample SAK-42, (e) PPL thin-section image showing the coarse-grained textures of the meta-granite, (f) BSE image showing the diverse mineral assemblage of the dark patches surrounded by coarse-grained K-feldspar and quartz. Qz, quartz; Pl, plagioclase; Afs, alkali feldspar; Bt, biotite; Ms, muscovite; Zrn, zircon; Ap, apatite; Ttn, titanite; Mnz, monazite.

diagram (Fig. 4a; Middlemost, 1994), and are peraluminous (Fig. 4b; Shand, 1943). The trace elements were normalized to the ocean-ridge granite (ORG) values of Pearce *et al.* (1984). Samples from the Izvorovo Pluton have similar trace element profiles, characterized by enrichments in K, Rb, Ba, Th and Ce and Sm relative to Ta, Nb, Hf, Zr, Y and Yb (Fig. 4c). These patterns show a resemblance to patterns from the Permian Kirklareli Pluton and Late Carboniferous to Early Permian Sakar Batholith; however, samples from Kirklareli Pluton have stronger negative Ta–Nb anomalies. The rare earth elements (REEs) were normalized to chondrite values of McDonough & Sun (1995; Fig. 4b). The samples show fractionation of the light REE (LREE) relative to heavy REE (HREE), and have negative Eu anomalies (0.31–0.35). These patterns are within the range of samples from Sakar Batholith and Kirklareli Pluton.

### 5.b. U–Pb zircon dating of Izvorovo meta-granitoids

LA-ICP-MS U–Th–Pb isotopic data of the analysed zircons for the samples SAK-40, SAK-41 and SAK-42 are listed in Table S1, in the Supplementary Material available online at <https://doi.org/10.1017/S0016756821000650>. Dates are reported as  $^{206}\text{Pb}$ – $^{238}\text{U}$  ages.

Orthogneiss sample SAK-40 from west of Mladinovo contains oscillatory zoned zircons that are euhedral to subhedral. Zircons are up to 180  $\mu\text{m}$  in length with aspect ratios of 1:1 and 1:2 (Fig. 5a). Some of the zircons have thin rims (up to 8  $\mu\text{m}$  in width), which were not analysed during this study. Thirty-one analyses were made on 30 zircon grains, from which 28 analyses are concordant (<5 % disc.; Table S1, in the Supplementary Material available online at <https://doi.org/10.1017/S0016756821000650>; Fig. 6a). From all the concordant data, one analysis is identified as of being a mixture of rim and oscillatory zoned zircon core in BSE and CL post-imaging, and is therefore excluded from further consideration in this study. The remaining data range from c. 248 Ma to c. 440 Ma, with a significant cluster on concordia between c. 248 Ma and c. 262 Ma (Fig. 6a). This cluster of 25 analyses defines a weighted mean  $^{206}\text{Pb}$ – $^{238}\text{U}$  age of  $254 \pm 2$  Ma (MSWD = 1.5; Fig. 6b). This age is interpreted as the crystallization age of the magmatic protolith. Two older analyses come from zircon cores (Fig. 5a) and are interpreted as inherited components.

Augen gneiss sample SAK-41 from Oryahovo contains zircons that are elongated and euhedral to subhedral. Zircons are up to 220  $\mu\text{m}$  in length, with aspect ratios of 1:1 to 4:1 (Fig. 5b). All zircons have strong oscillatory zonation. Some of the grains contain



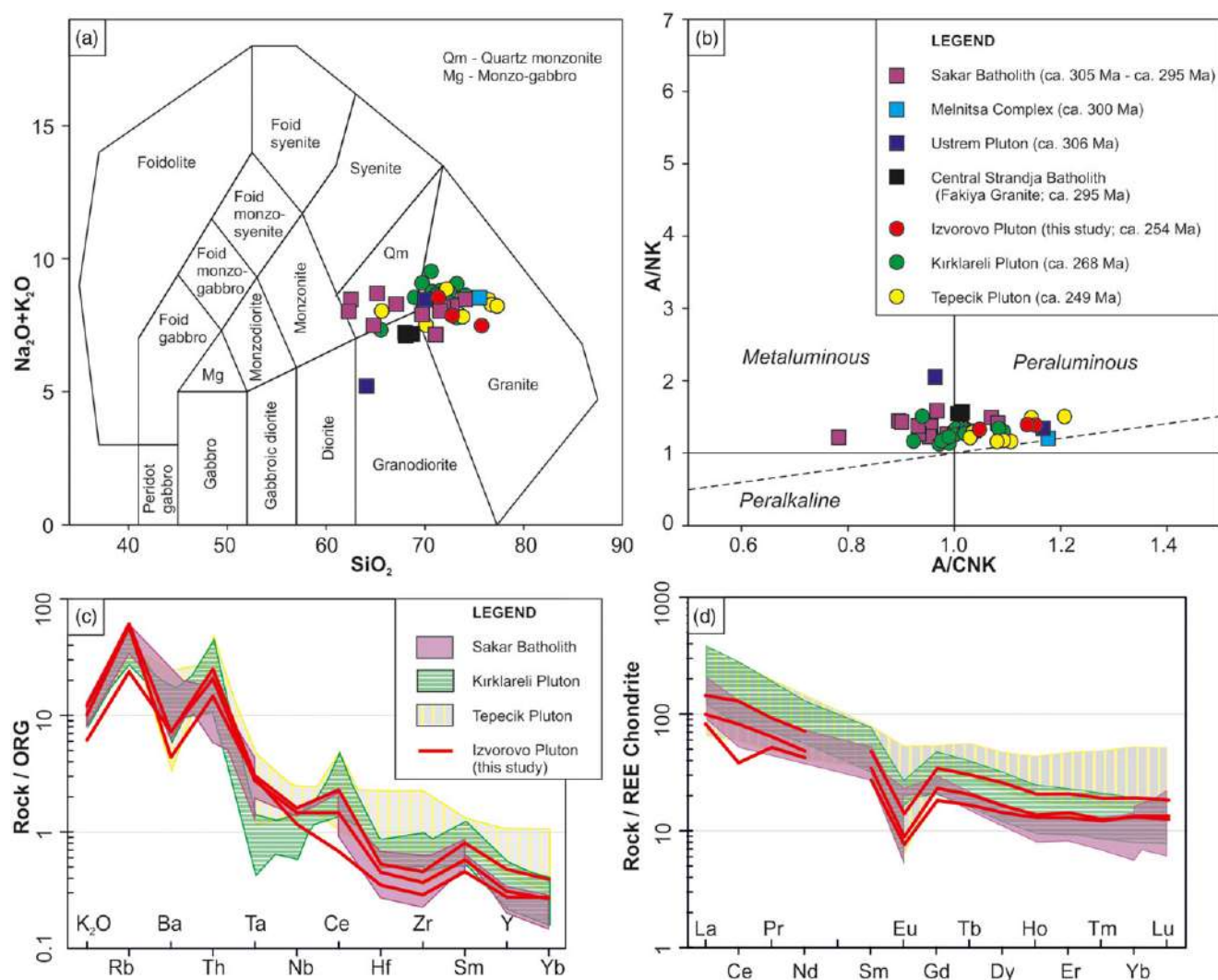


**Fig. 4.** (Colour online) Major and trace elements diagrams for meta-granitoids and gneisses from the Strandja Zone: (a) total alkali vs silica (TAS) diagram (Middlemost, 1994); (b) A/NK vs A/CNK plot of Shand (1943); (c) ocean ridge granite (ORG)-normalized diagram with normalization values after Pearce *et al.* (1984); (d) chondrite-normalized REE diagram with normalization values from McDonough & Sun (1995). Data from previous studies are from: Sunal *et al.* (2006), Kamenov *et al.* (2010), Machev *et al.* (2015), Aysal *et al.* (2018), Bonev *et al.* (2019a), and are given in Table S2 (in the Supplementary Material available online at <https://doi.org/10.1017/S0016756821000650>).

thin rims (~5 to ~10 µm in width), which were not analysed during this study. A total of 32 analyses were obtained from 27 grains (Table S1, in the Supplementary Material available online at <https://doi.org/10.1017/S0016756821000650>; Fig. 6c), of which 30 analyses were concordant (<5 % disc.). From all the concordant analyses, nine analyses were excluded from further consideration because they were obtained from mixed domains as revealed by BSE and CL post-analysis imagery. Of the remaining data, 21 data points from 19 grains with concordant  $^{206}\text{Pb}$ – $^{238}\text{U}$  ages ranging from c. 251 Ma to c. 269 Ma define a weighted mean  $^{206}\text{Pb}$ – $^{238}\text{U}$  age of  $256 \pm 3$  Ma (MSWD = 3.5). Although these data scatter beyond analytical uncertainty more than the cluster of data points in sample SAK-40, the calculated ages are within analytical uncertainty between the two samples. Thus, c. 256 Ma is interpreted as the emplacement age of the gneiss protolith.

Meta-granite sample SAK-42 from southwest of Izvorovo contains mostly subhedral, and stubby to elongate zircons (up to 240 µm in length, with aspect ratios of 1:1 to 3:1; Fig. 5c), and exhibiting oscillatory zoning. Some of the zircons have thin rims (up to 8 µm in width), which were not analysed during this study.

Thirty-two analyses from 30 grains were obtained (Table S1, in the Supplementary Material available online at <https://doi.org/10.1017/S0016756821000650>; Fig. 6d), of which two data points were discordant (>5 % disc.), and four were identified as mixed zones in post-analytical BSE and CL imaging, and were therefore excluded from further consideration. The remaining 26 data points range from c. 240 Ma to c. 460 Ma, of which 24 analyses scatter along concordia between c. 240 Ma and c. 263 Ma, with a weighted mean  $^{206}\text{Pb}$ – $^{238}\text{U}$  age of  $251 \pm 3$  Ma (MSWD = 3.5). This age is within analytical error of the crystallization age of the orthogneiss igneous protolith (SAK-40), and is interpreted as the crystallization age of the meta-granite. The two older analyses come from zircon cores and are interpreted as inherited components.

## 6. Discussion

### 6.a. Interpretation of geochronology and its regional context

All three samples from the Izvorovo Pluton yielded similar U–Pb zircon ages, ranging between  $251 \pm 3$  Ma and  $256 \pm 3$  Ma, with a



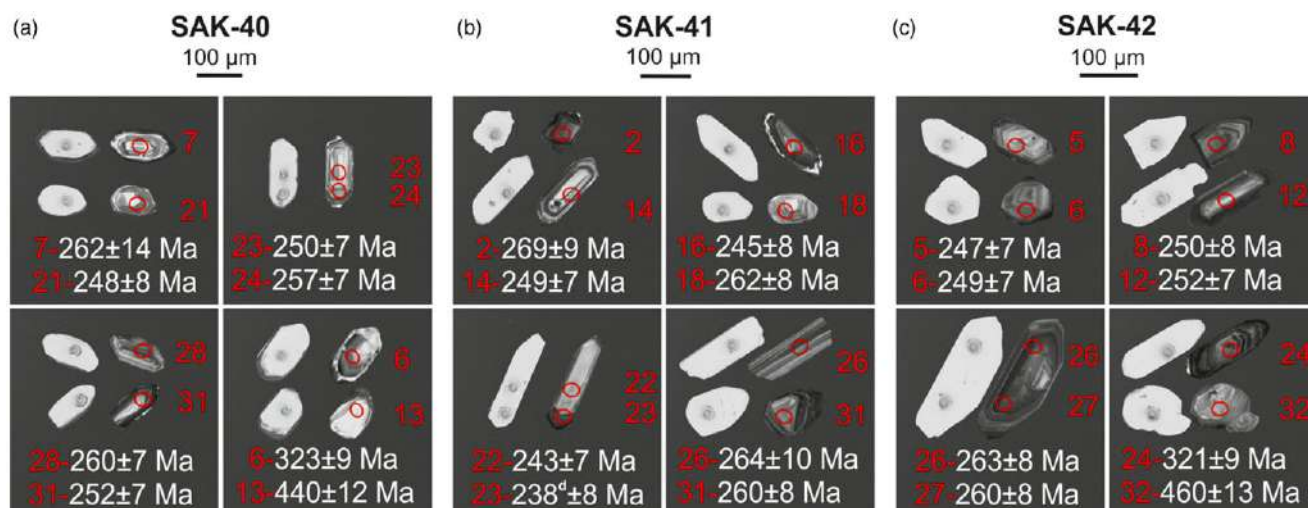


**Fig. 5.** (Colour online) BSE and CL images of representative zircons from: (a) sample SAK-40; (b) sample SAK-41; (c) sample SAK-42. Numbers represent the grain number, reported values are  $^{206}\text{Pb}/^{238}\text{U}$  ages, all presented ages are concordant (<5 % disc.) except for one discordant analysis (denoted d, which is disc. >5 %), and the white circles represent the laser ablation spot.

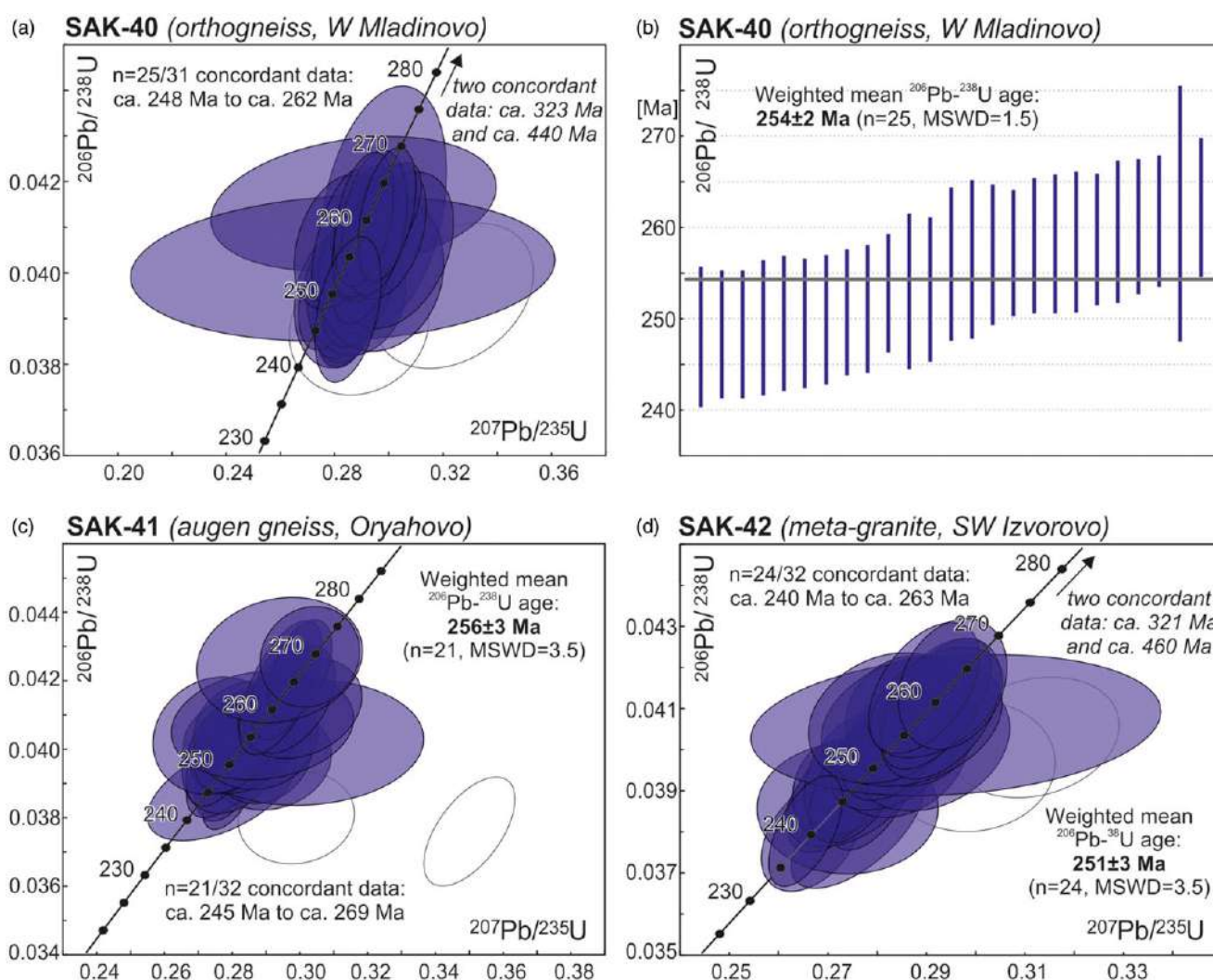


**Fig. 6.** (Colour online) LA-ICP-MS zircon U-Th-Pb analyses for sample: (a, b) SAK-40 (orthogneiss); (c) sample SAK-41 (augen gneiss); (d) sample SAK-42 (meta-granite); Wetherill Concordia diagrams (after Wetherill, 1956) are shown in (a), (b) and (d); the data shown as filled ellipses are used for age calculations, and black ellipses are discordant data (>5 %); analyses of mixed domains are not shown. All data-point error ellipses and error bars are at the 2 $\sigma$  uncertainty level.

weighted mean  $^{206}\text{Pb}/^{238}\text{U}$  age of  $254 \pm 5$  Ma. The time interval between  $251 \pm 3$  Ma and  $256 \pm 3$  Ma is considered as the crystallization age of the Izvorovo Pluton. This shows that both varieties of equigranular and porphyritic meta-granite from the Izvorovo Pluton, which used to be regarded as two different units of meta-granite and migmatite (Kozhoukharov & Kozhoukharova, 1973), are coeval. Within the zircon populations of the samples, xenocrysts were detected. Some inherited cores were analysed, and yielded concordant ages at 460–440 Ma and c. 320 Ma (Table S1, in the Supplementary Material available online at <https://doi.org/10.1017/S0016756821000650>). A 460–440 Ma magmatic episode within the Sakar Unit was recently described by Bonev *et al.* (2019a), who dated leucocratic stock meta-granites exposed to the east of the Sakar Batholith at  $462 \pm 3$  Ma. The younger population of zircon xenocrysts is consistent with 320–310 Ma ages obtained from zircons commonly found within the Sakar Batholith (Bonev *et al.* 2019a; Pristavova *et al.* 2019). The 320–310 Ma zircons documented from the Sakar Batholith are interpreted by Bonev *et al.* (2019a) and Pristavova *et al.* (2019) as ‘ante-crysts’, i.e. a group of crystals from an earlier pulse of magma which were incorporated by a later pulse. This suggests the occurrence of at least one earlier magmatic pulse in the Late Carboniferous within the Sakar Unit.

The crystallization age of the Izvorovo Pluton post-dates the emplacement of the Sakar Batholith (305–295 Ma; Peytcheva *et al.* 2016; Bonev *et al.* 2019a; Pristavova *et al.* 2019). Additionally, the Izvorovo Pluton underwent a later Late Jurassic to Early Cretaceous deformation and metamorphic event (Chatalov, 1990; Bonev *et al.*, 2020b), which is clearly visible in outcrop and in the petrographic data obtained from samples SAK-40 and SAK-41. The presented geochronological data invalidate the interpretation of Ivanov *et al.* (2001) and Gerdjikov (2005) that syn-kinematic magmatism (of assumed Late Jurassic to Early Cretaceous age) was the heat source for Early Alpine metamorphism. Thus, the question about the origin of the ‘anomalous’ high-grade metamorphism in the Sakar Mountains relative to the adjacent units remains open.

The Izvorovo Pluton is the first Permian–Triassic plutonic body described within the Sakar Unit, and is clearly emplaced 40 Myr later than Late Carboniferous – Early Permian intrusives such as the Sakar Batholith and coeval intrusions (c. 305 – c. 295 Ma; Peytcheva *et al.* 2016; Bonev *et al.* 2019a; Pristavova *et al.* 2019; Fig. 7; Table S3 in the Supplementary Material available online at <https://doi.org/10.1017/S0016756821000650>). Recently, new U–Pb ages ranging between 245 and 230 Ma were presented for the Harmanli Block Magmatic Complex (Bonev *et al.* 2019b) and St Iliya Heights (near Svetlina; Bonev *et al.* 2020a), located in the southwestern and northern part of the Sakar Unit (Fig. 2a), respectively. This shows that the magmatic evolution of the region is more complex than previously envisaged.

Although the Izvorovo Pluton provides the first evidence of Late Permian magmatism within the Sakar Unit, other Permian and Early Triassic plutons are known from the eastern part of the Strandja Zone. These plutons include the c. 268 Ma Kırklareli Pluton (Aysal *et al.* 2018), the c. 252 Ma Ömeroba Pluton (Natal'in *et al.* 2016; Fig. 7), and the c. 249 Ma Tepecik Pluton, which is located near Istanbul in the southeastern Strandja Zone (Aysal *et al.* 2018). For more detailed information about the published U–Pb zircon ages from Late Carboniferous to Triassic magmatic rocks in the Strandja Zone, see Table S3 in the Supplementary Material available online at <https://doi.org/10.1017/S0016756821000650>. Additionally, there are other published Pb–Pb ages for felsic bodies within the Strandja Unit which

were obtained by the single-zircon stepwise evaporation method (Table S3, in the Supplementary Material available online at <https://doi.org/10.1017/S0016756821000650>; Okay *et al.* 2001; Sunal *et al.* 2006); however, the inability to evaluate various factors (e.g. discordance) in such data means these ages will not be discussed further in this study.

### 6.b. Geochronological and geochemical arguments for two-stage magmatism in the Strandja Zone

Felsic to intermediate intrusive magmatism has played an important role in the crustal evolution of the Strandja Zone, as shown in Figure 7. The new geochronological data from this study and from the literature show that extensive magmatism began in the Late Carboniferous, and is almost continuous until the Triassic in both key components of the Strandja Zone, i.e. the Sakar and Strandja units (Table S3, in the Supplementary Material available online at <https://doi.org/10.1017/S0016756821000650>). The tectonic setting of the Strandja Zone is controversial and depends on the interpreted location of the zone with respect to (1) Variscan collision and (2) the subduction of the Palaeo-Tethys Ocean beneath Laurussia. The first scenario invokes Variscan collision between Gondwana and Laurussia in the granitoid formation (post-collisional granites; post-COLG) in the Strandja Zone. The peri-Gondwana continental magmatic arc, which consisted of the Balkanides, Strandja, Sakarya and Caucasus (BASSAC Block), collided with the Moesia and Istanbul Zone in the Middle Carboniferous (MOIS Block; Okay & Topuz, 2017). Within the Strandja Zone, Variscan metamorphism is observed in the pre-Late Carboniferous basement, which was affected by both Variscan and Early Alpine metamorphism (e.g. Okay *et al.* 2001). The exact age of Variscan metamorphism in the Strandja Zone remains unknown, but it is well established from the Balkanides (c. 340 – 330 Ma; Carrigan *et al.* 2006; Antić *et al.* 2016; Balkanska *et al.* 2021). The second scenario assumes that subduction of the Palaeo-Tethys Ocean beneath Laurussia played a primary role, resulting in various intrusions of volcanic-arc granites (VAG) in the Strandja Zone (Okay *et al.* 2001; Natal'in *et al.* 2016; Peytcheva *et al.* 2016; Aysal *et al.* 2018; Bonev *et al.* 2019a). This scenario is presented by Aysal *et al.* (2018), who suggested subduction-related magmatism with a transition from Permian arc magmatism to Middle Permian – Early Triassic back-arc magmatism. Rift-related felsic magmatism has also been proposed by some authors (i.e. Okay & Nikishin, 2015) for the surrounding regions (e.g. the Western Pontides). Rifting along a continental margin may be associated with back-arc basin development. The sedimentary rocks of the Topolovgrad Group in the Sakar Unit (Chatalov, 1990; Zagorchev *et al.* 2009) could have been deposited in this basin, which potentially initiated as a back-arc basin located in the northern part of the zone during the Permian–Triassic.

Geochemically, the Late Carboniferous to Early Triassic granitoids of the Strandja Zone are typical of either calc-alkaline volcanic-arc or post-collisional granites. The meta-granitoids from the Strandja Zone (Fig. 8a) plot within the post-collisional granite (post-COLG) field, which overlaps with the volcanic-arc granite (VAG) field on the Rb vs Y + Nb diagram (Pearce, 1996, after Pearce *et al.* 1984). The Rb–Hf–Ta ternary diagram (Harris *et al.* 1986; Fig. 8b) indicates that the Late Carboniferous to Early Permian Sakar Batholith and Late Permian Izvorovo Pluton plot within the collisional granite field, whereas data from the Permian Kırklareli Pluton, and most of the data from the Early Triassic Tepecik Pluton, lie within the VAG field. However, as was



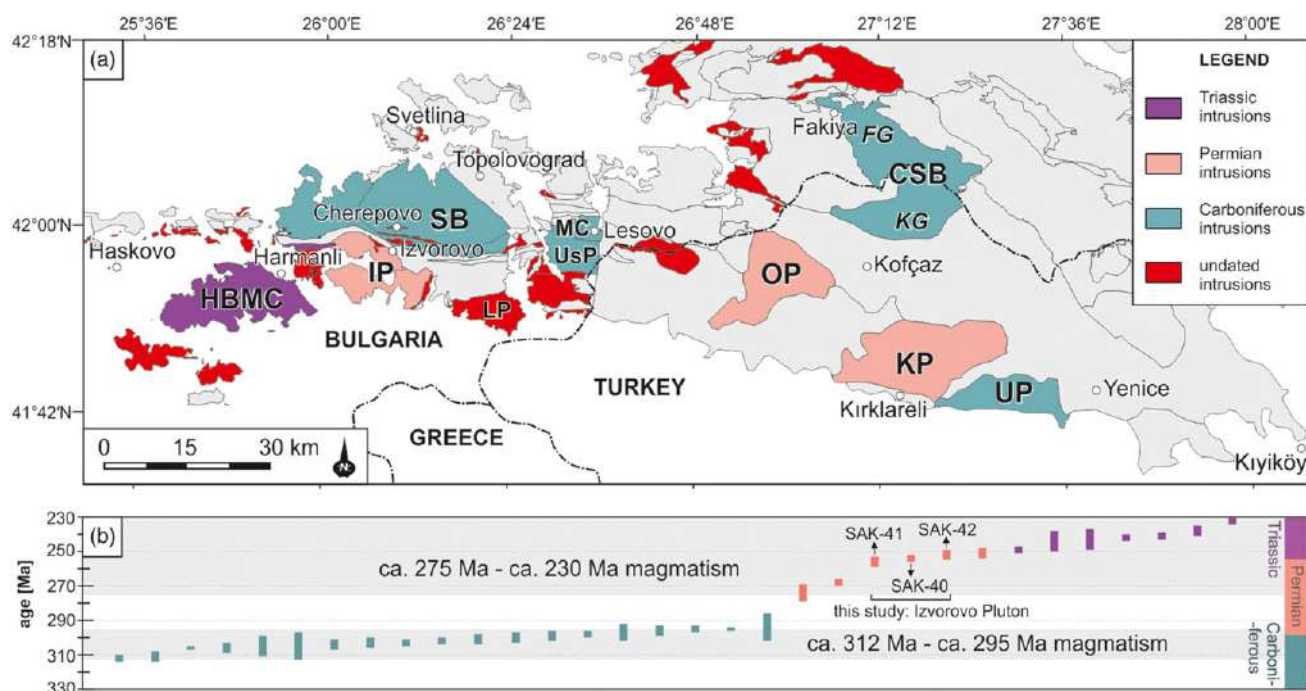


**Fig. 7.** (Colour online) Spatial and temporal distribution of the Late Carboniferous to Triassic magmatic rocks in the Strandja Zone: (a) geological map showing classification of plutonic bodies according to their age of emplacement (HBMK = Harmanli Block Magmatic Complex, IP = Izvorovo Pluton, SB = Sakar Batholith, LP = Levka Pluton, MC = Melnitsa Complex, UsP = Ustrem Pluton, OP = Ömeroba Pluton, KP = Kırklareli Pluton, UP = Üsküp Pluton, CSB = Central Strandja Batholith consisting of FG = Fakiya granite and KG = Kula granite); (b) summary of U–Pb zircon age determinations from all dated plutonic bodies within the Strandja Zone. Data sources are given in Table S3 (in the Supplementary Material available online at <https://doi.org/10.1017/S0016756821000650>).

shown by Harris *et al.* (1986), not all post-COLG magmas demonstrate the degree of Ta enrichment defined by the boundaries in Figure 8b. The geochemical data of the Late Carboniferous to Early Triassic meta-granitoids of the Strandja Zone also do not show a systematic trend in the temporal evolution of the magma chemistry, or in the tectonic setting inferred from those geochemical data. However, this interpretation is only based on empirical assumptions from geochemical diagrams, and can additionally be disturbed by Rb mobilization due to weathering or metamorphism which affected the granitoids.

The Late Carboniferous to Triassic magmatism is assigned by many authors as related to the subduction of the Palaeo-Tethys Ocean beneath the southern margin of Laurussia (Sunal *et al.* 2006; Natal'in *et al.* 2016; Aysal *et al.* 2018; Bonev *et al.* 2019a) with further magmatism in a back-arc setting in the Middle Triassic (Aysal *et al.* 2018). This interpretation is supported by published geochronological data which grouped all the intrusions as a single long-lived magmatic event. However, in this study, two stages (Late Carboniferous and Permian–Triassic) of magmatism in the Strandja Zone are now proposed. The first episode took place in the Late Carboniferous between *c.* 312 Ma and *c.* 295 Ma (Table S3, in the Supplementary Material available online at <https://doi.org/10.1017/S0016756821000650>; Georgiev *et al.* 2012; Machev *et al.* 2015; Natal'in *et al.* 2016; Peytcheva *et al.* 2016; Bonev *et al.* 2019a; Pristavova *et al.* 2019). It started with the intrusion of several small unnamed bodies described from the Kasatura and Kaletpe regions near Kiyiköy in the Strandja Unit (Fig. 1; Natal'in *et al.* 2016), and was followed by extensive emplacement of large plutons between *c.* 305 Ma and 295 Ma, e.g. the Sakar and Central Strandja batholiths. However, the presence of *c.* 320 to *c.* 310 Ma zircon antecrysts within plutonic rocks of the Sakar Batholith, Ustrem Pluton and Melnitsa Complex (Bonev *et al.* 2019a)

suggests that this early-stage magmatism was voluminous within the Strandja Zone. It confirms similarities to neighbouring areas where felsic intrusions with ages of *c.* 320–310 Ma are widespread, e.g. the Sakarya Zone (Ustaömer *et al.* 2012, 2013) and the eastern Mediterranean realm (Meinhold *et al.* 2008). Following the *c.* 312 to *c.* 295 Ma magmatic activity, after *c.* 20 Myr of quiescence, a more extended period of magmatism began in the Permian at *c.* 275 Ma, and which ceased in the Triassic by *c.* 230 Ma. The ages of the granitic bodies from this period are well established from the Strandja Unit (Natal'in *et al.* 2016; Aysal *et al.* 2018), whereas previously there was no evidence of coeval magmatism within the Sakar Unit. However, in this study, *c.* 251 Ma to *c.* 256 Ma ages for the Izvorovo Pluton are documented from the Sakar Unit. Additionally, *c.* 245 Ma to *c.* 230 Ma ages were presented for the Harmanli Block Magmatic Complex and St Iliya Heights (Bonev *et al.* 2019b, 2020a; Fig. 7).

These new data allow for the division of felsic to intermediate magmatism within the Strandja Zone into two age groups: (1) a short Late Carboniferous (*c.* 312 to *c.* 295 Ma) extensive magmatic event; and (2) Permian–Triassic magmatism (*c.* 275 to *c.* 230 Ma; Fig. 7b). These two age groups show significant differences in the characteristics of the zircon populations. The first group of Late Carboniferous granites show that within the population of typical oscillatory-zoned zircons, inherited components and antecrysts play an important role. In the *c.* 298 Ma albitized Sakar granitoid (Kanatara Quarry, Sakar Batholith), a considerable part of the analysed grains yielded ages between *c.* 330 Ma and *c.* 310 Ma, and were interpreted as antecrysts (Pristavova *et al.* 2019). Similar results were obtained from a *c.* 296 Ma porphyritic granite near Planinovo in the Sakar Batholith (sample S14), where half of the concordant zircon data range from *c.* 340 Ma to *c.* 310 Ma, and were interpreted as antecrysts. There is also a minor population

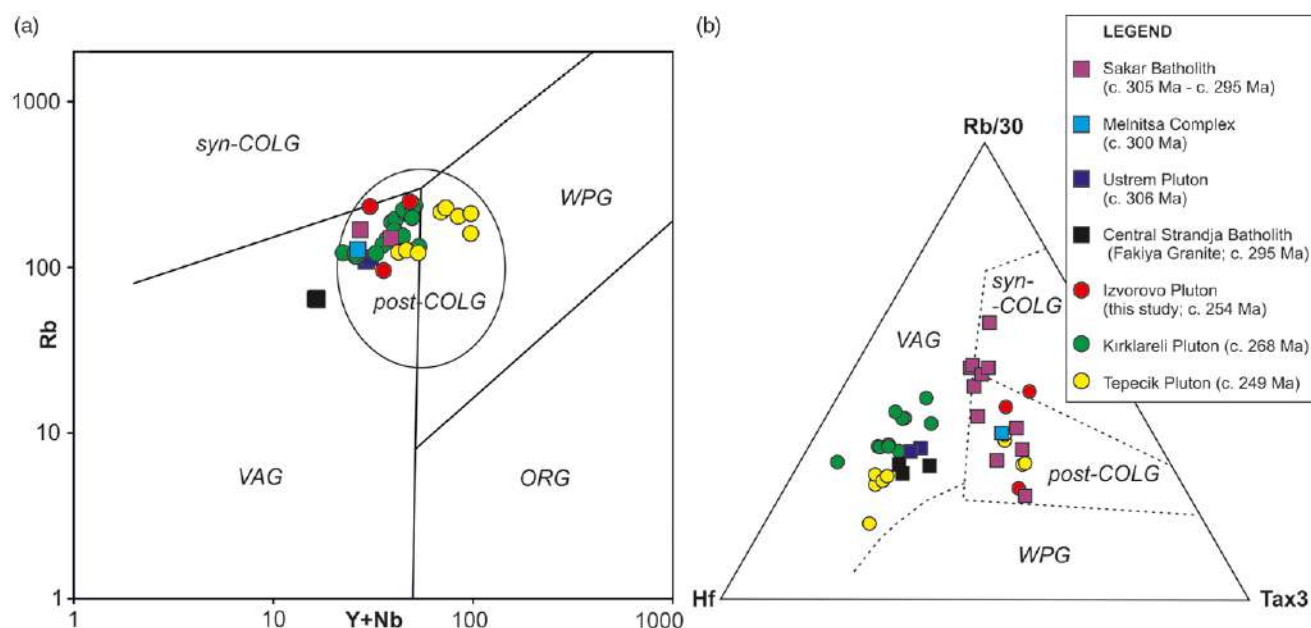


**Fig. 8.** (Colour online) Diagrams for discriminating the tectonic settings of granitic rocks: (a) the Rb-(Y + Nb) diagram (after Pearce, 1996, modified from Pearce *et al.* 1984); (b) the Rb-Hf-Ta ternary diagram (after Harris *et al.* 1986, modified from Pearce *et al.* 1984) distinguishing volcanic-arc granite (VAG), within-plate granite (WPG), syn-collisional granite (syn-COLG) and post-collisional granite (post-COLG). Data from previous studies are from Sunal *et al.* (2006), Kamenov *et al.* (2010), Machev *et al.* (2015), Aysal *et al.* (2018), Bonev *et al.* (2019a) and are given in Table S2 (in the Supplementary Material available online at <https://doi.org/10.1017/S0016756821000650>).

of xenocrysts (at c. 556 Ma and c. 636 Ma; Bonev *et al.* 2019a). A c. 295 Ma equigranular granite (Balgarska Polyana, Sakar Batholith, sample S4), dated by Bonev *et al.* (2019a), also contains abundant xenocrystic material (almost half of the concordant data) within the zircon population, with a broad age spectrum between c. 600 Ma and c. 370 Ma. The dominance of 330–310 Ma antecrysts within zircon populations was also detected from a c. 306 Ma meta-quartz diorite from the Ustrem Pluton (sample S36) and a c. 300 Ma porphyritic meta-granite from the Melnitsa Complex (sample S18), where they represent ~80 % of the concordant data (Bonev *et al.* 2019a). Because Late Carboniferous granitoids contain a large spectrum of components inside the zircon population, with a variety of ages ranging between c. 600 Ma and 305–295 Ma (the age of intrusion), the group can be classified as inheritance-rich granitoids.

On the other hand, the second group of Permian–Triassic intrusions do not contain a significant amount of antecrysts and xenocrysts. Aysal *et al.* (2018) showed that the zircon population of the c. 268 Ma Kırklareli meta-granite (sample KG-1) contained only a few inherited cores. Another study published by Natal'in *et al.* (2016) showed that within the zircon population of a c. 244 Ma leucocratic dyke cutting the Kırklareli Pluton (sample KI-231), all of the xenocrysts have an age directly related to the age of Kırklareli Pluton. This age range is between c. 270 Ma and c. 250 Ma, and therefore probably comes from assimilation of the host rock. A sample of c. 252 Ma porphyritic meta-granite from Ömeroba Pluton (KI-233.3) contains only two xenocrysts, with ages of c. 360 Ma and c. 330 Ma, respectively (Natal'in *et al.* 2016). A c. 249 Ma meta-granitoid from Tepecik Pluton (sample CT-23) had no xenocrysts or antecrysts (Aysal *et al.* 2018). Samples from Izvorovo Pluton contain only a few xenocrysts dated at c. 440 Ma and c. 323 Ma (sample SAK-40) and at c. 460 Ma and c. 321 Ma (SAK-42), respectively. The Permian–Triassic group represents inheritance-poor granitoids.

Zircon saturation temperatures ( $T_{Zr}$ ) calculated from bulk-rock compositions (after Watson & Harrison, 1983; Table S2, in the Supplementary Material available online at <https://doi.org/10.1017/S0016756821000650>) were used to estimate temperatures at which the magma solidified. The temperature calculated for the Sakar Batholith ranges between 717 °C and 805 °C (with average of 760 °C), and for other Late Carboniferous intrusions it is in the range 760–811 °C (with an average of 775 °C). The calculation for Permian Kırklareli Pluton and Triassic Tepecik Pluton yielded temperatures between 778 °C and 852 °C (mean of 805 °C) and 766 °C and 851 °C (mean of 810 °C, excluding one outlier of 932 °C), respectively. The zircon saturation temperatures for Permian Izvorovo Pluton from this study vary between 756 °C and 787 °C (mean of 768 °C). Therefore the Late Carboniferous granitoids with abundant inheritance yield lower  $T_{Zr}$  than inheritance-poor Permian–Triassic rocks with the exception of Izvorovo Pluton. According to Miller *et al.* (2003), the zircon saturation temperature should be interpreted in different ways for inheritance-rich and inheritance-poor granitoids. Inherited zircon components present in the granitoids indicate that the source was zircon-saturated and Zr is present mainly in crystals rather than melt, and  $T_{Zr}$  gives the upper limit on magma temperature. The lack of zircon inherited components implies that the source was undersaturated, and therefore the  $T_{Zr}$  calculated for inheritance-poor granitoids indicates a minimum initial magma temperature (Miller *et al.* 2003). This shows significant differences in magma temperatures between the Late-Carboniferous and Permian–Triassic intrusions in the Strandja Zone, because the maximum magma temperatures calculated for the inheritance-rich Late Carboniferous granitoids does not exceed 760 °C (for Sakar Batholith) and 775 °C (for other coeval granitoids), whereas the minimum magma temperatures for Permian–Triassic intrusions are 768 °C, 805 °C and 810 °C for the Izvorovo, Kırklareli and Tepecik plutons, respectively. Miller *et al.* (2003) proposed that there is a fundamentally different

mechanism of melt production between inheritance-rich and -poor intrusions. Inheritance-poor granitoids are interpreted according to currently accepted modes of felsic magma generation (i.e. dehydration melting in the crust; fractionation of mantle melts, with or without crustal contamination) and without incorporation of the inherited component during transport. However, generation of 'colder', inheritance-rich magma requires a source of water to lower the melt temperature, as the most visible mechanism for large-scale melting at temperatures <800 °C is infiltration of a water-rich fluid phase (Miller *et al.* 2003). Therefore, the inheritance-rich Late Carboniferous granitoids in the Strandja Zone were generated in a tectonic setting that did not reach especially high temperatures but was associated with fluid influx. The inheritance-poor Permian–Triassic intrusions were generated in a hotter, less fluid-rich environment; such settings include extensional or transtensional (Miller *et al.* 2003). This may be attributed to a possible change in the tectonic setting across the Carboniferous–Permian boundary.

The Late Carboniferous intrusions from the Strandja Zone invite correlation with the other Variscan post-collisional granites in the Balkanides. As shown by Carrigan *et al.* (2005), the dominant magmatic episode in the Balkanides took place in the interval between *c.* 315 Ma and *c.* 290 Ma. These authors also highlight that the Variscan Orogen in Bulgaria and the surrounding areas does not include an older phase of *c.* 340 Ma to 325 Ma magmatism, which was confirmed by recent work (e.g. Balkanska *et al.* 2021). This implies a similar evolution of the Balkanides and the western part of the Variscan Orogeny exposed in the Iberian Massif, where *c.* 340 Ma to *c.* 325 Ma felsic intrusions are also absent (Dias *et al.* 1998; Fernández-Suárez *et al.* 2000). A correlation between *c.* 315 Ma to *c.* 290 Ma post-collisional magmatism of the Balkanides and the Late Carboniferous meta-granitoids from Strandja Zone was proposed by Peytcheva *et al.* (2016). This interpretation has been disputed by other studies, which grouped together Late Carboniferous and Permian intrusions in the Strandja Zone into one long-lived period of subduction-related magmatism (e.g. Sunal *et al.* 2006; Natalin *et al.* 2016; Aysal *et al.* 2018; Bonev *et al.* 2019a). However, in this study, it is shown that Late Carboniferous to Triassic felsic to intermediate magmatism in the Strandja Zone represents two separate temporal stages. The younger, Permian–Triassic group is attributed to either subduction-related magmatism according to earlier models proposed for the Strandja Zone (i.e. Bonev *et al.* 2019a) or a rift-related setting, e.g. as inferred for the Western Pontides (Okay & Nikishin, 2015), or both, assuming a transition from a Permian arc setting to a Middle Permian – Early Triassic back-arc setting (Aysal *et al.* 2018). A rift-related environment is probably more likely as it may facilitate the high-temperature conditions required for magma generation (Miller *et al.* 2003). A rift-related setting for Permian to Triassic granitoids in the Strandja Zone is supported by the occurrence of a Permian–Triassic sequence of sedimentary rocks in the Topolovgrad Group located in the northeastern part of Sakar Unit (Chatalov, 1990; Zagorchev *et al.* 2009), which potentially have a back-arc basin affinity.

## 7. Conclusions

This study presents the first evidence of Permian magmatism in the Sakar Unit of the Strandja Zone, detected from the *c.* 251 to 256 Ma Izvorovo Pluton dated in this study. These ages disprove the interpretation of the Izvorovo Pluton as a possible heat source for Late Jurassic to Early Cretaceous metamorphism in the Sakar Unit

proposed by Ivanov *et al.* (2001) and Gerdjikov (2005). The Izvorovo Pluton is one of the largest magmatic bodies within the Sakar Unit, which has a complex magmatic evolution. Permian magmatism has already been well documented in the Strandja Unit, therefore this study allows for better correlation between the various magmatic units within the Strandja Zone. The results presented here highlight the significance of long-lived Permian–Triassic magmatism within the Strandja Zone (Fig. 7). The large granitic bodies intruded into pre-Late Carboniferous basement throughout the whole area from the westernmost vicinity of the Strandja Zone near Harmanli, to the southeastern part located close to Istanbul. These plutons consist of variably deformed and metamorphosed granitoids, which show evidence of post-Triassic metamorphism and deformation. However, all the presented data (i.e. field observations, petrography, geochemistry and geochronology), indicate that even the strongly sheared porphyroclastic gneisses preserve their igneous origin. Permian–Triassic magmatism was preceded by Late Carboniferous to Early Permian (*c.* 312 to *c.* 295 Ma) intrusions known from both parts of the Strandja Zone (e.g. the Sakar and Central Strandja batholiths; Table S3, in the Supplementary Material available online at <https://doi.org/10.1017/S0016756821000650>). Between an intensive short-lived Late Carboniferous event and a series of long-lived Permian to Triassic magmatic events, there was *c.* 20 Myr of magmatic quiescence. These two groups were distinguished based on geochronological data, and supported by inherited zircon populations and zircon saturation temperatures.

The two stages of felsic to intermediate magmatism during the Late Carboniferous to Triassic are attributed to changes in tectonic setting. One possible scenario is emplacement of post-collisional Late Carboniferous granitoids associated with the Variscan Orogeny. This was followed by intrusion of Permian–Triassic granitoids connected either with subduction-related or rift-related settings. The subduction-related scenario is in agreement with the interpretation of the Variscan Belt evolution in the Black Sea region (Okay & Topuz, 2017), whereas the rift-related scenario is consistent with models proposed for the western part of Pontides (i.e. Okay & Nikishin, 2015). This emphasizes the significance of the Strandja Zone as a link in the evolution of the Balkanides and Pontides.

**Acknowledgements.** We wish to thank the Editor, Peter Clift, as well as Wolfgang Dörr and two anonymous reviewers for comments which improved the manuscript. This research was supported by a Preludium Grant awarded to A.S. from the National Science Centre (Narodowe Centrum Nauki), NCN, in Poland (grant agreement no. UMO-2018/29/N/ST10/00368). D.C. is supported in part by a research grant from Science Foundation Ireland (SFI) under Grant Number 13/RC/2092 and 13/RC/2092\_P2 and co-funded under the European Regional Development Fund and by PIPCO RSG and its member companies. The authors would like to thank Nikolay Gospodinov for logistical support during the field trip, and Rafał Juroszek for help with the BSE imaging, as well as Alex Kounov for scientific discussions.

**Declaration of interest.** The authors declare none

**Supplementary material.** To view supplementary material for this article, please visit <https://doi.org/10.1017/S0016756821000650>

## References

- Antić M, Peytcheva I, Von Quadt A, Kounov A, Trivić B, Serafimovski T, Tasev G, Gerdjikov I and Wetzel A (2016) Pre-Alpine evolution of a segment of the North-Gondwanan margin: geochronological and geochemical evidence from the central Serbo-Macedonian Massif. *Gondwana Research* 36, 523–44.



- Aysal N, Şahin SY, Güngör Y, Peytcheva I and Öngen S (2018) Middle Permian–Early Triassic magmatism in the Western Pontides, NW Turkey: geodynamic significance for the evolution of the Paleo-Tethys. *Journal of Asian Earth Sciences* **164**, 83–103.
- Balkanska E, Gerdjikov I, Georfiiev S, Lazarova A, Dörr W and Kounov A (2021) Structural and geochronological constraints on the magmatic and tectonic events in the pre-Alpine basement of the central parts of the Balkan fold-thrust belt (Central Stara Planina Mountains, Bulgaria). *International Journal of Earth Sciences* **110**, 1181–211.
- Bedi Y, Vasilev E, Dabovski C, Ergen A, Okuyucu C, Dogan A, Kagan Tekin U, Ivanova D, Boncheva I, Lakova I, Sachanski V, Kuscı I, Tuncay E, Gülnur Demiray D, Soykan H and Cemal Goncuoglu M (2013) New age data from the tectonostratigraphic units of the Istranca 'Massif' in NW Turkey: a correlation with SE Bulgaria. *Geologica Carpathica* **64**, 255–77.
- Bonev N, Filipov P, Raicheva R and Moritz R (2019a) Timing and tectonic significance of Paleozoic magmatism in the Sakar unit of the SakarStrandzha Zone, SE Bulgaria. *International Geology Review* **61**, 1957–79.
- Bonev N, Filipov P, Raicheva R and Moritz R (2019b) Triassic magmatism along the Maritsa river valley, Sakar-Strandzha Zone, Bulgaria. *Review of the Bulgarian Geological Society* **80**, 56–7.
- Bonev N, Filipov P, Raicheva R and Moritz R (2020a) Triassic magmatism along the Eurasian margin of the Palaeotethys: U–Pb zircon age constraints from the western part of the Sakar-Strandzha Zone, Bulgaria. *EGU General Assembly Conference Abstracts* 9122.
- Bonev N, Spikings R and Moritz R (2020b)  $^{40}\text{Ar}/^{39}\text{Ar}$  age constraints for an early Alpine metamorphism of the Sakar unit, Sakar–Strandzha zone, Bulgaria. *Geological Magazine* **157**, 2106–12.
- Bonin B, Azzouni-Sekkal A, Bussy F and Ferrag S (1998) Alkali-calcic and alkaline post-orogenic (PO) granite magmatism: petrologic constraints and geodynamic settings. *Lithos* **45**, 45–70.
- Boyadjiev S and Lilov P (1972) On the K–Ar dating of the South Bulgarian granitoids from Srednogie and Sakar-Strandja Zones. *Proceedings of the Geological Institute, ser. Geochemistry, Mineralogy, Petrography* **26**, 121–220 (in Bulgarian).
- Boyanov I, Kozhoukharov D and Savov S (1965) Geological structure of the southern slope of Sakar Mountain between the villages Radovets and Kostur. *Review of the Bulgarian Geological Society* **26**, 121–34 (in Bulgarian).
- Carrigan C, Mukasa S, Haydoutov I and Kolcheva K (2006) Neoproterozoic magmatism and Carboniferous high-grade metamorphism in the Sredna Gora Zone, Bulgaria: an extension of the Gondwana-derived Avalonian–Cadomian belt? *Precambrian Research* **147**, 404–16.
- Carrigan CW, Mukasa SB, Haydoutov I and Kolcheva K (2005) Age of Variscan magmatism from the Balkan sector of the orogen, central Bulgaria. *Lithos* **82**, 125–47.
- Cattò S, Cavazza W, Zattin M and Okay A (2018) No significant Alpine tectonic overprint on the Cimmerian Strandja Massif (SE Bulgaria and NW Turkey). *International Geology Review* **60**, 513–29.
- Chatalov G (1988) Recent developments in the geology of the Strandzha zone in Bulgaria. *Bulletin of the Technical University of Istanbul* **41**, 433–66.
- Chatalov GA (1990) *Geology of the Strandja Zone in Bulgaria. Geologica Balcanica, series operum singulorum* 4. Sofia: Bulgarian Academy of Sciences, 263 pp. (in Bulgarian).
- Dias G, Leterrier J, Mendes A, Simões PP and Bertrand JM (1998) U–Pb zircon and monazite geochronology of postcollisional Hercynian granitoids from the Central Iberian Zone (northern Portugal). *Lithos* **45**, 349–69.
- Dimitrov S (1956) Die kinetische Regionalmetamorphose der Jurassischen Ablagerungen und Leucogranite in Süd-Ost Bulgarien. *Abhandlungen des XX Internationalen Geologischen Kongress. In Mexico*, 327–33.
- Dimitrov S (1959) Kurze Übersicht der metamorphen Komplexe in Bulgarien. *Freiberger Forschungshefte, Reih. C, H.* **57**, 62–72.
- Fernández-Suárez J, Dunning GR, Jenner GA and Gutiérrez-Alonso G (2000) Variscan collisional magmatism and deformation in NW Iberia: constraints from U–Pb geochronology of granitoids. *Journal of the Geological Society* **157**, 565–76.
- Franke W, Ballèvre M, Cocks LRM, Torsvik TH and Żelaźniewicz A (2020) Variscan Orogeny. In *Encyclopedia of Geology*, 2nd edn. London: Academic Press, 338–49.
- Gallhofer D, Von Quadt A, Peytcheva I, Schmid SM and Heinrich CA (2015) Tectonic, magmatic, and metallogenic evolution of the Late Cretaceous arc in the Carpathian–Balkan orogen. *Tectonics* **34**, 1813–36.
- Gawęda A and Golonka J (2011) Variscan plate dynamics in the circum-Carpathian area. *Geodinamica Acta* **24**, 141–55.
- Georgiev S, Von Quadt A, Heinrich C, Peytcheva I and Marchev P (2012) Time evolution of rifted continental arc: integrated ID-TIMS and LAICPMS study of magmatic zircons from the Eastern Srednogie, Bulgaria. *Lithos* **154**, 53–67.
- Gerdjikov I (2005) Alpine metamorphism and granitoid magmatism in the Strandja Zone: new data from the Sakar Unit, SE Bulgaria. *Turkish Journal of Earth Sciences* **14**, 167–83.
- Harris NBW, Pearce JA and Tindle AG (1986) Geochemical characteristics of collision zone magmatism. In *Collision Tectonics* (eds MP Coward and AC Ries), pp. 67–81. Geological Society of London, Special Publication no. 19.
- Haydoutov I (1989) Precambrian ophiolites, Cambrian island arc, and Variscan suture in the South Carpathian–Balkan region. *Geology* **17**, 905–8.
- Himmerkus F, Anders B, Reischmann T and Kostopoulos D (2007) Gondwana-derived terranes in the northern Hellenides. In *4-D Framework of Continental Crust* (eds RDPCM Hatcher Jr, JH McBride and JR Martínez Catalán), pp. 379–90. Boulder, Colorado: Geological Society of America Memoir 200.
- Ivanov Z, Gerdjikov I and Kounov A (2001) New data and considerations about structure and tectonic evolution of Sakar region, SE Bulgaria. *Annuaire de l'Université de Sofia, Geology and Geography* **91**, 35–80 (in Bulgarian).
- Ivanov Ž (2017) *Tectonics of Bulgaria*. Sofia: Sofia University Press, 331 pp. (in Bulgarian).
- Janoušek V, Moyen JF, Martin H, Erban V and Farrow C (2016) *Geochemical Modelling of Igneous Processes: Principles and Recipes in R Language*. New York: Springer Geochemistry.
- Jordanov M, Sarov S, Georgiev ST, Marinova R, Dobrev G, Grozdev V, Balkanska E and Moskovska L (2008) *Explanatory Notes to the Geological Map of the Republic of Bulgaria 1: 50,000 sheet K-35-76-B (Harmanly)*. Sofia: Geocomplex, 60 pp.
- Kamenov BK, Vergilov V, Dabovski C, Vergilov I and Ivchinova L (2010) The Sakar Batholith: petrology, geochemistry and magmatic evolution. *Geochemistry, Mineralogy and Petrology* **48**, 1–37.
- Kozhoukharov D and Kozhoukharova E (1973) Stratigraphy and petrology of the Precambrian metamorphic rocks from the Sakar Mountain. *Bulletin of the Geological Institute – Series Geochemistry, Mineralogy and Petrography* **22**, 193–210 (in Bulgarian).
- Ludwig KR (2012) *Isoplot 3.75: A Geochronological Toolkit for Microsoft Excel*. Berkeley, California: Geochronology Center Special Publication 5.
- Machev PH, Ganey V and Klain L (2015) New LA-ICP-MS U–Pb zircon dating for Strandja granitoids (SE Bulgaria): evidence for two-stage late Variscan magmatism in the internal Balkanides. *Turkish Journal of Earth Sciences* **24**, 230–48.
- Mayringer F, Treloar PJ, Gerder A, Finger F and Shengelia D (2011) New age data from the Dzirula massif, Georgia: implications for the evolution of the Caucasian Variscides. *American Journal of Science* **311**, 404–41.
- McCann T (2008) *The Geology of Central Europe: Volume 1: Precambrian and Palaeozoic*. Geological Society of London, 748 pp.
- McDonough W and Sun SS (1995) The composition of the Earth. *Chemical Geology* **67**, 1050–6.
- Meinhold G, Reischmann T, Kostopoulos D, Lehnert O, Matukov D and Sergeev S (2008) Provenance of sediments during subduction of Palaeotethys: detrital zircon ages and olivolith analysis in Palaeozoic sediments from Chios Island, Greece. *Palaeogeography, Palaeoclimatology, Palaeoecology* **263**, 71–91.
- Michard A, Soulaïmani A, Hoepffner C, Ouanaimi H, Baïdier L, Rjimiati EC and Saddiqi O (2010) The South-Western branch of the Variscan Belt: evidence from Morocco. *Tectonophysics* **492**, 1–24.
- Middlemost E (1994) Naming materials in the magma/igneous rock system. *Earth Science Review* **37**, 215–24.
- Miller CF, McDowell SM and Mapes RW (2003) Hot and cold granites? Implications of zircon saturation temperatures and preservation of inheritance. *Geology* **31**, 529–32.

- Natal'in B, Sunal G, Gün E, Wang B and Zhiqing Y (2016) Precambrian to Early Cretaceous rocks of the Strandja Massif (northwestern Turkey): evolution of a long lasting magmatic arc. *Canadian Journal of Earth Sciences* **53**, 1312–35.
- Okay A, Nikishin AM (2015) Tectonic evolution of the southern margin of Laurasia in the Black Sea region. *International Geology Review* **57**(5–8), 1051–1076.
- Okay A, Satur M, Tüysüz O, Akyüz S and Chen F (2001) The tectonics of Strandja Massif: late-Variscan and mid-Mesozoic deformation and metamorphism in the northern Aegean. *International Journal of Earth Science* **90**, 217–33.
- Okay A and Topuz G (2017) Variscan orogeny in the Black Sea region. *International Journal of Earth Sciences* **106**, 569–92.
- Paton C, Hellstrom J, Paul B, Woodhead J and Hergt J (2011) Iolite: freeware for the visualisation and processing of mass spectrometric data. *Journal of Analytical Atomic Spectrometry* **26**, 2508–18.
- Pearce J (1996) Sources and settings of granitic rocks. *Episodes* **19**, 120–5.
- Pearce J, Harris N and Tindle AG (1984) Trace element discrimination diagrams for the tectonic interpretation of granitic rocks. *Journal of Petrology* **25**, 956–83.
- Petrus JA and Kamber BS (2012) VizualAge: a novel approach to laser ablation ICP-MS U-Pb geochronology data reduction. *Geostandards and Geoanalytical Research* **36**, 247–70.
- Peytcheva I, Georgiev S and Von Quadt A (2016) U/Pb ID-TIMS dating of zircons from the Sakar-Strandzha Zone: new data and old questions about the Variscan orogeny in SE Europe. In *Proceedings of the Annual Conference of the Bulgaria Geological Society 'Geosciences 2016'*, pp. 71–72. Sofia: Bulgarian Geological Society.
- Pointon MA, Cliff RA and Chew DM (2012) The provenance of Western Irish Namurian Basin sedimentary strata inferred using detrital zircon U-Pb LA-ICP-MS geochronology. *Geological Journal* **47**, 77–98.
- Pristavova S, Tzankova N, Gospodinov N and Filipov P (2019) Petrological study of metasomatic altered granitoids from Kanarata Deposit, Sakar Mountain, southeastern Bulgaria. *Journal of Mining and Geological Sciences* **62**, 53–61.
- Sengör AMC (1979) Mid-Mesozoic closure of Permo Triassic Tethys and its implications. *Nature* **279**, 590–3.
- Sengör AMC (1984) The cimmeric orogenic system and the tectonics of Eurasia. *Geological Society of America, Special Paper* 195.
- Sengör AMC, Altiner D, Cin A, Ustaömer T and Hsü KJ (1988) Origin and assembly of the Tethyside orogenic collage at the expense of Gondwana Land. Gondwana and Tethys (ed. MG Audley-Charles), pp. 119–81. *Geological Society of London, Special Publication* no. 37.
- Shand SJ (1943) *Eruptive Rocks: their Genesis, Composition, Classification, and Their Relation to Ore-Deposits, with a Chapter on Meteorite*. New York: Wiley.
- Sláma J, Košler J, Condon DJ, Crowley JL, Gerdes A, Hanchar JM, Horstwood MSA, Morris GA, Nasdala L and Norberg N (2008) Plešovice zircon: a new natural reference material for U–Pb and Hf isotopic microanalysis. *Chemical Geology* **249**, 1–35.
- Spahić D and Gaudenyu T (2018) Primordial geodynamics of Southern Carpathian-Balkan basements (Serbo-Macedonian Mass): Avalonian vs. Cadomian arc segments. *Proceedings of the Geologists' Association* **130**, 142–56.
- Stampfli GM (2000) Tethyan oceans. In *Tectonics and Magmatism in Turkey and the Surrounding Area* (eds E Bozkurt, JA Winchester and JDA Piper), pp. 1–23. Geological Society of London, Special Publication no. 173.
- Stampfli GM and Kozur HW (2006) Europe from the Variscan to the Alpine cycles. In *European Lithosphere Dynamics* (eds DG Gee and RA Stephenson), pp. 57–82. Geological Society of London Memoir 32.
- Stephan T, Kroner U, Romer RL and Rösel D (2019) From a bipartite Gondwanan shelf to an arcuate Variscan belt: the early Paleozoic evolution of northern Peri-Gondwana. *Earth-Science Reviews* **192**, 491–512.
- Sunal G, Natal'in BA, Satir M and Toraman E (2006) Paleozoic magmatic events in the Strandja Massif, NW Turkey. *Geodinamica Acta* **19**, 283–300.
- Szopa K, Sałacińska A, Gumsley AP, Chew D, Petrov P, Gawęda A, Zagórska A, Deput E, Gospodinov N and Banasik K (2020) Two-stage Late Jurassic to Early Cretaceous hydrothermal activity in the Sakar Unit of southeastern Bulgaria. *Minerals* **10**, 266. doi: 10.3390/min10030266.
- Tzankova N and Pristavova S (2007a) New data about petrography and mineralogy of garnet-bearing mica schists in the frame of the Sakar pluton, SE Bulgaria. *Comptes rendus de l'Académie bulgare des Sciences* **60**, 159–64.
- Tzankova N and Pristavova S (2007b) Metamorphic evolution of garnet-bearing schists from Sakar Mountain, southeastern Bulgaria. *Comptes rendus de l'Académie bulgare des Sciences* **60**, 271–8.
- Ustaömer PA, Ustaömer T and Robertson AHF (2012) Ion probe U–Pb dating of the Central Sakarya Basement: a peri-Gondwana terrane intruded by Late Lower Carboniferous subduction/collision-related granitic rocks. *Turkish Journal of Earth Sciences* **21**, 905–32.
- Ustaömer T, Robertson AHF, Robertson AHF, Ustaömer PA, Gerdes A and Peytcheva I (2013) Constraints on Variscan and Cimmerian magmatism and metamorphism in the Pontides (Yusufeli–Artvin area), NE Turkey from U–Pb dating and granite geochemistry. In *Geological Development of Anatolia and the Easternmost Mediterranean Region* (eds AHF Robertson, O Parlak and UC Ünlügenç), pp. 49–74. Geological Society of London, Special Publication no. 372.
- Von Raumer JF (2013) Pre-Mesozoic Alpine basements: their place in the European Paleozoic framework. *GSA Bulletin* **125**, 89–108.
- Watson EB and Harrison TM (1983) Zircon saturation revisited: temperature and composition effects in a variety of crustal magma types. *Earth and Planetary Science Letters* **64**, 295–304.
- Wetherill GW (1956) Discordant uranium-lead ages, I. *Eos, Transactions of the American Geophysical Union* **37**, 320–6.
- Wiedenbeck M, Alle P, Corfu F, Griffin WL, Meier M, Oberli FV, Von Quadt A, Roddick JC and Spiegel W (1995) Three natural zircon standards for U–Th–Pb, Lu–Hf, trace element and REE analyses. *Geostandards Newsletter* **19**, 1–23.
- Wiedenbeck M, Hanchar JM, Peck W, Sylvester P, Valley J, Whitehouse M, Kronz A, Morishita Y, Nasdala L, Fiebig J, Franchi I, Girard J-P, Greenwood RC, Hinton R, Kita N, Mason PRD, Norman M, Ogasawara M, Piccoli PM, Rhede D, Satoh H, Schulz-Dobrick B, Skår O, Spicuzza MJ, Terada K, Tindle A, Togashi S, Vennemann T, Xie Q and Zheng Y-F (2004) Further characterisation of the 91500 zircon crystal. *Geostandards and Geoanalytical Research* **28**, 9–39.
- Zagorchev I, Dabovski CH and Nikolov T (2009) *Geology of Bulgaria, Volume II, Part 5: Mesozoic Geology*. Sofia: 'Prof. Marin Drinov' Academic Publishing House, 355 pp. (in Bulgarian).
- Zulauf G, Dörr W, Fisher-Spurlock SC, Gerder A, Chatzaras V and Xypolias P (2014) Closure of the Paleotethys in the External Hellenides: constraints from U–Pb ages of magmatic and detrital zircons (Crete). *Gondwana Research* **28**, 642–67.



# Variscan magmatic evolution of the Strandja Zone (Southeast Bulgaria and northwest Turkey) and its relationship to other north Gondwanan margin terranes

Anna Sałacińska<sup>a,b,\*</sup>, Ianko Gerdjikov<sup>c</sup>, Alexandre Kounov<sup>d</sup>, David Chew<sup>e</sup>, Krzysztof Szopa<sup>b</sup>, Ashley Gumsley<sup>b</sup>, Izabela Kocjan<sup>a</sup>, Beata Marciniak-Maliszewska<sup>f</sup>, Foteini Drakou<sup>e</sup>

<sup>a</sup> Institute of Geological Sciences Polish Academy of Science, Research Centre in Kraków, Senacka 1, 31-002, Poland

<sup>b</sup> Institute of Earth Sciences, Faculty of Natural Sciences, University of Silesia in Katowice, Będzińska 60, 41-200 Sosnowiec, Poland

<sup>c</sup> Faculty of Geology and Geography, Sofia University "St. Kliment Ohridski", 15 Tzar Osvoboditel Blvd., 1504 Sofia, Bulgaria

<sup>d</sup> Department of Environmental Sciences, Basel University, 4056 Basel, Switzerland

<sup>e</sup> Department of Geology, School of Natural Sciences, Trinity College Dublin, Ireland

<sup>f</sup> Faculty of Geology, University of Warsaw, Żwirki i Wigury 93, 02-089 Warsaw, Poland

## ARTICLE INFO

### Article history:

Received 26 November 2021

Revised 1 April 2022

Accepted 24 April 2022

Available online 30 April 2022

Handling Editor: S. Kwon

### Keywords:

Strandja Zone

Sakar Unit

Levka Pluton

Sakar Batholith

U-Pb zircon dating

## ABSTRACT

The Strandja Zone, straddling the border between Bulgaria and Turkey, is often assigned to either the Balkanide or the Pontide thrust belts of the Alpine orogen in the Black Sea region. Previous studies have considered this zone, which originated on the North Gondwanan margin, as part of a Late Carboniferous to Triassic magmatic arc associated with the subduction of the Paleo-Tethys Ocean beneath Eurasia. Magmatism has been regarded as representing one continuous or two separate stages occurring under different tectonic settings. We present new LA-ICP-MS U-Pb zircon ages together with field, petrographic and geochemical studies of variably deformed granites from the Sakar Batholith and Levka Pluton of the Sakar Unit in the Strandja Zone. The new U-Pb ages from Sakar Batholith (ca. 306 Ma) and Levka Pluton (ca. 319 Ma) demand a re-evaluation of previously published U-Pb crystallisation ages from these magmatic bodies. The U-Pb age reported for the Levka Pluton also provides an upper age limit for the timing of Variscan metamorphism. The Late Carboniferous to Early Permian magmatic evolution of the Strandja Zone displays a strong resemblance to that of the Sredna Gora Zone. Both units, probably together with Serbo-Macedonian Metamorphic Complex and Sakarya Zone, were part of the metamorphic core of the Variscan Orogen.

© 2022 The Authors. Published by Elsevier B.V. on behalf of International Association for Gondwana Research. This is an open access article under the CC BY license (<http://creativecommons.org/licenses/by/4.0/>).

## 1. Introduction

The evolution of Paleozoic Earth was concurrent with the formation of the last known supercontinent, Pangea, with one of the most important events during its assembly being the final collision between Gondwana and Laurussia in the Late Carboniferous (e.g., Matte 1986; Kroner et al., 2008; Kroner and Romer 2013; Stephan et al., 2019; Franke et al., 2020). A product of this collision was the Variscan Orogen, which is well exposed today in large

areas of Western and Central Europe (e.g., Stephan et al., 2019; Franke et al., 2020). Remnants of this orogen, often strongly overprinted by younger tectonic events, occur as far southeast as the Black Sea region, where the Strandja Zone, one of the least studied areas in the southeastern Europe, is located (Fig. 1a) (e.g., Şengör et al., 1988; Okay and Topuz, 2017; Şengün et al., 2020; Balkanska et al., 2021). The zone is located between the peri-Gondwana terranes of the Balkanides (Sredna Gora and Rhodope zones) to the north and west, and the Pontides to the east and south (Istanbul and Sakarya zones; Fig. 1a), and is often variously assigned to either tectonic belt (e.g., Chatalov, 1990; Okay et al., 2001; Sunal et al., 2006; Ustaömer et al., 2012; Aysal et al., 2018). The palaeogeographic position of the Strandja Zone and its relationship with neighbouring units during the Variscan orogeny is also still unclear. The few studies that have addressed these problems, considered this region to represent a Late Carboniferous

\* Corresponding author at: Institute of Geological Sciences Polish Academy of Science, Research Centre in Kraków, Senacka 1, 31-002 Kraków, Poland.

E-mail addresses: [anna.salacinska@twarda.pan.pl](mailto:anna.salacinska@twarda.pan.pl) (A. Sałacińska), [a.kounov@unibas.ch](mailto:a.kounov@unibas.ch) (A. Kounov), [chewd@tcd.ie](mailto:chewd@tcd.ie) (D. Chew), [krzysztof.szopa@us.edu.pl](mailto:krzysztof.szopa@us.edu.pl) (K. Szopa), [ashley.gumsley@us.edu.pl](mailto:ashley.gumsley@us.edu.pl) (A. Gumsley), [ndkocjan@cyf-kr.edu.pl](mailto:ndkocjan@cyf-kr.edu.pl) (I. Kocjan), [b.maliszewska@uw.edu.pl](mailto:b.maliszewska@uw.edu.pl) (B. Marciniak-Maliszewska), [drakouf@tcd.ie](mailto:drakouf@tcd.ie) (F. Drakou).



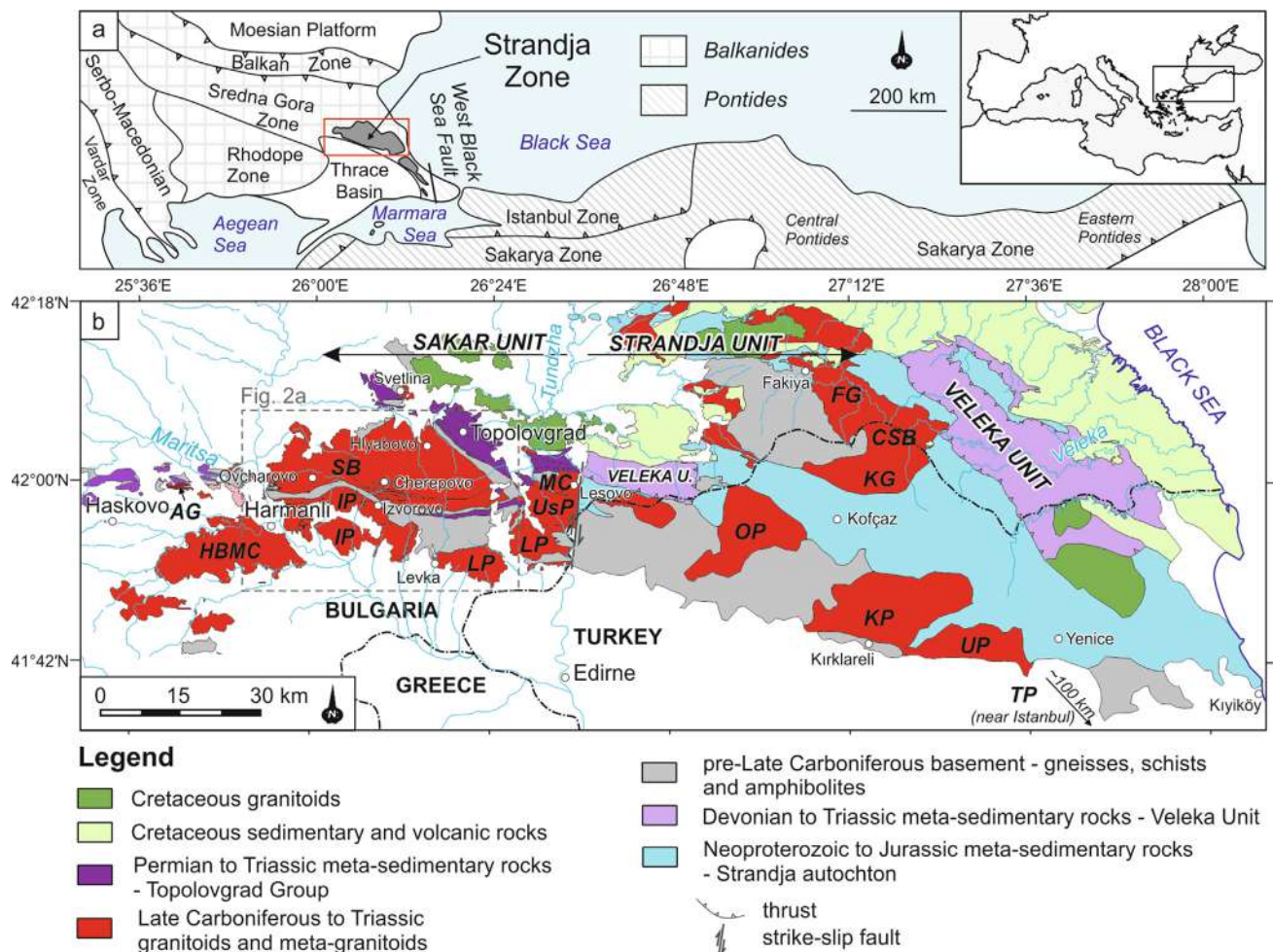


**Fig. 1.** (a) Map presenting the Strandja Zone and the surrounding major tectonic units (inset); (b) Geological map of the Strandja Zone with major Late Carboniferous to Triassic plutonic bodies: AG – Aleksandrovo Granite, CSB – Central Strandja Batholith consist of FG – Fakiya granite and KG – Kula granite, HBMC – Harmanli Block Magmatic Complex, IP – Izvorovo Pluton, KP – Kırklareli Pluton, LP – Levka Pluton, MC – Melnița Complex, OP – Ömeroba Pluton, SB – Sakar Batholith, UP – Üsküp Pluton, UsP – Ustrem Pluton, TP – Tepecik Pluton (modified after [Okay et al., 2001](#); [Gerdjikov 2005](#); [Natal'in et al., 2016](#); [Sačaniška et al., 2021](#)).

to Triassic magmatic arc associated with the subduction of the Paleozoic Tethys Ocean beneath Eurasia (e.g., Okay and Topuz, 2017; Aysal et al., 2018; Bonev et al., 2019, 2021). In their review paper on the Variscan evolution of the Black Sea region, Okay and Topuz (2017) suggest that some units of the Balkanides, such as the Sredna Gora and Balkan zones, were also part of this magmatic arc, although several other studies infer the existence of a Variscan shear zone (e.g., Gerdjikov et al., 2007; Carrigan et al., 2005; Balkanska et al., 2021) or even an oceanic suture between them (e.g., Haydoutov, 1989). The model of continuous arc-related magmatism in the Strandja Zone from the Late Carboniferous to the Triassic (e.g., Aysal et al., 2018; Bonev et al., 2019, 2021) was challenged by Sałacińska et al. (2021), who distinguished two separate stages of Late Carboniferous to Early Permian and Late Permian to Triassic magmatic activity, related to possible changes in tectonic setting in the Permian. The latter interpretation is in agreement with the model of distinct syn- and post-Variscan phases in the evolution of the Strandja Zone suggested by Okay and Topuz (2017). The timing and conditions of Variscan metamorphism affecting the pre-Permian basement of this segment of the Northern Gondwana margin (Şahin et al., 2014; Yılmaz et al., 2021; Žak et al., 2021), remains an open question (e.g., Okay et al., 2001).

Voluminous Late Carboniferous to Triassic felsic magmatism is documented within the Strandja Zone (Fig. 1b), with a substantial

amount of new U-Pb geochronological data from these magmatic rocks published in the last decade (Georgiev et al., 2012; Machev et al., 2015; Natal'in et al., 2016; Peytcheva et al., 2016; Aysal et al., 2018; Pristavova et al., 2019; Bonev et al., 2019, 2021; Akgündüz et al., 2021; Sałacińska et al., 2021). For example, the most recent studies on Triassic magmatism from the Sakar Unit (Izvorovo Pluton, Sałacińska et al., 2021; Harmanli Block Magmatic Complex and surrounding areas, Bonev et al., 2021), provide important insights into the potential correlation of the Sakar and Strandja units of the Strandja Zone and other Variscan basement units in the Balkanides and Pontides.

In this study, we present new laser ablation-inductively coupled plasma-mass spectrometry (LA-ICP-MS) U-Pb zircon ages together with geochemical and petrographic studies coupled with field observations from the Sakar Batholith, the largest intrusive body in the Sakar Unit of the Strandja Zone (Fig. 1b; e.g., Kamenov et al., 2010), and the Levka Pluton of the Lesovo Magmatic Complex (Boyanov et al., 1965), as well as field observations from their country rock envelope (Fig. 1b). We also report the first isotopic age for Levka Pluton, which provides an upper age limit for the timing of Variscan metamorphism. Our new U-Pb ages from Sakar Batholith and Levka Pluton also requires a re-evaluation of previously published U-Pb crystallisation ages of these magmatic bodies (e.g., Bonev et al., 2019). Therefore LA-ICP-MS U-Pb zircon dating was coupled with detailed zircon petro-

rography and careful consideration of factors such as possible Pb loss due to younger metamorphic events. The new ages, together with petrographic and geochemical data from Sakar Batholith and Levka Pluton, are compiled into a detailed data set that includes previously published U-Pb geochronological and geochemical data from the Late Carboniferous to Triassic intrusive and extrusive rocks of the Strandja Zone. Such a compilation allows for a better understanding of the Variscan evolution of the area and correlation with neighbouring units.

## 2. Geological setting

The Strandja Zone, alternatively named the Strandzha or Sakar-Strandja (Strandzha) Zone, Strandja (Strandzha) or Instranca Masif, represents a northwest-southeast-trending mountain belt straddling the border between Bulgaria and Turkey, that is comprised of pre-Late Cretaceous autochthonous and allochthonous units (Fig. 1, e.g., Boyadiev and Lilov, 1972; Okay et al., 2001; Bedi et al., 2013; Natal'in et al., 2016; Ivanov, 2017; Aysal et al., 2018). The zone was affected by upper greenschist- to amphibolite-facies Late Jurassic to Early Cretaceous metamorphism and deformation, related to what is called in the local literature Early Alpine or Cimmerian orogenesis (e.g., Ivanov et al., 2001; Gerdjikov, 2005; Cattò et al., 2018; Vladinova et al., 2019; Szopa et al., 2020; Bonev et al., 2020). An earlier Variscan metamorphic event is reported from the Strandja zone in Turkey (e.g., Okay et al., 2001; Sunal et al., 2011). The contact of the Strandja Zone with the Rhodope Metamorphic Complex is poorly constrained due to the Cenozoic sedimentary cover of the Thrace Basin, which also overlies the southern part of the Strandja Zone (Fig. 1). To the southeast, the Strandja Zone is bordered by the Istanbul Zone of the Pontides, from which it is separated by the West Black Sea Fault (Okay et al., 1994) (Fig. 1). To the north, the Strandja Zone is covered by volcano-sedimentary rocks of the Sredna Gora Zone, part of the larger Late Cretaceous Apuseni-Banat-Timok-Sredna Gora magmatic arc (e.g., Chatalov, 1990; Gallhofer et al., 2015). The rocks of the Strandja Zone are also intruded by several plutons associated with this magmatic arc.

The Strandja Zone in Bulgaria is subdivided into three units: the Sakar, Strandja and Veleka units, based on their differing Late Jurassic to Early Cretaceous evolution. These differences include their structural position, degree of deformation and metamorphism, as well as their stratigraphic characteristics (Chatalov, 1990; Gerdjikov, 2005). The Sakar and Strandja units (Fig. 1) consist of pre-Late Carboniferous metamorphic rocks intruded by variably deformed and metamorphosed Late Carboniferous to Triassic felsic to intermediate magmatic rocks (e.g., Okay et al., 2001; Natal'in et al., 2016; Bonev et al., 2021; Sałacińska et al., 2021). The protolith of the gneisses, schists and amphibolites within the metamorphic basement includes Neoproterozoic-Cambrian (Şahin et al., 2014; Natal'in et al., 2016) and Ordovician (Bonev et al., 2019) felsic magmatic rocks and sedimentary rocks with Cambrian (maximum) depositional ages (Vladinova et al., 2018; Vladinova and Georgieva, 2020), interpreted to represent part of a peri-Gondwanan terrane(s) (e.g., Stampfli, 2000; Okay and Topuz, 2017; Žak et al., 2021). The basement rocks of the Sakar Unit are overlain by a Permian to Triassic amphibolite-facies meta-sedimentary sequence called the Topolovgrad Group (Fig. 1; e.g., Chatalov, 1990), which differs in facies and degree of metamorphism from coeval sedimentary sequences of the Strandja Unit.

The Veleka Unit, which tectonically overlies the Strandja Unit (Gerdjikov, 2005), comprises two stratigraphically and lithologically distinct entities of probable Paleozoic to Triassic age.

### 2.1. Late Carboniferous to Triassic magmatism of the Sakar Unit

Late Carboniferous to Triassic intermediate to felsic magmatic rocks intruded the metamorphic basement of the Sakar Unit (e.g., Okay et al., 2001; Natal'in et al., 2016; Bonev et al., 2019, 2021; Sałacińska et al., 2021). The largest coherent magmatic body in the area – the Sakar Batholith, is located in the central part of the Sakar Unit (Kamenov et al., 2010; Fig. 1b). The Lesovo Magmatic Complex is situated south of the Sakar Batholith (~350 km<sup>2</sup>), and is separated from it by a belt of basement rocks (Fig. 1b). The extent of the Lesovo Magmatic Complex has been a topic of debate. The complex was first defined by Boyanov et al. (1965) and described in detail by Kozhoukharov and Kozhoukharova (1973). Later, Chatalov (1992) separated the porphyritic meta-granite and meta-rhyolite of the northeastern part of the complex, and defined it as the Late Paleozoic volcano-plutonic Melnitsa Complex. Recently, Bonev et al. (2019) provided ages of ca. 300–297 Ma for Melnitsa Complex. Furthermore, field mapping and structural data allowed Ivanov et al. (2001) to separate the deformed and metamorphosed rocks of the Lesovo Magmatic Complex into three magmatic bodies – the Ustrem, Levka and Izvorovo plutons (Fig. 1b). Bonev et al. (2019) also presented an age of ca. 306 Ma for the Ustrem Pluton (Fig. 1b), and interpreted it as the crystallisation age of the entire Lesovo Complex. The boundary between the neighbouring ca. 306 Ma Ustrem and Levka plutons does not crop out (Fig. 1b), and therefore whether it represents one single magmatic complex remains uncertain. Due to Cenozoic sedimentary cover, the true extent of the ca. 256–251 Ma Izvorovo Pluton (Sałacińska et al., 2021) is not well-established. However, based on lithological similarities, Jordanov et al. (2008) suggested that the Harmanli Block Magmatic Complex could be the westernmost continuation of the Izvorovo Pluton (Fig. 1b). Both magmatic bodies are composed of metamorphosed and deformed granitoids, predominantly K-feldspar porphyritic granites.

The focus of this study is the Sakar Batholith and Levka Pluton (Fig. 1b, 2a). The Sakar Batholith is composed of three types of granitoids (Kamenov et al., 2010). Equigranular and porphyritic granites are the major components, whereas leucocratic granitoids occur mostly as small elongated bodies close to the batholith margins (Kamenov et al., 2010; Pristavova et al., 2019). The Sakar Batholith is deformed mostly along its periphery and is locally affected by albitization (Pristavova et al., 2019; Szopa et al., 2020), likely the product of a metasomatic process related to the Late Jurassic – Early Cretaceous hydrothermal activity during the Early Alpine/Cimmerian orogeny (Szopa et al., 2020). Published ages of the batholith range between ca. 305 Ma and ca. 295 Ma (Peytcheva et al., 2016; Bonev et al., 2019; Pristavova et al., 2019).

The Levka Pluton is also a large body, cropping out over ~ 150 km<sup>2</sup>, consisting of equigranular medium-grained biotite granodiorites and granites. The northern intrusive contact of the Levka Pluton with its metamorphosed country rocks is reworked by Early Alpine deformation (Gerdjikov, 2005). Due to the lack of geochronological data, the Levka Pluton was previously regarded as Late Carboniferous in age based on structural observations (Gerdjikov, 2005).

## 3. Sampling strategy

In this study, three rock samples (SAK-13, SAK-24 and SAK-27) were collected from different parts of Sakar Batholith. Sampled areas were previously mapped as equigranular and porphyritic parts of the batholith (Fig. 2a), however all three samples represent porphyritic granites (Fig. 2b,c,d). One sample of granodiorite, SAK-33, was collected from Levka Pluton (Fig. 2). Sample locations, rock types and mineral assemblages are listed in Table 1.



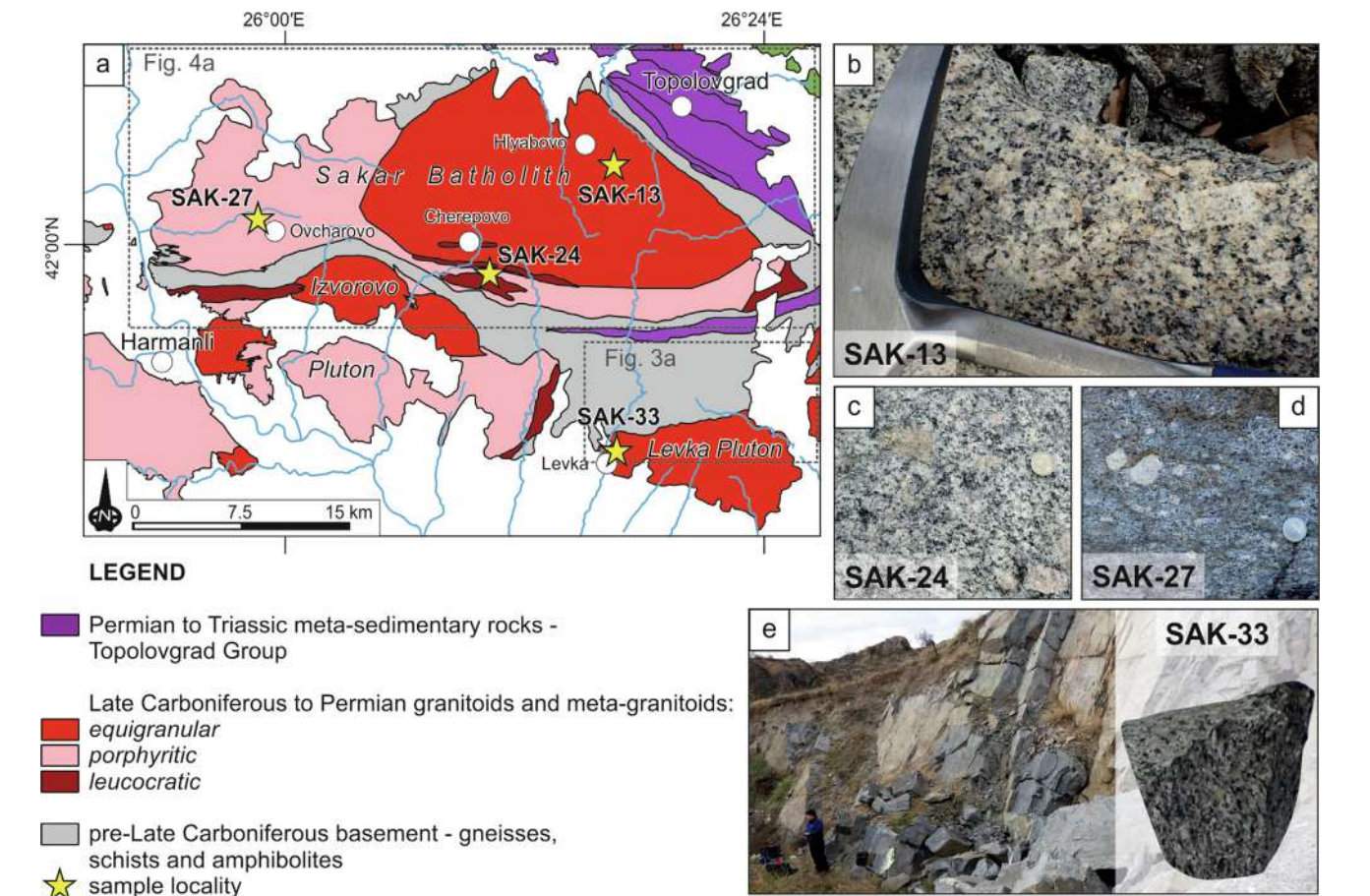


**Fig. 2.** (a) Geological map of the Sakar Unit with sample localities and samples (modified after Okay et al., 2001; Gerdjikov, 2005; Natal'in et al., 2016; Sałacińska et al., 2021); (b, c, d) porphyritic granites from the Sakar Batholith (SAK-13, SAK-24, SAK-27), (e) granodiorite from the Levka Pluton (SAK-33).

**Table 1**  
Sample localities and modal mineral assemblages. Modal abundance is given in %, unless < 1%, i.e. accessory (•). Qz, quartz; Pl, plagioclase; Afs, alkali feldspar; Bt, biotite; Ms, muscovite; Ser, sericite; Zrn, zircon; Ap, apatite; Ttn, titanite; Ep, epidote.

Sample	Lithology		Locality	Latitude		Longitude			
SAK-13	porphyritic monzogranite		Sakar Batholith, 2 km SE Hlyabovo	42°02'59.0"N		26°16'11.0"E			
SAK-24	porphyritic monzogranite		Sakar Batholith, 3 km SE Cherepovo	41°59'03.4"N		26°10'16.1"E			
SAK-27	porphyritic monzogranite		Sakar Batholith, 1.5 km NW Ovcharovo	42°01'09.1"N		25°59'05.2"E			
SAK-33	granodiorite		Levka Pluton, in Levka	41°52'44.9"N		26°16'21.2"E			
Sample	Qz	Pl	Afs	Bt	Ms	Zrn	Ap	Ttn	Ep
SAK-13	~25	~40	~25	~10	• (Ser)	•	•	•	
SAK-24	~25	~40	~25	~10	• (Ser)	•	•	•	•
SAK-27	~20	~40	~30	~5	~5	•	•	•	
SAK-33	~20	~40	~15	~20	~5	•	•	•	

The porphyritic granites, representing the major component of the Sakar Batholith, were sampled in order to better constrain variations in the crystallisation age of the different parts of the pluton, which ranges between ca. 305 Ma and ca. 295 Ma (Peytcheva et al., 2016; Pristavova et al., 2019; Bonev et al., 2019). These porphyritic granites are weakly to moderately deformed, however, all three rock samples were collected from undeformed to non-foliated outcrops. The porphyritic granite sample SAK-13, was collected from an abandoned quarry ~ 2 km southeast of Hlyabovo (northeastern part of the Sakar Batholith; Fig. 2a,b). In this quarry, small mafic enclaves (up to 15 cm in diameter) were observed. Porphyritic granite sample SAK-24 comes from an active quarry located

~3 km southeast of Cherepovo (south-central part of the batholith; Fig. 2a,c). In this quarry, the granite is intruded by pale, garnet-rich granitoids of unknown age. Porphyritic granite sample SAK-27 was collected from a road cut, ~1.5 km north-west of Ovcharovo (western part of the batholith; Fig. 2a,d). Granodiorite sample SAK-33 comes from a small abandoned quarry located in the northern outskirts of Levka (Levka Pluton; Fig. 2a,e). In this quarry dark homogenous granodiorite showing solid-state deformation and development of a planar fabric is exposed. This sampling strategy aimed not only to provide ages of undated magmatic bodies in the Sakar Unit, but also to constrain

the timing of an early high-grade deformation event in the metamorphic country rocks which predates the granitoid emplacement.

## 4. Analytical procedures

### 4.1. Sample preparation

Four granitoid samples (SAK-13, SAK-24, SAK-27 and SAK-33) were analysed in this study. Thin sections and petrographic observations were made in the Institute of Earth Sciences at the University of Silesia in Katowice, Sosnowiec, Poland, using an Olympus BX-51 optical polarising microscope; and a ThermoFisher Scientific Phenom XL Scanning Electron Microscope (SEM) with back-scattered electron (BSE) imagery coupled to an energy dispersive spectrometer (EDS). The mineral chemical analyses were made using a Cameca SX100 electron microprobe at the Laboratory of Electron Microscopy, Microanalysis and X-Ray Diffraction (Faculty of Geology, University of Warsaw, Warsaw, Poland) according to procedures described in the Supplementary Table 1 ([dataset] Sałacińska et al., 2022).

The most homogeneous parts of the samples were selected for whole-rock geochemical analysis. The samples were first crushed using a jaw crusher and pulverised in an agate ball mill to a fine-grained powder. The material was then coned and quartered before being analysed for major and trace elements in Bureau Veritas Analytical Laboratories in Vancouver, Canada. Major elements were analysed using X-ray fluorescence (XRF) spectrometry. Trace elements, including rare earth elements (REE) were analysed by ICP-MS. The volatile content on each sample was obtained by loss on ignition determinations (LOI). The geochemical data were then plotted using the GeoChemical Data toolkit (GCDkit) of Janoušek et al. (2016).

Zircon grains were separated from each sample in the Sample Preparation Laboratory at the Institute of Geological Sciences, Polish Academy of Sciences in Krakow, Poland. The separation process included crushing, sieving through a 0.315 mm mesh, panning, density separation, and finally hand-picking using a standard binocular microscope. The zircon grains were then cast in epoxy resin mounts of 25 mm diameter, and ground and polished to half-grain thickness to expose the zircon interiors. The zircon grains were imaged in transmitted and reflected light microscopy using the same equipment as employed in the petrographic observations. Additionally, cathodoluminescence (CL) imagery was undertaken at the Institute of Earth Sciences, University of Silesia in Katowice using a FET Phillips 30 SEM to reveal the internal structure of the zircon grains. A 15 kV accelerating voltage, and a beam current of 1 nA was employed. All the imaging techniques were employed for spot selection before U-Th-Pb isotopic analyses.

### 4.2. Sample analysis

Zircon grains from samples SAK-13, SAK-24, SAK-27 and SAK-33 underwent U-Th-Pb isotopic analyses in the Department of Geology, Trinity College Dublin, Ireland. A Photon Machines Analyte Excite 193 nm ArF excimer laser-ablation system with a HelEx 2- vol ablation cell, coupled to an Agilent 7900 mass spectrometer was used for the analyses. Line scans on NIST612 standard glass were used to tune the instruments, by obtaining a Th/U ratio close to unity and low oxide production rates (i.e.,  $\text{ThO}^+/\text{Th}^+$  typically < 0.15%). A circular laser spot of 24  $\mu\text{m}$  was used, with a repetition rate of 11 Hz. Helium carrier gas was fed into the laser cell at  $\sim 0.4 \text{ l. min}^{-1}$ , and was mixed with an aerosol of  $\sim 0.6 \text{ l. min}^{-1}$  Ar make-up gas and  $11 \text{ ml. min}^{-1}$   $\text{N}_2$ . During each analysis, eight isotopes ( $^{90}\text{Zr}$ ,  $^{202}\text{Hg}$ ,  $^{204}\text{Pb}$ ,  $^{206}\text{Pb}$ ,  $^{207}\text{Pb}$ ,  $^{208}\text{Pb}$ ,  $^{232}\text{Th}$  and  $^{238}\text{U}$ ) were measured. Each analysis comprised 27.3 s of ablation (300 shots) and

12 s of washout time. The latter portions of the washout time were used for baseline measurements. The data reduction of raw U-Th-Pb isotopic data was undertaken using the freeware IOLITE package (Paton et al., 2011), with the “VizualAge” data reduction scheme (Petrus and Kamber, 2012). Conventional sample-standard bracketing was then applied to account for both downhole fractionation and long-term drift in isotopic or elemental ratios by normalising all ratios to those of the U-Th-Pb reference materials. The primary U-Pb calibration standard was 91,500 zircon ( $^{206}\text{Pb}$ - $^{238}\text{U}$  age of  $1065.4 \pm 0.6 \text{ Ma}$ ; Wiedenbeck et al., 1995; Wiedenbeck et al., 2004) and secondary standards of the Plešovice zircon ( $^{206}\text{Pb}$ - $^{238}\text{U}$  age of  $337.13 \pm 0.37 \text{ Ma}$ ; Sláma et al., 2008) and WRS 1348 zircon ( $^{206}\text{Pb}$ - $^{238}\text{U}$  age of  $526.26 \pm 0.70$ ; Pointon et al., 2012) were also used. The secondary standards yielded respective ages of  $337.5 \pm 1.9 \text{ Ma}$  ( $^{206}\text{Pb}$ - $^{238}\text{U}$  weighted mean age,  $n = 22$ ) and  $522.6 \pm 3.9 \text{ Ma}$  ( $^{206}\text{Pb}$ - $^{238}\text{U}$  weighted mean age,  $n = 24$ ), for the session with samples SAK-13, SAK-24, SAK-27 and respective ages of  $336.9 \pm 2.0 \text{ Ma}$  ( $^{206}\text{Pb}$ - $^{238}\text{U}$  weighted mean age,  $n = 20$ ) and  $530.0 \pm 4.7 \text{ Ma}$  ( $^{206}\text{Pb}$ - $^{238}\text{U}$  weighted mean age,  $n = 18$ ) for the session with sample SAK-33.

After the LA-ICP-MS analyses, the zircon grains were imaged again using BSE and CL in order to inspect the laser ablation craters for admixtures of growth zones. The final geochronological data reduction employed Isoplot 3.75 (Ludwig, 2012) and also for the generation of concordia diagrams. All data are listed at the  $2\sigma$  level and include decay constant errors. Data with an absolute discordance of < 5% ( $^{206}\text{Pb}/^{238}\text{U}$  vs  $^{207}\text{Pb}/^{235}\text{U}$ ) were treated as concordant data.

## 5. Results

### 5.1. Structural observations on the relationship between the analysed plutons and their country rocks

#### 5.1.1. Levka Pluton

The country rocks of Levka Pluton are heterogeneous, consisting of various high-grade metamorphic rocks, including paragneisses, garnet and two-mica schists, amphibolites, orthogneisses, lenses of meta-gabbros and meta-ultrabases and rare migmatites. Metamorphosed country rocks also occur as metre- to hundred-metre-in-size xenoliths restricted mainly to the northern periphery of the pluton along its contact (Fig. 3). Similar xenoliths are also observed within the Sakar Batholith, especially along its periphery (Fig. 4c, d).

These rocks have experienced penetrative deformation during a post-Triassic event as evidenced by the fact that the planar and linear fabrics can be traced undisrupted not only in the Late Carboniferous Levka granodiorites (Fig. 3) but also further north into the narrow strip of Triassic meta-sedimentary rocks of the Topolovgrad Group (Fig. 2). There, the pelitic lithologies within the Mesozoic sequence are transformed into garnet-staurolite schists. The foliation strikes SW-NE to WSW-ENE often bearing a SE- to E-plunging lineation defined by mica and stretched quartz aggregates. Kinematic indicators such as asymmetric boudins and sheared porphyroclasts indicate top-to-the-NW or W sense of shear.

An earlier fabric can be observed at several localities. In the eastern part of the studied area, this fabric is preserved in a low-strain domain ( $\sim 3 \text{ km}^2$ ), sandwiched between two separate bodies of Levka-type intrusives (area with a cross-hatched pattern in the NE corner of Fig. 3a) where a high-grade gneissic and migmatitic fabric ( $S_1$ ) is preserved (Fig. 3b). Elsewhere, the  $S_1$  fabric is reworked and transposed parallel to the  $S_2$  fabric, with the  $S_1$  fabric only recognizable in hinge zones of metre- to decametre-scale  $F_2$  folds which have predominantly NE-SW trending fold axes



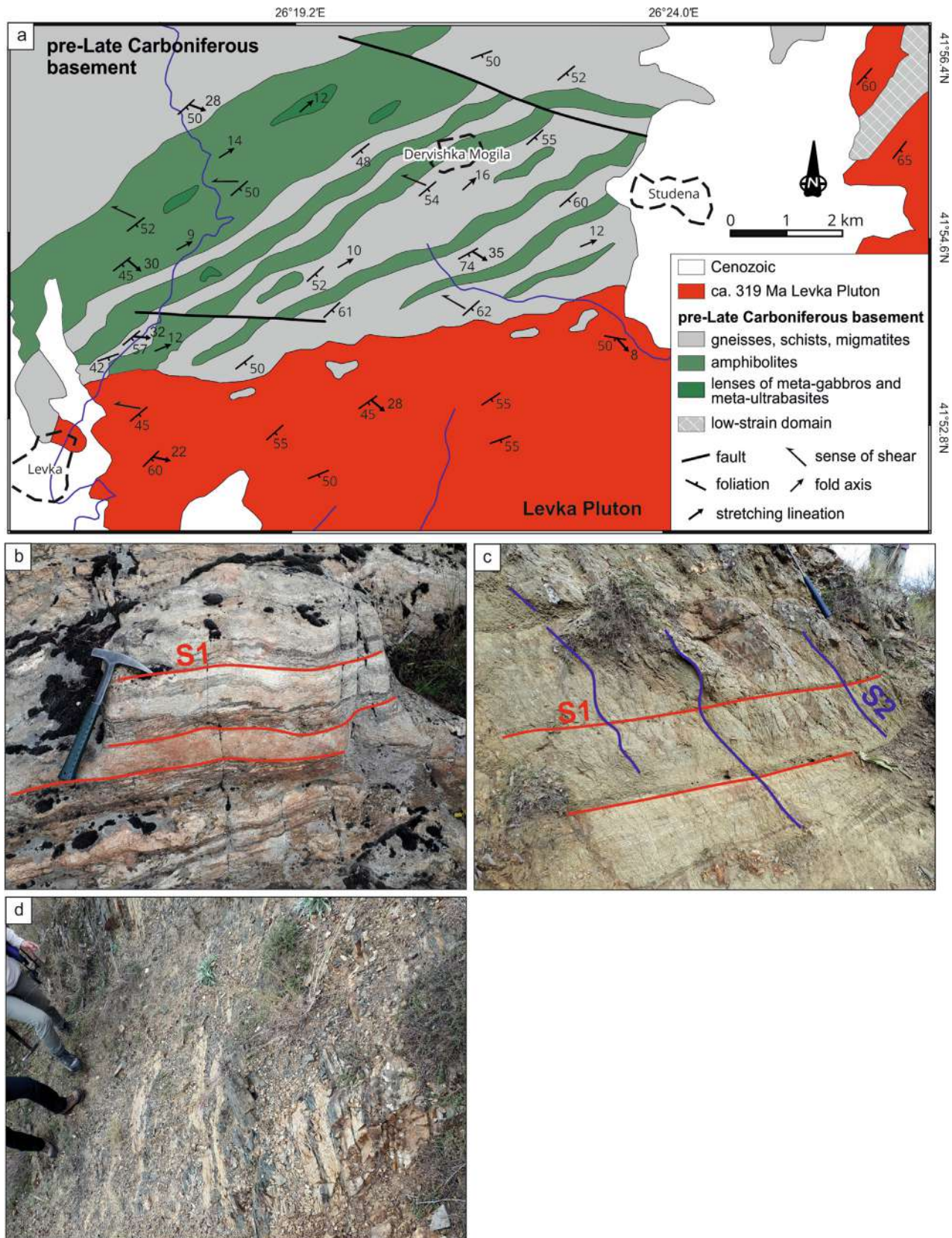


**Fig. 3.** (a) Geological map of the northern contact of Levka Pluton with the metamorphic country rocks (modified after Kouzhokharova and Kouzhokharov, 1973). (b) Field photograph of migmatitic gneisses from a low-strain country rock domain (location: 26°26'45.00"E; 41°55'30.00"N). (c) Field photo of gneissic-migmatitic layering ( $S_1$ ) cut by weakly developed foliation ( $S_2$ ; 26°17'0.00"E; 41°53'31.00"N). (d) Field photograph of a decameter-scale xenolith of amphibolites penetrated by swarm of foliation-parallel leucogranitic dykes; northern margin of the pluton, along the Levka river valley (location: 26°16'46.00"E; 41°53'19.00"N).



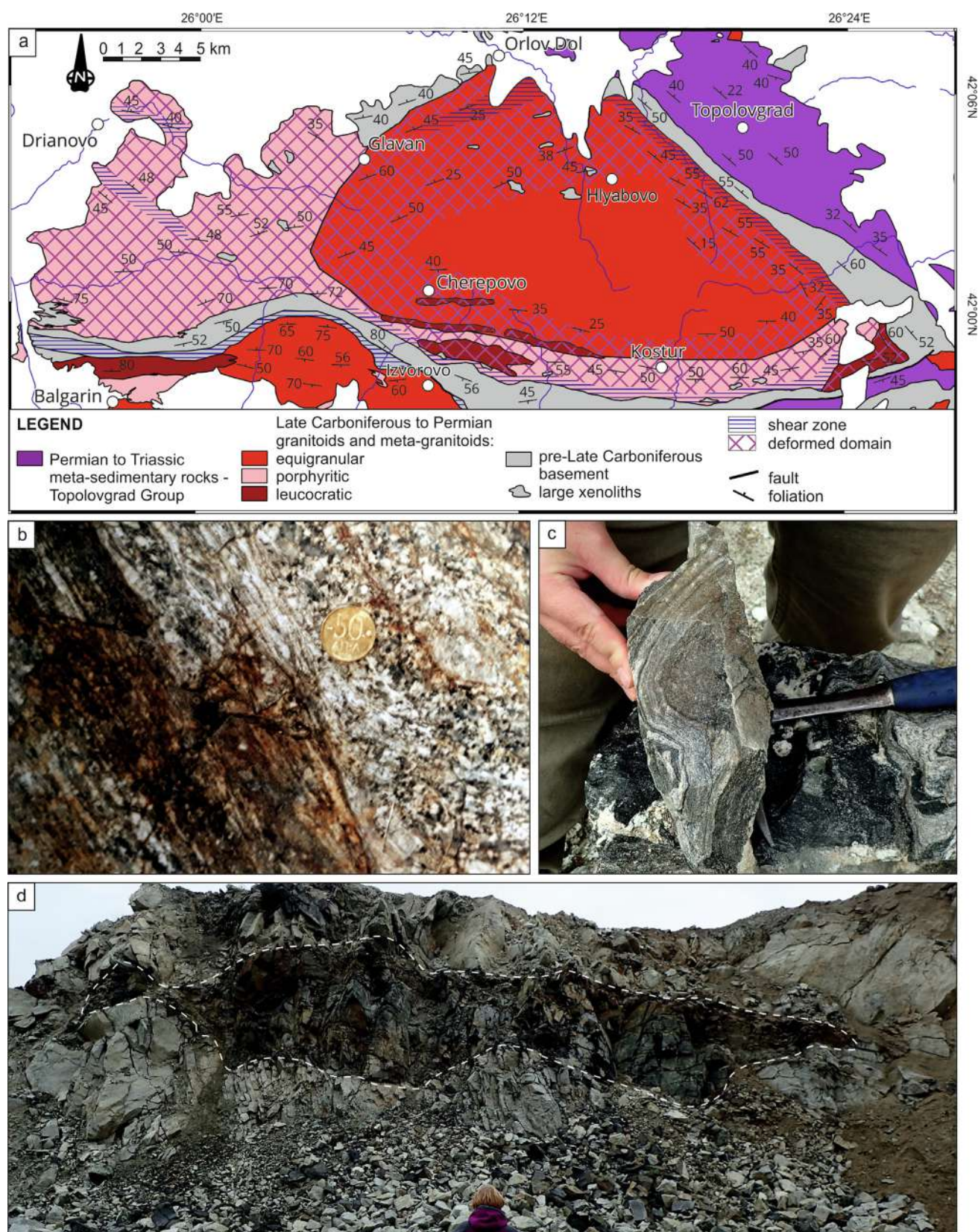


**Fig. 4.** (a) Geological map of the Sakar Batholith and a portion of its country rocks (modified after Kouzhokharova and Kouzhokharov, 1973). (b) Field photograph of the strain gradient from weakly foliated granite to ultramylonite; Drianovo shear zone, NW margin of the Sakar Batholith (location: 25°57'16,85"E; 42°5'23,11"N). (c,d) Field photographs of xenoliths of deformed and metamorphosed country rocks in the Sakar Batholith, Kanarata Quarry, north of Hlyabovo (location: 26°16'28,00"E; 42°5'2,00"N).



(Fig. 3c), and axial planes parallel to the main  $S_2$  foliation. However, older pre-Late Carboniferous metamorphism and deformation clearly occurred as suggested by the presence of xenoliths of metamorphic rocks in the ca. 319 Ma Levka Pluton (Fig. 3d).

### 5.1.2. Sakar Batholith

The Sakar Batholith is characterised by an uneven solid-state deformation overprint. The undeformed portion occurs only in the central, equigranular, part of the batholith, whereas the western, porphyritic portion together with most of the periphery of the batholith is penetratively deformed (Fig. 4a). Several, up to 300 m wide, discrete shear zones are observed (Fig. 4a).

The foliation in the eastern part of the granites is defined by stretched quartz, mica flakes and elongated and recrystallized feldspars. The fabric is generally parallel to the batholith contacts and the foliation in the country rocks. In the deformed zone an intensification of solid-state deformation is observed toward the pluton margin. This is best observed in the southern margin of the batholith where the weakly developed foliation and/or centimetre to metre thick individual shear zones grade into mylonites to ultramylonites developed along the pluton contact (Fig. 4b).

The western part of the batholith (west of the Glavan-Izvorovo line) is penetratively deformed, with the foliation dipping steeply to moderately to the north. Two high-strain zones (NE and SE of Drianovo) have been identified in this domain, where the granites are transformed into K-feldspar porphyroclastic augen gneisses. The Sakar Batholith itself contains a lot of xenoliths of deformed and metamorphosed country rocks (e.g., xenoliths in the Kanarata Quarry, north of Hlyabovo, Fig. 4c,d). The fact that deformed and metamorphosed xenoliths have been observed in the undeformed part of the batholith clearly suggests that their deformation and metamorphism must predate granite emplacement.

### 5.2. Petrographic observations and whole-rock geochemistry

The chemical composition of the minerals and the results of whole-rock geochemical analyses are provided in Supplementary Tables 1 and 2 ([dataset] Sałacińska et al., 2022).

Sample SAK-13 (Sakar Batholith) represents a weakly deformed porphyritic granite with no visible mesoscopic development of planar fabric. The sample consists of K-feldspar porphyrocrysts, quartz, plagioclase and biotite. Partially recrystallized K-feldspar ( $Or_{91-95}Ab_{5-9}An_0$ ) porphyrocrysts display tartan twinning characteristic of microcline and exsolved lamellae and irregular intergrowths of albite (perthite; Fig. 5a). Plagioclase reveals core-mantle structures with the internal parts of plagioclase (oligoclase,  $Or_{1-2}Ab_{75-82}An_{17-24}$ ) altered to sericite and external parts affected by the recrystallisation of subgrains (Fig. 5b). Some quartz crystals are recrystallized and occur as subgrains, whereas primary quartz displays undulose extinction (Fig. 5c). In many places, recrystallized quartz shows grain boundary migration features (Fig. 5a). The biotite plots in the central part of the annite-phlogopite and siderophyllite-eastonite diagram. Accessory minerals include F-OH apatite, titanite and zircon (Fig. 5d). They occur mostly within biotite nests or on the contact between biotite and optically transparent minerals. F-OH apatite and partially altered titanite (Fig. 5d) are significantly bigger than zircon crystals, and are up to 300–400  $\mu m$  in diameter. Although in hand specimens they appear to be undeformed, microscopic observations reveal a clear solid-state overprint.

Sample SAK-24 (Sakar Batholith), which represents weakly deformed porphyritic granite with no visible mesoscopic development of a planar fabric, shows textural and mineral compositions similar to sample SAK-13 (Fig. 5e,f). However, in the former the titanite crystals are homogeneous. Additionally, sample SAK-24

contains secondary epidote (Fig. 5e,f) which suggests more alteration compared to the sample SAK-13.

Sample SAK-27 (Sakar Batholith) represents a weakly foliated porphyritic granite containing K-feldspar porphyrocrysts ( $Or_{94-95}Ab_{5-6}An_0$ ), quartz, plagioclase (albite-oligoclase,  $Or_{0-1}Ab_{83-94}An_{5-16}$ ), biotite and muscovite (Fig. 5e,f). The metamorphic overprint is shown by dynamic recrystallisation of quartz crystals, undulose extinction of primary quartz and recrystallisation of the marginal parts of the K-feldspar porphyrocrysts (Fig. 5g,h). The foliation is defined by alignment of biotite flakes and quartz ribbons. Plagioclase is altered to sericite. Accessory minerals include large homogenous F-OH apatite crystals (up to 600  $\mu m$  in diameter) and smaller zircons (up to 200  $\mu m$  in diameter).

Sample SAK-33 (Levka Pluton) represents a foliated granodiorite, which is composed of aggregates of recrystallised quartz and primary quartz crystals with undulose extinction, partially altered plagioclase (oligoclase,  $Or_{1-2}Ab_{71-79}An_{20-28}$ ), biotite, muscovite and partially recrystallized K-feldspar ( $Or_{92-95}Ab_{5-8}An_0$ ), with accessory titanite, F-OH apatite and zircon (Fig. 5i,j). The content of dark ferromagnesian minerals (mainly biotite) is significantly higher than in the porphyritic granites of the Sakar Batholith. Sample SAK-33 shows deformation and development of planar fabric in both outcrop as well as at the microscopic scale.

Whole-rock major- and trace-element compositions of the four analysed samples (SAK-13, SAK-24, SAK-27 from the Sakar Batholith and SAK-33 from the Levka Pluton) together with a compilation of published data from other Late Carboniferous to Triassic intrusions of the Strandja Zone are presented in Supplementary Table 2 ([dataset] Sałacińska et al., 2022). The samples from Sakar Batholith are silica-rich (69.6–70.7 wt%  $SiO_2$ ) and plot in the monzogranite field on a QAPF diagram, whereas the sample from the Levka Pluton contains less silica (66.9 wt%  $SiO_2$ ) and alkalis (6.7 wt%  $Na_2O + K_2O$ ) and is classified as granodiorite (Fig. 6a; Streckeisen, 1974). All samples are peraluminous (Fig. 6b; Shand, 1943).

The trace elements were normalised to the ocean-ridge granite (ORG) values of Pearce et al. (1984) and plotted on a multi-element (spider) diagram. The samples from the Sakar Batholith and Levka Pluton have similar trace element patterns, characterised by enrichment in K, Rb, Ba, Th and Ce and Sm relative to Ta, Nb, Hf, Zr, Y and Yb (Fig. 6c).

The rare earth elements (REEs) were normalised to the chondrite values of McDonough and Sun (1995; Fig. 6d), and plotted on a multi-element diagram. The samples show fractionation of the light REE (LREE) relative to heavy REE (HREE), and have negative Eu anomalies. These Eu anomalies appear slightly more pronounced in the sample from the Levka Pluton (0.35) than from the Sakar Batholith (0.27–0.33).

### 5.3. U-Pb zircon dating

LA-ICP-MS U-Th-Pb isotopic data for the analysed zircons from samples SAK-13, SAK-24, SAK 27 of the Sakar Batholith and SAK-33 of the Levka Pluton are listed in Supplementary Table 3 ([dataset] Sałacińska et al., 2022). All of the analysed zircon crystals are presented in Supplementary Fig. 1 ([dataset] Sałacińska et al., 2022). Dates are reported as  $^{206}Pb$ - $^{238}U$  weighted mean ages with  $2\sigma$  error uncertainties.

The granitoid samples (SAK-13, SAK-24 and SAK-27) from the Sakar Batholith contain similar populations of euhedral to subhedral zircon crystals up to 180  $\mu m$  in length and aspect ratios of 1:1 to 1:3 (Fig. 7a-c). The zircons have strong oscillatory zonation and some of the crystals contain distinctive cores and/or thin rims (~5 to ~10  $\mu m$  in width). In this study, the thin rims were not analysed and only a few analyses come from cores.

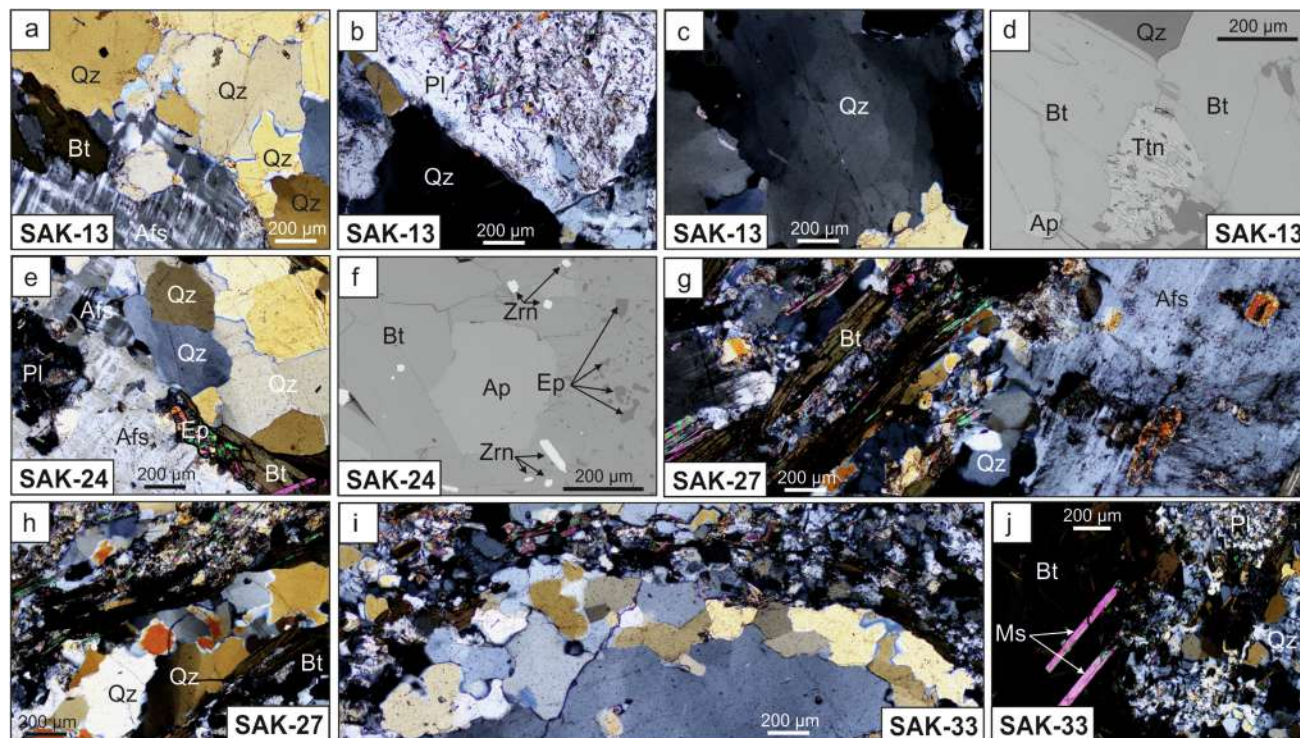


**Fig. 5.** Petrographic images of the porphyritic granites from the Sakar Batholith (a, b, c, d – SAK-13; e, f – SAK-24; g, h – SAK-27) and granodiorite from the Levka Pluton (i, j – SAK-33). (a, b, c) Thin sections in cross-polarised light (XPL) showing (a) a K-feldspar porphyroclast with tartan twinning characteristic of microcline and recrystallized quartz with grain boundary migration features; (b) a plagioclase crystal, which reveals a core-mantle structure with the internal parts altered to sericite and external parts affected by recrystallisation of subgrains; (c) primary quartz crystal, which display undulose extinction; (d) a BSE image of F-OH apatite and heterogeneous titanite; (e) thin section in XPL showing a K-feldspar with tartan twinning, plagioclase altered to sericite, recrystallized quartz with grain boundary migration features and secondary epidote; (f) a BSE image showing alteration to secondary epidote; (g, h, i, j) thin section in XPL showing (g) dynamic recrystallisation of quartz crystals and recrystallisation of marginal parts of the K-feldspar porphyroclasts; (h) dynamic recrystallisation of quartz crystals and undulose extinction of primary quartz; (i) dynamic recrystallisation of quartz crystals; (j) two-mica intergrowths and recrystallised subgrains of quartz. Abbreviations in pictures: Qz, quartz; Pl, plagioclase; Afs, alkali feldspar; Bt, biotite; Ms, muscovite; Ep, epidote; Zrn, zircon; Ap, apatite; Ttn, titanite.

#### 5.3.1. Porphyritic granite sample SAK-13 (Sakar Batholith)

A total of 39 analyses were obtained from 35 zircon crystals (Supplementary Table 3, [dataset] Sałacińska et al., 2022; Fig. 8a). Two discordant (>5% disc.) and two analyses from mixed domains, as revealed by BSE and CL post-imaging, were excluded from the age calculations. From the other 35 concordant data, 28 data points form a cluster of  $^{206}\text{Pb}$ - $^{238}\text{U}$  ages ranging from ca. 293 Ma to ca. 308 Ma, and define a weighted mean  $^{206}\text{Pb}$ - $^{238}\text{U}$  age of  $301 \pm 2$  Ma (MSWD = 0.6). This age is interpreted as the emplacement of the granite. The remaining six analyses from oscillatory-zoned zircons scatter along concordia with ages ranging from ca. 322 Ma to ca. 335 Ma and one analysis from a zircon core is significantly older (ca. 608 Ma). These analyses are interpreted as antecrysts and a xenocryst, respectively.

#### 5.3.2. Porphyritic granite sample SAK-24 (Sakar Batholith)

Thirty-two concordant (<5% disc.) analyses from 31 crystals were obtained (Supplementary Table 4, [dataset] Sałacińska et al., 2022; Fig. 8b) from this sample. All data points range from ca. 298 Ma to ca. 517 Ma, whereas 28 of them form a cluster between ca. 298 Ma and ca. 316 Ma, with a weighted mean  $^{206}\text{Pb}$ - $^{238}\text{U}$  age of  $305 \pm 2$  Ma (MSWD = 1.2). This age is interpreted as related to the crystallisation of the granite. The four older analyses, coming from zircon cores, are interpreted as inherited components.

#### 5.3.3. Porphyritic granite sample SAK-27 (Sakar Batholith)

From this sample, 39 analyses from 38 crystals were obtained (Supplementary Table 3, [dataset] Sałacińska et al., 2022; Fig. 8c),

and only five data points were discordant (>5% disc.). The 34 concordant data points range from ca. 295 Ma to ca. 1755 Ma, and 29 of them form a cluster with ages between ca. 295 Ma and ca. 314 Ma, with a weighted mean  $^{206}\text{Pb}$ - $^{238}\text{U}$  age of  $306 \pm 2$  Ma (MSWD = 0.7). This age is interpreted as the crystallisation of the granite. The remaining five analyses scatter along the concordia with ages ranging from ca. 576 Ma to ca. 1755 Ma. These data come from zircon cores and are interpreted as inherited components.

#### 5.3.4. Granodiorite sample SAK-33 (Levka Pluton)

This sample contains oscillatory-zoned zircons that are euhedral to subhedral. Zircons are up to 180  $\mu\text{m}$  long with aspect ratios of 1:1 to 1:3 (Fig. 7d). Some of the zircons have thin rims ( $\sim 5$  to  $\sim 10$   $\mu\text{m}$  in width), which were not analysed during this study. A total of 34 spot analyses were obtained from 33 zircon crystals (Supplementary Table 3, [dataset] Sałacińska et al., 2022; Fig. 8d). From all 34 data points, six analyses come from mixed domains as revealed by BSE and CL post-imaging and are therefore excluded from further consideration. The remaining 28 data are concordant and range from ca. 310 Ma to ca. 869 Ma, with a significant cluster on the concordia between ca. 310 Ma and ca. 329 Ma. The cluster of 17 analyses defines a weighted mean  $^{206}\text{Pb}$ - $^{238}\text{U}$  age of  $319 \pm 3$  Ma (MSWD = 1.2). This age is interpreted as the crystallisation age of the granodiorite. The remaining 11 analyses scatter along the concordia with ages ranging from ca. 440 Ma to ca. 869 Ma. These data come from zircon cores and are interpreted as inherited components.



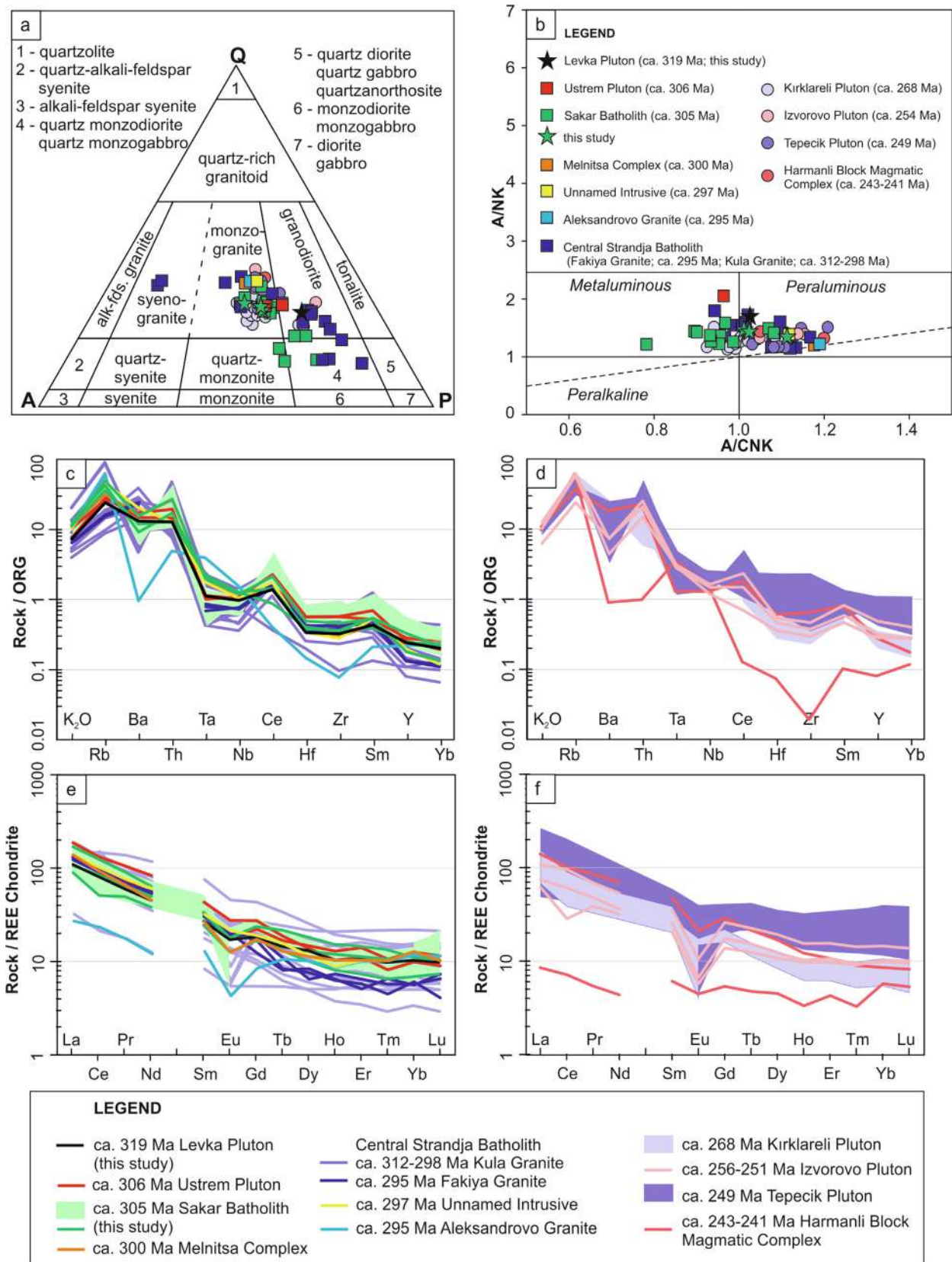


**Fig. 6.** Major and trace elements diagrams for meta-granitoids and gneisses from the Strandja Zone: (a) QAPF (Q – quartz, A – alkali feldspar, P – plagioclase, F – feldspathoids or foids) diagram (Streckeisen 1974); (b) A/CNK vs. A/NK plot of Shand (1943); (c, d) Ocean ridge granite (ORG)-normalised multi-element diagram after Pearce et al. (1984); (e, f) Chondrite-normalised REE diagram after McDonough and Sun (1995). Data from previous studies are from: Sunal et al. (2006), Kamenov et al. (2010), Machev et al. (2015), Aysal et al. (2018), Bonev et al. (2019, 2021), Akgündüz et al. (2021), Sałacińska et al. (2021) and are given in Supplementary Table 2 ([dataset] Sałacińska et al., 2022).

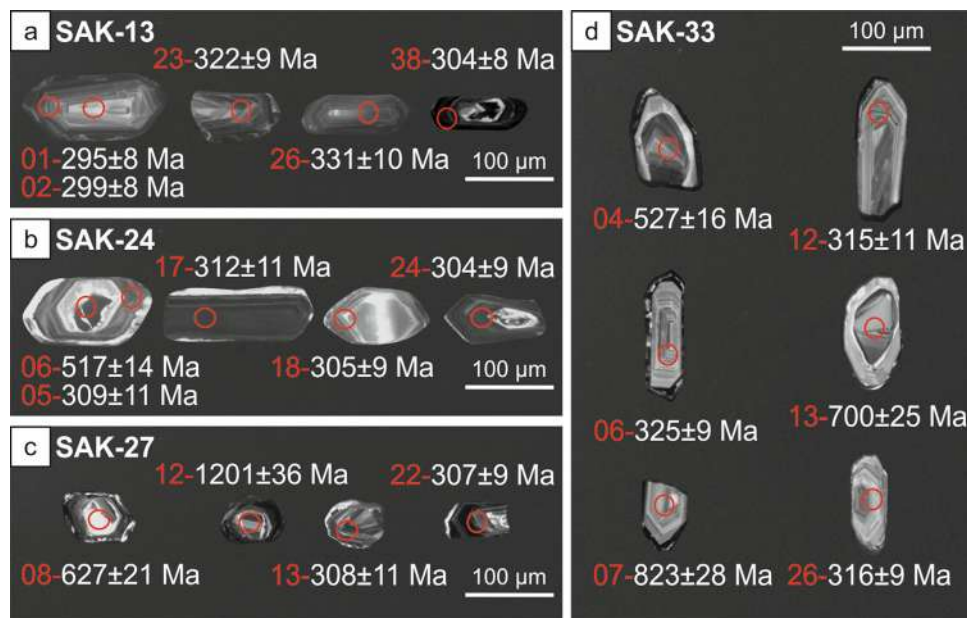


**Fig. 7.** BSE and CL images of representative zircons from the Sakar Batholith (a, b, c) and Levka Pluton (d). (a) Sample SAK-13; (b) sample SAK-24; (c) sample SAK-27; (d) sample SAK-33). Numbers represent the grain number, reported values are  $^{206}\text{Pb}/^{238}\text{U}$  ages, all presented ages are concordant (<5% disc.); red circles represent the laser ablation spot. (For interpretation of the references to colour in this figure legend, the reader is referred to the web version of this article.)

## 6. Discussion

### 6.1. Comparison of new geochronological results with previously published data from Strandja Zone

In this study, we present the first U-Pb age of the Levka Pluton ( $319 \pm 3$  Ma) and three new ages of the Sakar Batholith ranging between  $306 \pm 2$  Ma and  $301 \pm 2$  Ma. These ages reveal that the Levka Pluton is the oldest Late Carboniferous intrusion currently documented in the Sakar Unit.

The lithological similarities between the Levka and Ustrem plutons led Boyanov et al. (1965) and Kozhoukharov and Kozhoukharova (1973) to consider them as part of one single magmatic complex. However, the age of  $306 \pm 3$  Ma reported by Bonev et al. (2019) for the latter differs significantly from the age of  $319 \pm 3$  Ma for Levka Pluton obtained in this study. The calculation presented by Bonev et al. (2019) for their sample S36 from the Ustrem Pluton (Lesovo Complex), based on the seven youngest concordant zircons (Fig. 9a,b), interpreted as the only analysed autocrusts, yielded a weighted mean  $^{206}\text{Pb}$ - $^{238}\text{U}$  age of  $306 \pm 3$  Ma (MSWD = 0.43) and a concordia age of  $306 \pm 1$  Ma (MSWD = 2.3). However, the concordant data from this sample spread continuously along the concordia between ca. 327 Ma and ca. 303 Ma, without any distinctive clustering (Fig. 9a,b). Bonev et al. (2019) considered all crystals older than ca. 313 Ma as antecrusts, and excluded them from the age calculation, although it is possible that the observed continuous spread along concordia is due to partial Pb loss in some of the younger crystals caused by Late Jurassic to Early Cretaceous metamorphism rather than a mixture of auto- and antecrusts. Such cases of spread along the concordia data are often reported from magmatic rocks which have experienced complex Pb loss during a subsequent metamorphic event (e.g., Ashwal et al., 1999; Halpin et al., 2005, 2012; Bomparola et al., 2007).

Accordingly, a calculation based on all 36 concordant data of sample S36 of Bonev et al. (2019), spreading between ca. 327

and ca. 303 Ma, yields a weighted mean  $^{206}\text{Pb}$ - $^{238}\text{U}$  age of  $315 \pm 2$  Ma (MSWD = 2.3; Fig. 8a,b). Such an age for the Ustrem Pluton, which probably represents a minimum age of the emplacement of the meta-quartz diorite, overlaps within analytical error the emplacement age of Levka Pluton presented in this study. The Levka and Ustrem plutons also show a similar distribution of concordant U-Pb analyses within a similar time interval between ca. 330 – ca. 300 Ma. In this study, the zircon population from the Levka Pluton is interpreted as autocrusts, whereas the zircon data from the Ustrem Pluton are interpreted by Bonev et al. (2019) as coming from both autocrusts and antecrusts (Fig. 10). Comparison of inherited components in these two plutons is impossible because xenocrystic cores have only been analysed from the Levka Pluton in this study (Fig. 10).

Existing U-Pb zircon age constraints on the Sakar Batholith range between 305 Ma and 295 Ma, and not all ages are within analytical uncertainty (Supplementary Table 4, [dataset] Sałacińska et al., 2022; Peytcheva et al., 2016; Pristavova et al., 2019; Bonev et al., 2019). The ages from the Sakar Batholith presented in this study (ca. 306–301 Ma) overlap within analytical uncertainty with the ID-TIMS crystallisation age of  $305 \pm 6$  Ma reported by Peytcheva et al. (2016). We consider the age of  $306 \pm 2$  Ma (this study) as closest to the crystallisation age of the Sakar Batholith. We consider the ages presented by Pristavova et al. (2019) of ca. 298 Ma and Bonev et al. (2019) of ca. 296–295 Ma as younger than the true crystallisation age of the Sakar Batholith for the same reasons as those presented concerning the Ustrem pluton. They were calculated only on the basis of the youngest concordant data, with slightly older concordant data excluded and likely affected by Pb loss, probably associated with Late Jurassic to Early Cretaceous metamorphism. The Sakar Batholith, together with other intrusive and extrusive rocks of similar age including the > ca. 300 Ma Melnitsa Complex, the > ca. 295 Ma Aleksandrovo Granite and the > ca. 295 Ma Kavachki meta-volcanic rocks (Bonev et al., 2019, 2021), represent a significant part of the Sakar Unit (Fig. 11). This shows the important role of Late Carboniferous to Early Permian magmatism in the evolution

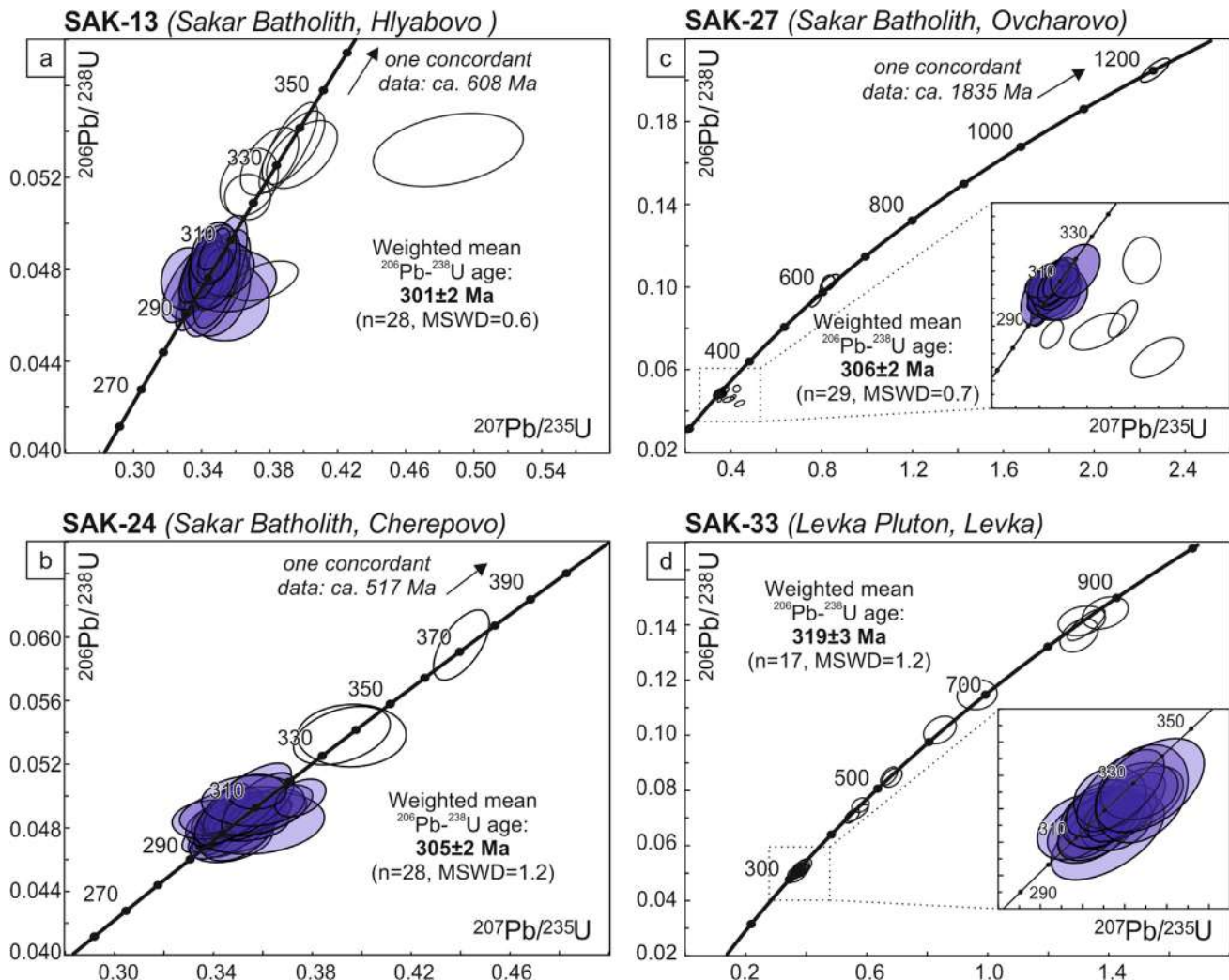


**Fig. 8.** LA-ICP-MS zircon U-Th-Pb analyses presented on Wetherill Concordia diagrams (after Wetherill, 1956) for samples of: (a) porphyritic granite SAK-13; (b) porphyritic granite SAK-24; (c) porphyritic granite SAK-27; (d) granodiorite SAK-33; the data shown as filled ellipses are used for age calculations; analyses of mixed domains are not shown.

of the Sakar Unit and the Strandja Zone as a whole, as magmatic bodies of the same age range are reported also from the Strandja Unit. This includes (Supplementary Table 4, [dataset] Sałacińska et al., 2022) the Central Strandja Batholith (ca. 295–294 Ma Fakiya Granite; Georgiev et al., 2012; Machev et al., 2015; ca. 312–298 Ma Kula Granite; Akgündüz et al., 2021), the ca. 301–299 Ma Üsküp Pluton (Okay et al., 2001; Natal'in et al., 2016), the ca. 302 Ma Zhelezkovo Gabbro (Georgiev et al., 2012; Peytcheva et al., 2016) and other ca. 306–303 Ma unnamed intrusive and extrusive rocks (Natal'in et al., 2016).

The concordant zircon data reported as autocrysts, antecrysts and xenocrysts in the Late Carboniferous to Early Permian intrusive and extrusive rocks of the Sakar Unit (Fig. 9; Supplementary Table 5, [dataset] Sałacińska et al., 2022), shows that 85% of the analyses range between ca. 344 Ma and ca. 291 Ma. This suggests that although the oldest dated Late Carboniferous intrusion is the ca. 319 Ma Levka Pluton, older concordant data from antecrystic and xenocrystic zircons (Fig. 10) imply that the magma evolution may have started as early as ca. 344 Ma, although intrusions of this age are as yet unknown from the study area.

The Sakar Unit also includes other large intrusions such as the Izvorovo Pluton and the Harmanli Block Magmatic Complex (Fig. 1b and 11). The Harmanli Block Magmatic Complex was

described by Jordanov et al. (2008) as a potential westernmost extension of the Izvorovo Pluton, although published ages of ca. 256–251 Ma for the latter (Sałacińska et al., 2021a), and ca. 243–241 Ma for the former (Bonev et al., 2021), exclude such a correlation. However, it is noted that the U-Pb age calculations for samples from Harmanli Block Magmatic Complex and other coeval extrusive rocks (e.g., Prochorovo Formation), presented in Bonev et al. (2021) were again made only on a subset (i.e., the youngest crystals) of the zircon population, where slightly older concordant data were excluded without detailed explanation. The zircon U-Pb data spread along concordia in samples from the Harmanli Block Magmatic Complex ranges from 270 to 239 Ma for Bonev et al. (2021) sample S79 and 268 Ma – 239 Ma for sample S83, without any statistically important clustering (Fig. 9c,d). Assuming again that this age scatter is a direct consequence of partial Pb loss during the Late Jurassic to Early Cretaceous metamorphic event, we consider the ages reported by Bonev et al. (2021) as only presenting minimum crystallisation ages. Thus, the correlation between Izvorovo Pluton and Harmanli Block Magmatic Complex is still possible and requires additional research. Prolonged Permian-Triassic magmatic activity is also well documented in the Strandja Unit, such as the ca. 268 Ma Kirkklareli Pluton, the



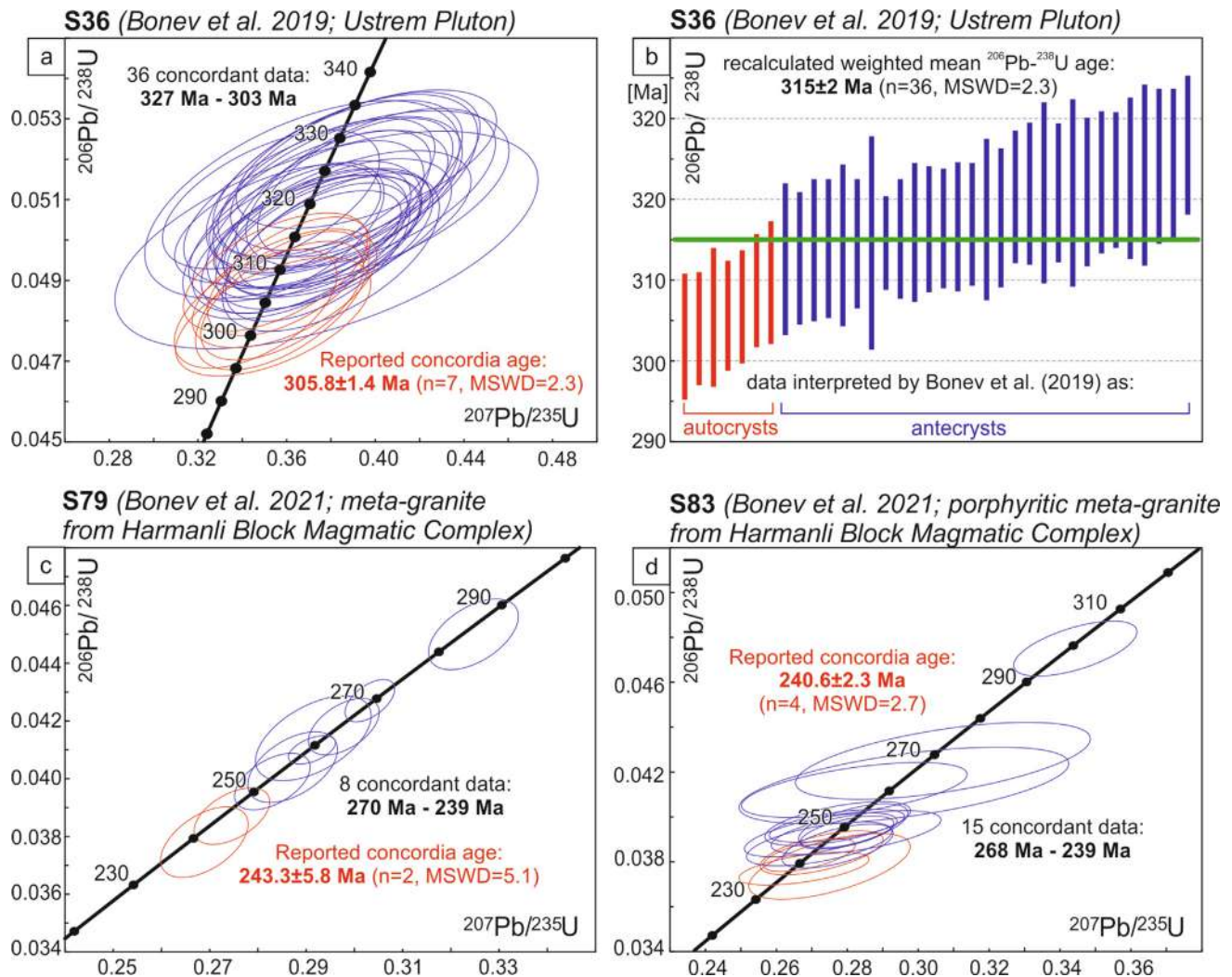


**Fig. 9.** Recalculation of the LA-ICP-MS zircon U-Th-Pb analyses from samples presented by Bonev et al. (2019, 2021): (a, b) meta-quartz diorite S36 from the Ustrem Pluton of Lesovo Complex; (c) meta-granite S79 and (d) K-feldspar porphyritic meta-granite S83, both from Harmanli Block Magmatic Complex; Wetherill Concordia diagrams (after Wetherill, 1956) are shown in (a), (c) and (d); the data shown as red ellipses were used for age calculations by Bonev et al. (2019, 2021); discordant data are not shown. (For interpretation of the references to colour in this figure legend, the reader is referred to the web version of this article.)

ca. 252 Ma Ömeroba Pluton and the ca. 249 Ma Tepecik Pluton (Natal'in et al., 2016; Aysal et al., 2018).

We excluded from further discussion the ages of the Radevo granite, the Svetlina meta-granite and one unnamed intrusive within the basement reported by Bonev et al. (2021), as all are based on only one single concordant data point (Supplementary Table 4, [dataset] Sałacińska et al., 2022).

## 6.2. Interpretation of the geochemical data and magma generation temperature in a regional context

Previously published geochemical data together with new data presented in this study show that the Late Carboniferous to Triassic granitoids from the Strandja Zone are a heterogeneous group of granitoids with mostly a monzogranite to granodiorite composition (Fig. 6a) and are transitional between metaluminous-peraluminous to peraluminous compositions (Fig. 6b). The trace element and REE patterns of the Sakar Batholith and Levka Pluton presented in this study are similar to earlier published data from the Sakar Batholith, as well as to the Late Carboniferous to Early Permian Ustrem Pluton, Melnitsa Complex, some samples from the Kula Granite of the Central Strandja Batholith and another

unnamed intrusion from the Sakar Unit (Fig. 6c,e). Samples from the Central Strandja Batholith represented by the Fakiya Granite and some samples from the Kula Granite show slightly stronger fractionation of HREE and a lack of Eu anomalies. Akgündüz et al. (2021) suggested that the trace element and REE variations in samples of the Kula Granite result from magma mixing, fractional crystallization and partial melting processes. Additionally, the ca. 295 Ma Aleksandrovo Granite has distinct trace element and REE patterns, which are interpreted as derived from melt associated with the last stage of the regional magmatic evolution (Bonev et al., 2021). Generally similar trace elements and REE features are also documented from the Permian to Triassic Kırklareli, Izvorovo and Tepecik plutons, as well as from the Harmanli Block Magmatic Complex, with the exception of one sample from the latter, which is again interpreted as a product of the final stage of the magmatic evolution (Fig. 6d,f).

In some recent studies from the Strandja Zone (e.g., Bonev et al., 2019, 2021; Akgündüz et al., 2021), the geochemical data described above (Fig. 6c-f) coupled with discrimination diagrams, were used to determine the tectonic setting of the Late Carboniferous to Triassic magmatism in the region. Based on these data, Bonev et al. (2019, 2021) and Akgündüz et al. (2021) supported the previously proposed

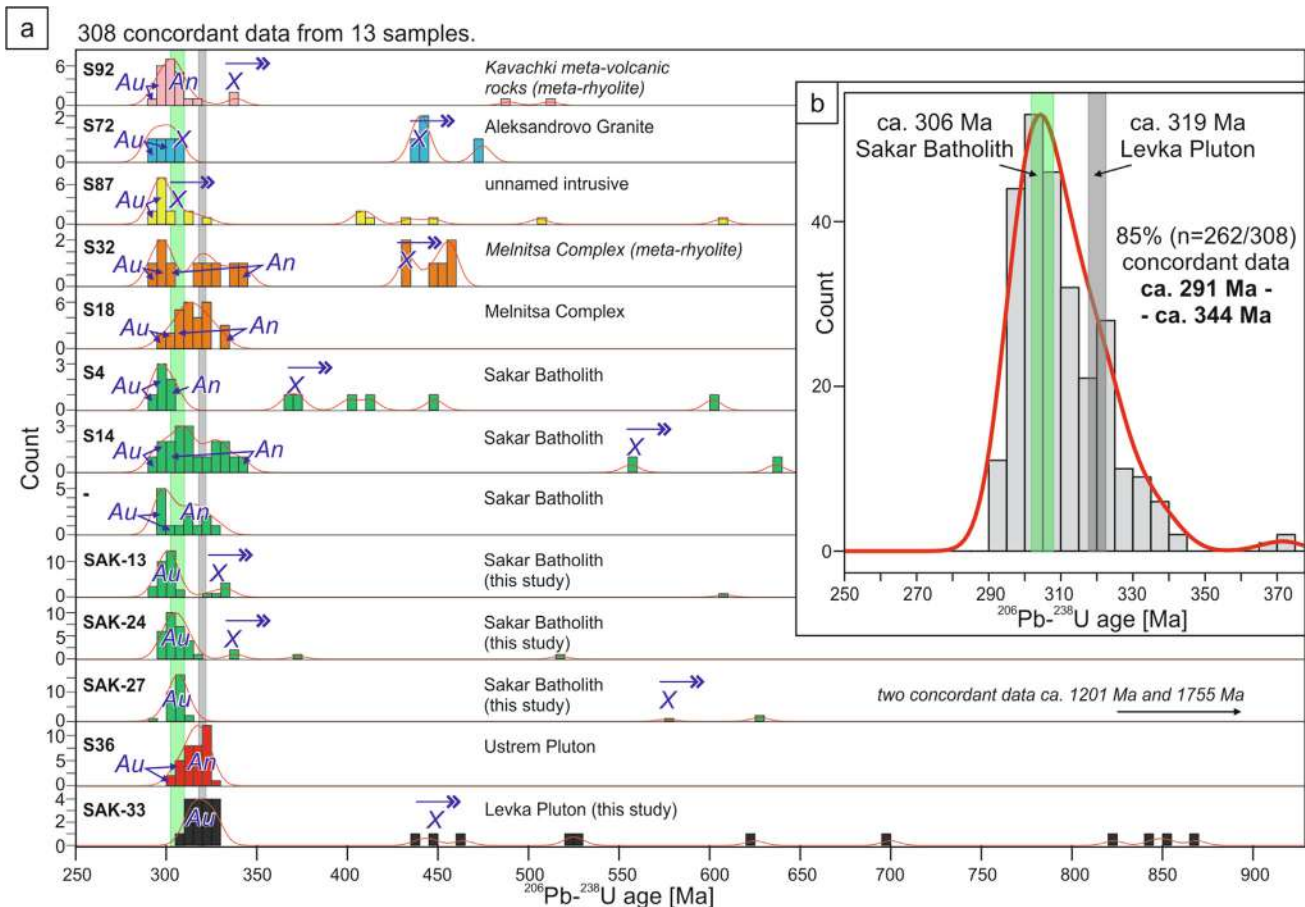


**Fig. 10.** Compilation of concordant U-Pb data from Late Carboniferous to Early Permian magmatic rocks from the Sakar Unit, which were interpreted by various authors as coming from autocrystic (Au), antecrystic (An) or xenocrystic (X) zircon crystals. Colours indicate different units (a) Distribution of the ages from 13 samples of intrusive and extrusive rocks. (b) Distribution of compiled data from all samples show a major range of ages (ca. 290 Ma to ca. 350 Ma). Data sources: [Pristavova et al., 2019](#); [Bonev et al., 2019, 2021](#); [Sałacińska et al., 2021a](#); and this study.

idea that all the Late Carboniferous to Triassic magmatic rocks were part of one long-lived magmatic arc associated with subduction and eventual closure of the Paleo-Tethys Ocean to the south of the Strandja Zone ([Sunal et al., 2006](#); [Natal'in et al., 2016](#); [Aysal et al., 2018](#); [Bonev et al., 2019](#)). However, magmatic arc signatures (e.g. the REE, Nb and Ta anomalies) can be also inherited from the source rocks, as is often the case in post-collision granites, thus making arc vs post-collision granites difficult to distinguish (e.g. [Pearce et al., 1984](#); [Harris et al., 1986](#); [Pearce, 1996](#)).

[Sałacińska et al. \(2021\)](#) used differences in the zircon populations and zircon saturation temperature ( $T_{\text{Zr}}$ ) of the different magma generations to suggest that the felsic intrusive and extrusive rocks in the Strandja Zone represent two distinctive groups: one Late Carboniferous to Early Permian and the other Late Permian to Triassic, the likely products of different tectonic environments. These authors also stated that generally it is not possible to distinguish post-collisional from magmatic arc granites based only on geochemical data, and agreed with [Peytcheva et al. \(2016\)](#) that Late Carboniferous to Early Permian magmatism was probably associated with the last stages of the Variscan orogeny, similar to coeval granitoids from the Balkan and Sredna Gora zones (e.g. [Haydoutov and Yanev, 1997](#); [Balkanska et al., 2021](#)).

A compilation of all published concordant U-Pb analyses from Late Carboniferous to Early Permian granitoids of Sakar Unit ([Fig. 9](#)) reveals that most of the samples contain antecrystic and xenocrystic zircons. According to [Miller et al. \(2003\)](#), inherited zircon components in granitoids indicate that they were zircon satu-

rated at their source, and as Zr is present mainly in crystals rather than melt, the zircon saturation temperatures ( $T_{\text{Zr}}$ ) should place an upper limit on the magma temperature. Therefore,  $T_{\text{Zr}}$  calculated from bulk-rock compositions (after [Watson and Harrison, 1983](#), Supplementary Table 2, [dataset] [Sałacińska et al., 2022](#)) could be used for determinations of the upper limit of magma crystallisation temperatures (after [Miller et al., 2003](#)). The calculation of  $T_{\text{Zr}}$  for samples from this study shows that there is no significant difference in  $T_{\text{Zr}}$  between the Levka Pluton (746 °C) and the Sakar Batholith (778–758 °C, average of 760 °C), and other Late Carboniferous to Early Permian intrusions for which calculations were made based on data from previous studies ([Kamenov et al., 2010](#); [Bonev et al., 2019, 2021](#); [Akgündüz et al., 2021](#)). These results are similar to the average  $T_{\text{Zr}}$  (766 °C) for inheritance-rich “cold” granitoids presented by [Miller et al. \(2003\)](#), who proposed that there is a fundamentally different mechanism of melt production between inheritance-rich (“cold”) and inheritance-poor (“hot”) intrusions. Generation of inheritance-rich magma requires lowering of the melt temperature below 800 °C, probably by infiltration of a water-rich fluid phase ([Miller et al., 2003](#)), which is in agreement with the interpretation of Sakar Batholith magma genesis presented by [Kamenov et al. \(2010\)](#). Additionally, “cold” magmas are relatively rich in crystals, and therefore tend to form plutons rather than erupt ([Miller et al., 2003](#)).

Zircon populations of the Late Permian to Triassic magmatic rocks from Strandja Zone are inheritance-poor and yield higher  $T_{\text{Zr}}$  (768 °C, 805 °C, 810 °C for the Izvorovo, Kırklareli, Tepecik plu-



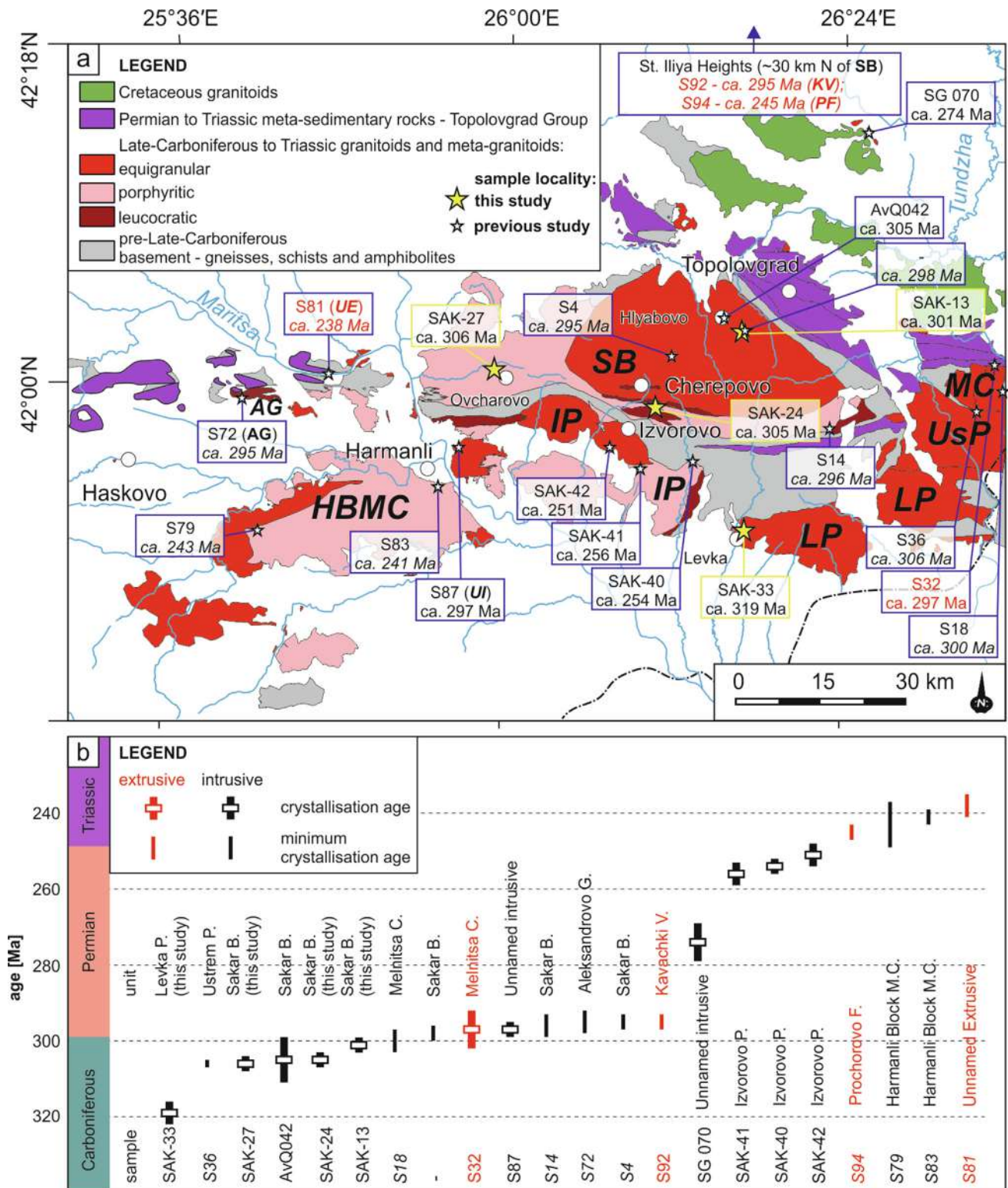


**Fig. 11.** Spatial and temporal distribution of the Late Carboniferous to Triassic magmatic rocks in the Sakar Unit with re-interpretation of their crystallisation ages: (a) geological map showing classification of intrusive (black text) and extrusive (red text) rocks according to their age of emplacement with re-interpretation of the part of published ages as minimum crystallization ages (italic). AG – Aleksandrovo Granite, HBMC – Harmanli Block Magmatic Complex, IP – Izvorovo Pluton, KV – Kavachki meta-volcanic rocks, LP – Levka Pluton, MC – Melnitsa Complex, PF – Prochorovo Formation, SB – Sakar Batholith, UsP – Ustrem Pluton, UI – unnamed intrusive, UE – unnamed extrusive; (b) Summary of U-Pb zircon age determinations from all dated magmatic bodies within the Strandja Zone. Data sources: Georgiev et al., 2012; Peytcheva et al., 2016; Pristavova et al., 2019; Bonev et al., 2019, 2021; Salacińska et al., 2021a; and this study. (For interpretation of the references to colour in this figure legend, the reader is referred to the web version of this article.)

tons, respectively) than Late Carboniferous to Early Permian group as shown by Salacińska et al. (2021). Calculation of  $T_{Zr}$  for the Triassic Harmanli Block Magmatic Complex based on data published

by Bonev et al. (2021) gives a temperature of 811 °C and 574 °C, with the latter coming from meta-granite interpreted as derived from the last stage of magma evolution. These plutons are also

inheritance-poor. Generation of such “hot” granites do not require the presence of fluid during magma generation due to high melt temperature (Miller et al., 2003).

The approach presented above allows for distinguishing two groups of granitoids based on different thermal conditions during the magma generation. To better resolve this problem and more conclusively determine the tectonic setting related to the regional Late Carboniferous to Triassic magma evolution, additional geochemical analysis such as isotopic (e.g., Hf, O) studies on zircon crystals could also be undertaken.

### 6.3. Comparison of the Variscan evolution of the Strandja and Sredna Gora zones

Although the Strandja Zone shares several similarities with the neighbouring units of the North Gondwanan margin in the Balkanides (e.g., Sredna Gora and Balkan zones; Fig. 1a) and the Pontides (Sakarya Zone, Fig. 1a), detailed studies concerning their common Variscan evolution are rare. Okay and Topuz (2017) were the first to note that all these units comprise basement of predominantly Late Neoproterozoic to Early Paleozoic sedimentary and igneous rocks deformed and metamorphosed during the Early Carboniferous, and intruded by Late Carboniferous to Permian granitoids (Fig. 12). They suggested that these units were part of a single continental magmatic arc since the Late Devonian, which consequently collided with Laurussia. Bonev et al. (2019, 2021) also considered the Strandja Zone, together with Serbo-Macedonian and Rhodope zones, as part of a long-lived Late Carboniferous to Middle Triassic magmatic arc formed along the active continental margin of the Eurasian plate during subduction of the Palaeo-Tethys oceanic lithosphere.

The existence of a common continental magmatic arc since the Late Devonian, including all the units of the Balkanides as suggested by Okay and Topuz (2017) is questioned by the presence of a Variscan shear zone separating the Sredna Gora metamorphic basement from the Balkan Zone pre-Permian basement (Fig. 12; Carrigan et al., 2005; Gerdjikov et al., 2007; Balkanska et al., 2021). The latter was metamorphosed at low- to medium-grade greenschist facies conditions during the Variscan orogeny, whereas the former complex shows evidence of a multi-stage Variscan metamorphic evolution including early high-pressure (HP) metamorphism (Gaggero et al., 2009; Gerdjikov et al., 2014), followed by Early Carboniferous high-temperature (HT) metamorphism accompanied by migmatization (Carrigan et al., 2006; Žák et al., 2021). It is suggested that these two units were finally juxtaposed along a Variscan shear zone between ca. 337 and ca. 314 Ma (Balkanska et al., 2021), most likely at ~ 334 Ma when pervasive retrogression of the Sredna Gora migmatites under greenschist- to lower amphibolite-facies conditions took place (Gerdjikov et al., 2010).

There are several similarities concerning the pre-, syn- and post-Variscan orogenic evolution between the Sredna Gora and Strandja zones. Recent detrital zircon U-Pb geochronological studies suggest that both units share a very similar metamorphic basement of Gondwana origin. This includes a sedimentary protolith with a Cambrian maximum depositional age (Vladinova et al., 2018; Žák et al., 2021) and intruded by Cambrian and Ordovician granitoids (e.g., Peytcheva and Von Quadt, 2004; Carrigan et al., 2006; Şahin et al., 2014; Lazarova et al., 2015; Bonev et al., 2019; Vladinova and Georgieva, 2020; Yılmaz et al., 2021). All these rocks were metamorphosed at high-grade conditions during the Variscan (e.g., Okay et al., 2001; Carrigan et al., 2005; Sunal et al., 2011; Balkanska et al., 2021), although evidence for the HP event is only

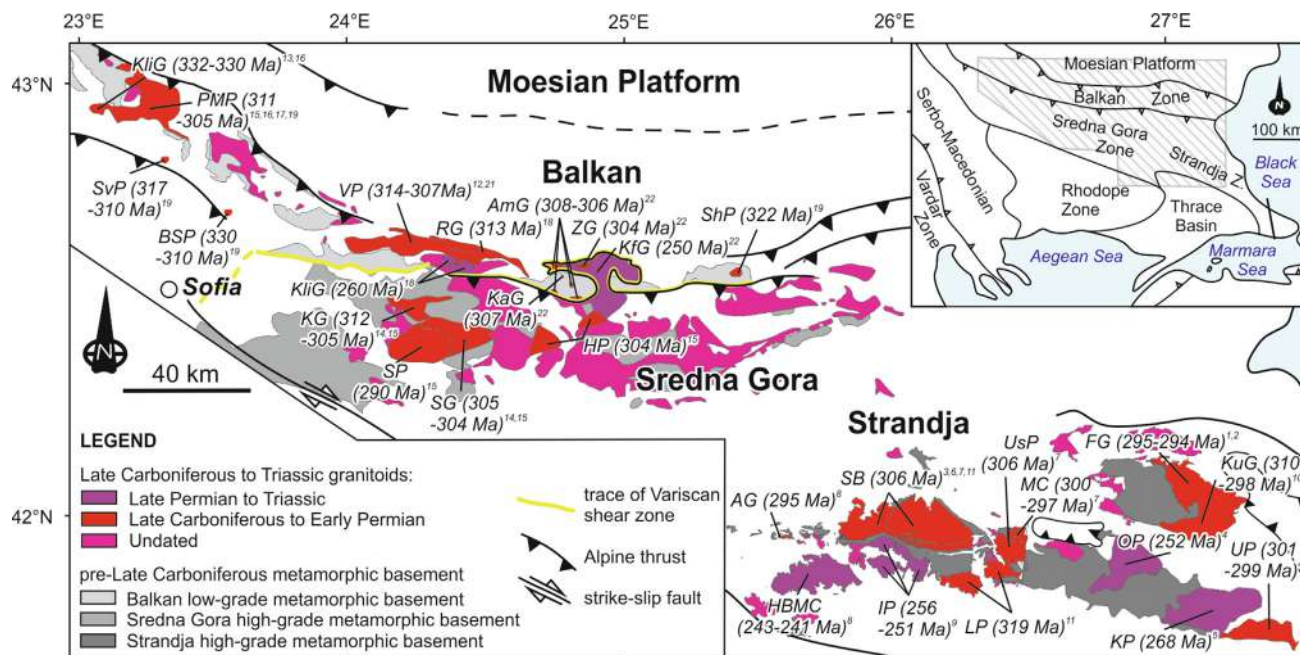


**Fig. 12.** Summary geological map of the Late Carboniferous to Triassic granitoids and its basement rocks in the Strandja, Sredna Gora and Balkan zones. Abbreviations for Strandja Zone: AG - Aleksandrovo Granite; FG - Fakiya Granite; HBMC - Harmanli Block Magmatic Complex; IP - Izvorovo Pluton; KuG - Kula Granite; KP - Kırklareli Pluton; MC - Melnitsa Complex; OP - Ömeroba Pluton; SB - Sakar Batholith; UP - Üsküp Pluton; UsP - Ustrem Pluton; TP - Tepecik Pluton; and for Balkan and Sredna Gora zones: AmG - Ambaritsa Granite; BSP - Buhovo-Seslavtsi Pluton; HP - Hisarya Pluton; KG - Koprivshitsa Granite; KaG - Kazan Granite; KFG - Kalofer Granite; Klig - Klisura Granite; PMP - Petrohan-Mezdrea Pluton; RG - Ribaritsa Granite; SG - Smilovene Granite; SP - Strelcha Pluton; ShP - Shipka Pluton; SvP - Svidnya Pluton; VP - Vezhen Pluton; ZG - Zhaltets Granodiorite. Data sources for the Strandja Zone: (1) Georgiev et al., 2012; (2) Machev et al., 2015; (3) Peytcheva et al., 2016; (4) Natal'in et al., 2016; (5) Aysal et al., 2018; (6) Pristavova et al., 2019; (7) Bonev et al., 2019; (8) Bonev et al., 2021; (9) Salacińska et al., 2021; (10) Akgündüz et al., 2021; (11) this study. Data source for Sredna Gora and Balkan zones: (12) Kamenov et al., 2002; (13) Malinov et al., 2004; (14) Peytcheva et al., 2004a; (15) Carrigan et al., 2005; (16) Peytcheva et al., 2006; (17) Nedialkov et al., 2007; (18) Antonov et al., 2010; (19) Dyulgerov et al., 2018; (20) Peytcheva et al., 2018; (21) Georgiev et al., 2020; (22) Balkanska et al., 2021.



reported for the Sredna Gora Zone (Gaggero et al., 2009; Trapp et al., 2020). In this study we have presented clear evidence for the existence of a pre-Alpine high-grade metamorphic and deformational event in the Sakar Unit, likely accompanied by anatexis (Fig. 3 and Fig. 4), which is most probably of Variscan age, as it is affecting Ordovician granitoids (Bonev et al., 2019) and cut by the Late Carboniferous Levka Pluton.

Voluminous Late Carboniferous to Triassic granitoid emplacement (Fig. 12) is common for the Strandja (e.g., Georgiev et al., 2012; Machev et al., 2015; Peytcheva et al., 2016; Natal'in et al., 2016; Aysal et al., 2018; Pristavova et al., 2019; Bonev et al., 2019, 2021; Akgündüz et al., 2021; Sałacińska et al., 2021; this study) and Sredna Gora zones (e.g., Kamenov et al., 2002; Malinov et al., 2004; Peytcheva et al., 2004a, 2006, 2018; Carrigan et al., 2005; Nedialkov et al., 2007; Antonov et al., 2010; Dyulgerov et al., 2018; Georgiev et al., 2020; Balkanska et al., 2021). In both zones these granitoids have not experienced Variscan deformation and therefore are considered as post-tectonic (Carrigan et al., 2005), except some granites in the Sredna Gora Zone intruded within a long-lived shear zone which developed along the contact with the Balkan Zone (Balkanska et al., 2021). All these similarities between the Strandja and Sredna Gora zones suggest that during Variscan time they were part of the metamorphic core of the orogen.

#### 6.4. Comparison of the Variscan evolution of the Strandja Zone with other neighbouring units

Structural and geochronological studies from the Serbo-Macedonian Zone show that this metamorphic complex also shares a similar Variscan evolution with other parts of Balkanides, including the Strandja Zone, although the amount of felsic magma emplacement, especially of Late Carboniferous granitoids, is reduced in the Serbo-Macedonian Zone (e.g., Peytcheva et al., 2015; Antić et al., 2016). Differences in the ages of granitoid emplacement and the amount of magmatism in the Variscan units of the Black Sea region is confirmed by data from the Sakarya Zone in Turkey (Fig. 1b). There, unlike the Sredna Gora and Strandja basement, where *syn*-tectonic granitoids are not reported, Carboniferous *syn*-tectonic granitoids and associated extrusive rocks are predominant (ca. 336–319 Ma, Topuz et al., 2010; Ustaömer et al., 2012, 2013; Şengün and Koralay, 2017; Dokuz et al., 2017; Şengün et al., 2020). In fact, the Late Carboniferous to Early Permian post-tectonic intrusions in the Sakarya Zone represent only a minor component (ca. 302–294 Ma; Karlı et al., 2016; Okay and Topuz, 2017). In this zone, upper amphibolite- to granulite facies-metamorphism accompanied by anatexis took place between ca. 340 Ma and ca. 330 Ma (Okay, 1996; Topuz et al., 2004).

The high-grade metamorphic core of the Variscan orogen (Serbo-Macedonian, Sredna Gora and Sakarya zones) is juxtaposed with low-grade Precambrian to lower Paleozoic rocks of the Balkan Zone (e.g., Haydoutov, 1989; Balkanska et al., 2021). Their contact likely represents a Variscan shear zone (Fig. 12; e.g., Carrigan et al., 2005; Gerdjikov et al., 2007; Balkanska et al., 2021). In this zone, granitoid magmatism, which started in the Early Carboniferous (Fig. 12; Klisura granite, ~332 Ma), post-dates the main Variscan phase of metamorphism (Buzzy et al., 2010; Peytcheva et al., 2018; Balkanska et al., 2021). However, deformation continued in discrete shear zones until ~306 Ma, as was suggested by the structural and geochronological analysis of pre-, syn- and post-tectonic granites (Balkanska et al., 2021).

The Rhodope Zone has also been compared to the neighbouring Strandja Zone (Bonev et al., 2019, 2021). It represents a large high-grade metamorphic complex which experienced a long and multi-stage tectonic evolution including *syn*-metamorphic thrusting during the Jurassic and Cretaceous followed by large-scale extension and core complex formation in the Cenozoic (i.e., Burg, 2012, for review).

Late-Carboniferous to Permian orthogneisses have been reported from all the units of this metamorphic complex (e.g., Ovtcharova et al., 2002, 2004; Peytcheva et al., 2004b; Cornelius, 2008; Turpaud and Reischmann, 2010), where their Variscan structural position and evolution was obscured by the strong Alpine overprint.

#### 6.5. The problem of deciphering the tectonic settings of the Late Carboniferous to Triassic magmatism in the Black Sea region

The tectonic setting for magma genesis and evolution in the Carboniferous to Triassic in the Black Sea region and especially in the Balkanide units is not fully understood. Carrigan et al. (2005) suggested that Late Carboniferous to Permian magmatic activity in the Balkanides was related to continued subduction under Laurussia. Peytcheva et al. (2018), however, advocated a collisional setting for the Early Carboniferous granitoids from the Western Balkan Zone and a *syn*- to post-collisional setting for the Late Carboniferous to Permian magmatism in the rest of the Balkanides. The Early Triassic granitoids in the Serbo-Macedonian Zone are interpreted as post-collisional (e.g., Zidarov et al., 2007; Peytcheva et al., 2009, 2015) or rift-related (e.g., Himmerkus et al., 2009; Antić et al., 2016), whereas no clear conclusions were made about the tectonic setting of coeval magmatic rocks from the other parts of the Balkanides. Recently Bonev et al. (2019, 2021) suggested that Late Carboniferous to Triassic magmatic rocks in Strandja Zone are products of continental arc magmatism related to the Paleo-Tethys Ocean subduction beneath proto-Europe, although Kamenov et al. (2010) consider emplacement of the Sakar Batholith related to a post-collisional tectonic setting.

However, in the studies above, determining the tectonic settings during the different stages of the Variscan orogeny was mostly based on geochemical signatures of the magmatic rocks. The only real field evidence for the existence of Paleo-Tethys subduction in the Black Sea region comes from the Sakarya Zone, where the Triassic Karakaya subduction-accretionary complex crops out. This complex contains Late Triassic high pressure (HP) eclogites and blueschists (e.g., Okay and Göncüoğlu, 2004) as well as blocks of Devonian, Carboniferous and Permian radiolarian cherts (Okay et al., 2011), most probably representing fragments of Paleo-Tethys oceanic crust. As documented by Okay and Topuz (2017), such accretionary complexes are not known in the Balkanides, including the Strandja Zone, and farther west in Central Europe, which indicates that the Sakarya Zone marks the westernmost limit of the Paleo-Tethys Ocean. Middle Triassic eclogitic gabbros (Liati, 2005) and ca. 200 Ma ultra-HP metamorphism (dated by U-Th-Pb on monazite, Petrik et al., 2016), in the Intermediate Terrane of Rhodope Metamorphic Complex may be also related to Paleo-Tethys Ocean subduction (Petrik et al., 2016). Upper Triassic turbidites which could be correlated with those from the Karakaya Complex are part of the allochthonous Veleka Unit of Strandja Zone. This unit represents a NW-vergent nappe whose root zone is still unknown (e.g., Gerdjikov, 2005). On the other hand, the Permian to Early Triassic sedimentary rocks which lie unconformably over the Variscan crystalline basement in the Balkanides, as well as the Sakar Unit of Strandja Zone comprise continental clastic sequences, and are associated with felsic volcanic rocks (e.g., Chatalov, 1990; Cortesogno et al., 2004; Bonev et al., 2021) which are interpreted as related to the Strandja Zone volcanic arc (Bonev et al., 2021) or late orogenic extensional collapse in the Balkanides (Cortesogno et al., 2004).

From the above discussion it is apparent that absolute dating of magmatic rocks backed up by geochemical analysis is not sufficient to discriminate the tectonic conditions during different phases of orogenic evolution. These processes can only be unravelled when combined with detailed studies on the metamorphic, deformational and basin evolution.



## 7. Conclusions

Based on the results presented in this study, coupled with a reinterpretation of previous work we can draw the following conclusions:

1. The ca. 319 Ma Levka Pluton of the Sakar Unit is the oldest Late Carboniferous intrusion documented so far in the Strandja Zone. The distribution of all the concordant U-Pb data from Levka and Ustrem plutons shows strong similarities. A reinterpretation of the previously reported crystallisation age of the Ustrem pluton, together with geochemical similarities between both plutons, suggests that they were probably part of the same large magmatic body.
2. The structural field observations along the contact of Levka Pluton with its country rocks provides clear evidence for the existence of Variscan deformation and metamorphism in the Strandja Zone, as well as the upper age limit of this event (>319 Ma).
3. The presence of antecrystic and xenocrystic zircons in samples of Late Carboniferous to Early Permian magmatic rocks with concordant U-Pb ages as old as ca. 344 Ma suggests that the magmatic evolution in the Strandja Zone may have started at this time, although intrusions of this age are still not directly dated.
4. A reinterpretation of previously reported U-Pb zircon geochronological data from the Sakar Batholith, together with those presented in this study, shows that the intrusion was most likely emplaced at ca. 306 Ma.
5. The zircon population characteristics, together with the estimated  $T_{Zr}$  of different plutons from the Strandja Zone support the hypothesis of the existence of two distinct groups (suites): Late Carboniferous to Early Permian “cold” and Late Permian to Triassic “hot” granitoids, separated by 20 Myr of magmatic quiescence.
6. The Late Carboniferous to Early Permian magmatic evolution of the Strandja Zone displays a strong resemblance to that of the Sredna Gora Zone. Further similarities of the basement protoliths, showing clear Gondwanan affinities, and their Variscan metamorphism implies both units, probably together with Serbo-Macedonian Metamorphic Complex and Sakarya Zone, were part of the metamorphic core of the Variscan Orogen.

## CRedit authorship contribution statement

**Anna Sałacińska:** Conceptualization, Data curation, Formal analysis, Funding acquisition, Investigation, Methodology, Project administration, Resources, Visualization, Writing – original draft, Writing – review & editing. **Ianko Gerdjikov:** Conceptualization, Formal analysis, Investigation, Methodology, Resources, Supervision, Visualization, Writing – original draft, Writing – review & editing. **Alexandre Kounov:** Conceptualization, Investigation, Supervision, Visualization, Writing – original draft, Writing – review & editing. **David Chew:** Formal analysis, Funding acquisition, Investigation, Validation, Writing – review & editing. **Krzysztof Szopa:** Formal analysis, Investigation, Project administration, Supervision, Writing – review & editing. **Ashley Gumsley:** Investigation, Writing – review & editing. **Isabella Kocjan:** Formal analysis, Writing – review & editing. **Beata Marciniak-Maliszewska:** Formal analysis, Validation, Writing – review & editing. **Foteini Drakou:** Formal analysis, Validation, Writing – review & editing.

## Declaration of Competing Interest

The authors declare that they have no known competing financial interests or personal relationships that could have appeared to influence the work reported in this paper.

## Acknowledgements

This research was supported by a Preludium Grant awarded to AS from the National Science Centre (Narodowe Centrum Nauki), NCN, in Poland (grant agreement no. UMO-2018/29/N/ST10/00368). DC is supported in part by a research grant from Science Foundation Ireland (SFI) under Grant Number 13/RC/2092\_P2 (iCrag, the SFI Research Centre in Applied Geosciences). The authors would like to thank Nikolay Gospodinov for logistical support during the field work. We wish to thank the Editor, Sanghoon Kwon, as well as Boris Natal'in, Mihai Ducea and Tobias Stephan for constructive reviews which helped to improve the manuscript.

## Appendix A. Supplementary material

Supplementary data to this article can be found online at <https://doi.org/10.1016/j.gr.2022.04.013>.

## References

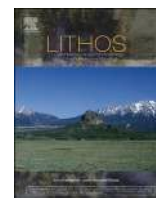
- Akgündüz, S., Aysal, N., Peytcheva, I., Yilmaz, Ş., Güngör, Y., 2021. Geochronology, geochemistry and tectono-magmatic evolution of the upper Carboniferous–lower Permian Kula pluton in the Istranca (Strandja) Massif, NW Turkey. *Geol. Carpathica* 72 (5), 373–394. <https://doi.org/10.31577/GeolCarp.72.5.2>.
- Antić, M., Peytcheva, I., von Quadt, A., Kounov, A., Trivić, B., Serafimovski, T., Tasev, G., Gerdjikov, I., Wetzel, A., 2016. Pre-Alpine evolution of a segment of the North-Gondwanan margin: geochronological and geochemical evidence from the central Serbo-Macedonian Massif. *Gondwana Res.* 36, 523–544. <https://doi.org/10.1016/j.gr.2015.07.020>.
- Antonov, M., Gerdjikov, S., Metodiev, L., Kiselinov, Ch., Sirakov, V., Valev, V., 2010. Explanatory note to the geological map of the Republic of Bulgaria scale 1:50000: Map sheet K-35-37-B Pirdop, Geocomplex, Sofia.
- Ashwal, L.D., Tucker, R.D., Zinner, K., 1999. Slow cooling of deep crustal granulites and Pb-loss in zircon. *Geochim. Cosmochim. Acta* 63 (18), 2839–2851. [https://doi.org/10.1016/S0016-7037\(99\)00166-0](https://doi.org/10.1016/S0016-7037(99)00166-0).
- Aysal, N., Şahin, S.Y., Güngör, Y., Peytcheva, I., Öngen, S., 2018. Middle Permian–Early Triassic magmatism in the Western Pontides, NW Turkey: geodynamic significance for the evolution of the Paleo-Tethys. *J. Asian Earth Sci.* 164, 83–103. <https://doi.org/10.1016/j.jseas.2018.06.026>.
- Balkanska, E., Gerdjikov, I., Georгиев, S., Lazarova, A., Dörr, W., Kounov, A., 2021. Structural and geochronological constraints on the magmatic and tectonic events in the pre-Alpine basement of the central parts of the Balkan fold-thrust belt (Central Stara Planina Mountains, Bulgaria). *Int. J. Earth Sci.* 110, 1181–1211. <https://doi.org/10.1007/s00531-021-02011-1>.
- Bedi, Y., Vasilev, E., Dabovski, C., Ergen, A., Okuyucu, C., Dogan, A., Kagan Tekin, U., Ivanova, D., Boncheva, I., Lakova, I., Sachanski, V., Kuscu, I., Tumcay, E., Gülnur Demiray, D., Soykan, H., Cemal Goncuoglu, M., 2013. New age data from the tectonostratigraphic units of the Istranca “Massif” in NW Turkey: a correlation with SE Bulgaria. *Geol. Carpathica* 64 (4), 255–277. <https://doi.org/10.2478/geoca-2013-0019>.
- Bomparola, R.M., Ghezzi, C., Belousova, E., Griffin, W.L., O'Reilly, S.Y., 2007. Resetting of the U-Pb zircon system in cambro-ordovician intrusives of the Deep Freeze range, Northern Victoria Land, Antarctica. *J. Petrology* 48 (2), 327–364. <https://doi.org/10.1093/petrology/egl064>.
- Bonev, N., Filipov, P., Raicheva, R., Moritz, R., 2021. Evidence of late palaeozoic and middle triassic magmatism in the sakar-strandzha zone, SE Bulgaria: regional geodynamic implications. *Int. Geol. Rev.* (in press). doi: 10.1080/00206814.2021.1917008.
- Bonev, N., Filipov, P., Raicheva, R., Moritz, R., 2019. Timing and tectonic significance of Paleozoic magmatism in the Sakar unit of the Sakar-Strandzha Zone, SE Bulgaria. *Int. Geol. Rev.* 61 (16), 1957–1979. <https://doi.org/10.1080/00206814.2019.1575090>.
- Bonev, N., Spikings, R., Moritz, R., 2020.  $^{40}\text{Ar}/^{39}\text{Ar}$  age constraints for an early Alpine metamorphism of the Sakar unit, Sakar-Strandzha zone, Bulgaria. *Geol. Mag.* 157 (12), 2106–2112. <https://doi.org/10.1017/S0016756820000953>.
- Boyadjiev, S., Lilov, P., 1972. On the K-Ar dating of the South Bulgarian granitoids from Srednogorie and Sakar-Strandja Zones, in: *Proceedings of the Geological Institute, ser. Geochemistry, Mineralogy, Petrography* 26 (2), 121–220 (in Bulgarian).

- Boyakov, I., Kozhoukharov, D., Savov, S., 1965. Geological structure of the southern slope of Sakar Mountain between the villages Radovets and Kostur. *Revi. Bulgarian Geol. Soc.* 26 (2), 121–134. In Bulgarian.
- Burg, J.-P., 2012. Rhodope: from Mesozoic convergence to Cenozoic extension. Review of petro-structural data in the geochronological frame. *J. Virtual Explor.* 42, 1–44. <https://doi.org/10.3809/jvirtex.2011.00270>.
- Carrigan, C.W., Mukasa, S.B., Haydoutov, I., Kolcheva, K., 2005. Age of Variscan magmatism from the Balkan sector of the orogen, central Bulgaria. *Lithos* 82, 125–147. <https://doi.org/10.1016/j.lithos.2004.12.010>.
- Carrigan, C., Mukasa, S., Haydoutov, I., Kolcheva, K., 2006. Neoproterozoic magmatism and Carboniferous high-grade metamorphism in the Sredna Gora Zone, Bulgaria: an extension of the Gondwana-derived Avalonian-Cadomian belt? *Precambrian Res.* 147, 404–416. <https://doi.org/10.1016/j.precamres.2006.01.026>.
- Cattò, S., Cavazza, W., Zattin, M., Okay, A., 2018. No significant Alpine tectonic overprint on the Cimimerian Strandja Massif (SE Bulgaria and NW Turkey). *Int. Geol. Rev.* 60 (4), 513–529. <https://doi.org/10.1080/00206814.2017.1350604>.
- Chatalov, A., 1992. Petrological characteristics of the rocks of the Melnitsa orthometamorphic complex, Sakar Mountains. *Rev. Bulgarian Geol. Soc.* 53, 99–112. In Bulgarian.
- Chatalov, G.A., 1990. Geology of the Strandja zone in Bulgaria: *Geologica Balcanica, Series Opum Singulorum* 4. Sofia, Publishing house of Bulgarian Academy of Sciences, 263 p. (in Bulgarian).
- Cornelius, N.K., 2008. UHP metamorphic rocks of the Eastern Rhodope Massif, NE Greece: New constraints from petrology, geochemistry and zircon ages. Ph.D. thesis, Johannes Gutenberg University of Mainz, 173 p.
- Cortesogno, L., Gaggero, L., Ronchi, A., Yanev, S., 2004. Late orogenic magmatism and sedimentation within Late Carboniferous to early permian basins in the Balkan terrane (Bulgaria): geodynamic implications. *Int. J. Earth Sci.* 93, 500–520. <https://doi.org/10.1007/s00531-004-0410-y>.
- Dokuz, A., Külekçi, E., Aydınçakır, E., Kandemir, R., Alçiçek, M.C., Pecha, M.E., Sünnetçi, K., 2017. Cordierite-bearing strongly peraluminous Cebre Rhyolite from the eastern Sakarya Zone, NE Turkey: constraints on the Variscan Orogeny. *Lithos* 278–281, 285–302. <https://doi.org/10.1016/j.lithos.2017.02.002>.
- Dylugorov, M., Ovtcharova-Schaltegger, M., Ulianov, A., Schaltegger, U., 2018. Timing of high-K alkaline magmatism in the Balkan segment of southeast European Variscan edifice: ID-TIMS and LA-ICP-MS study. *Int. J. Earth Sci.* 107, 1175–1192. <https://doi.org/10.1007/s00531-017-1527-0>.
- Franke, W., Ballèvre, M., Cocks, L.R.M., Torsvik, T.H. and Żelaźniewicz, A., 2020. Variscan Orogeny. *Encyclopedia of Geology*. second ed. pp. 338–349. doi: 10.1016/B978-0-08-102908-4.00022-9.
- Gaggero, L., Buzzi, L., Haydoutov, I., Cortesogno, L., 2009. Eclogite relics in the Variscan orogenic belt of Bulgaria (SE Europe). *Int. J. Earth Sci.* 98 (8), 1853–1877. <https://doi.org/10.1007/s00531-008-0352-x>.
- Gallhofer, D., Von Quadt, A., Peytcheva, I., Schmid, S.M., Heinrich, C.A., 2015. Tectonic, magmatic, and metallogenic evolution of the Late Cretaceous arc in the Carpathian-Balkan orogen. *Tectonics* 34 (9), 1813–1836. <https://doi.org/10.1002/2015TC003834>.
- Georgiev, S., Gerdjikov, I., Peytcheva, I., Makaveev, P., 2020. Time frame of the Carboniferous tectonic and magmatic activity in the area of Vezhen pluton, Bulgaria. In: *Proceedings of the annual geological conference “Geosciences 2020”*. Bulgarian Geol. Soc. 81, pp. 72–74.
- Georgiev, S.V., Quadt, A., Heinrich, C., Peytcheva, I., Marchev, P., 2012. Time evolution of rifted continental arc: integrated ID-TIMS and LAICPMS study of magmatic zircons from the Eastern Srednogie, Bulgaria. *Lithos* 154, 53–67. <https://doi.org/10.1016/j.lithos.2012.06.020>.
- Gerdjikov, I., 2005. *Alpine Metamorphism and Granitoid Magmatism in the Strandja Zone: New Data from the Sakar Unit, SE Bulgaria*. *Turkish J. Earth Sci.* 14, 167–183.
- Gerdjikov, I., Georgiev, N., Dimov, D., Lazarova, A., 2007. The different faces of supposedly single thrust: a reevaluation of the Vezhen thrust, Central Balkanides. In: *Proceedings of the Annual Geological Conference “Geosciences 2007”*, Bulgarian Geological Society, pp. 24–26.
- Gerdjikov, I., Ruffet, G., Lazarova, A., Vangelov, D., Balkanska, E., Bonev, K., 2010. 40Ar/39Ar geochronological constraints of a Variscan transpression in Central Stara Planina Mountain. In: *Proceedings of the Annual Geological Conference “Geosciences 2010”*. Bulgarian Geological Society, pp. 109–110.
- Gerdjikov, I., Kounov, A., Vangelov, D., 2014. The Paleozoic Balkan terrane: a re-evaluation. In: *Proceedings of the Annual Geological Conference “Geosciences 2014”*. Bulgarian Geological Society, pp. 43–44.
- Halpin, J.A., Gerakites, C.L., Clarke, G.L., Belousova, E.A., Griffin, W.L., 2005. In-situ U-Pb geochronology and Hf isotope analyses of the Rayner Complex, east Antarctica. *Contrib. Mineral. Petrol.* 148, 689–706. <https://doi.org/10.1007/s00410-004-0627-6>.
- Halpin, J.A., Daczko, N.R., Milan, L.A., Clarke, G.L., 2012. Decoding near-concordant U-Pb zircon ages spanning several hundred million years: recrystallisation, metamictisation or diffusion? *Contrib. Mineral. Petrol.* 163, 67–85. <https://doi.org/10.1007/s00410-011-0659-7>.
- Harris, N.B.W., Pearce, J.A., Tindle, A.G., 1986. Geochemical characteristics of collision zone magmatism. *Geol. Soc. Spec. Publ.* 19, 67–81. <https://doi.org/10.1144/GSL.SP.1986.019.01.04>.
- Haydoutov, I., 1989. Precambrian ophiolites, Cambrian island arc, and Variscan suture in the South Carpathian-Balkan region. *Geology* 17 (10), 905–908. [https://doi.org/10.1130/0091-7613\(1989\)017<0905:POCIAA>2.3.CO;2](https://doi.org/10.1130/0091-7613(1989)017<0905:POCIAA>2.3.CO;2).
- Haydoutov, I., Yanev, S., 1997. The Protomoesian microcontinent of the Balkan Peninsula – a peri-Gondwanaland piece. *Tectonophysics* 272, 303–313. [https://doi.org/10.1016/S0040-1951\(96\)00264-8](https://doi.org/10.1016/S0040-1951(96)00264-8).
- Himmerkus, F., Reischmann, T., Kostopoulos, D., 2009. Triassic rift-related meta-granites in the Internal Hellenides, Greece. *Geol. Mag.* 146 (2), 252–265. <https://doi.org/10.1017/S001675680800592X>.
- Ivanov, Z., Gerdjikov, I., Kounov, A., 2001. New data and considerations about structure and tectonic evolution of Sakar region, SE Bulgaria. *Annuaire de l'Université de Sofia, Geology and Geography* 91, 35–80 (in Bulgarian).
- Ivanov, Z., 2017. *Tectonics of Bulgaria*. Sofia University Press, Sofia, 331 p. (in Bulgarian).
- Janoušek, V., Moya, J.F., Martin, H., Erban, V., Farrow, C., 2016. *Geochemical Modelling of Igneous Processes—Principles and Recipes in R Language*. Springer Geochemistry, New York, p. 346.
- Jordanov, M., Sarov, S., Georgiev, S.T., Marinova, R., Dobrev, G., Grozdev, V., Balkanska, E., Moskovska, L., 2008. Explanatory notes to the Geological Map of the Republic of Bulgaria 1: 50000, sheet K-35-76-B (Harmanly). *Geocomplex, Sofia*, pp. 1–60.
- Kamenov, B.K., von Quadt, A., Peytcheva, I., 2002. New insight into petrology, geochemistry and dating of the Vejen pluton, Bulgaria. *Bulgarian Acad. Sci. Geochim. Mineral. Petrol.* 39, 3–25.
- Kamenov, B.K., Vergilov, V., Dabovski, C., Vergilov, I., Ivchinova, L., 2010. The Sakar batholith – petrology, geochemistry and magmatic evolution. *Bulgarian Acad. Sci. Geochim. Mineral. Petrol.* 48, 1–37.
- Karsli, O., Dokuz, A., Kandemir, R., 2016. Subduction-related Late Carboniferous to Early Permian Magmatism in the Eastern Pontides, the Camlik and Casurluk plutons: insights from geochemistry, whole-rock Sr–Nd and in situ zircon Lu–Hf isotopes, and U–Pb geochronology. *Lithos* 266–267, 98–114. <https://doi.org/10.1016/j.lithos.2016.10.007>.
- Kozhoukharov, D., Kozhoukharova, E., 1973. Stratigraphy and petrology of the Precaubrian metamorphic rocks from the Sakar Mountain: bulletin of the Geological Institute – Series Geochemistry. *Mineral. Petrogr.* 22, 193–210. In Bulgarian.
- Kroner, U., Mansy, J.-L., Mazur, S., Aleksandrowski, P., Hann, H., Huckriede, H., Lacquement, F., Lamarche, J., Ledru, P., Pharaoh, T., Zedler, H., Zen, A., Zulauf, G., 2008. Variscan tectonics. In: McCann (Eds.), *The Geology of Central Europe: Volume 1: Precambrian and Palaeozoic*. Geological Society of London. doi: 10.1144/CEV1P.11.
- Kroner, U., Romer, R., 2013. Two plates – many subduction zones: the Variscan orogeny reconsidered. *Gondwana Res.* 24, 298–329. <https://doi.org/10.1016/j.gr.2013.03.001>.
- Lazarova, A., Naydenov, K., Petrov, N., Grozdev, V., 2015. Cambrian magmatism, Variscan high-grade metamorphism and imposed greenschist facies shearing in the Central Sredna Gora basement units (Bulgaria). *Geol. Carpathica* 66, 443–454. <https://doi.org/10.1515/geoca-2015-0037>.
- Liati, A., 2005. Identification of repeated Alpine (ultra) high-pressure metamorphic events by U–Pb SHRIMP geochronology and REE geochemistry of zircon: the Rhodope zone of Northern Greece. *Contrib. to Mineral. Petrol.* 150, 608–630. <https://doi.org/10.1007/s00410-005-0038-3>.
- Ludwig, K.R., 2012. *Isoplot 3.75: A Geochronological Toolkit for Microsoft Excel*. Berkeley Geochronology Center Special Publication 5.
- Machev, P.H., Ganev, V., Klain, L., 2015. New LA-ICP-MS U–Pb zircon dating for Strandja granitoids (SE Bulgaria): evidence for two-stage late Variscan magmatism in the internal Balkanides. *Turkish J. Earth Sci.* 24, 230–248. <https://doi.org/10.3906/yer-1407-21>.
- Malinov, O., von Quadt, A., Peytcheva, I., Aladjov, T., Aladjov, A., Naydenova, S., Djambazov, S., 2004. The Klissura Granite in the Western Balkan – questions and answers from new field and isotopic studies. In: *Annual Scientific Conference “Geology 2004”*, 16–17.12.2004, Bulgarian Geological Society, abstract, pp. 51–53.
- Matte, P., 1986. Tectonics and plate tectonics model for the Variscan belt of Europe. *Tectonophysics* 126, 329–374. [https://doi.org/10.1016/0040-1951\(86\)90237-4](https://doi.org/10.1016/0040-1951(86)90237-4).
- McDonough, W., Sun, S.S., 1995. The composition of the Earth. *Chem. Geol.* 67 (5), 1050–1056. [https://doi.org/10.1016/0009-2541\(94\)00140-4](https://doi.org/10.1016/0009-2541(94)00140-4).
- Miller, C.F., McDowell, S.M., Mapes, R.W., 2003. HOT AND COLD GRANITES? Implications of zircon saturation temperatures and preservation of inheritance. *Geology* 31, 529–532. [https://doi.org/10.1130/0091-7613\(2003\)031<0529:HACGIO>2.0.CO;2](https://doi.org/10.1130/0091-7613(2003)031<0529:HACGIO>2.0.CO;2).
- Natal'in, B.A., Sunal, G., Gün, E., Wang, B.O., Zhiqing, Y., 2016. Precambrian to Early Cretaceous rocks of the Strandja Massif (northwestern Turkey): evolution of a long lasting magmatic arc. *Can. J. Earth Sci.* 53 (11), 1312–1335.
- Nedialkov, R., Platevoet, B., Peytcheva, I., von Quadt, A., Vangelova, V., 2007. Geochemistry and U–Pb zircon dating of the Mezhdredya granitic pluton: Bulgarian Geological Society, National Conference with International Participation “Geosciences 2007”, Abstracts, pp. 101–102.
- Okay, A.I., Göncüoğlu, M.C., 2004. Karakaya Complex: a review of data and concepts. *Turkish J. Earth Sci.* 13, 77–95.
- Okay, A., Satur, M., Tüysüz, O., Akýüz, S., Chen, F., 2001. The tectonics of Strandja Massif: late-Variscan and mid-Mesozoic deformation and metamorphism in the northern Aegean. *Int. J. Earth Sci.* 90, 217–233. <https://doi.org/10.1007/s005310000104>.
- Okay, A.I., Şengör, A.M.C., Görür, N., 1994. Kinematic history of the opening of the Black Sea and its effects on the surrounding regions. *Geology* 22, 267–270. [https://doi.org/10.1130/0091-7613\(1994\)022<0267:KHOTOO>2.3.CO;2](https://doi.org/10.1130/0091-7613(1994)022<0267:KHOTOO>2.3.CO;2).

- Okay, A.I., Noble, J., Tekin, U.K., 2011. Devonian radiolarian ribbon cherts from the Karakaya Complex, northwest Turkey: implications for the Paleo-Tethyan evolution. *C. R. Palevol* 10, 1–10. <https://doi.org/10.1016/j.crpv.2010.12.002>.
- Okay, A., Topuz, G., 2017. Variscan orogeny in the Black Sea region. *Int. J. Earth Sci.* 106, 569–592. <https://doi.org/10.1007/s00531-016-1395-z>.
- Okay, A.I., 1996. Granulite facies gneisses from the Pulur region, Eastern Pontides. *Turkish J. Earth Sci.* 5, 55–61.
- Ovtcharova, M., Cherneva, Z., von Quadt, A. and Peytcheva, I., 2002. Migmatitic geochronology and geochemistry - a key to understanding the exhumation of the Madan dome (Bulgaria). In: *Proceeding of Goldschmidt Conference, Geochim. Cosmochim. Acta* 66, Abstract, Supplement 1, A573.
- Ovtcharova, M., von Quadt, A., Cherneva, Z., Sarov, S., Heinrich, C., Peytcheva, I., 2004. U-Pb dating of zircon and monazite from granulites and migmatites in the core and eastern periphery of the Central Rhodopean Dome, Bulgaria. *Goldschmidt Conference, Geochim. Cosmochim. Acta* 68 (11), Abstract, Supplement, A664.
- Paton, C., Hellstrom, J., Paul, B., Woodhead, J., Hergt, J., 2011. Iolite: freeware for the visualisation and processing of mass spectrometric data. *J. Anal. At. Spectrom.* 26, 2508–2518. <https://doi.org/10.1039/C1JA10172B>.
- Pearce, J., 1996. Sources and settings of granitic rocks. *Episodes* 19 (4), 120–125. <https://doi.org/10.18814/epiugs/1996/v19i4/005>.
- Pearce, J., Harris, N., Tindle, A.G., 1984. Trace element discrimination diagrams for the tectonic interpretation of granitic rocks. *J. Petrol.* 25, 956–983. <https://doi.org/10.1093/petrology/25.4.956>.
- Petrík, I., Janák, M., Froitzheim, N., Georgiev, N., Yoshida, K., Sasinková, V., Konečný, P., Milovská, S., 2016. Triassic to Early Jurassic (c. 200 Ma) UHP metamorphism in the Central Rhodopes: evidence from U-Pb-Th dating of monazite in diamond-bearing gneiss from Chepelare (Bulgaria). *J. Metamorph. Geol.* 34, 265–291. <https://doi.org/10.1111/jmg.12181>.
- Petrus, J.A., Kamber, B.S., 2012. VisualAge: a novel approach to laser ablation ICP-MS U-Pb geochronology data reduction. *Geostand. Geanal. Res.* 36, 247–270. <https://doi.org/10.1111/j.1751-908X.2012.00158.x>.
- Peytcheva, I., von Quadt, A., 2004. The Palaeozoic protoliths of Central Srednogie, Bulgaria: records in zircons from basement rocks and Cretaceous magmatites. In: *5th International Symposium on Eastern Mediterranean Geology, Thessaloniki, Greece, Abstract, Conference Volume*, pp. 11–19.
- Peytcheva, I., von Quadt, A., Frank, M., Nedialkov, R., Kamenov, B., Heinrich, C., 2004a. Timing and magma evolution of Upper Cretaceous rocks in Medet Cupporphyry deposit: isotope-geochronological and geochemical constraints. In: *Annual Scientific Conference "Geology 2004"*, 16–17.12.2004, Bulgarian Geological Society, abstract, pp. 57–59.
- Peytcheva, I., von Quadt, A., Malinov, O., Tacheva, E., Nedialkov, R., 2006. Petrochan and Klissura plutons in Western Balkan: relationships, in situ and single grain U-Pb zircon/monazite dating and isotope tracing. In: *Proceedings of the Joint Conference of the Bulgarian Geophysical and Geological Societies "Geosciences 2006"*, abstracts, pp. 221–224.
- Peytcheva, I., Von Quadt, A., Sarov, S., Voinova, E., Kolcheva, K., 2009. Ordovician protoliths of metamorphic rocks in Eastern Pirin - Western Rhodopes: Are they part of the Ograzhdan Unit? In: *Proceedings of Conference of the Bulgarian Geological Society "Geosciences 2009"*: Sofia, Bulgarian Geological Society, pp. 17–18.
- Peytcheva, I., Georgiev, S., Von Quadt, A., 2016. U/Pb ID-TIMS dating of zircons from the Sakar-Strandzha Zone: New data and old questions about the Variscan orogeny in SE Europe. In: *Proceedings of Annual Conference of the Bulgaria Geological Society "Geosciences 2016"*: Sofia, Bulgarian Geological Society, pp. 71–72.
- Peytcheva, I., von Quadt, A., Ovtcharova, M., Handler, R., Neubauer, F., Salnikova, E., Kostitsyn, Y., Sarov, S., Kolcheva, K., 2004b. Metagranitoids from the eastern part of the Central Rhodopean Dome (Bulgaria): U-Pb, Rb-Sr and 40Ar/39Ar timing of emplacement and exhumation and isotope-geochemical features. *Mineral. Petrol.* 82, 1–31. <https://doi.org/10.1007/s00710-004-0039-3>.
- Peytcheva, I., Macheva, L., Von Quadt, A., Zidarov, N., 2015. Gondwana-derived units in Ograzhdan and Belasitsa Mountains, Serbo-Macedonian Massif (SW Bulgaria): combined geochemical, petrological and U-Pb zircon-xenotime age constraints. *Geol. Balcanica* 44 (1–3), 51–84.
- Peytcheva, I., Tacheva, E., von Quadt, A., Nedialkov, R., 2018. U-Pb zircon and titanite ages and Sr-Nd-Hf isotope constraints on the timing and evolution of the Petrohan-Mezdrea pluton (Western Balkan Mts, Bulgaria). *Geol. Balcanica* 47 (2), 25–46. <https://doi.org/10.52321/GeolBalc.47.2.25>.
- Pointon, M.A., Cliff, R.A., Chew, D.M., 2012. The provenance of Western Irish Namurian Basin sedimentary strata inferred using detrital zircon U-Pb LA-ICP-MS geochronology. *Geol. J.* 47, 77–98. <https://doi.org/10.1002/gj.1335>.
- Pristavova, S., Tzankova, N., Gospodinov, N., Filipov, P., 2019. Petrological study of metasomatic altered granitoids from Kanarata Deposit, Sakar Mountain, southeastern Bulgaria. *J. Mining Geol. Sci.* 62, 53–61.
- Şahin, S.Y., Aysal, N., Güngör, Y., Peytcheva, I., Neubauer, F., 2014. Geochemistry and U-Pb zircon geochronology of metagranites in Istranca (Strandja) Zone, NW Pontides, Turkey: implications for the geodynamic evolution of Cadomian orogeny. *Gondwana Res.* 26 (2), 755–771. <https://doi.org/10.1016/j.gr.2013.07.011>.
- Sałacińska, A., Gerdjikov, I., Gumsley, A., Szopa, K., Chew, D., Gawęda, A., Kocjan, I., 2021. Two stages of Late Carboniferous to Triassic magmatism in the Strandja Zone of Bulgaria and Turkey. *Geol. Mag.* 158 (12), 2151–2164. <https://doi.org/10.1017/S0016756821000650>.
- Sałacińska, A., Gerdjikov, I., Kounov, A., Chew, D., Szopa, K., Gumsley, A., Kocjan, I., Marciniak-Maliszewska, B., Drakou, F., 2022. Data for "Variscan magmatic evolution of the Strandja Zone (Southeast Bulgaria and Northwest Turkey) and its relationship to other North Gondwanan margin terranes". Mendeley Data V2. <https://doi.org/10.17632/vwdgwh2rc5.2>.
- Şengör, A.M.C., Altiner, D., Cin, A., Ustaömer, T., Hsü, K.J., 1988. Origin and assembly of the Tethyside orogenic collage at the expense of Gondwana Land: Gondwana and Tethys. *Geol. Soc. Spec. Publ.* 37, 119–181. <https://doi.org/10.1144/GSL.SP.1988.037.01.09>.
- Şengün, F., Koralay, O.E., 2017. Early Variscan magmatism along the southern margin of Laurasia: geochemical and geochronological evidence from the Biga Peninsula, NW Turkey. *Int. J. Earth Sci.* 106, 811–826. <https://doi.org/10.1007/s00531-016-1334-z>.
- Şengün, F., Koralay, O.E., Kristoffersen, M., 2020. Zircon U-Pb age and Hf isotopic composition of the Carboniferous Gönen granitoid in the western Sakarya Zone of Turkey. *Turkish J. Earth Sci.* 29, 617–628. <https://doi.org/10.3906/yer-1910-7>.
- Shand, S.J., 1943. *Eruptive Rocks. Their Genesis, Composition, Classification, and Their Relation to Ore-deposits with a Chapter on Meteorite*. Wiley, New York.
- Sláma, J., Košler, J., Condon, D.J., Crowley, J.L., Gerdes, A., Hancher, J.M., Horstwood, M.S.A., Morris, G.A., Nasdala, L., Norberg, N., Schaltegger, U., Schoene, B., Tubrett, M.N., Whitehouse, M.J., 2008. Plešovice zircon—a new natural reference material for U-Pb and Hf isotopic microanalysis. *Chem. Geol.* 249 (1–2), 1–35.
- Stampfli, G.M., 2000. Tethyan oceans. In: Bozkurt, E., Winchester, J.A., Piper, J.D.A., (Eds.), *Tectonics and Magmatism in Turkey and the Surrounding Area: Geol. Soc. Spec. Publ.* 173, pp. 1–23. doi: 10.1144/GSL.SP.2000.173.01.01.
- Stephan, T., Kroner, U., Romer, R.L., Rösel, D., 2019. From a bipartite Gondwanan shelf to an arcuate Variscan belt: The early Paleozoic evolution of northern Peri-Gondwana. *Earth-Sci. Rev.* 192, 491–512. <https://doi.org/10.1016/j.earscirev.2019.03.012>.
- Streckeisen, A., 1974. Classification and nomenclature of plutonic rocks. *Geol. Rundsch.* 63, 773–786. <https://doi.org/10.1007/BF01820841>.
- Sunal, G., Natal'in, B.A., Satir, M., Toraman, E., 2006. Paleozoic magmatic events in the Strandja Massif, NW Turkey. *Geodin. Acta* 19 (5), 283–300.
- Sunal, G., Satir, M., Natal'in, B.A., Topuz, G., Vonderschmidt, O., 2011. Metamorphism and diachronous cooling in a contractional orogen: the Strandja Massif, NW Turkey. *Geol. Mag.* 148 (4), 580–596.
- Szopa, K., Sałacińska, A., Gumsley, A.P., Chew, D., Petrov, P., Gawęda, A., Zagórska, A., Deput, E., Gospodinov, N., Banasik, K., 2020. Two-stage late Jurassic to early Cretaceous hydrothermal activity in the Sakar unit of Southeastern Bulgaria. *Minerals* 10, 266. <https://doi.org/10.3390/min10030266>.
- Topuz, G., Alther, R., Kalt, A., Satir, M., Werner, O., Schwartz, W.H., 2004. Aluminous granulites from the Pulur Complex, NE Turkey: a case of partial melting, efficient melt extraction and crystallisation. *Lithos* 72, 183–207. <https://doi.org/10.1016/j.lithos.2003.10.002>.
- Topuz, G., Altherr, R., Siebel, W., Schwarz, W.H., Zack, T., Hasözbeke, A., Barth, M., Satir, M., Şen, C., 2010. Carboniferous high-potassium I-type granitoid magmatism in the Eastern Pontides: the Gümüşhane pluton (NE Turkey). *Lithos* 116 (1–2), 92–110.
- Trapp, S., Janák, M., Fassmer, K., Froitzheim, N., Münker, C., Georgiev, N., 2020. Variscan ultra-high-pressure eclogite in the Upper Allochthon of the Rhodope Metamorphic Complex (Bulgaria). *Terra Nova* 33 (2), 174–183. <https://doi.org/10.1111/ter.12503>.
- Turpaud, P., Reischmann, T., 2010. Characterisation of igneous terranes by zircon dating: implications for UHP occurrences and suture identification in the Central Rhodope, northern Greece. *Int. J. Earth Sci.* 99, 567–591. <https://doi.org/10.1007/s00531-008-0409-x>.
- Ustaömer, T., Robertson, A.H.F., Ustaömer, P.A., Gerdes, A., Peytcheva, I., 2013. Constraints on Variscan and Cimmerian magmatism and metamorphism in the Pontides (Yusufeli-Artvin area), NE Turkey from U-Pb dating and granite geochemistry. *Geol. Soc. Spec. Publ.* 372 (1), 49–74. <https://doi.org/10.1144/SP372.13>.
- Ustaömer, P.A., Ustaömer, T., Robertson, A.H.F., 2012. Ion probe U-Pb dating of the central Sakarya basement: a peri-Gondwana Terrane intruded by late lower carboniferous subduction/collision-related granitic rocks. *Turkish J. Earth Sci.* 21 (6), 905–932. <https://doi.org/10.3906/yer-1103-1>.
- Vladinova, T., Georgieva, M., 2020. New data on the westernmost part of the Sakar unit metamorphic basement, SE Bulgaria. In: *Proceedings of National Conference "Geosciences 2020"*: Sofia, Bulgarian Geological Society, 81(3), pp. 105–107.
- Vladinova, T., Georgieva, M., Bosse, V., Cherneva, Z., 2018. U-Pb detrital zircons geochronology from metasedimentary rocks of the Sakar Unit, Sakar-Strandzha zone, SE Bulgaria. In: *Proceedings of National Conference "Geosciences 2018"*: Sofia, Bulgarian Geological Society 79(3), pp. 67–68.
- Vladinova, T., Georgieva, M., Peytcheva, I., 2019. U-Pb geochronology and geochemistry of rutiles from metaconglomerate in the Sakar-Strandzha zone, SE Bulgaria. In: *Proceedings of National Conference "Geosciences 2019"*: Sofia, Bulgarian Geological Society, 80(3), pp. 91–93.
- Watson, E.B., Harrison, T.M., 1983. Zircon saturation revisited: Temperature and composition effects in a variety of crustal magma types. *Earth Planet. Sci. Lett.* 64, 295–304. [https://doi.org/10.1016/0012-821X\(83\)90211-X](https://doi.org/10.1016/0012-821X(83)90211-X).
- Wetherill, G.W., 1956. Discordant uranium-lead ages. *I. Eos. Trans. Am. Geophys. Union* 37 (3), 320–326. doi: 10.1029/TR037i003p00320.
- Wiedenbeck, M., Alle, P., Corfu, F., Griffin, W.L., Meier, M., Oberli, F.V., Von Quadt, A., Roddick, J.C., Spiegel, W., 1995. Three natural zircon standards for U-Th-Pb, Lu-

- Hf, trace element and REE analyses. *Geostand. Newsl.* 19, 1–23. <https://doi.org/10.1111/j.1751-908X.1995.tb00147.x>.
- Wiedenbeck, M., Hanchar, J.M., Peck, W., Sylvester, P., Valley, J., Whitehouse, M., Kronz, A., Morishita, Y., Nasdala, L., Fiebig, J., Franchi, I., Girard, J.-P., Greenwood, R.C., Hinton, R., Kita, N., Mason, P.R.D., Norman, M., Ogasawara, M., Piccoli, P.M., Rhede, D., Satoh, H., Schulz-Dobrick, B., Skär, O., Spicuzza, M.J., Terada, K., Tindle, A., Togashi, S., Vennemann, T., Xie, Q., Zheng, Y.-F., 2004. Further characterisation of the 91500 zircon crystal. *Geostand. Geoanal. Res.* 28 (1), 9–39. <https://doi.org/10.1111/j.1751-908X.2004.tb01041.x>.
- Yılmaz, I., Şahin, S.Y., Aysal, N., Güngör, Y., Akgündüz, A., and Bayhan, U.C., 2021. Geochronology, geochemistry and tectonic setting of the Cadomian (Ediacaran–Cambrian) magmatism in the Istranca (Strandja) Massif: new insights into magmatism along the northern margin of Gondwana in NW Turkey. *International Geology Review*. <https://doi.org/10.1080/00206814.2021.1901249>. In press.
- Žak, J., Svojtka, M., Gerdjikov, I., Kounov, A., Vangelov, D.A., 2021. The Balkan terranes: a missing link between the eastern and western segments of the Avalonian–Cadomian orogenic belt? *Int. Geol. Rev.* <https://doi.org/10.1080/00206814.2020.1861486>. in press.
- Zidarov, N., Tarassova, E., Peytcheva, I., von Quadt, A., Andreichev, V., Titorenkova, R., 2007. Petrology, geochemistry and age dating of Skrut granitoids – new evidence for Early Triassic magmatism in Belasitsa Mountain (SW Bulgaria). *Geol. Balcanica* 36, 17–29.





# An Early Cretaceous thermal event in the Sakar Unit (Strandja Zone, SE Bulgaria/NW Turkey) revealed based on U—Pb rutile geochronology and Zr-in-rutile thermometry

Anna Gumsley<sup>a,b,\*</sup>, Krzysztof Szopa<sup>b</sup>, David Chew<sup>c</sup>, Ianko Gerdjikov<sup>d</sup>, Petras Jokubauskas<sup>e</sup>, Beata Marciniak-Maliszewska<sup>e</sup>, Foteini Drakou<sup>c</sup>

<sup>a</sup> Institute of Geological Sciences Polish Academy of Science, Research Centre in Kraków, Senacka 1, 31-002, Poland

<sup>b</sup> Institute of Earth Sciences, Faculty of Natural Sciences, University of Silesia in Katowice, Będzińska 60, 41-200 Sosnowiec, Poland

<sup>c</sup> Department of Geology, School of Natural Sciences, Trinity College Dublin, Ireland

<sup>d</sup> Faculty of Geology and Geography, Sofia University "St. Kliment Ohridski", 15 Tzar Osvoboditel Blvd., 1504 Sofia, Bulgaria

<sup>e</sup> Faculty of Geology, University of Warsaw, Żwirki i Wigury 93, 02-089 Warsaw, Poland

## ARTICLE INFO

### Keywords:

Strandja Zone  
Sakar Unit  
U—Pb rutile dating  
Zr-in-rutile thermometry  
Early Alpine metamorphism

## ABSTRACT

The Strandja Zone (SE Bulgaria/ NW Turkey) comprises tectonic units affected by Late Jurassic to Early Cretaceous upper greenschist- to amphibolite-facies metamorphism. A contemporaneous tectonothermal event occurred in the Rhodope Metamorphic Complex, which has led to many authors correlating both zones. Three tectonic units can be distinguished in the Bulgarian part of the Strandja Zone: the Sakar, Strandja and Veleka units. This study focuses on albitized rocks of the Sakar Unit that are suspected to be related to this tectonothermal event. Albitized samples were collected from the Late Carboniferous Sakar Batholith, while for comparison country-rock orthogneiss unaffected by albitization was also analyzed. Geochemical and petrological studies indicate that albitization was coupled with the removal of quartz and the growth of rutile-rich aggregates replacing titanite. U—Pb rutile dating of an orthogneiss (ca. 154 Ma) confirms Late Jurassic amphibolite-facies conditions, whereas rutile from albitized metagranitoids yields Early Cretaceous ages (ca. 125–116 Ma). Zr-in-rutile thermometry reveals similar crystallization temperatures (~530–620 °C) for the albitized Sakar granitoids and country rock orthogneiss. U—Pb zircon and titanite dating implies a Late Carboniferous crystallization age for various granitoids forming the Sakar Batholith. Our results indicate that at least some parts of the Sakar Unit were affected by thermal events and associated albitization in the Early Cretaceous. However, this did not lead to the formation of a new penetrative fabric, unlike in the Rhodopes, where contemporaneous regional metamorphism is associated with penetrative deformation.

## 1. Introduction

The Strandja Zone straddles the Bulgarian and Turkish border (Fig. 1) between the Balkanides and Pontides and comprises various pre-Late Cretaceous tectonic units (Aysal et al., 2018; Chatalov, 1990; Natal'in et al., 2016; Okay et al., 2001). These units were affected by Late Jurassic to Early Cretaceous upper greenschist- to amphibolite-facies metamorphism known in the local literature as the Early Alpine or Cimmerian event (Bonev et al., 2020; Gerdjikov, 2005; Şengör et al., 1984; Szopa et al., 2020; Vladinova et al., 2019). The duration of this metamorphic episode is estimated between ca. 167 Ma and ca. 114 Ma

based on different geochronological systems including U—Pb rutile, apatite and titanite dating (Szopa et al., 2020; Vladinova et al., 2019); Ar—Ar dating of muscovite, sericite, biotite and hornblende (Bonev et al., 2020; Elmas et al., 2011); and Rb—Sr dating of biotite and muscovite (Okay et al., 2001; Sunal et al., 2011, Supplementary Table 1). This metamorphic overprint is interpreted as either a single event followed by subsequent (diachronous) cooling (Bonev et al., 2020; Sunal et al., 2011) or two discrete thermal events (Szopa et al., 2020). Some authors have suggested that the albitization that locally affects the northern part of the Sakar Unit in the western Strandja Zone is also connected with the Early Alpine event (Kamenov et al., 2010; Pristavova

\* Corresponding author at: Institute of Geological Sciences Polish Academy of Science, Research Centre in Kraków, Senacka 1, 31-002, Poland.

E-mail addresses: [anna.salacinska@twarda.pan.pl](mailto:anna.salacinska@twarda.pan.pl) (A. Gumsley), [krzysztof.szopa@us.edu.pl](mailto:krzysztof.szopa@us.edu.pl) (K. Szopa), [chewd@tcd.ie](mailto:chewd@tcd.ie) (D. Chew), [janko@gea.uni-sofia.bg](mailto:janko@gea.uni-sofia.bg) (I. Gerdjikov), [p.jokubauskas@uw.edu.pl](mailto:p.jokubauskas@uw.edu.pl) (P. Jokubauskas), [b.maliszewska@uw.edu.pl](mailto:b.maliszewska@uw.edu.pl) (B. Marciniak-Maliszewska), [drakouf@tcd.ie](mailto:drakouf@tcd.ie) (F. Drakou).

<https://doi.org/10.1016/j.lithos.2023.107186>

Received 6 September 2022; Received in revised form 13 April 2023; Accepted 15 April 2023

Available online 19 April 2023

0024-4937/© 2023 Elsevier B.V. All rights reserved.

et al., 2019; Szopa et al., 2020). In the zone of albitization Szopa et al. (2020) recognized two stages of hydrothermal activity during Early Alpine metamorphism and suggested that the albitization event was connected with one of the Early Alpine tectonothermal episodes in the Late Jurassic or Early Cretaceous.

A Late Jurassic – Early Cretaceous metamorphic event is also well documented in the neighbouring Rhodope Metamorphic Complex (Fig. 1), where it reached (ultra-) high-grade metamorphic conditions (see the summary in Burg, 2012; Gautier et al., 2017). The Early Alpine evolution of the Strandja Zone may help to better understand the regional significance of these Late Jurassic – Early Cretaceous tectonic processes.

Albitization is a replacement of alkali and plagioclase feldspars by albite (e.g., Hövelmann et al., 2010; Norberg et al., 2011), and it is known from various rocks and tectonic settings in Earth's upper crust, e.g., as a fluid-driven alteration of granitoids (Engvik et al., 2008; Kent et al., 2000; Lee and Parsons, 1997; Mark, 1998; Petersson and Eliasson, 1997; Plümpner and Putnis, 2009) or diagenetic alteration of sedimentary rocks (e.g., Ramseyer et al., 1992 and reference therein). The albitization of granitoids can be caused by deuteritic fluids circulating in the latest stages of magma evolution (Lee and Parsons, 1997; Petersson and Eliasson, 1997) or by post-magmatic hydrothermal fluids of external origin (Kent et al., 2000; Lee and Parsons, 1997; Mark, 1998). The source of hydrothermal fluids is usually difficult to determine (Lee and Parsons, 1997; Mark, 1998; Plümpner and Putnis, 2009). The process can be regional in scale but often affects localised zones (Engvik et al., 2008; Kent et al., 2000). The estimated P-T conditions for hydrothermal fluids

causing albitization do not exceed 650 °C and are typically in the range of 2–4 kbar (Engvik et al., 2008; Kent et al., 2000). Albitization is often associated with other processes, such as the removal of quartz (Petersson and Eliasson, 1997), the formation of minerals of the scapolite group (Engvik et al., 2008) or the formation of ore deposits (Kent et al., 2000; Mark, 1998). Most albitized granitoids form by fluid-induced alteration of their original magmatic mineralogy (Plümpner and Putnis, 2009) and, in this study, are described with the prefix 'meta' to distinguish them from unaltered variants.

Zr-in-rutile thermometry (Tomkins et al., 2007; Watson et al., 2006; Zack et al., 2004) is a powerful petrological tool which allows unravelling part of the thermal evolution of rutile-bearing rocks affected by medium- to (ultra-) high-grade metamorphism (e.g., Ewing et al., 2015, 2013; Kooijman et al., 2012; Luvizotto et al., 2009a; Luvizotto and Zack, 2009; Meinhold, 2010; Wang et al., 2021; Zack and Luvizotto, 2006). In medium-grade rutile-bearing metamorphic rocks, U–Pb rutile dating (closure temperature of the U–Pb rutile system of >500–640 °C; Cherniak, 2000; Kooijman et al., 2010) coupled with Zr-in-rutile thermometry allows constraining the timing of peak metamorphism.

This study focuses on rutile-bearing rocks to unravel the timing and temperature conditions of the Early Alpine metamorphism in the Strandja Zone and the superimposed albitization which affected the northern part of the Sakar Unit. It investigates: 1) links between regional metamorphism and albitization; and 2) the influence of albitization on accessory minerals such as zircon, titanite and rutile commonly used as geochronometers. Rutile-bearing rocks were sampled in an albitized part of the Sakar Batholith and from country-rock orthogneisses (Fig. 2).

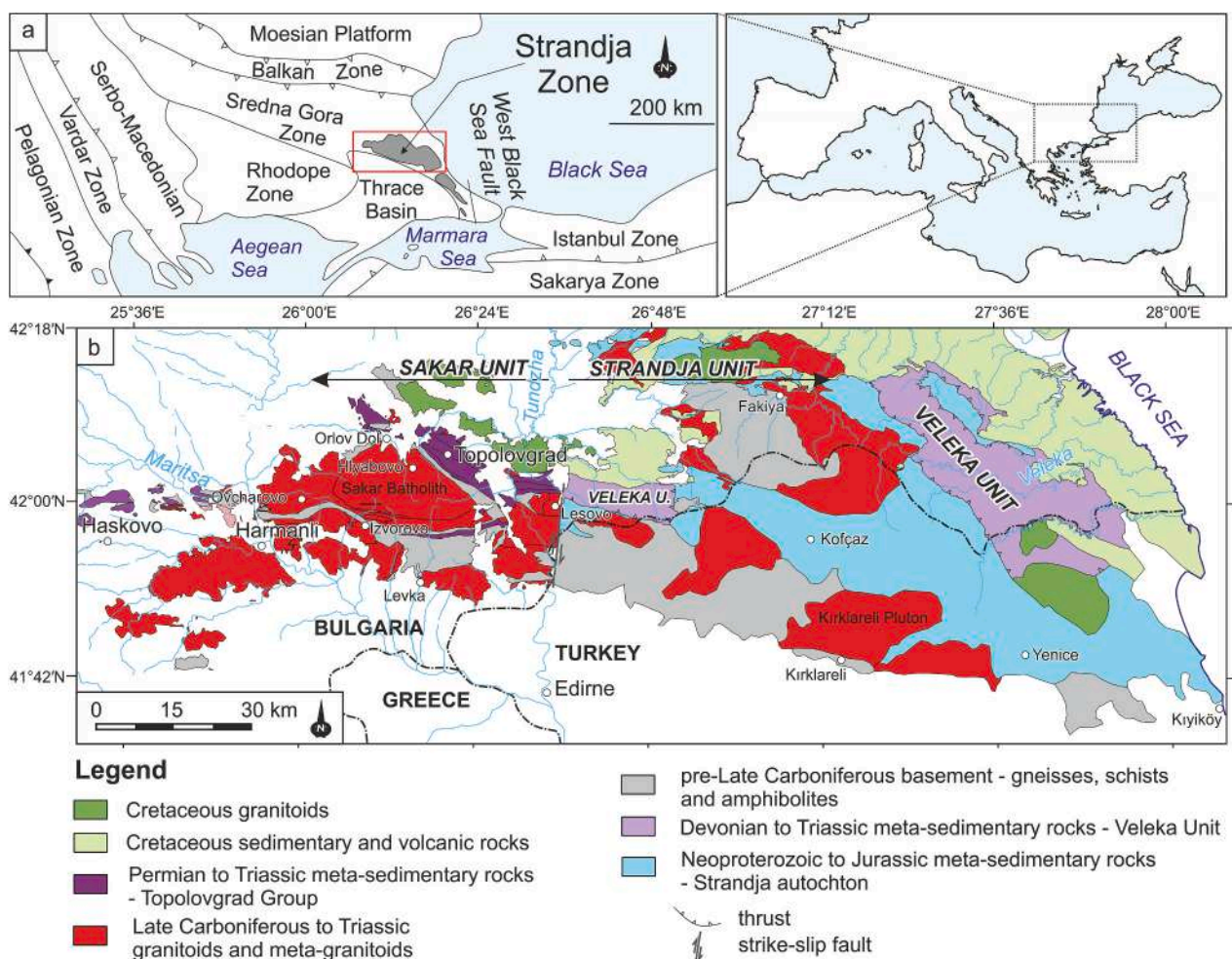
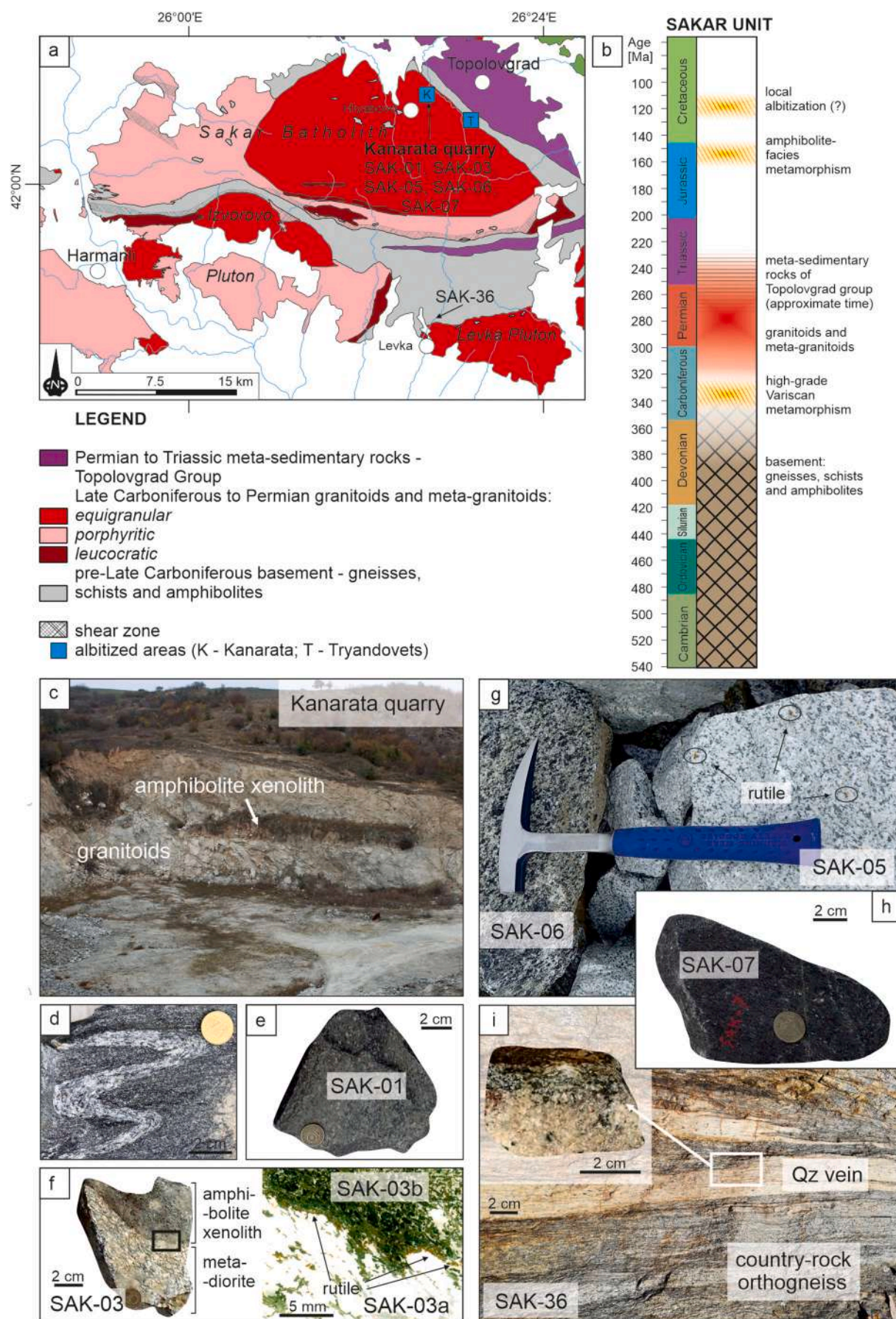


**Fig. 1.** (a) Location of the Strandja Zone and the surrounding major tectonic units; (b) Geological map of the Strandja Zone (modified after Okay et al., 2001; Gerdjikov, 2005; Natal'in et al., 2016; Salacińska et al., 2021, 2022).





(caption on next page)

**Fig. 2.** (a) Geological map of the Sakar Unit with sample localities marked (modified after Gerdjikov, 2005; Salacińska et al., 2021, 2022); (b) column with major events of the Sakar Unit; (c) outcrop in Kanarata quarry (northern part of the Sakar Batholith; near Hlaybovo) showing a large amphibolite xenolith in the granitoids; (d) deformed and metamorphosed amphibolite xenolith from Kanarata quarry; (e–h) rock samples from Kanarata quarry: (e) melanocratic metadiorite (SAK-01), (f) albitized metadiorite with an amphibolite xenolith (SAK-03), (g) leucocratic metadiorite (SAK-05) and granodiorite (SAK-06), (h) amphibolite xenoliths (SAK-07); (i) rock sample of country rock orthogneiss (SAK-36) cut by a quartz vein (southern of the Sakar Batholith, near Levka).

The U–Pb rutile dating was coupled with Zr-in-rutile thermometry and geochemical and petrological studies. Furthermore, U–Pb zircon and titanite dating were applied to confirm the Late Carboniferous crystallization age of the Sakar granitoids.

## 2. Geological setting

The Strandja Zone is a NW-SE-trending mountain belt in south-eastern Bulgaria and north-western Turkey (Fig. 1). It is bordered by the Sredna Gora Zone and Rhodope Metamorphic Complex to the north and west, respectively, and the Thrace Basin and Istanbul Zone to the south and south-east (Fig. 1a). The Strandja Zone comprises pre-Late Cretaceous autochthonous and allochthonous units, parts of which were affected by at least two metamorphic events (Fig. 1b, 2b, e.g., Aysal et al., 2018; Chatalov, 1990; Natal'in et al., 2016; Okay et al., 2001; Salacińska et al., 2022): 1) Late Carboniferous Variscan high-grade metamorphism and deformation (e.g., Okay et al., 2001; Salacińska et al., 2022; Sunal et al., 2011); and 2) an upper greenschist- to amphibolite-facies Late Jurassic to Early Cretaceous event (Bonev et al., 2020; Gerdjikov, 2005; Szopa et al., 2020; Vladinova et al., 2019). Three tectonic units can be distinguished in the Bulgarian part of the Strandja Zone – the Sakar, Strandja and Veleka units (Chatalov, 1990; Gerdjikov, 2005). The Sakar and Strandja units display many similarities. Both units consist of pre-Late Carboniferous high-grade para- and orthogneisses, garnet two-mica schists, amphibolites, meta-gabbros and meta-ultrabasic lenses and migmatites (Natal'in et al., 2016; Şahin et al., 2014). Detrital zircon U–Pb geochronology suggests a maximum Cambrian age for the migmatitic paragneisses of the Sakar Unit (Vladinova et al., 2018; Vladinova and Georgieva, 2020), while the orthogneisses have Neoproterozoic–Cambrian and Ordovician maximum ages (Bonev et al., 2019; Natal'in et al., 2016; Şahin et al., 2014). The high-grade metamorphic rocks are intruded by Late Carboniferous to Triassic intermediate to felsic magmatic rocks. The pre-Alpine basement thus comprises both high-grade metamorphic rocks and magmatic rocks. Along with the Triassic–Jurassic cover, this basement was variously affected by Early Alpine metamorphism and deformation (e.g., Okay et al., 2001; Natal'in et al., 2016; Aysal et al., 2018; Salacińska et al., 2021, 2022; Bonev et al., 2022). One of the primary differences between the Sakar and Strandja units is the metamorphic grade of the overlying Permian to Triassic meta-sedimentary sequences. In the Sakar Unit, the Triassic Topolovgrad Group is metamorphosed to amphibolite-facies, whereas coeval meta-sedimentary rocks in the Strandja Unit were affected by lower-grade metamorphism and deformation (Chatalov, 1990).

### 2.1. Early Alpine metamorphism in the Strandja Zone

#### 2.1.1. Early Alpine metamorphism in the Sakar Unit

From the Sakar Unit, Vladinova et al. (2019) reported a low-precision age of  $167 \pm 35$  Ma for metamorphic rutile growth with Zr-in-rutile temperatures ranging from 530 °C to 610 °C (calculations after Watson et al., 2006) in a metabreccia-conglomerate of the lowermost part of Topolovgrad Group (Fig. 1b). Recently, Bonev et al. (2020) presented  $^{40}\text{Ar}/^{39}\text{Ar}$  amphibole and white mica age data from a country-rock amphibolite and a metasandstone of the lower part of Topolovgrad Group respectively, and suggested protracted cooling of these rocks from the amphibolite facies to greenschist facies between ca. 141–126 Ma.

Geothermobarometry on garnet-bearing schists from the middle part

of Topolovgrad Group indicates prograde metamorphism from ~410 °C to ~660 °C and 3.5–8 kbar to 6.5–9 kbar (Tzankova and Pristavova, 2007). These P–T conditions are consistent with the plagioclase–hornblende geothermobarometry constraints of Chavdarova and Machev (2017). These authors calculated temperatures and pressures in the range of 510–555 °C and 6–8 kbar for amphibolites of the Topolovgrad Group, and 625–635 °C and 6.5–8 kbar for amphibolites of the pre-Late Carboniferous country rocks. A post-Triassic albitization process, which affected the northern part of the Sakar Batholith (e.g., locally in Hlyabovo and Tryandovets; Fig. 2; Kamenov et al., 2010; Pristavova et al., 2019) is probably associated with this Early Alpine event. Szopa et al. (2020) suggested that albitization was associated with one of the discrete stages of hydrothermal activity either at ca. 149 Ma or ca. 114 Ma.

#### 2.1.2. Early Alpine metamorphism in the Strandja Unit

Geochronological studies from the Strandja Unit have also documented Early Alpine metamorphism. Okay et al., 2001 reported a Rb–Sr biotite - whole rock age of  $155 \pm 2$  Ma (2 $\sigma$ ) from the Kırklareli metagranite (Fig. 1b) and interpreted it as related to greenschist-facies metamorphism. Working in the vicinity of the Kırklareli Pluton and its country rock envelope, Sunal et al. (2011) determined P–T conditions of 6–8 kbar at 485–530 °C for the epidote-amphibolite-facies domain. Peak metamorphism at ca. 160 Ma was implied based on Rb–Sr muscovite ages of  $162.9 \pm 1.6$  Ma to  $149.1 \pm 2.1$  Ma (2 $\sigma$ ) obtained from the southern part of the studied area. Rb–Sr biotite ages decreased from  $153.9 \pm 1.5$  Ma in the south to  $134.4 \pm 1.3$  Ma (2 $\sigma$ ) in the north, indicating diachronous cooling.  $^{40}\text{Ar}/^{39}\text{Ar}$  dating of hornblende, biotite and white mica from various lithologies in the south-eastern part of the Strandja Unit have yielded ages between ca. 156 Ma and ca. 119 Ma (Elmas et al., 2011).

### 2.2. The Sakar Batholith and later albitization

One of the largest magmatic bodies in the Sakar Unit is the Sakar Batholith that records heterogeneous Early Alpine overprint (Kamenov et al., 2010; Pristavova et al., 2019; Salacińska et al., 2022). The Sakar Batholith is composed of two major textural variants of equigranular and porphyritic granitoids, and minor leucocratic granitoids, whose composition varies from monzogranite to granodiorite and quartz-monzodiorite (e.g., Kamenov et al., 2010; Fig. 2a). Leucocratic granitoids are mainly represented by small elongated bodies that occur close to the batholith margins (Kamenov et al., 2010; Pristavova et al., 2019). These peripheral parts are the most heterogeneous, contain the largest xenoliths (up to hundreds of meters wide), and are locally affected by superimposed albitization, best exposed in Kanarata quarry (Fig. 2c; Pristavova et al., 2019; Szopa et al., 2020) located 3 km NE of Hlaybovo. The rocks in the quarry comprise fine- to medium-grained equigranular leuco-, meso- and melanocratic granitoids affected by various degrees of albitization (Fig. 2e,g), which change their composition toward diorite (Pristavova et al., 2019). Albitization is most pronounced in the leucocratic Sakar granitoids (Pristavova et al., 2019). U–Pb dating of these rocks yielded a crystallization age of  $298 \pm 2$  Ma (2 $\sigma$ ; Pristavova et al., 2019), similar to other ages obtained from the Sakar Batholith (Bonev et al., 2019; Peytcheva et al., 2016; Salacińska et al., 2022). The granitoids contain amphibolite xenoliths, ranging from centimetres to several meters in size (Fig. 2c; e.g., Pristavova et al., 2019; Salacińska et al., 2022) and are cut by various aplitic dykes and hydrothermal veins (Pristavova et al., 2019; Szopa et al., 2020). In many places, the contacts



between xenoliths and granite are obliterated, or the amphibolite xenoliths are completely weathered and resulting cavities are filled by secondary mineralization (Pristavova et al., 2019). This mineralization formed during two hydrothermal episodes at  $149 \pm 7$  Ma and  $114 \pm 1$  Ma (Szopa et al., 2020). The xenoliths have a visible foliation (Pristavova et al., 2019).

### 3. Sample strategy

Samples for this study were collected from Kanarata quarry which contains rocks variously affected by albitization (SAK-01; SAK-03; SAK-05 – strongly albitized; SAK-07 – weakly albitized; SAK-06 – non albitized), located in the north-eastern part of the Sakar Batholith and from the orthogneiss country rock (north of Levka), close to the ca. 319 Ma Levka Pluton (SAK-36; Fig. 2). Sample locations are listed in Table 1.

The rock samples collected from Kanarata quarry (Hlaybovo; Fig. 2c–h) are: melanocratic metadiorite sample SAK-01; leucocratic metadiorite sample SAK-05; granodiorite sample SAK-06 and fine-grained amphibolite xenolith sample SAK-07. Additionally, sample SAK-03 (metadiorite) was collected from the same granitoid body as SAK-06 (granodiorite), with SAK-06 representing the non-albitized and massive central part of the body and SAK-03 collected from the albitized contact zone between granitoid and an amphibolite xenolith, and thus includes both rock types. These rocks were sampled to reveal the rock-forming processes and alteration (primarily albitization) of the various types of granitoids and determine the timing of granitoid emplacement and the superimposed albitization process.

Sample SAK-36 was collected from country-rock orthogneiss in the southern part of the Sakar Unit. At this locality, the orthogneiss is cut by a quartz vein (up to 10 cm thick) along which rutile grew in the orthogneiss. The sample represents the contact zone of the quartz vein and orthogneiss, and consists of both rock types (Fig. 2i). This sample was collected to confirm the age of the Early Alpine metamorphic event affecting the Sakar Unit.

### 4. Analytical procedures

Petrographic observations on thin sections were conducted using an Olympus BX-51 optical polarising microscope; and a ThermoFisher Scientific Phenom XL Scanning Electron Microscope (SEM) with back-scattered electron (BSE) detector coupled to an energy-dispersive spectrometer (EDS) in the Institute of Earth Sciences at the University of Silesia in Katowice, Sosnowiec, Poland. Mineral chemical analyses were undertaken by Electron Probe Microanalysis (EPMA) at the Laboratory

of Electron Microscopy, Microanalysis and X-Ray Diffraction (Faculty of Geology, University of Warsaw, Warsaw, Poland) using two microprobes – a Cameca SX100 and a Cameca SXFiveFE. The EPMA procedures for rock-forming minerals and accessory titanite and epidote are described in Supplementary Table 2, whereas the EPMA procedures used for rutile and zircon are provided in Supplementary Table 3.

Four homogeneous rock samples (SAK-01, SAK-05, SAK-06, SAK-07) were selected for whole-rock geochemical analysis. The samples were crushed by a jaw crusher and pulverized in an agate ball mill. The fine-grained powder was analyzed at Bureau Veritas Analytical Laboratories in Vancouver, Canada, using X-ray fluorescence (XRF) spectrometry for major elements and inductively coupled plasma-mass spectrometry (ICP-MS) for trace elements, including rare-earth elements (REE). The volatile content on each sample was obtained by loss on ignition (LOI) determination.

Zircon (SAK-01, SAK-05 and SAK-06), titanite (SAK-06) and rutile (SAK-01, SAK-05 and SAK-36) crystals were separated in the Sample Preparation Laboratory at the Institute of Geological Sciences, Polish Academy of Sciences in Krakow, Poland. The separation process included crushing, sieving using a 0.315 mm mesh, panning and density separation. Crystals were then hand-picked using a standard binocular microscope. The zircon, titanite and rutile crystals were then cast in epoxy resin mounts of 25 mm diameter, and ground and polished to half-thickness to expose the crystal interiors, followed by transmitted and reflected light microscopy, and by SEM with BSE using the same equipment as for the petrographic observations. Zircon crystals were also imaged by SEM with cathodoluminescence (CL) at the Institute of Earth Sciences, the University of Silesia in Katowice, using a FET Phillips 30 SEM to reveal the internal structure of the zircons. A 15 kV accelerating voltage and a beam current of 1 nA were applied. Spot selection for U-Th-Pb isotopic analyses was guided by these images.

U-Th-Pb isotopic analyses were carried out at the Department of Geology, Trinity College Dublin, Ireland. A Photon Machines Analyte Excite 193 nm ArF excimer laser-ablation system with a HelEx 2-volume ablation cell, coupled to an Agilent 7900 mass spectrometer was employed. Line scans on NIST612 standard glass were used to tune the instrument, by obtaining a Th/U ratio close to unity and low oxide production rates (i.e.,  $\text{ThO}^+/\text{Th}^+$  typically  $<0.15\%$ ). A circular laser spot of 24  $\mu\text{m}$  was used for zircon and a 36 or 47  $\mu\text{m}$  spot was used for titanite and rutile, with the spot diameter constant for each session. A repetition rate of 11 Hz and a fluence of  $2.25 \text{ J}\cdot\text{cm}^{-2}$  was employed. The helium carrier gas was fed into the laser cell at  $\sim 0.4 \text{ l}\cdot\text{min}^{-1}$  and was mixed with  $\sim 0.6 \text{ l}\cdot\text{min}^{-1}$  Ar make-up gas and  $11 \text{ ml}\cdot\text{min}^{-1}$   $\text{N}_2$ . Each analysis comprised 27.3 s of ablation (300 shots) and 12 s of washout

**Table 1**

Sample localities and modal mineral assemblages. Modal abundance is given in %, unless  $<1\%$ , i.e., accessory (•). Qz, quartz; Pl, plagioclase; Afs, alkali feldspar; Amp, Amphibole; Bt, biotite; Ms., muscovite; Rt, rutile; Ttn, titanite; Zrn, zircon; Ap, apatite; Ep, epidote; Mnz, monazite; Chl, chlorite; Py, pyrite.

Sample	Lithology	Qz	Pl	Afs	Amp	Bt	Ms	Rt	Ttn	Zrn	Ap	Ep	Mnz	Ilm	Mag	Chl	Py
KANARATA QUARRY - north part of the Sakar Batholith (42°05'00.0"N; 26°16'24.0"E)																	
SAK-01	melanocratic metadiorite	~5	~50		~40			•	•	•	•	•					
SAK-03	metadiorite with amphibolite xenolith (contact zone)																
SAK-03a	metadiorite part of sample SAK-03	~5	~60		~15			•		•	•						
SAK-03b	amphibolite xenolith part of sample SAK-03		~30		~65			•	•	•	•	•					
SAK-05	leucocratic metadiorite	~5	~85		~5			•		•	•	•	•				
SAK-06	granodiorite	~20	~40	~15		~15	~5		•	•	•	•					
SAK-07	amphibolite xenolith		~35		~60			•	•	•	•	•		•	•		
COUNTRY ROCKS - north of Levka (41°53'31.30"N; 26°17'0.10"E)																	
SAK-36	orthogneiss cut by quartz vein																
SAK-36a	orthogneiss	~15	~50		~30			•	•	•	•			•			•
SAK-36b	transition zone between orthogneiss and quartz vein	~55	~30		~10						•	•				•	

time; the latter portions of the washout were used for baseline measurements. The data reduction of raw U–Th–Pb isotopic data was undertaken using the freeware IOLITE package (Paton et al., 2011), with the “VizualAge” data reduction scheme (Petrus and Kamber, 2012) for zircon, and the “VizualAge UcompPbine” data reduction scheme (Chew et al., 2014) for titanite and rutile which can account for the presence of variable common Pb in the primary age reference material. Common Pb in the titanite and rutile standards was corrected using the  $^{207}\text{Pb}$ -based correction method. Conventional sample-standard bracketing was then applied to account for both downhole fractionation and long-term drift in isotopic or elemental ratios by normalizing all ratios to those of the U–

Th–Pb reference materials. The primary U–Pb calibration standard was 91500 zircon ( $^{206}\text{Pb}$ – $^{238}\text{U}$  age of  $1065.4 \pm 0.6$  Ma; Wiedenbeck et al., 1995; Wiedenbeck et al., 2004). Secondary standards used were the Plešovice zircon ( $^{206}\text{Pb}$ – $^{238}\text{U}$  age of  $337.13 \pm 0.37$  Ma; Sláma et al., 2008) and the WRS 1348 zircon ( $^{206}\text{Pb}$ – $^{238}\text{U}$  age of  $526.26 \pm 0.70$ ; Pointon et al., 2012) which yielded respective ages of  $337.0 \pm 1.7$  Ma ( $^{206}\text{Pb}$ – $^{238}\text{U}$  weighted mean age,  $n = 13$ ) and  $528.6 \pm 4.4$  Ma ( $^{206}\text{Pb}$ – $^{238}\text{U}$  weighted mean age,  $n = 20$ ), for the session with sample SAK-01, and  $337.1 \pm 1.9$  Ma ( $^{206}\text{Pb}$ – $^{238}\text{U}$  weighted mean age,  $n = 4$ ) and  $527.6 \pm 3.4$  Ma ( $^{206}\text{Pb}$ – $^{238}\text{U}$  weighted mean age,  $n = 9$ ) for the session with samples SAK-05 and SAK-06.

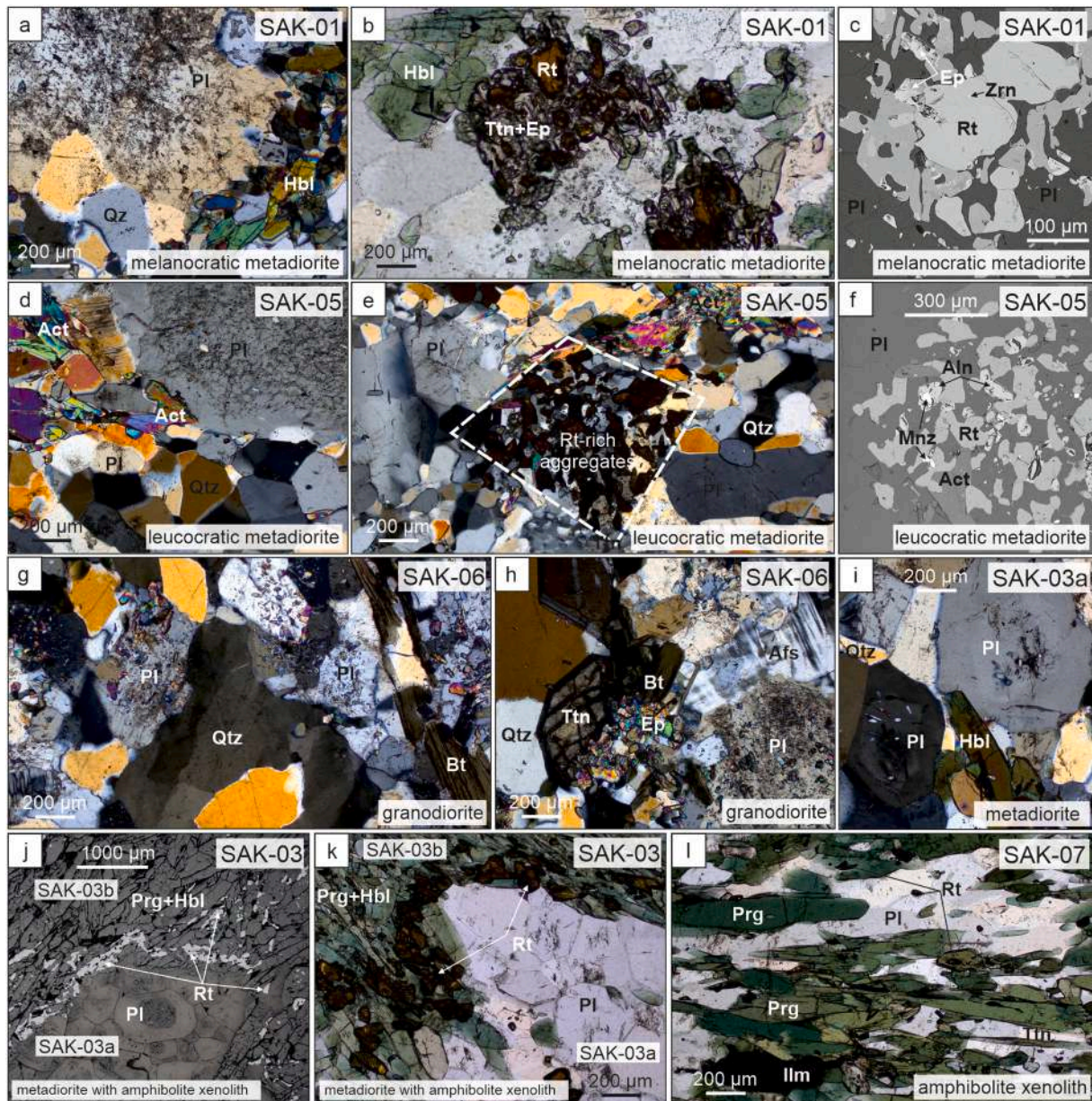


**Fig. 3.** Petrographic images of the rock samples from Kanarata quarry (north part of the Sakar Batholith): a, b, c, – SAK-01; d, e, f – SAK-05; g, h – SAK-06; i, j, k – SAK-03; l – SAK-07. (a) thin section in cross-polarised light (XPL) showing sericitization of a large plagioclase; (b) thin section in plane-polarised light (PPL) showing rutile-rich aggregates; (c) BSE image of rutile, titanite and titanite aggregates; (d, e) thin section in XPL showing (d) two generations of plagioclase; (e) rutile-rich aggregates and primary quartz with undulose extinction; (f) BSE image of rutile, allanite and monazite aggregates; (g, h, i) thin section in XPL showing (g) plagioclase partially altered to sericite and epidote and quartz with undulose extinction; (h) K-feldspar with tartan twinning characteristic of microcline, sericitized plagioclase and euhedral crystals of titanite surrounded by epidote; (i) plagioclase with a core-rim structure; (j, k) thin section in reflected light (j) and in PPL (k) showing a contact enriched in rutile between albitized granodiorite and an amphibolite xenolith; (l) foliated amphibolite xenolith. Abbreviations in the pictures: Act, actinolite; Afs, alkali feldspar; Aln, allanite; Bt, biotite; Ep, epidote; Hb, hornblende; Ilm, ilmenite; Mnz, monazite; Pl, plagioclase; Prg, pargasite; Rt, rutile; Ttn, titanite; Qtz, quartz.



For titanite analyses, OLT-1 ( $^{206}\text{Pb}/^{238}\text{U}$  TIMS age of  $1014.8 \pm 2.0$  Ma; Kennedy et al., 2010) was used as the primary U–Pb age reference material. The secondary age standards were MKED1 titanite ( $^{207}\text{Pb}/^{206}\text{Pb}$  TIMS age of  $1521.02 \pm 0.55$  Ma; Spandler et al., 2016) and BLR-1 titanite ( $^{206}\text{Pb}/^{238}\text{U}$  TIMS age of  $1047.1 \pm 0.4$  Ma; Aleinikoff et al., 2007) which yielded  $^{207}\text{Pb}$ -corrected ages of  $1506 \pm 13$  Ma and  $1036.8 \pm 6.9$  Ma, respectively, using the Stacey and Kramers (1975) terrestrial Pb evolution model for the age of crystallization. NIST 612 standard glass was used as the titanite trace-element reference material with  $^{43}\text{Ca}$  employed as an internal elemental standard.

R10 rutile (U–Pb TIMS age of ca. 1090 Ma; Luvizotto et al., 2009b) was analyzed as the primary rutile standard while R19b rutile (weighted mean  $^{206}\text{Pb}/^{238}\text{U}$  TIMS age of  $489.5 \pm 0.9$  Ma; Zack et al., 2011) and R13 rutile (U–Pb SIMS concordia age of  $504 \pm 4$  Ma; Schmitt and Zack, 2012) were used as secondary standards. During the course of analysis, the secondary reference materials yielded weighted average  $^{207}\text{Pb}$ -corrected ages of  $497.0 \pm 2.6$  Ma and  $510.1 \pm 4.6$  Ma respectively.

After the LA-ICP-MS zircon analyses, the crystals were imaged again using BSE and CL to inspect the laser ablation craters for inadvertent mixtures of growth zones. The final data reduction and presentation on the concordia diagrams were undertaken using the Isoplot 3.75 macro for Microsoft Excel (Ludwig, 2012). All dates are reported at the 2 $\sigma$  confidence level and include decay constant errors.

## 5. Results

### 5.1. Petrography

The rock types and mineral assemblages are listed in Table 1. Mineral compositions are provided in Supplementary Tables 2 and 3.

The majority of the granitoids from Kanarata quarry (SAK-01, SAK-05, SAK-06) are weakly deformed rocks with no visible mesoscopic development of a planar fabric. Foliation is observed in the contact zone of granitoids with xenoliths (SAK-03) and in the external parts of large xenoliths (SAK-07).

Sample SAK-01 is an albitized melanocratic metadiorite consisting of plagioclase and amphibole (magnesian-hornblende), with minor quartz and accessory rutile, titanite, epidote, apatite and zircon. Two generations of the plagioclase are present: 1) large (up to 1 cm) crystals with a core ( $\text{Or}_{0.1}\text{Ab}_{69.74}\text{An}_{26.31}$ ) - rim ( $\text{Or}_{0.1}\text{Ab}_{80.85}\text{An}_{15.20}$ ) structure; and 2) fine-grained recrystallized plagioclase (oligoclase,  $\text{Or}_{0.1}\text{Ab}_{81.85}\text{An}_{15.19}$ ), compositionally similar to the rims of the larger crystals (Fig. 3a). Quartz occurs in subordinate amounts, mostly as recrystallized subgrains. Accessory minerals (predominantly rutile, titanite and epidote) form aggregates of euhedral to subhedral crystals (Fig. 3b,c).

Sample SAK-05 is an albitized leucocratic metadiorite and consists of plagioclase, minor amphibole (actinolite) and quartz. Accessory minerals include rutile, allanite, zircon, apatite and monazite. Plagioclase occurs as 1) large crystals, with interiors altered to sericite; and 2) recrystallized euhedral crystals (Fig. 3d), and both types have a similar composition (albite,  $\text{Or}_{0.1}\text{Ab}_{90.96}\text{An}_{4.9}$ ). Primary quartz displays undulose extinction (Fig. 3e). Accessory minerals are euhedral to subhedral and form rutile-rich aggregates near amphibole in the plagioclase-rich groundmass (Fig. 3e,f). Monazite is surrounded by allanite or is almost completely broken down into allanite and apatite. Many allanite crystals have epidote rims.

Sample SAK-06 was collected from a non-albitized equigranular granodiorite consisting of plagioclase, quartz, biotite, muscovite and K-feldspar with accessory titanite, epidote, apatite and zircon. Plagioclase (oligoclase,  $\text{Or}_{0.1}\text{Ab}_{76.78}\text{An}_{21.23}$ ) is partially altered to sericite and epidote (Fig. 3g,h). Primary quartz displays undulose extinction (Fig. 3h), whereas recrystallized quartz usually shows grain boundary migration features (Fig. 3g). K-feldspar displays tartan twinning characteristic of microcline (Fig. 3h). Biotite and minor muscovite form intergrowths. Large euhedral crystals of titanite (up to 600  $\mu\text{m}$ ) are partially altered on their rims and surrounded by epidote (Fig. 3h).

Epidote occurs mostly as an alteration product; however, primary euhedral epidote is also observed.

Sample SAK-03 was sampled at the contact between the granitoid and amphibolite xenoliths which were both albitized. The granitoid part was transformed to metadiorite (SAK-03a) and contains plagioclase with a core-rim structure (Fig. 3i,j) which has lower anorthite content (oligoclase,  $\text{Or}_{0.1}\text{Ab}_{81.89}\text{An}_{11.19}$ ) than the plagioclase of its unaltered equivalent (massive granodiorite sample SAK-06). Plagioclase cores are altered to sericite (Fig. 3i,j). It also contains less quartz than sample SAK-06 and no K-feldspar, biotite and muscovite. Instead, magnesian-hornblende is present (Fig. 3i), which is similar in composition to amphibole from sample SAK-01. The amphibolite part of the sample (SAK-03b) consists mainly of plagioclase (oligoclase,  $\text{Or}_{0.1}\text{Ab}_{82.92}\text{An}_{8.18}$ ) and amphibole (magnesian-hornblende and pargasite; Fig. 3j,k). Compared to sample SAK-07, the plagioclase is enriched in Na. Rutile aggregates are pronounced along the contact between metadiorite and amphibolite (Fig. 3j,k). Both parts of this sample are enriched in Na and depleted in K compared to the unalbitized sample SAK-06.

Sample SAK-07 is an amphibolite xenolith and consists of plagioclase (oligoclase,  $\text{Or}_{0.1}\text{Ab}_{76.79}\text{An}_{21.24}$ ), amphibole (pargasite; Fig. 3l) and accessory rutile, zircon, apatite, titanite, epidote, ilmenite and magnetite. Accessory minerals are mostly euhedral and are randomly distributed within the amphibole-plagioclase groundmass.

Sample SAK-36 represents a non-albitized country-rock orthogneiss in contact with a quartz vein (Fig. 4a). The orthogneiss (SAK-36a) consists of plagioclase (oligoclase,  $\text{Or}_{0.1}\text{Ab}_{57.79}\text{An}_{43.20}$ ), amphibole (magnesian-hornblende and minor pargasite) and quartz with accessory ilmenite, rutile, apatite and zircon (Fig. 4b). Along the quartz vein, a transition zone (SAK-36b) is enriched in quartz, but minor amphibole and plagioclase are also present together with epidote, chlorite and apatite (Fig. 4c).

### 5.2. Whole rock geochemistry

Whole-rock major- and trace-element compositions of four samples analyzed herein and previously published data are presented in Supplementary Table 4.

The granitoid samples represent felsic to intermediate rocks with variable silica contents (57.5–66.6 wt%  $\text{SiO}_2$ ) and plot in the granodiorite (SAK-06) and diorite/gabbro (SAK-01, SAK-05) fields on a QAPF diagram (Streckeisen, 1974; Fig. 5a) and are metaluminous (Shand, 1943; Fig. 5b). Within the Sakar Batholith, dioritic samples are identified only from albitized Kanarata quarry (Pristavova et al., 2019; Fig. 5a, b).

The granodiorite sample SAK-06 has a similar trace element pattern to other granitoids from Sakar Batholith (Kamenov et al., 2010; Bonev et al., 2019; Salacińska et al., 2022; Fig. 5c). Metadiorites SAK-01 and SAK-05 have distinctive patterns similar to other albitized rocks (Pristavova et al., 2019). The differences are manifested by low K, Rb, Ba contents and more positive Th and Ce anomalies (Fig. 5c). The granitoid samples show fractionation of the light REE (LREE) relative to the heavy REE (HREE) and have negative Eu anomalies similar to samples of the Sakar Batholith (Fig. 5d).

### 5.3. Petrographic and chemical characteristics of titanite, zircon and rutile

#### 5.3.1. Titanite

The chemical composition of the titanite from melanocratic metadiorite SAK-01, granodiorite SAK-06 and amphibolite xenolith SAK-07 is provided in Supplementary Table 2 (EPMA data) and 5 (LA-ICP-MS data).

Titanites from melanocratic metadiorite SAK-01 and amphibolite xenolith SAK-07 are colourless, homogeneous, and occur as euhedral to subhedral crystals up to 200  $\mu\text{m}$  in length (Fig. 3b,c,l). Titanites from granodiorite SAK-06 are large (up to 600  $\mu\text{m}$  in length), brown and

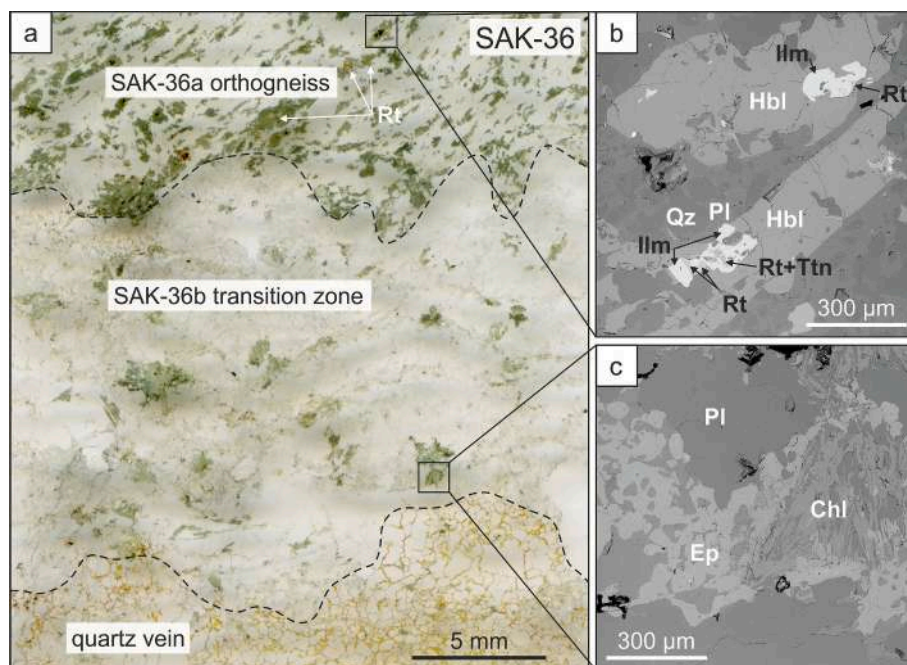


**Fig. 4.** Petrographic images of the country-rock orthogneiss (SAK-36) collected from the contact zone with a quartz vein: (a) thin section in PPL showing the transition zone between orthogneiss and a quartz vein; (b, c) BSE images of (b) orthogneiss containing rutile crystals; (c) the transition zone between orthogneiss and a quartz vein containing epidote and chlorite aggregates. Abbreviations in the pictures: Chl, chlorite; Ep, epidote; Hb, hornblende; Ilm, ilmenite; Pl, plagioclase; Rt, rutile; Ttn, titanite; Qz, quartz.

euhedral with patchy zonation revealed in BSE (Fig. 3h; Fig. 6a). Light-coloured BSE domains occur in the internal portions of the crystals, whereas the margins are significantly darker (Fig. 6a). This reflects the changes in chemical composition from light to dark domains with increasing contents of  $\text{CaO}$ ,  $\text{TiO}_2$ ,  $\text{SiO}_2$  and a decreasing content of  $\text{Fe}_2\text{O}_3$ . Light domains have a low Al/Fe ratio ( $\sim 1.0$ – $1.1$ ), which is slightly elevated in intermediate domains ( $1.0$ – $1.8$ ), and high ( $3.4$ – $2.7$ ) in dark domains. Light domains are enriched in REE and Y in comparison to dark domains (Fig. 6b). Titanite crystals from samples SAK-01 and SAK-07 have a similar composition to the dark domains in SAK-06.

Based on an Al vs Fe (a.p.f.u.) diagram after Aleinikoff et al. (2002), light and medium-grey domains (in BSE) of titanite from sample SAK-06 have a magmatic origin. The BSE-dark domains of titanite from sample SAK-06 and homogeneous titanites from samples SAK-01 and SAK-07 have a metamorphic origin (Fig. 6c).

LA-ICP-MS trace-element data from the cores of titanites from granodiorite sample SAK-06 (Supplementary Table 5) show that all analyzed domains are rich in REE and have high but variable Y contents. Sixty analyses (from a total of 66) have Th/U ratios  $>1$  (up to 16), which suggests a magmatic origin (i.e., Aleinikoff et al., 2002). The chondrite-normalized REE diagram after McDonough and Sun (1995) shows La depletion, followed by flat to HREE-depleted REE patterns with slight to moderate negative Eu anomalies (0.95 to 0.41; Fig. 6d).

### 5.3.2. Zircon

Zircons can be classified into two groups: 1) zircon associated with rutile (SAK-01, SAK-03, SAK-05); and 2) unassociated “free” zircons (Fig. 7). The first group occurs as tiny inclusions in rutile (zircons up to 5  $\mu\text{m}$  in length; sporadically up to 10–15  $\mu\text{m}$ ) along rutile rims and in their vicinity (zircon up to 20  $\mu\text{m}$  in length; Fig. 7a–f). The second group consists of large crystals up to 220  $\mu\text{m}$  in length (Fig. 7g) and this group was used for U–Pb dating.

### 5.3.3. Rutile

Rutile occurs in melanocratic metadiorite (SAK-01), the metadiorite with the amphibolite xenolith (SAK-03), leucocratic metadiorite (SAK-05), amphibolite xenolith (SAK-07) and in the orthogneiss (SAK-36a).

Rutiles from melanocratic (SAK-01) and leucocratic (SAK-05) metadiorites occur as euhedral to subhedral crystals up to 200–300  $\mu\text{m}$  long

and in aggregates with other accessory minerals (Fig. 3b,c,e,f; Fig. 7a,f). They are homogeneous in BSE images, with no indication of zoning or preservation of more than one generation of rutile. The occurrence of small (up to 10–15  $\mu\text{m}$  in length) euhedral zircons included in rutile or their vicinity is commonly observed.

Sample SAK-03 (the metadiorite with the amphibolite xenolith) contains rutiles in both lithologies (SAK-03a,b) and in the contact zone (Fig. 7b–e). Rutile from the metadiorite portion occurs as homogeneous anhedral to subhedral crystals up to 100–200  $\mu\text{m}$  long, closely associated with amphiboles (Fig. 7d). Rutiles from the amphibolitic portion are similar, but are occasionally surrounded by anhedral titanite (Fig. 7e). The contact zone is particularly enriched in rutile aggregates and is macroscopically visible as a brown band between the metadioritic and amphibolitic portions of the sample (Fig. 7b,c). These rutiles contain inclusions of numerous zircons (up to 5  $\mu\text{m}$  in length, sporadically 10–15  $\mu\text{m}$ ) while larger zircons (up to 20  $\mu\text{m}$  in length) commonly occur near the rutile or along their edges (section 5.2.2). Some rutiles are surrounded by a rim of titanite (Fig. 7b).

Rutile from amphibolite xenolith SAK-07 occurs mainly as homogeneous euhedral to subhedral crystals (up to 100  $\mu\text{m}$ ) randomly distributed in the host rock matrix (Fig. 7h). Sporadically, rutile with titanite and titanomagnetite form a complex aggregate as pseudomorphs after almost completely replaced ilmenite (Figure 7i).

Rutile from the orthogneiss (SAK-36) is homogeneous, mostly subhedral ( $\sim 100$   $\mu\text{m}$ ), and often coexists with ilmenite (Fig. 7 j, k). Some ilmenite grains are partially transformed into a mixture of fine-grained rutile and other phases (Fig. 7l).

The chemical composition of rutile is provided in Supplementary Table 3. The Si concentration was used to monitor inclusions, and all data with Si  $>200$  ppm were excluded (following Zack et al., 2004).

### 5.4. Ti-in-zircon and Zr-in-rutile thermometers

The mineral assemblage of zircon, rutile and quartz allows application of the Ti-in-zircon and Zr-in-rutile thermometers (Watson et al., 2006). However, the identification of zircon coexisting with rutile is crucial. Large zircons from granitoids (SAK-01, SAK-03, SAK-05) exhibit oscillatory zonation in CL (Fig. 9) and are interpreted as igneous phases (Late Carboniferous; section 5.4.1). The growth of small zircon



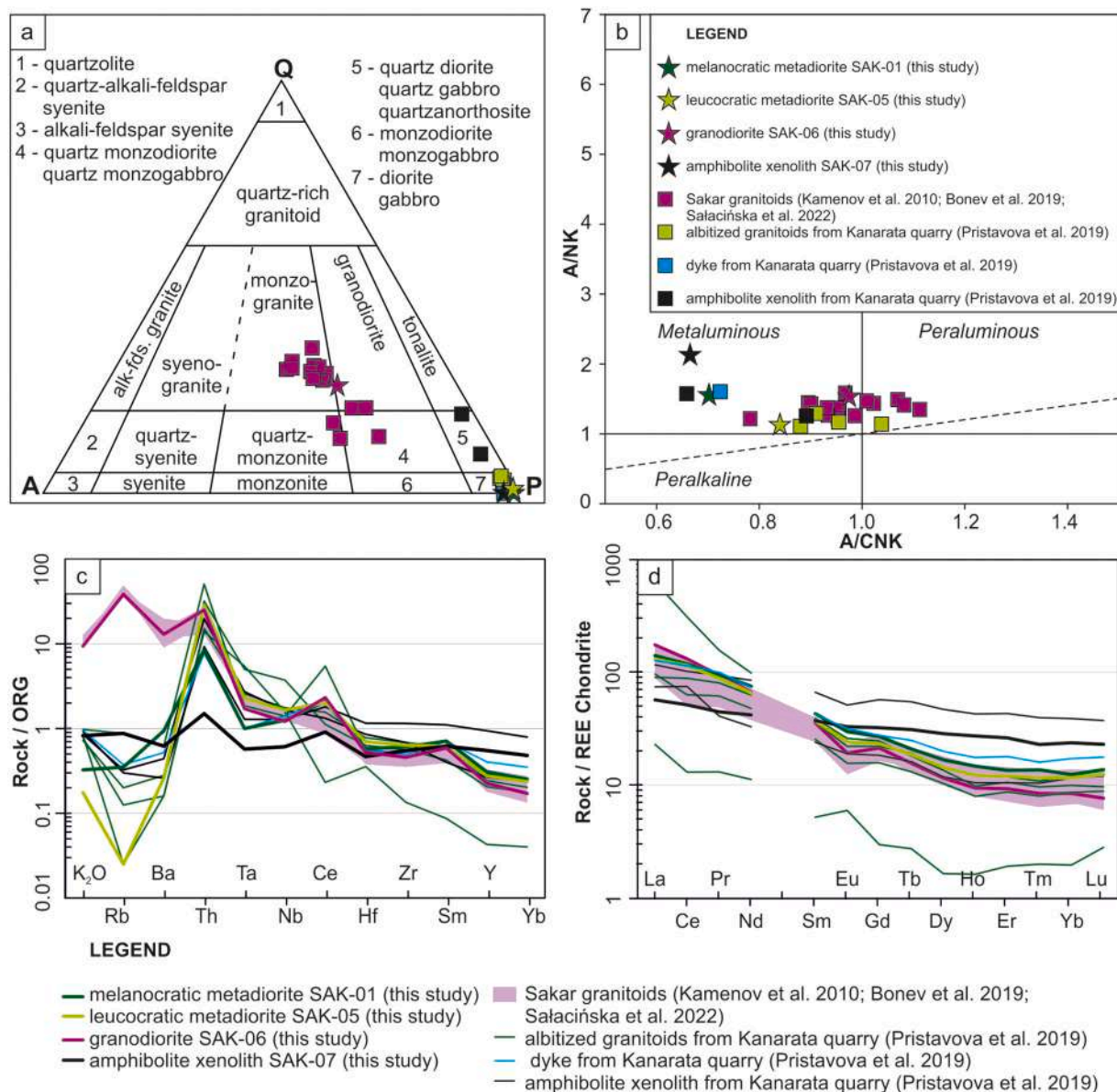


**Fig. 5.** Major and trace element diagrams for Sakar granitoids and other rocks from Kanarata quarry (northern part of the Sakar Batholith): (a) QAPF (Q – quartz, A – alkali feldspar, P – plagioclase, F – feldspathoids or foids) diagram (Streckeisen, 1974); (b) A/NK vs. A/CNK plot of Shand (1943); (c) Ocean ridge granite (ORG)-normalized multi-element diagram after Pearce et al. (1984); (d) Chondrite-normalized REE diagram after McDonough and Sun (1995). Data from previous studies are from: Kamenov et al. (2010), Bonev et al. (2019), Pristavova et al. (2019); Salacińska et al. (2022) and are given in Supplementary Table 4.

associated with rutile is interpreted as being associated with Early Alpine metamorphic processes. The Ti contents of these zircons range between 1223 ppm and 5448 ppm (SAK-01, SAK-03; Supplementary Table 3), thus yielding exceedingly high Ti-in-zircon temperatures (1465 °C–1961 °C; after Watson et al., 2006).

The Zr-in-rutile temperatures yield similar temperatures for the different rocks in Kanarata quarry (calculation after Watson et al., 2006; Fig. 8a; Supplementary Table 3). These temperatures range between ~540 °C and 620 °C. Temperatures calculated for rutiles from the orthogneiss (SAK-36) scatter from 490 °C to 665 °C (excluding two data points with Zr contents below the detection limit) with the main population between ~530 °C and 600 °C (average of  $562 \pm 20$  °C,  $n = 26/31$ ; Fig. 8a). Pressure-dependent temperature calculations after Tomkins et al. (2007) were undertaken using the minimum (3.5 kbar) and maximum (9 kbar) pressure values estimated for the Strandja Zone (e.g., Tzankova and Pristavova, 2007). For the higher pressures, the temperatures calculated after Tomkins et al. (2007) are comparable to those

calculated after Watson et al. (2006), and are slightly lower at lower pressures (Fig. 8b).

### 5.5. U–Pb geochronology

#### 5.5.1. U–Pb zircon and titanite dating

LA-ICP-MS U–Th–Pb isotopic data are listed in Supplementary Table 6. U–Pb dates are reported as  $^{206}\text{Pb}$ – $^{238}\text{U}$  weighted mean ages (zircon) or as a lower intercept age (titanite), both with  $2\sigma$  age uncertainties.

The granitoid samples (SAK-01, SAK-05 and SAK-06) contain similar populations of euhedral to subhedral zircon grains up to 220  $\mu\text{m}$  in length and aspect ratios of 1:2 to 1:3 (Fig. 9a–c). The zircons have strong oscillatory zonation, and some grains contain distinctive cores.

Thirty-four analyses were obtained from the melanocratic metadiorite (SAK-01) on 32 zircon grains (Fig. 10a). Two discordant (>5% disc.) analyses were excluded from further consideration. The remaining

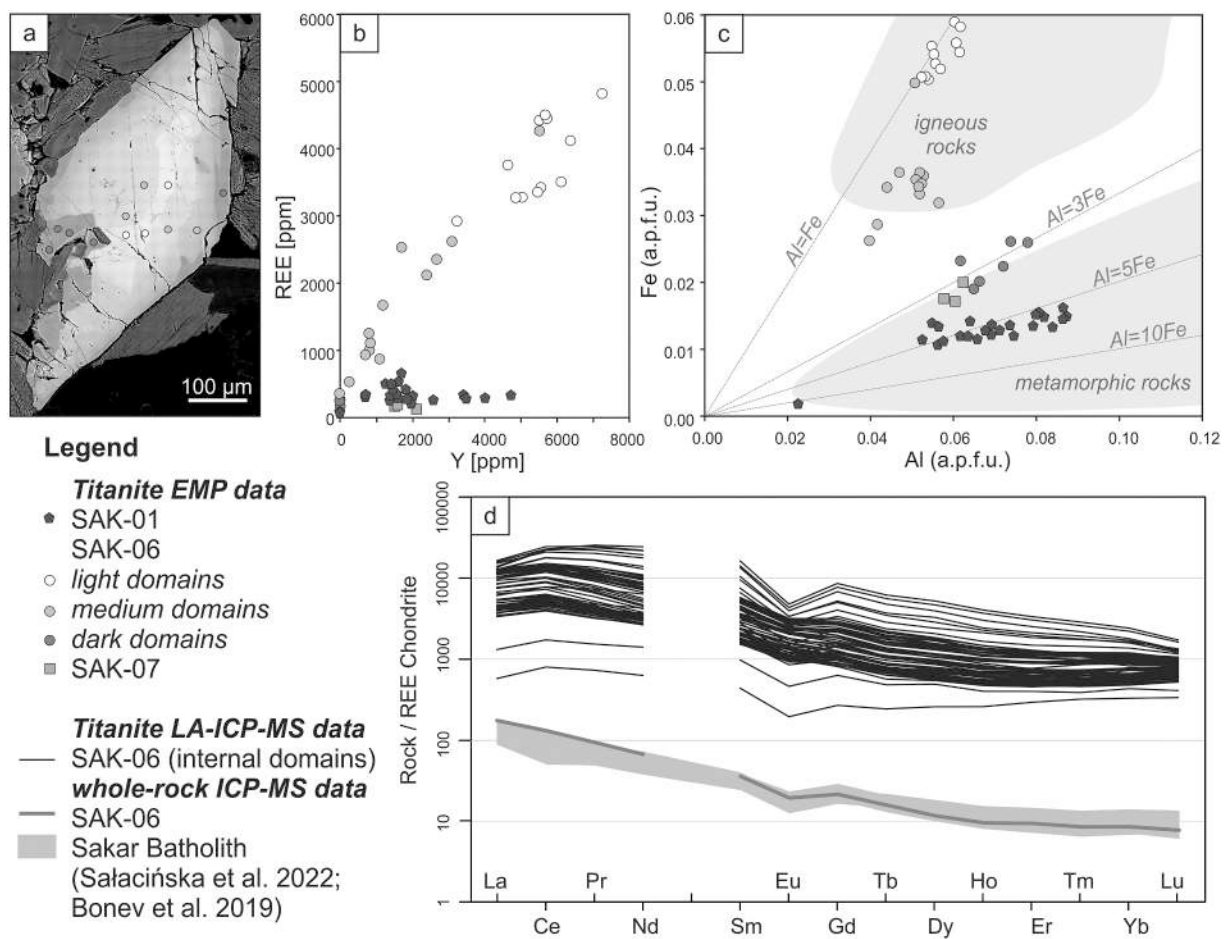


**Fig. 6.** Titanite from the Kanarata quarry (northern part of Sakar Batholith, Sakar Unit of the western Strandja Zone). (a) BSE images from granodiorite SAK-06 of euhedral titanite recrystallized on the crystal margins; small circles represent EMP location spots; (b) REE versus Y [ppm] plot; (c) classification diagram of Al (atom per formula unit; a.p.f.u.) plotted versus Fe (a.p.f.u.) after Aleinikoff et al. (2002); (d) REE normalized to chondrite (McDonough and Sun, 1995).

32 concordant data points range from ca. 462 Ma to ca. 294 Ma. Thirty-one concordant analyses scatter along the Concordia between ca. 342 Ma and ca. 294 Ma, with a significant cluster of twenty-seven data yielding a weighted mean  $^{206}\text{Pb}$ – $^{238}\text{U}$  age of  $304 \pm 2$  Ma (MSWD = 2.8); when the excess variance (1.5%) on the weighted mean  $^{206}\text{Pb}$ – $^{238}\text{U}$  age of the WRS validation material is taken into account, the external uncertainty on this weighted mean age is  $304 \pm 4.5$  Ma. These Late Carboniferous zircons probably represent a mixture of autocrusts and antecrusts. One analysis from a zircon core is significantly older (ca. 462 Ma) and is interpreted as a xenocryst.

For the leucocratic metadiorite (SAK-05), thirty-two concordant (<5% disc.) analyses from 31 grains were obtained (Fig. 10b). The BSE and CL post-imaging revealed that one analysis comes from a mixed domain, which was therefore excluded from further consideration. The remaining data points range from ca. 308 Ma to ca. 286 Ma, with a weighted mean  $^{206}\text{Pb}$ – $^{238}\text{U}$  age of  $301 \pm 2$  Ma (MSWD = 1.9). This age is interpreted as the crystallization age of the granitoid.

For granodiorite SAK-06, thirty-eight analyses from 37 oscillatory-zoned zircons were obtained (Fig. 10c). All data points spread along the Concordia with ages between ca. 320 Ma to ca. 292 Ma, without any distinctive cluster. Based on the isotopic data and textural observations in CL, partial Pb loss is detected within zircon grains, e.g. where younger dates of ca. 296 Ma are obtained from cores, whereas slightly older dates of ca. 300 Ma comes from oscillatory-zoned rims (Fig. 9c, analyses 19,20). Therefore, this data set is interpreted as a mixture of antecrystic and autocrystic zircons, variously affected by partial Pb loss.

Granodiorite sample SAK-06 contains large titanite crystals (up to

600  $\mu\text{m}$  in length) from which sixty-six analyses were obtained. All data points are highly discordant due to high proportions of common Pb relative to radiogenic Pb, and lie on an unanchored Tera–Wasserburg discordia line with a lower intercept age of  $297 \pm 5$  Ma (MSWD = 14) and a  $^{207}\text{Pb}/^{206}\text{Pb}$  initial ratio of  $0.872 \pm 0.094$  provided by the upper intercept (Fig. 10d).

#### 5.5.2. U–Pb rutile dating

LA-ICP-MS U–Th–Pb isotopic data of the analyzed rutile are listed in Supplementary Table 7. The data points are highly discordant due to high proportions of common Pb relative to radiogenic Pb. For the rutile, dates are reported as lower intercept ages with  $2\sigma$  age uncertainties calculated based on an unanchored Tera–Wasserburg discordia line.

For the melanocratic metadiorite (SAK-01), 78 analyses of rutile were obtained, which yielded a lower intercept age of  $125 \pm 4$  Ma (MSWD = 3.2) and a highly radiogenic  $^{207}\text{Pb}/^{206}\text{Pb}$  initial ratio of  $0.126 \pm 0.016$  provided by the upper intercept of the discordia line (Fig. 11a).

For the leucocratic metadiorite (SAK-05), a total of 103 rutile analyses were obtained and yielded a lower intercept age of  $116 \pm 7$  Ma (MSWD = 4.6); again with a highly radiogenic  $^{207}\text{Pb}/^{206}\text{Pb}$  initial ratio of  $0.101 \pm 0.013$  (Fig. 11b).

Forty-three analyses were obtained from rutiles of the orthogneiss sample SAK-36, which are distributed along the discordia line with a lower intercept age of  $154 \pm 4$  Ma (MSWD = 1.14) and a  $^{207}\text{Pb}/^{206}\text{Pb}$  initial ratio of  $0.828 \pm 0.015$  (Fig. 11c).

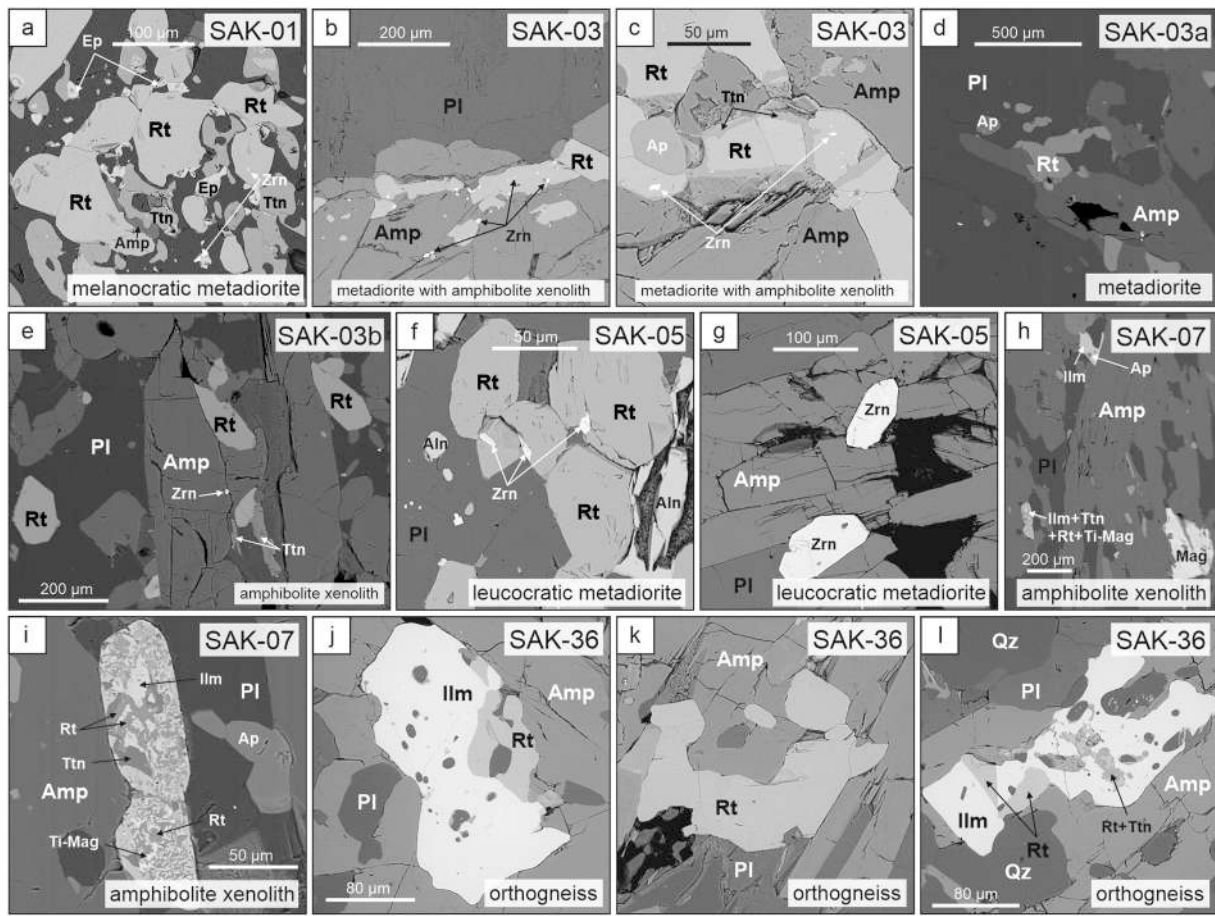


**Fig. 7.** BSE images of the accessory phases from rutile-bearing rocks of the Sakar Unit. (a) rutile containing small zircon in an accessory mineral aggregate from melanocratic metadiorite SAK-01; (b, c) contact zone between metadiorite and an amphibolite xenolith, which is enriched in rutile with associated zircon (SAK-03); with some of the rutile surrounded by titanite (c); (d) rutile from the metadiorite (SAK-03a); (e) rutile and associated titanite from the amphibolite xenolith (SAK-03b); (f) rutile and associated small zircon in the rutile-rich aggregates from leucocratic metadiorite (SAK-05); (g) large zircon crystals from leucocratic metadiorite (SAK-05); (h, i) accessory minerals from the amphibolite xenolith (SAK-07) with ilmenite replaced by rutile, titanite and titanomagnetite (i); (j, k, l) rutile and ilmenite from orthogneiss SAK-36.

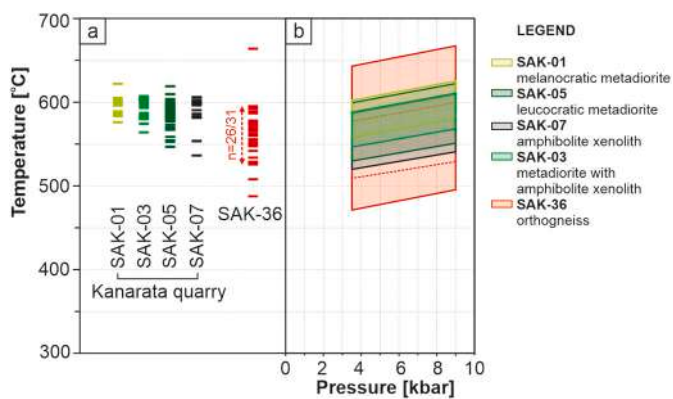


**Fig. 8.** Rutile from Kanarata quarry (northern part of the Sakar Batholith) and country-rock orthogneiss (south of the Sakar Batholith, near Levka): (a, b) diagram showing Zr-in-rutile temperatures calculated (a) after Watson et al. (2006), (b) after Tomkins et al. (2007) for pressures of 3.5–9 kbar previously estimated for the Sakar Unit.

## 6. Discussion

### 6.1. U–Pb geochronology

#### 6.1.1. Zircon and titanite

On the basis of U–Pb zircon geochronology, previous studies inferred an emplacement age of the Sakar Batholith between ca. 306 Ma and ca. 295 Ma (Bonev et al., 2019; Peytcheva et al., 2016; Pristavova et al., 2019; Salacińska et al., 2022) and reported that zircon populations contain both autocrystic and antecrystic components. Salacińska et al. (2022) suggested that these zircons were variously affected by partial Pb-loss due to Late Jurassic to Early Cretaceous metamorphism. The Late Carboniferous emplacement age of the Sakar granitoids is supported by a ca. 297 Ma age of the igneous titanite from granodiorite SAK-06. Sample SAK-05, an elongated leucocratic body dated by U–Pb zircon at ca. 301 Ma represents the youngest pulse of the Sakar Batholith (Kamenov et al., 2010). It indicates that the emplacement of different phases of the Sakar Batholith occurred within a relatively short time interval in the Late Carboniferous.

#### 6.1.2. Rutile

Samples SAK-01 and SAK-05 yield U–Pb Tera-Wasserburg lower intercept ages of  $125 \pm 4$  Ma and  $116 \pm 7$  Ma respectively. The  $^{207}\text{Pb}/^{206}\text{Pb}$  initial ratios for samples SAK-01 and SAK-05 ( $0.126 \pm 0.016$  and  $0.101 \pm 0.013$ , respectively) are much lower than the values



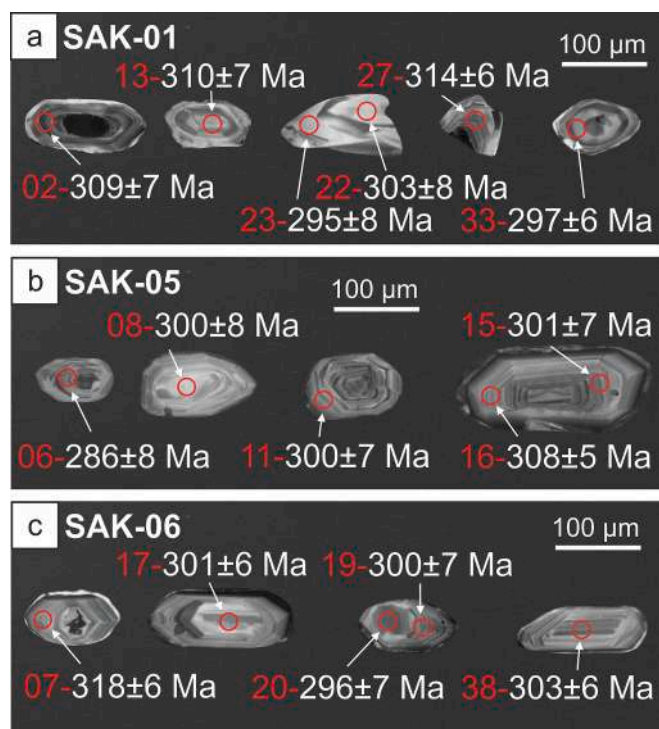


**Fig. 9.** CL images of representative zircons from the various granitoids in Kanarata quarry of the Sakar Batholith (a) sample SAK-01; (b) sample SAK-05; (c) sample SAK-06; red numbers represent the analyses number, reported values are  $^{206}\text{Pb}/^{238}\text{U}$  ages, all presented ages are concordant (<5% disc.); red circles represent the laser ablation spot. (For interpretation of the references to colour in this figure legend, the reader is referred to the web version of this article.)

predicted by any terrestrial Pb-evolution model (0.844–0.843 ratios for an age of ca. 125–116 Ma; [Stacey and Kramers, 1975](#)). The U–Pb rutile data could be interpreted as the oldest  $^{206}\text{Pb}/^{238}\text{U}$  dates (ca. 175–180 Ma in both samples) representing a minimum crystallization age, and the younger Early Cretaceous dates representing either recrystallization or Pb loss during subsequent metamorphism at ca. 120 Ma. This is possible, although analyses free of common Pb would be expected to define a mixing line on the Tera–Wasserburg concordia from ca. 180 Ma to ca. 120 Ma, while any analyses with incorporation of common Pb would be dispersed above this discordia line. This is not observed in either sample – the analyses lie on discordias and the older  $^{206}\text{Pb}/^{238}\text{U}$  analyses have systematically higher  $^{207}\text{Pb}/^{206}\text{Pb}$  ratios. Instead, it is argued below that the ca. 120 Ma U–Pb lower intercept ages constrain the timing of the peak Early Cretaceous thermal event, and that the initial lead incorporated during rutile growth was highly radiogenic. Importantly, it is emphasised either interpretation of the Tera–Wasserburg systematics of the U–Pb rutile data imply a ca. 120 Ma metamorphic event.

Incorporation of highly radiogenic initial lead is typical of mineral growth from a local geochemical reservoir influenced by the breakdown of a U-rich mineral (e.g., [Romer, 2001](#)). The initial lead isotopic composition of the metamorphic phases should be consistent with the mean lead composition of the precursor ([Romer, 2001](#)). U–Pb zircon dating shows that various granitoids are Late Carboniferous in age. The less albitized granodiorite (sample SAK-06) contains igneous domains in the internal parts of the titanite ([Fig. 6](#)), which provide a ca. 297 Ma age ([Fig. 10d](#)). The U–Pb titanite data from these Late Carboniferous granitoids yield a weighted mean  $^{207}\text{Pb}/^{206}\text{Pb}$  ratio of  $0.1057 \pm 0.0066$ , similar to the initial lead composition of the rutile data for samples SAK-01 and SAK-05. This ratio, coupled with a weighted mean  $^{238}\text{U}/^{206}\text{Pb}$  ratio of  $19.09 \pm 0.38$  of the titanite, was used to construct an average titanite data-point ellipse ('AvTtn' on [Fig. 11a](#)), which lies very close to

the discordia line of the rutile data (SAK-01); modelling the Pb evolution of this 'AvTtn' analysis shows that at ca. 125 Ma it yields a  $^{207}\text{Pb}/^{206}\text{Pb}$  ratio of 0.14198 (Supplementary Fig. 1), which is just within uncertainty of the  $^{207}\text{Pb}/^{206}\text{Pb}$  initial ratio for sample SAK-05 ( $0.126 \pm 0.016$ ) from the same quarry which exhibits rutile growth at  $125 \pm 4$  Ma. This provides further indication that the low (highly radiogenic) initial lead isotopic composition in rutile was inherited from igneous titanite and suggests that mineral aggregates in samples SAK-01 and SAK-05 are likely pseudomorphs after Early Alpine breakdown of Late Carboniferous titanite.

The well constrained ca. 154 Ma rutile age from sample SAK-36 is significantly older than those obtained from samples SAK-01 and SAK-05; however, the Zr-in-rutile temperatures are comparable. Therefore, the ca. 154 Ma age is interpreted as a record of a separate metamorphic event.

## 6.2. Igneous versus metamorphic origin of the accessory phases

The accessory phases in this study represent primary magmatic and metamorphic minerals. The less albitized granodiorite (SAK-06) contains euhedral crystals of titanite, epidote, apatite and zircon. Such an accessory mineral assemblage is characteristic of the equigranular and porphyritic granitoids of the Sakar Batholith ([Bonev et al., 2019](#); [Kamenov et al., 2010](#); [Śalacińska et al., 2022](#)). The titanite in granodiorite (SAK-06) yields evidence for dissolution-precipitation based on patchy zonation visible in BSE, which likely formed during a hydrothermal event ([Fig. 6a](#)). However, the igneous composition of the titanites is preserved in their internal domains. The primary titanites are interpreted as an early crystallizing phase based on their euhedral morphology and similar features of both titanite and the whole-rock REE patterns ([Fig. 6d](#); e.g., [Pan et al., 2018](#)). Other accessory minerals in the granodiorite do not show features characteristic of dissolution-precipitation.

Rutile, titanite, REE-enriched epidote, apatite and zircon from the melanocratic (SAK-01) and rutile, allanite, apatite, zircon and monazite from leucocratic (SAK-05) metadiorites form aggregates with shapes similar to those of igneous titanite in sample SAK-06 ([Fig. 3b,c,e,f](#)) and are interpreted as pseudomorphs after titanite. Breakdown of mineral precursors such as ilmenite, biotite or titanite can form rutile during high-grade metamorphism, but it is also known from medium-grade rocks (e.g., [Angiboust and Harlov, 2017](#); [Luvizotto et al., 2009a](#); [Luvizotto and Zack, 2009](#); [Meinhold, 2010](#)). The interpretation of titanite as a precursor of the rutile-rich aggregates in metadiorites is supported by U–Pb isotopic evidence (see section 6.1.2). The metamorphic titanite in the melanocratic metadiorite may have grown as a result of the high CaO content in the rock (7.1 wt%) and may also explain the absence of monazite, which coexists with allanite in granitoids with only intermediate contents of CaO (e.g., [Lee and Bastron, 1967](#)). In the mafic xenoliths (SAK-03b, SAK-07) and orthogneiss (SAK-36), metamorphic rutiles formed due to ilmenite breakdown, which is supported by textural evidence ([Fig. 7h–l](#)).

Zircon crystals (~100–220 µm in length) from the metadiorites (SAK-01, SAK-05) have no metamorphic rims but these samples contain a population of small zircons (mostly ~5–10 µm in length) associated with rutile, observed also in the contact zone between metadiorite and a mafic xenolith (SAK-03; [Fig. 7a–f](#)). Similar zircons have been described from high- and ultrahigh-temperature metamorphic rocks (e.g., [Ewing et al., 2013](#); [Kooijman et al., 2012](#)) and were interpreted to have formed by Zr expulsion during cooling. However, this model does not appear applicable to this study. The small zircons have very high-Ti concentrations (1223–5448 ppm), corresponding to unrealistically high Ti-in-zircon temperatures (1465 °C–1961 °C). Assuming that igneous titanite crystals (with average ~420 ppm Zr; Supplementary Table 5) were precursors of the rutile-rich aggregates in the metadiorites, these local geochemical reservoirs could contain more Zr than rutile was able to incorporate at medium temperatures (540–620 °C). From this excess of



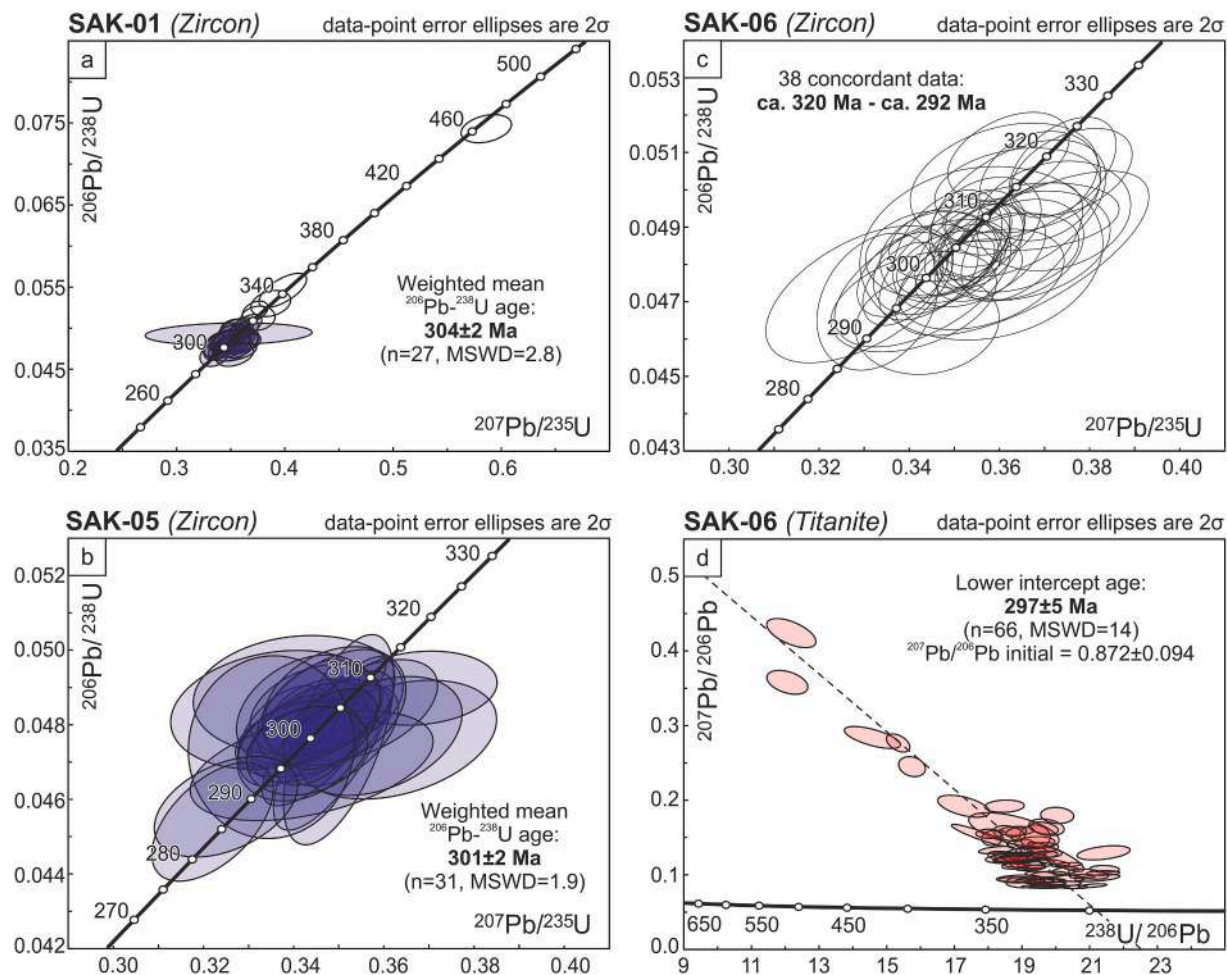


**Fig. 10.** LA-ICP-MS U-Th-Pb analyses of zircon presented on Wetherill Concordia diagrams (a, b, c) and titanite presented on a Tera-Wasserburg Concordia diagram (d) for samples of: (a) melanocratic metadiorite SAK-01; (b) leucocratic metadiorite SAK-05; (c, d) granodiorite SAK-06; the data shown as filled ellipses are used for age calculations; analyses of mixed domains are not shown.

Zr, small zircons could then crystallize although the high-Ti contents remain difficult to explain – it is possible the excitation volume in the zircon caused by the EPMA electron beam partly extends into the Ti-rich rutile host.

### 6.3. Rock-forming processes of Sakar granitoids and its superimposed albitization

Previous studies of the Sakar Batholith have shown that the major granitoid components are metaluminous to slightly peraluminous equigranular and porphyritic monzogranite, granodiorite and quartz-monzodiorite (e.g., Bonev et al., 2019; Kamenov et al., 2010; Salacina et al., 2022). These rocks have a common magmatic evolution on a calc-alkaline series caused by fractionation of ferromagnesian minerals and plagioclase with local re-distribution of  $\text{Na}_2\text{O}$  related to the superimposed albitization (e.g., Kamenov et al., 2010; Pristavova et al., 2019). Elongated leucocratic bodies or veins (up to few meters wide) are a minor component of the batholith, and occur mostly along the batholith peripheries, whereas granitoids richer in ferromagnesian minerals (mostly biotite) are associated with the assimilation of country rocks (Kamenov et al., 2010; Pristavova et al., 2019). This study investigated all types of granitoids, which are affected to varying degrees by superimposed albitization. The massive part of granodiorite (SAK-06) is almost unaltered and is similar to the equigranular component of the Sakar granitoid. The assimilation of country-rock amphibolites caused the formation of a melanocratic variety of the Sakar granitoid (SAK-01)

with a lower content of  $\text{SiO}_2$  and higher content of  $\text{CaO}$  and  $\text{MgO}$ . Leucocratic metadiorite (SAK-05) contains a lower amount of  $\text{Fe}_2\text{O}_3$ , presumably resulting from late-stage fractional crystallization. Both the melanocratic (SAK-01) and leucocratic (SAK-05) metadiorites have elevated values of  $\text{Na}_2\text{O}$  and are depleted in  $\text{K}_2\text{O}$ ,  $\text{Rb}$ ,  $\text{Ba}$  (Fig. 5c) and  $\text{Cs}$  ( $<0.1$  ppm), which is attributed to the albitization process. The REE patterns (Fig. 5d) were not affected by either country rock contamination or the albitization process. The heterogeneity of the thermal overprint can be explained by fluid-induced alteration with preferable migration paths along weakened, fractured parts, such as contact zones between massive granitoids, xenoliths and elongated leucocratic bodies. The most albitized rocks contain rutile-rich aggregates, which occur as pseudomorphs after titanite (SAK-01, SAK-05) or along the contact zone of different rock types (SAK-03). Therefore, we attribute their formation to the albitization process. Albitization causes the replacement of K-feldspar and Ca-plagioclase by albite, which is related to a dissolution-precipitation processes (e.g., Engvik et al., 2008). Complete albitization of granitic rocks usually involves the dissolution of quartz (dequartzification or episyenitization) and micas (e.g., Petersson and Eliasson, 1997; Boulvais et al., 2007). This is consistent with our observations of the absence of mica and the presence of only minor amounts of quartz in the albitized metadiorites (SAK-01, SAK-05, SAK-03a).

The associated mineral reactions can be inferred based on comparing granodiorite samples SAK-06 (effectively unaltered) and SAK-03 (partial albitization). The albitization of the plagioclase was relatively minor

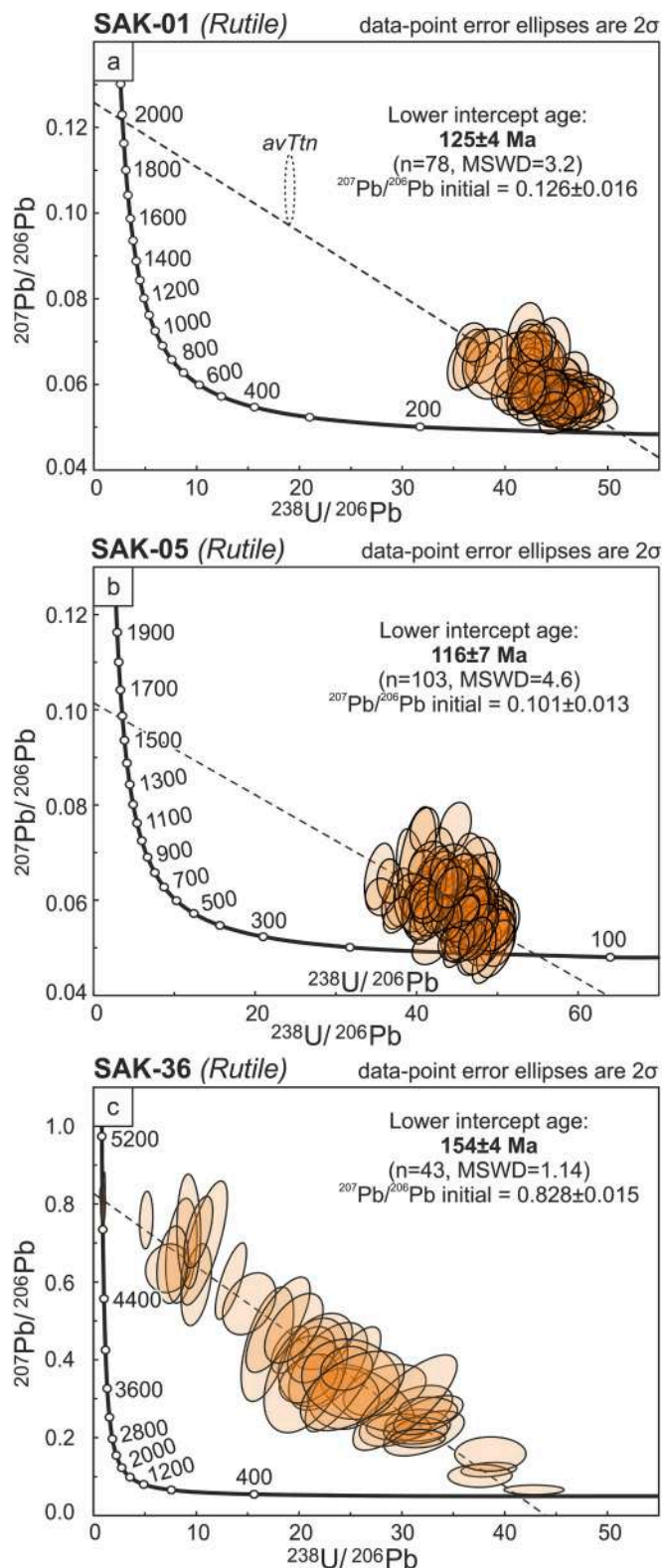


**Fig. 11.** LA-ICP-MS rutile U-Th-Pb analyses presented on Tera-Wasserburg Concordia diagrams for samples of: (a) melanocratic metadiorite SAK-01; (b) leucocratic metadiorite SAK-05; (c) orthogneiss SAK-36; the data shown as filled ellipses are used for age calculations.

and involved only small changes in chemical composition from oligoclase (SAK-06) to albite (SAK-03a). K-feldspar (SAK-06) was replaced by albite, and dissolution of quartz occurred (20% modal volume in SAK-06 falling to 5% in SAK-3a). Compared to the biotite with minor muscovite observed in SAK-06, sample SAK-03 contains magnesio-hornblende. Primary accessory phases differ as well, with primary titanite and epidote present in SAK-06 and absent in SAK-03, which instead contains rutile.

A simplified albitization reaction can be proposed:

Oligoclase + quartz + K-feldspar + phlogopite + minor muscovite + accessory titanite, epidote, zircon, apatite +  $\text{Na}^{2+}$  +  $\text{H}_2\text{O}$  → albite + magnesio-hornblende + minor quartz + accessory rutile, zircon, apatite +  $\text{K}^+$  +  $\text{SiO}_4^{4-}$ , where,

- 1)  $\text{Na}^+$  comes from the fluid, and was responsible for the albitization of oligoclase and K-feldspar;
- 2)  $\text{Ca}^{2+}$  incorporated in magnesio-hornblende comes from albitization of oligoclase and from accessory titanite and epidote;
- 3)  $\text{K}^+$  was released to the fluid from K-feldspar, biotite and muscovite;
- 4) Dissolution of quartz released a significant amount of silica, which helped form albite and magnesio-hornblende, with excess delivered to the fluid.

#### 6.4. Significance of metamorphic ages in a local and regional context

Previous studies of the Sakar Unit documented amphibolite-facies metamorphism (temperatures in the range of 510–660 °C) between ca. 167 Ma and ca. 124 Ma (Bonev et al., 2020; Chavdarova and Machev, 2017; Tzankova and Pristavova, 2007; Vladinova et al., 2019). These temperatures are comparable to the Zr-in-rutile temperatures presented in this study (~530–620 °C). The U–Pb rutile dating shows that the Sakar Unit was affected by two events: at ca. 154 Ma and at ca. 125–116 Ma (Fig. 11), which both reached similar temperatures. The  $^{40}\text{Ar}/^{39}\text{Ar}$  dating of amphibole from country-rock amphibolites sampled close to country-rock orthogneiss SAK-36 yielded an age of  $141 \pm 2$  Ma (Bonev et al., 2020), which when integrated with this study, provides a time interval of ca. 154–141 Ma for amphibolite-facies metamorphism. Our study indicates that fluid migration and element redistribution linked to the albitization also caused the growth of metamorphic rutile at ca. 125–116 Ma. From the same locality, Szopa et al. (2020) documented two stages of hydrothermal activity based on U–Pb dating of apatite (ca. 149 Ma) and titanite (ca. 114 Ma), with the titanite representing a texturally later set of minerals from the same vein. We interpret these two stages as connected to the ca. 154 Ma and ca. 125–116 Ma metamorphic events detected in this study. The source of the Early Cretaceous fluid is unknown. Albitization caused new mineral growth and recrystallization, however, the albitized rocks did not acquire a new deformation-related fabric.

None of the studies from the Strandja Unit have documented a younger (Early Cretaceous) amphibolite-facies regional thermal episode similar to the event detected in the northern part of the Sakar Unit.

Evidence for Late Jurassic to Early Cretaceous metamorphism is preserved in the neighbouring Rhodope Metamorphic Complex (Fig. 1; e.g., Burg, 2012; Gautier et al., 2017). Many studies emphasize the common Late Jurassic to Early Cretaceous evolution of the Rhodopes and Strandja Zone (e.g., Bonev et al., 2020; Natal'in et al., 2016; Okay et al., 2001; Sunal et al., 2011). However, it is important to notice that the Strandja Zone was apparently not affected by the high-grade metamorphic event documented in the Rhodope Metamorphic Complex, which reached (ultra-) high-pressure granulite-facies conditions in the Late Jurassic – Early Cretaceous (e.g., Bauer et al., 2007; Liati, 2005; Liati et al., 2016; Moulas et al., 2017). Additionally the Rhodopes were subsequently affected by polycyclic amphibolite-facies Alpine metamorphism in the Late Cretaceous and the Cenozoic (see summary in Burg, 2012; Gautier et al., 2017).

## 7. Conclusions

The results of this study led to the following conclusions:

1. The Sakar Batholith in the Strandja Zone contains several varieties of Late Carboniferous granitoids that formed due to the interaction between granitic magma and country rocks, and through fractional crystallization.
2. Early Alpine amphibolite-facies metamorphism affected the Strandja Zone in the Late Jurassic. However, at least part of the study area was re-heated to similar temperatures (~530–620 °C) in the Early Cretaceous.
3. The Early Cretaceous event is associated with albitization which caused new mineral growth and recrystallization but did not result in formation of a new penetrative fabric.
4. There is no clear connection between regional metamorphism and albitization. Albitization was local, was coupled with the removal of quartz and affected only the northern part of the Sakar Batholith. The degree of albitization was strongly dependent on fluid migration pathways. Fluid migration led to the formation of rutile-rich aggregates which record the timing and temperatures of this albitization event. Rutile-rich aggregates formed due to the alteration of primary titanites.
5. Late Jurassic – Early Cretaceous thermal events in the Strandja Zone were synchronous with Early Alpine metamorphism in Rhodope Metamorphic Complex.

Supplementary data to this article can be found online at <https://doi.org/10.1016/j.lithos.2023.107186>.

## CRediT authorship contribution statement

**Anna Gumsley:** Conceptualization, Data curation, Formal analysis, Funding acquisition, Investigation, Methodology, Project administration, Resources, Visualization, Writing – original draft, Writing – review & editing. **Krzysztof Szopa:** Formal analysis, Supervision, Validation, Writing – review & editing. **David Chew:** Formal analysis, Funding acquisition, Methodology, Validation, Writing – review & editing. **Ianko Gerdjikov:** Supervision, Writing – review & editing. **Petrus Jokubauskas:** Formal analysis, Validation, Writing – review & editing. **Beata Marciniak-Maliszewska:** Formal analysis, Validation, Writing – review & editing. **Foteini Drakou:** Formal analysis, Validation, Writing – review & editing.

## Declaration of Competing Interest

The authors declare that they have no known competing financial interests or personal relationships that could have appeared to influence the work reported in this paper.

## Acknowledgements

This research was supported by a Preludium Grant awarded to Anna Gumsley from the National Science Centre (Narodowe Centrum Nauki), NCN, in Poland (grant agreement no. UMO-2018/29/N/ST10/00368). David Chew is supported in part by a research grant from Science Foundation Ireland (SFI) under Grant Number 13/RC/2092\_P2 (iCrag, the SFI Research Centre in Applied Geosciences). The authors would like to thank Nikolay Gospodinov for logistical support during the field work. We wish to thank the Editor, Nadia Malaspina, as well as Michael Bröcker, Andrew Kylander-Clark and anonymous reviewer for constructive reviews which helped to improve the manuscript.

## References

- Aleinikoff, J.N., Wintsch, R.P., Fanning, C.M., Dorais, M.J., 2002. U-Pb geochronology of zircon and polygenetic titanite from the Glastonbury complex, Connecticut, USA: an integrated SEM, EMPA, TIMS, and SHRIMP study. *Chem. Geol.* 188 (1–2), 125–147. [https://doi.org/10.1016/S0009-2541\(02\)00076-1](https://doi.org/10.1016/S0009-2541(02)00076-1).
- Aleinikoff, J.N., Wintsch, R.P., Tollo, R.P., Unruh, D.M., Fanning, C.M., Schmitz, M.D., 2007. Ages and origins of rocks of the Killingworth dome, south-Central Connecticut: implications for the tectonic evolution of southern New England. *Am. J. Sci.* 307 (1), 63–118. <https://doi.org/10.2475/01.2007.04>.
- Angiboust, S., Harlov, D., 2017. Ilmenite breakdown and rutile-titanite stability in metagranitoids: Natural observations and experimental results. *Am. Mineral.* 102 (8), 1696–1708. <https://doi.org/10.2138/am-2017-0604>.
- Aysal, N., Şahin, S.Y., Güngör, Y., Peytcheva, I., Öngen, S., 2018. Middle Permian–Early Triassic magmatism in the Western Pontides, NW Turkey: geodynamic significance for the evolution of the Paleo-Tethys. *J. Asian Earth Sci.* 164, 83–103. <https://doi.org/10.1016/j.jseaes.2018.06.026>.
- Bauer, C., Rubatto, D., Krenn, K., Proyer, A., Hoinkes, G., 2007. A zircon study from the Rhodope metamorphic complex, N-Greece: Time record of a multistage evolution. *Lithos* 99, 207–228. <https://doi.org/10.1016/j.lithos.2007.05.003>.
- Bonev, N., Filipov, P., Raicheva, R., Moritz, R., 2019. Timing and tectonic significance of Paleozoic magmatism in the Sakar unit of the Sakar-Strandzha Zone, SE Bulgaria. *Int. Geol. Rev.* 61 (16), 1957–1979. <https://doi.org/10.1080/00206814.2019.1575090>.
- Bonev, N., Spinkings, R., Moritz, R., 2020. <sup>40</sup>Ar/<sup>39</sup>Ar age constraints for an early Alpine metamorphism of the Sakar unit, Sakar-Strandzha zone, Bulgaria. *Geol. Mag.* 157 (12), 2106–2112. <https://doi.org/10.1017/S0016756820000953>.
- Bonev, N., Filipov, P., Raicheva, R., Moritz, R., 2022. Evidence of late Palaeozoic and Middle Triassic magmatism in the Sakar-Strandzha Zone, SE Bulgaria: regional geodynamic implications. *Int. Geol. Rev.* 64 (9) <https://doi.org/10.1080/00206814.2021.1917008>, 1199–1215.
- Boulvais, P., Ruffet, G., Cornichet, J., Mermet, M., 2007. Cretaceous albitization and dequartzification of Hercynian peraluminous granite in the Salvezines Massif (French Pyrénées). *Lithos* 93 (1–2), 89–106. <https://doi.org/10.1016/j.lithos.2006.05.001>.
- Burg, J.P., 2012. Rhodope: from Mesozoic convergence to Cenozoic extension. Review of petro-structural data in the geochronological frame. *J. Virtual Explor.* 42, 1–44. <https://doi.org/10.3809/jvirtex.2011.00270>.
- Chatalov, G.A., 1990. Geology of the Strandja Zone in Bulgaria: *Geologica Balcanica, Series Operum Singulorum* 4. Publishing house of Bulgarian Academy of Sciences, Sofia, 263 p. (in Bulgarian).
- Chavdarova, S., Machev, P., 2017. Amphibolites from Sakar Mountain – geological position and petrological features. In: *Proceeding of the National Conference with International Participation “GEOSCIENCES 2017”* Bulgarian Geological Society, pp. 49–50.
- Cherniak, D.J., 2000. Pb diffusion in rutile. *Contrib. Mineral. Petrol.* 139 (2), 198–207. <https://doi.org/10.1007/PL00007671>.
- Chew, D.M., Petrus, J.A., Kamber, B.S., 2014. U-Pb LA-ICPMS dating using accessory mineral standards with variable common Pb. *Chem. Geol.* 363, 185–199. <https://doi.org/10.1016/j.chemgeo.2013.11.006>.
- Elmas, A., Yilmaz, I., Yiğitbaş, E., Ullrich, T., 2011. A late Jurassic-early cretaceous metamorphic core complex, Strandja Massif, NW Turkey. *Int. J. Earth Sci.* 100, 1251–1263. <https://doi.org/10.1007/s00531-010-0540-3>.
- Engvik, A.K., Putnis, A., Fitz Gerald, J.D., Austrheim, H., 2008. Albitization of granitic rocks: the mechanism of replacement of oligoclase by albite. *Can. Mineral.* 46 (6), 1401–1415. <https://doi.org/10.3749/canmin.46.6.1401>.
- Ewing, T.A., Hermann, J., Rubatto, D., 2013. The robustness of the Zr-in-rutile and Ti-in-zircon thermometers during high-temperature metamorphism (Ivrea-Verbano Zone, northern Italy). *Contrib. Mineral. Petrol.* 165 (4), 757–779. <https://doi.org/10.1007/s00410-012-0834-5>.
- Ewing, T.A., Rubatto, D., Beltrando, M., Hermann, J., 2015. Constraints on the thermal evolution of the Adriatic margin during Jurassic continental break-up: U–Pb dating of rutile from the Ivrea–Verbano Zone, Italy. *Contrib. Mineral. Petrol.* 169, 44. <https://doi.org/10.1007/s00410-015-1135-6>.
- Gautier, P., Bosse, V., Cherneva, Z., Didier, A., Gerdjikov, I., Tiepolo, M., 2017. Polycyclic alpine orogeny in the Rhodope metamorphic complex: the record in migmatites from the Nestos shear zone (N. Greece). *Bull. Soc. Geol. Fr.* 188 (6), 1–28. <https://doi.org/10.1051/bsgf/2017195>.
- Gerdjikov, I., 2005. Alpine Metamorphism and Granitoid Magmatism in the Strandja Zone: New Data from the Sakar Unit, SE Bulgaria. *Turk. J. Earth Sci.* 14 (2), 167–183.
- Hövelmann, J., Putnis, A., Geisler, T., Schmidt, B.C., Golla-Schindler, U., 2010. The replacement of plagioclase feldspars by albite: Observations from hydrothermal experiments. *Contrib. Mineral. Petrol.* 159, 43–59. <https://doi.org/10.1007/s00410-009-0415-4>.
- Kamenov, B.K., Vergilov, V., Dabovski, C., Vergilov, I., Ivchinova, L., 2010. The Sakar batholith – petrology, geochemistry and magmatic evolution. *Bulg. Acad. Sci. Geochim. Mineral. Petrol.* 48, 1–37.
- Kennedy, A.K., Kamo, S.L., Nasdala, L., Timms, N.E., 2010. Grenville skarn titanite: potential reference material for Sims U–Th–Pb analysis. *Can. Mineral.* 48 (6), 1423–1443. <https://doi.org/10.3749/canmin.48.6.1423>.
- Kent, A.J.R., Ashley, P.M., Fanning, C.M., 2000. Metasomatic alteration associated with regional metamorphism: an example from the Willyama Supergroup, South Australia. *Lithos* 54, 33–62. [https://doi.org/10.1016/S0024-4937\(00\)00021-9](https://doi.org/10.1016/S0024-4937(00)00021-9).



- Kooijman, E., Mezger, K., Berndt, J., 2010. Constraints on the U-Pb Systematics of Metamorphic Rutile from in Situ LA-ICP-MS Analysis. *Earth Planet. Sci. Lett.* 293 (3–4), 321–330. <https://doi.org/10.1016/j.epsl.2010.02.047>.
- Kooijman, E., Smit, M.A., Mezger, K., Berndt, J., 2012. Trace element systematics in granulite facies rutile: implications for Zr geothermometry and provenance studies. *J. Metamorph. Geol.* 30 (4), 397–412. <https://doi.org/10.1111/j.1525-1314.2012.00972.x>.
- Lee, D.E., Bastron, H., 1967. Fractionation of rare-earth elements in allanite and monazite as related to geology of the Mt. Wheeler mine area, Nevada. *Geochim. Cosmochim. Acta* 31 (3), 339–356. [https://doi.org/10.1016/0016-7037\(67\)90046-4](https://doi.org/10.1016/0016-7037(67)90046-4).
- Lee, M.R., Parsons, I., 1997. Dislocation formation and albitization in alkali feldspars from the Shap granite. *Am. Mineral.* 82, 557–570. <https://doi.org/10.2138/am-1997-5-616>.
- Liati, A., 2005. Identification of repeated Alpine (ultra) high-pressure metamorphic events by U-Pb SHRIMP geochronology and REE geochemistry of zircon: the Rhodope zone of Northern Greece. *Contrib. Mineral. Petrol.* 150, 608–630. <https://doi.org/10.1007/s00410-005-0038-3>.
- Liati, A., Theye, T., Fanning, C.M., Gebauer, D., Rayner, N., 2016. Multiple subduction cycles in the Alpine orogeny, as recorded in single zircon crystals (Rhodope zone, Greece). *Gondwana Res.* 29, 199–207. <https://doi.org/10.1016/j.gr.2014.11.007>.
- Ludwig, K.R., 2012. Berkeley Geochronology Center, Special Publication No. 5 A Geochronological Toolkit for Microsoft Excel.
- Luvizotto, G.L., Zack, T., 2009. Nb and Zr Behavior in Rutile during High-Grade Metamorphism and Retrogression: an example from the Ivrea-Verbano Zone. *Chem. Geol.* 261 (3–4), 303–317. <https://doi.org/10.1016/j.chemgeo.2008.07.023>.
- Luvizotto, G.L., Zack, T., Triebold, S., Von Eynatten, H., 2009a. Rutile occurrence and trace element behavior in medium-grade metasedimentary rocks: example from the Erzgebirge, Germany. *Mineral. Petrol.* 97 (3–4), 233–249. <https://doi.org/10.1007/s00710-009-0092-z>.
- Luvizotto, G.L., Zack, T., Meyer, H.P., Ludwig, T., Triebold, S., Kronz, A., Munker, C., Stockli, D.F., Prowatke, S., Klemme, S., Jacob, D.E., von Eynatten, H., 2009b. Rutile crystals as potential trace element and isotope mineral standards for microanalysis. *Chem. Geol.* 261 (3–4), 346–369. <https://doi.org/10.1016/j.chemgeo.2008.04.012>.
- Mark, G., 1998. Albitite formation by selective pervasive sodic alteration of tonalite plutons in the Cloncurry district, Queensland. *Aust. J. Earth Sci.* 45, 765–774. <https://doi.org/10.1080/08120099808728431>.
- McDonough, W.F., Sun, S., 1995. The composition of the Earth. *Chem. Geol.* 120 (3–4), 223–253. [https://doi.org/10.1016/0009-2541\(94\)00140-4](https://doi.org/10.1016/0009-2541(94)00140-4).
- Meinhold, G., 2010. Rutile and its applications in Earth Sciences. *Earth-Sci. Rev.* 102 (1–2), 1–28. <https://doi.org/10.1016/j.earscirev.2010.06.001>.
- Moulas, E., Schenker, F.L., Burg, J.-P., Kostopoulos, D., 2017. Metamorphic conditions and structural evolution of the Kesirir-Kardamos dome: Rhodope metamorphic complex (Greece-Bulgaria). *Int. J. Earth Sci.* 106, 2667–2685. <https://doi.org/10.1007/s00531-017-1452-2>.
- Natal'in, B., Sunal, G., Gün, E., Wang, B., Zhiqing, Y., 2016. Precambrian to early cretaceous rocks of the Strandja Massif (northwestern Turkey): evolution of a long lasting magmatic arc. *Can. J. Earth Sci.* 53 (11), 1312–1335. <https://doi.org/10.1139/cjes-2016-0026>.
- Norberg, N., Neusser, G., Wirth, R., Harlov, D., 2011. Microstructural evolution during experimental albitization of K-rich alkali feldspar. *Contrib. Mineral. Petrol.* 162, 531–546. <https://doi.org/10.1007/s00410-011-0610-y>.
- Okay, A., Satur, M., Tüysüz, O., Akyüz, S., Chen, F., 2001. The tectonics of Strandja Massif: late-Variscan and mid-Mesozoic deformation and metamorphism in the northern Aegean. *Int. J. Earth Sci.* 90 (2), 217–233. <https://doi.org/10.1007/s005310000104>.
- Pan, L.C., Hu, R.Z., Bi, X.W., Li, C., Wang, X.S., Zhu, J.J., 2018. Titanite major and trace element compositions as petrogenetic and metallogenic indicators of Mo ore deposits: examples from four granite plutons in the southern Yidun arc, SW China. *Am. Mineral.* 103 (9), 1417–1434. <https://doi.org/10.2138/am-2018-6224>.
- Paton, C., Hellstrom, J., Paul, B., Woodhead, J., Hergt, J., 2011. Iolite: Freeware for the visualisation and processing of mass spectrometric data. *J. Anal. At. Spectrom.* 26 (12), 2508–2518. <https://doi.org/10.1039/c1ja10172b>.
- Pearce, J.A., Harris, N.B.W., Tindle, A.G., 1984. Trace element discrimination diagrams for the tectonic interpretation of granitic rocks. *J. Petrol.* 25 (4), 956–983. <https://doi.org/10.1093/petrology/25.4.956>.
- Petersson, J., Eliasson, T., 1997. Mineral evolution and element mobility during episyntization (dequartzification) and albitization in the postkinematic Bohus granite, Southwest Sweden. *Lithos* 42, 123–146. [https://doi.org/10.1016/S0024-4937\(97\)00040-6](https://doi.org/10.1016/S0024-4937(97)00040-6).
- Petrus, J.A., Kamber, B.S., 2012. VisualAge: A Novel Approach to Laser Ablation ICP-MS U-Pb Geochronology Data Reduction. *Geostand. Geanal. Res.* 36 (3), 247–270. <https://doi.org/10.1111/j.1751-908X.2012.00158.x>.
- Peytcheva, I., Georgiev, S., von Quadt, A., 2016. U/Pb ID-TIMS dating of zircons from Sakar-Strandzha Zone: new data and old questions about the Variscan orogeny in SE Europe. In: *Proceeding of the National Conference with International Participation "GEOSCIENCES 2016"*. Bulgarian Geological Society, pp. 71–72.
- Plümpner, O., Putnis, A., 2009. The complex hydrothermal history of granitic rocks: Multiple feldspar replacement reactions under subsolidus conditions. *J. Petrol.* 50, 967–987. <https://doi.org/10.1093/petrology/egp028>.
- Pointon, M.A., Cliff, R.A., Chew, D.M., 2012. The provenance of Western Irish Namurian Basin sedimentary strata inferred using detrital zircon U-Pb LA-ICP-MS geochronology. *Geol. J.* 47 (1), 77–98. <https://doi.org/10.1002/gj.1335>.
- Pristavova, S., Tzankova, N., Gospodinov, N., Filipov, P., 2019. Petrological study of metasomatic altered granitoids from Kanarata Deposit, Sakar Mountain, southeastern Bulgaria. *J. Min. Geol. Sci.* 62, 53–61.
- Ramseyer, K., Boles, J.R., Lichtner, P.C., 1992. Mechanism of plagioclase albitization. *J. Sediment. Petrol.* 62, 349–356. <https://doi.org/10.1306/d42678fc-2b26-11d7-8648000102c1865d>.
- Romer, R.L., 2001. Lead incorporation during crystal growth and the misinterpretation of geochronological data from low-<sup>238</sup>U/<sup>204</sup>Pb metamorphic minerals. *Terra Nova* 13 (4), 258–263. <https://doi.org/10.1046/j.1365-3121.2001.00348.x>.
- Şahin, S.Y., Aysal, N., Güngör, Y., Peytcheva, I., Neubauer, F., 2014. Geochemistry and U-Pb zircon geochronology of metagranites in Istranca (Strandja) Zone, NW Pontides, Turkey: implications for the geodynamic evolution of Cadomian orogeny. *Gondwana Res.* 26 (2), 755–771. <https://doi.org/10.1016/j.gr.2013.07.011>.
- Salacińska, A., Gerdjikov, I., Gumsley, A., Szopa, K., Chew, D., Gawęda, A., Kocjan, I., 2021. Two stages of late Carboniferous to Triassic magmatism in the Strandja Zone of Bulgaria and Turkey. *Geol. Mag.* 158 (12), 2151–2164. <https://doi.org/10.1017/S0016756821000650>.
- Salacińska, A., Gerdjikov, I., Kounov, A., Chew, D., Szopa, K., Gumsley, A., Kocjan, I., Marciniak-Maliszewska, B., Drakou, F., 2022. Variscan magmatic evolution of the Strandja Zone (Southeast Bulgaria and Northwest Turkey) and its relationship to other north Gondwanan margin terranes. *Gondwana Res.* 109, 253–273. <https://doi.org/10.1016/j.gr.2022.04.013>.
- Schmitt, A.K., Zack, T., 2012. High-sensitivity U-Pb rutile dating by secondary ion mass spectrometry (SIMS) with an O<sup>2+</sup> primary beam. *Chem. Geol.* 332–333, 65–73. <https://doi.org/10.1016/j.chemgeo.2012.09.023>.
- Şengör, A.M.C., Yılmaz, Y., Sungurlu, O., 1984. Tectonics of the Mediterranean Cimmerides: Nature and evolution of the western termination of Paleo-Tethys. In: Dixon, J.E., Robinson, A.H.F. (Eds.), *The Geological Evolution of the Eastern Mediterranean*, 17. Geological Society of London Special Publication, pp. 77–112. <https://doi.org/10.1144/GSL.SP.1984.017.01.04>.
- Shand, J., 1943. *Eruptive Rocks: Their Genesis, Composition, and Classification, with a Chapter on Meteorites*. Wiley, New York.
- Sláma, J., Košler, J., Condon, D.J., Crowley, J.L., Gerdes, A., Hanchar, J.M., Horstwood, M., Morris, G.A., Nasdala, L., Norberg, N., Schaltegger, U., Schoene, B., Tubrett, M., Whitehouse, M., 2008. Plešovice zircon - A new natural reference material for U-Pb and Hf isotopic microanalysis. *Chem. Geol.* 249 (1–2), 1–35. <https://doi.org/10.1016/j.chemgeo.2007.11.005>.
- Spandler, C., Hammerli, J., Sha, P., Hilbert-Wolf, H., Hu, Y., Roberts, E., Schmitz, M., 2016. MKD1: A new titanite standard for in situ analysis of Sm-Nd isotopes and U-Pb geochronology. *Chem. Geol.* 425, 110–126. <https://doi.org/10.1016/j.chemgeo.2016.01.002>.
- Stacey, J.S., Kramers, J.D., 1975. Approximation of terrestrial lead isotope evolution by a two-stage model. *Earth Planet. Sci. Lett.* 26 (2), 207–221. [https://doi.org/10.1016/0012-821X\(75\)90088-6](https://doi.org/10.1016/0012-821X(75)90088-6).
- Streckeisen, A., 1974. Classification and Nomenclature of Plutonic Rocks Recommendations. *Geol. Rundsch.* 63 (4), 773–786. <https://doi.org/10.1007/BF01820841>.
- Sunal, G., Satir, M., Natal'in, B.A., Topuz, G., Vonderschmidt, O., 2011. Metamorphism and diachronous cooling in a contractional orogen: the Strandja Massif, NW Turkey. *Geol. Mag.* 148 (4), 580–596. <https://doi.org/10.1017/S0016756810001020>.
- Szopa, K., Salacińska, A., Gumsley, A.P., Chew, D., Petrov, P., Gawęda, A., Zagórska, A., Deput, E., Gospodinov, N., Banasik, K., 2020. Two-stage late Jurassic to early cretaceous Hydrothermal activity in the Sakar Unit of Southeastern Bulgaria. *Minerals* 10, 266. <https://doi.org/10.3390/min10030266>.
- Tomkins, H.S., Powell, R., Ellis, D.J., 2007. The pressure Dependence of the Zirconium-in-Rutile Thermometer. *J. Metamorph. Geol.* 25 (6), 703–713. <https://doi.org/10.1111/j.1525-1314.2007.00724.x>.
- Tzankova, N., Pristavova, S., 2007. Metamorphic evolution of garnet-bearing schists from Sakar mountain southeastern Bulgaria. *Compt. Rend. L'Acad. Bulg. Sci.* 60 (3), 271–278.
- Vladinova, T., Georgieva, M., 2020. New data on the westernmost part of the Sakar unit metamorphic basement, SE Bulgaria. In: *Proceeding of the National Conference with International Participation "GEOSCIENCES 2020"*, 81(3). Bulgarian Geological Society, pp. 105–107.
- Vladinova, T., Georgieva, M., Cherneva, Z., 2018. U-Pb detrital zircons geochronology from metasedimentary rocks of the Sakar Unit, Sakar-Strandzha zone, SE Bulgaria. In: *Proceeding of the National Conference with International Participation "GEOSCIENCES 2018"*, 79. Bulgarian Geological Society, pp. 67–68.
- Vladinova, T., Georgieva, M., Peytcheva, I., 2019. U-Pb geochronology and geochemistry of rutiles from metaconglomerate in the Sakar-Strandzha zone, SE Bulgaria. In: *Proceeding of the National Conference with International Participation "GEOSCIENCES 2019"*, 80(3). Bulgarian Geological Society, pp. 91–93.
- Wang, C., Rao, S., Shi, K., Bagas, L., Chen, Q., Zhu, J., Duan, H., Liu, L., 2021. Rutile in amphibolite facies metamorphic rocks: a rare example from the east qinling orogen, China. *Appl. Sci.* 11, 18. <https://doi.org/10.3390/app11188756>.
- Watson, E.B., Wark, D.A., Thomas, J.B., 2006. Crystallization Thermometers for Zircon and Rutile. *Contrib. Mineral. Petrol.* 151 (4), 413–433. <https://doi.org/10.1007/s00410-006-0068-5>.
- Wiedenbeck, M., Allé, P., Corfu, F., Griffin, W.L., Meier, M., Oberli, F., Von Quadt, A., Roddick, J.C., Spiegel, W., 1995. Three natural zircon standards for U-Th-Pb, Lu-Hf, trace element and ree analyses. *Geostand. Newslett.* 19 (1), 1–23. <https://doi.org/10.1111/j.1751-908X.1995.tb00147.x>.
- Wiedenbeck, M., Hanchar, J.M., Peck, W.H., Sylvester, P., Valley, J., Whitehouse, M., Kronz, A., Morishita, T., Nasdala, L., Fiebig, J., Franchi, I., Girard, J.-P., Greenwood, R.C., Hinton, R., Kita, N., Mason, P.R.D., Norman, M., Ogasawara, M., Piccoli, P.M., Rhede, D., Satoh, H., Schulz-Dobrick, B., Skår, O., Spicuzza, M.J., Terada, K., Tindle, A., Togashi, S., Vennemann, T., Xie, Q., Zheng, Y.-F., 2004. Further characterisation of the 91500 zircon crystal. *Geostand. Geanal. Res.* 28 (1), 9–39. <https://doi.org/10.1111/j.1751-908X.2004.tb01041.x>.



- Zack, T., Luvizotto, G.L., 2006. Application of rutile thermometry to eclogites. *Mineral. Petrol.* 88 (1–2), 69–85. <https://doi.org/10.1007/s00710-006-0145-5>.
- Zack, T., Moraes, R., Kronz, A., 2004. Temperature dependence of Zr in rutile: Empirical calibration of a rutile thermometer. *Contrib. Mineral. Petrol.* 148 (4), 471–488. <https://doi.org/10.1007/s00410-004-0617-8>.
- Zack, T., Stockli, D.F., Luvizotto, G.L., Barth, M.G., Belousova, E., Wolfe, M.R., Hinton, R. W., 2011. In situ U-Pb rutile dating by LA-ICP-MS:  $^{208}\text{Pb}$  correction and prospects for geological applications. *Contrib. Mineral. Petrol.* 162 (3), 515–530. <https://doi.org/10.1007/s00410-011-0609-4>.